Welding Simulations of Aluminum Alloy Joints by Finite Element Analysis

Justin D. Francis

Thesis submitted to the Faculty of the
Virginia Polytechnic Institute and State University
in partial fulfillment of the requirements for the degree of

Master of Science
in
Aerospace Engineering

Dr. Eric Johnson, Chair
Dr. Rakesh Kapania
Dr. Zafer Gurdal
Dr. Tom-James Stoumbos

April 2002
Blacksburg, Virginia

Keywords: weld simulation, GMAW, aluminum, finite element analysis

Welding Simulations of Aluminum Alloy Joints by Finite Element Analysis

Justin D. Francis

(ABSTRACT)

Simulations of the welding process for butt and tee joints using finite element analyses are presented. The base metal is aluminum alloy 2519-T87 and the filler material is alloy 2319. The simulations are performed with the commercial software SYSWELD+®, which includes moving heat sources, material deposit, metallurgy of binary aluminum, temperature dependent material properties, metal plasticity and elasticity, transient heat transfer and mechanical analyses. One-way thermo-mechanical coupling is assumed, which means that the thermal analysis is completed first, followed by a separate mechanical analysis based on the thermal history.

The residual stress state from a three-dimensional analysis of the butt joint is compared to previously published results. For the quasi-steady state analysis the maximum residual longitudinal normal stress was within 3.6% of published data, and for a fully transient analysis this maximum stress was within 13% of the published result. The tee section requires two weld passes, and both a fully three-dimensional (3-D) and a 3-D to 2-D solid-shell finite elements model were employed. Using the quasi-steady state procedure for the tee, the maximum residual stresses were found to be 90-100% of the room-temperature yield strength. However, the longitudinal normal stress in the first weld bead was compressive, while the stress component was tensile in the second weld bead. To investigate this effect a fully transient analysis of the tee joint was attempted, but the excessive computer times prevented a resolution of the longitudinal residual stress discrepancy found in the quasi-steady state analysis. To reduce computer times for the tee, a model containing both solid and shell elements was attempted. Unfortunately, the mechanical analysis did not converge, which appears to be due to the transition elements used in this coupled solid-shell model.

Welding simulations to predict residual stress states require three-dimensional analysis in the vicinity of the joint and these analyses are computationally intensive and difficult. Although the state of the art in welding simulations using finite elements has advanced, it does not appear at this time that such simulations are effective for parametric studies, much less to include in an optimization algorithm.

Acknowledgments

First and foremost I would like to thank my parents, David and Karen, and my brother, Josh, for their continued support in my pursuit of my undergraduate degree, as well as this advanced degree. If not for their support I would not have been able to return to Virginia Tech to attend graduate school full-time.

I would also like to thank Dr. Tom Stoumbos who over the course of two years, planted the seed and encouraged my return to Virginia Tech to complete my master's degree. His support, and the support of General Dynamics Amphibious Systems, made this possible. It was Tom who introduced me to Dr. Eric Johnson and Dr. Rakesh Kapania and paved the way for my return to Virginia Tech. Once at Tech, Dr. Eric Johnson's guidance made it as painless as possible to complete my degree. I would also like to thank Dr. Rakesh Kapania, Dr. Zafer Gürdal, Dr. Scott Ragon, and John Coggin for their continued interest and challenges which helped shape this research.

I acknowledge the Dept. of the Navy, STTR Contract N00014-99-M-0253 of which ADOPTECH, Inc., Blacksburg, VA was the primary contractor, for the funding of this research effort, and the Interdisciplinary Center for Applied Mathematics at Virginia Tech for use of their SGI Origin 2000 computer facility.

Table of Contents

List of Tables

List of Figures

CHAPTER 1

Utilizing welding simulations in vehicle structural design

The background for this work is presented in this chapter. Finite element analysis in the optimal design of vehicle structures is discussed in the context of a project on the weight reduction of a military assault vehicle. A technique called global/local optimization is summarized, which is a method to include the results of numerically intensive, detailed analyses in the overall design algorithm. In particular, the structural detail of interest is the welded aluminum joint. The assault vehicle has numerous welded joints, and the aim of this work is to explore the possibility of using the results from detailed welding simulations in the global-local optimization scheme.

1.1 Finite Element Analysis in Vehicle Design

The design of complex vehicle structures such as the Advanced Amphibious Assault Vehicle (AAAV), shown in Figure 1.1 on page 2 , involves many factors such as cost, weight, and durability. The AAAV utilizes a planing hull design which can traverse seas at speeds of 25

knots, then land at beaches and become a tracked vehicle capable of speeds of 45 m.p.h. over diverse terrain [1]. Hence, these vehicles are subjected to a variety of random loads including hydrodynamic loads, rough terrain loads and blast loads. Designers of these vehicles face many challenges such as accurate modeling of the loads, accurate modeling of the vehicle structure and sub-components, and maintaining a balance of manufacturability, cost, and structural integrity. Finite element models are often developed for the analysis of these complex structures, and the amount of detail to include in the finite element analyses is always problematical.

Fig. 1.1 Advanced Amphibious Assault Vehicle (AAAV) [1]

Typically large, and computationally intensive finite element models are utilized to predict the overall response of a structure, including important quantities such as stresses and displacements [2]. Moreover, repetitive analyses are required in design algorithms, and execution of many finite element analyses usually demands approximations to reduce run times. Therefore, it is typical for finite element models of the overall structure to have reduced detail which does not take into account local design issues. Unfortunately, many of the local design details that are neglected in the overall vehicle finite element analysis have a strong influence on the response and failure characteristics of the vehicle, and must be accounted for during overall design of the vehicle.

1.2 Global/Local Optimization

An important objective in the optimization process of vehicle structural design is to reduce the weight of the vehicle without a failure of any kind occurring under service loads. However, the difficult issue is that of the level of detail to include in the finite element structural analysis to evaluate constraints. A method to include local design details early in the vehicle design process is called the global/local design methodology. A global/local optimization strategy for the overall design of complex structures such as the AAAV can account for the local details and their interaction with the global response of the vehicle. In the global/local approach, the overall design problem is decomposed into a global problem and a local problem. The global problem focuses on the design and analysis of the entire vehicle structure using simplified models, typically shell finite element models. At the global design level, the finite element model of the complete structure is used to compute the overall response of the structure and to assure that specified constraints on displacements and stresses are not violated. In the global finite element models the

flexibility of the joints between parts, such as the connection between the web of a stiffener and the skin, is ignored. The corresponding displacements and rotations of the structural elements adjacent to the connection are the same. For example, the joint between the two skin elements and stiffener element as shown in Figure 1.2 is assumed to be rigid. In the AAAV structure this joining of the stiffener to the skin is achieved by welding. Welding heat adversely affects weld-zone mechanical properties, and the strength of the weld area is less than that of the unaffected base metal. Also, residual stresses of significant magnitude are developed in the weld zone unless a post-weld heat treatment is performed to alleviate the residual stresses. Reduced strength, residual stresses, and joint flexibility that are ignored in the global finite element analysis, are represented in the local problem.

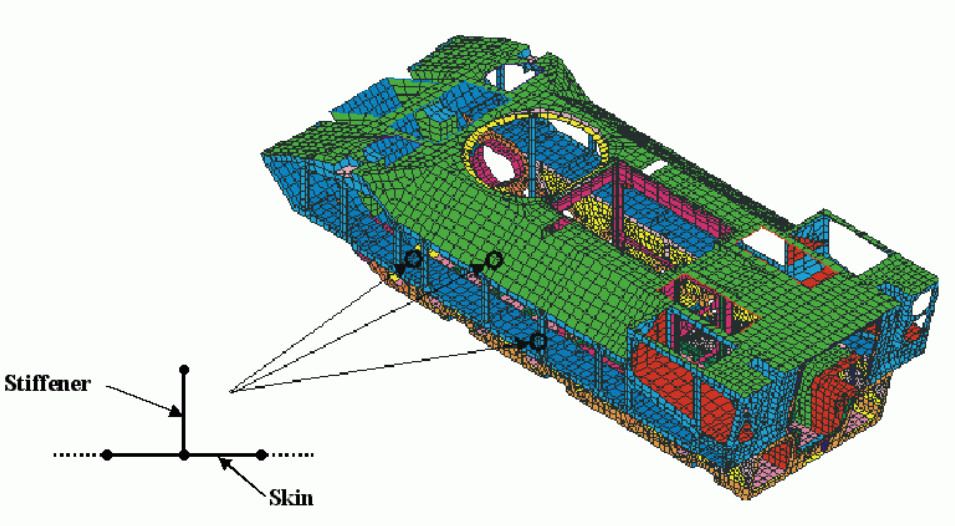

Fig. 1.2 Finite Element Model of AAAV with Skin/ Stiffener Configuration [2]

The local problem consists of refined finite element models of the weldment between the stiffener and skin to account for joint flexibility and reduced strength. Design variables as well as

joint displacements, or loads, determined in the global analysis are imposed on the local model of the welded joint. Then, the design variables unique to the local joint model are determined such that the joint design is optimal, where as an example, optimal means that the joint design has the largest factor of safety. This largest factor of safety is returned to the global optimization program to assess if there is a local failure of a particular joint, and if there is a joint that does not meet the specified minimum factor of safety, then the design optimization process is repeated to determine new values of the global design variables.

Before the optimization process begins in the global/local methodology, the local problems are optimally designed for a range of values of global design variables and global loads that are anticipated. These optimized local designs are then stored in a database and it this data based that is called by the global optimization program, rather than performing a local analysis and optimization iterations within a global optimization iteration. See Figure 1.3 . Interpolation of the data base for specified global variables is accomplish by what is called a response surface, which can be conceptualized as a surface representing the factor of safety plotted over the subspace of the global variables. In addition, for each set of values for the global variables there is a set of values for the local design variables associated with the maximum factor of safety. Once the local design data base is constructed, it can easily be used by the global optimization program to design the complete structure. The global/local design methodology is particularly advantageous when the configuration of the local problem is replicated many times in the global problem, as is the case in the AAAV structure where the skin-stiffener joint configuration occurs in many locations.

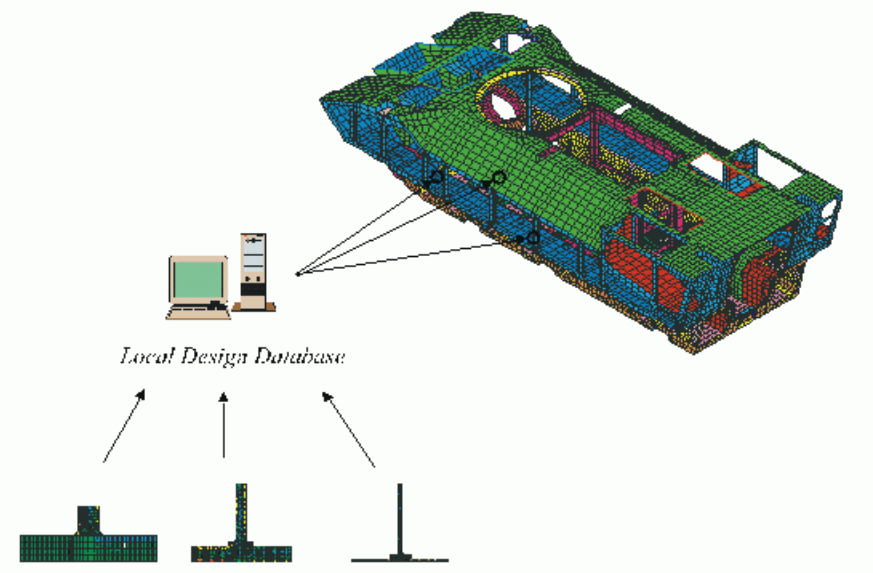

Fig. 1.3 Global/Local decomposition [2]

1.3 Weld Joint Model in Phase I

In the initial effort to demonstrate the potential of the global/local methodology, which was called Phase I [2], a simplified finite element model of the skin-stiffener joint was developed. The cross section of the finite element model of this skin-stiffener joint is shown in Figure 1.4 . As is shown in the figure, global design variables were the skin thickness t_1, stiffener height h, and stiffener width w. Local design variables were the flange width s, flange thickness t_2, and dimension l characterizing the weld size. The finite element analysis was three-dimensional as is shown in Figure 1.5 , with a depth equal to 0.5 cm. The model consisted of 948 brick elements and 5292 degrees of freedom.

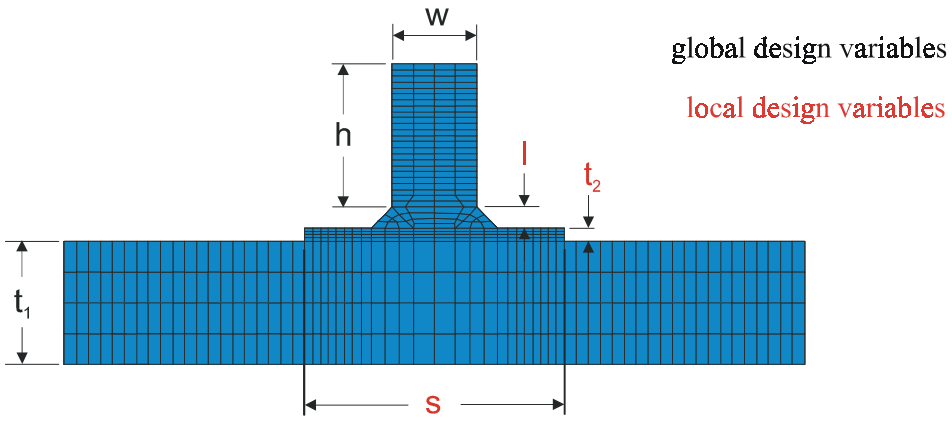

Fig. 1.4 Finite Element Model of Local Weld Joint with Design Variables [2]

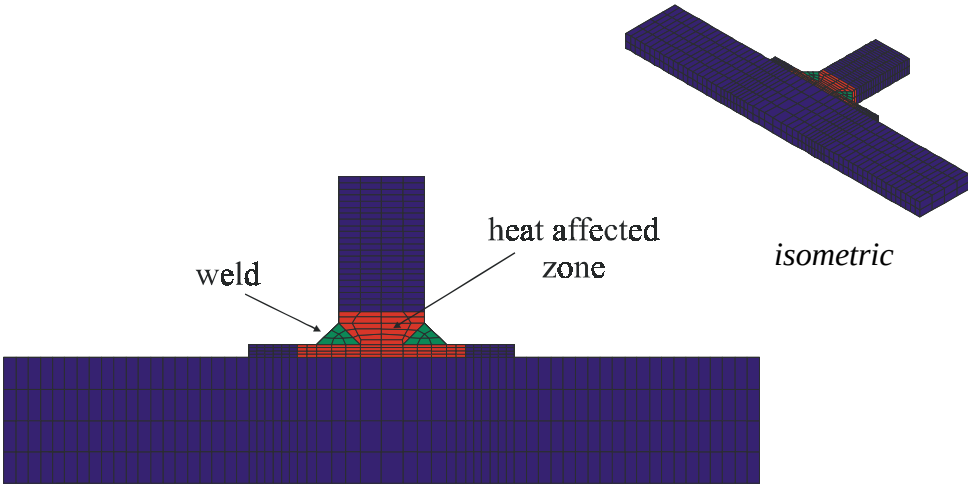

Fig. 1.5 Finite Element Model of Local Weld Joint depicting weld and heat affected zone [2]

Load data from the global model were the rotations and displacements shown in Figure 1.6 and Figure 1.7 . In the local coordinate system shown in Figure 1.7 , Δd_1 and Δd_2

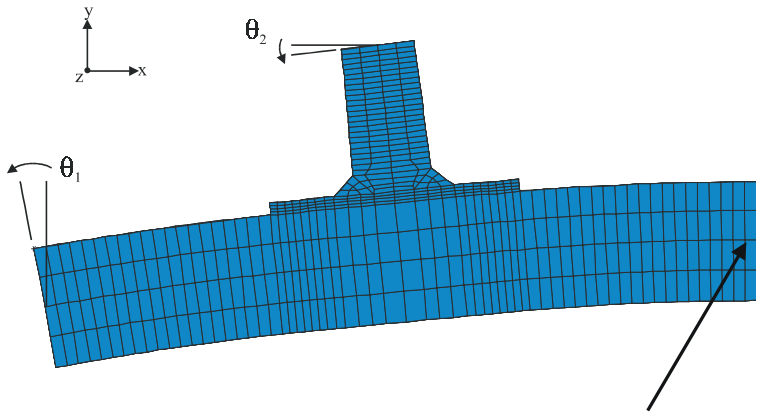

θ_1 and θ_2 measured relative to rotation at right end of skin

Fig. 1.6 Local model applied rotations [2]

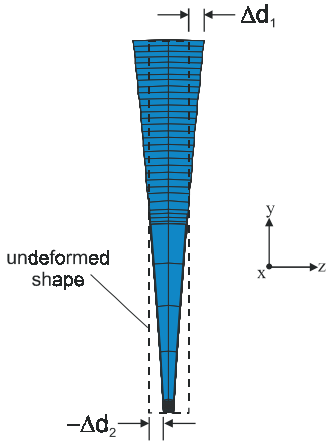

Δd_1 and Δd_2 are elongations, and account for tension/compression and longitudinal bending of the stiffener

Fig. 1.7 Local model applied displacements [2]

are elongations of the top of the stiffener and bottom of the skin in the *z*-direction to represent the longitudinal bending and extensional deformations of the stiffener. The weld zone size and heat

affected zone, or HAZ, were approximated based on the weld size and engineering experience, and are shown as the green and red shaded areas in Figure 1.5 . In the weld zone the yield strength of the material was degraded to a value of 152 MPa to account for the adverse effects of welding on the strength. The yield strength in the base metal unaffected by welding was 400 MPa. The factor of safety at a particular location was defined as the yield strength divided by the von Mises effective stress. Dependent upon the global design variables (t_1, h, w), as well as the loading (θ_1,θ_2,Δd_1, Δd_2), the local design variables (t_2, s, l) were determined to maximize the factor of safety for the joint. For a specified set of global design variables and applied loads, the global optimization program receives from the local design database, or response surface, the factor of safety for the joint [2].

Recently, there has been significant advancement in the finite element simulations of the welding process, and the literature on this subject is reviewed in Chapter 3. Hence, it is timely to assess if rationally-based finite element simulations can be used in place of the approximation of the reduction in joint strength as used in the Phase I effort.

1.4 Objective

The objective of this research is to determine the size of the weld zone and residual stress state of tee and butt joints using finite element simulations. The welds are continuous using the gas metal-arc process, the base metal is aluminum alloy 2519-T87, and the filler metal is aluminum alloy 2319. Details of the gas metal-arc welding (GMAW) process are discussed in Chapter 2. The SYSWELD+[1] software is used to perform the finite element simulations.

1. SYSWELD+ is the registered trademark of ESI Group, ESI North America, 13399 West Star, Shelby Township MI 48315-2701.

The complex nature of the welding process causes difficulty in analyzing and modeling by numerical methods. These complexities include: material and thermal properties which vary with temperature, transient heat transfer with complicated boundary conditions, moving heat sources, phase changes and transformations, complex residual stress states and the difficulties of making experimental measurements at high temperatures [11]. In addition to these complexities, finite element modeling of the weld process must include complex thermo-mechanical interactions, metallurgical transformations, material deposit, and moving heat sources. Accurate prediction of the thermal cycle in the weld joint is the first step when predicting residual stresses. Prediction of the temperature field requires a non-linear, 3-D analysis with temperature dependent material properties. Moving heat sources are used to generate the temperature fields during the welding process and material deposit is implemented using a variety of means. The temperature history is used for the calculation of the thermal stresses and displacement fields during and after the welding process [12]. In other words, once the thermal history is known, the plastic deformation due to the thermal expansion and contraction must be calculated [2]. A sample residual stress distribution as predicted by a weld simulation is shown in Figure 1.8 .

The finite element simulations of welding are so computationally intensive that it is impractical to execute them within the numerous iterations required in design algorithms. However, the global/local methodology was developed specifically to incorporate computationally intensive analyses into the design optimization program. Hence, it may be possible to use the results of the welding simulation in the local finite element models of the skin-stiffener joint in the structural design of the AAAV vehicle.

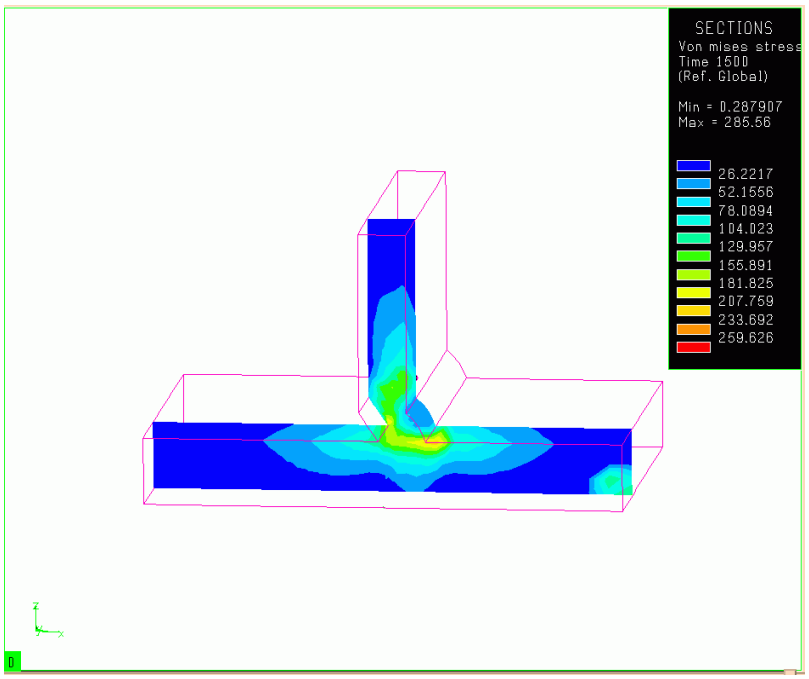

Fig. 1.8 Residual stress distribution in an aluminum alloy tee joint

1.5 Summary of Subsequent Chapters

The processes, procedures, and metallurgy of gas-metal arc welding of aluminum are presented in Chapter 2. In Chapter 3, the previous finite element analyses of welding are reviewed. The energy and constitutive equations governing a welding simulation are outlined in Chapter 4, while performing welding simulations utilizing the SYSWELD+® sofware is described in Chapter 5. The residual stress results for the tee and butt joints are reported in Chapter 6. Concluding remarks are given in Chapter 7.

CHAPTER 2

Processes and Metallurgy of Welding Aluminum Alloy

Aspects of the physics, metallurgy, and procedures involved in welding aluminum are discussed in this chapter.

2.1 Gas Metal Arc Welding Aluminum

The AAAV structure is primarily made of aluminum alloys, and aluminum alloys are usually fusion welded with the gas metal arc welding (GMAW) process, or the gas tungsten arc welding (GTAW or TIG) process. Fusion welding achieves the chemical bond formation, or welding, of parts through melting. A filler metal may be used to facilitate the process [3]. Examples of fusion welding are arc welding, gas welding, electron beam welding, and laser welding [4]. In general, GMAW is for heavier material while GTAW is for thicknesses to 3.175 mm (1/8 inch), though this is not a steadfast rule. In each process an inert gas is used to shield the weld arc and the weld pool. The difference in the processes are in the electrodes and type of power used. GMAW utilizes an aluminum filler wire as the electrode while GTAW

uses a nonconsumable tungsten electrode with aluminum filler material added separately. The arc used for GMA welding aluminum is direct-current, electrode-positive (DCEP) where the electrode is positive and the work is negative. The filler metal and the weld zone of the workpiece are melted. GTA welding aluminum may use direct-current electrode-negative (DCEN), direct-current electrode-positive (DCEP), or alternating current (AC). The GMAW process is either semiautomatic or automatic. During semiautomatic welding the gun is operated manually [5].

When exposed to air, aluminum and its alloys develop a self-limiting oxide surface film. The melting point of this oxide is above the melting point of pure aluminum, 1982^{o}C (3600 ^{o}F) compared to 1315 ^{o}C (2400 ^{o}F), respectively. This oxide film can preclude wetting between the base plate and the filler metal, but also flakes of oxide or dross can become entrapped within the weld metal, which reduces the weld ductility. If argon shielding is used, the DCEP breaks up the surface oxide on the base metal ahead of the weld pool. This cleaning action is thought to be caused by two phenomena, the inert-gas ions striking the plate and electrons leaving the base plate. Another important feature of the DCEP arc, is that the action propels the filler metal across the arc to the workpiece in line with the axis of the electrode, regardless of the orientation of the electrode. Combined with aluminum's low density, surface tension, and high cooling rate, gas metal arc welds can be made in horizontal, vertical, and overhead positions. High deposition rates are possible which results in greater weld strengths and less distortion than other fusion-welding processes [5].

Distinct microstructural regions occur in fusion welds as a result of the effects of heat. At the weld centerline is the fusion zone (FZ). The FZ is where the bonding by melting takes place; i.e., the heating causes the alloy to rise above its liquidis temperature. Outside the FZ is the partially melted zone (PMZ), where the temperature of the alloy was below the liquidis but above

the solidis. Outside the PMZ is the heat affected zone (HAZ), where the temperatures are lower, but still high enough to cause observable microstructural changes due to solid-phase transformations. At some further distance from the weld centerline is the unaffected base material, where the temperature rise was too low to cause any noticeable microstructural changes [6]. The weld zone (WZ) encompasses the fusion, partially melted, and heat affected zones.

2.1.1 Weld Quality

Ductility, fatigue strength and tensile strength of welded joints are adversely affected by the inclusion of porosity and dross. The main source of porosity in aluminum welds is due to entrapped gas within the weld puddle. Contaminants in the shielding gas, air and water, as well as contaminants in the base or filler metals can be the origin of these gases. The amount of gas which remains in the weld pool is a function of the cooling rate of the weld pool; i.e., the metal freezes before the gas has a chance to escape. Weld porosity in a weld joint is similar to the air bubbles trapped in an ice cube which was frozen rapidly. The generation of hydrogen from contaminants in the weld is also a cause of gas porosity in aluminum welds. Aluminum has a high solubility of hydrogen when molten, but solid aluminum can contain very little hydrogen, as shown in Figure 2.1 on page 15. As the weld pool cools, hydrogen gas is evolved, so if the cooling rate is too rapid the gas cannot rise to the surface. The gas therefore remains within the metal causing porosity. Furthermore, multi-pass welds exhibit more porosity than single-pass welds. Root passes generally contain less porosity than later, top passes [5].

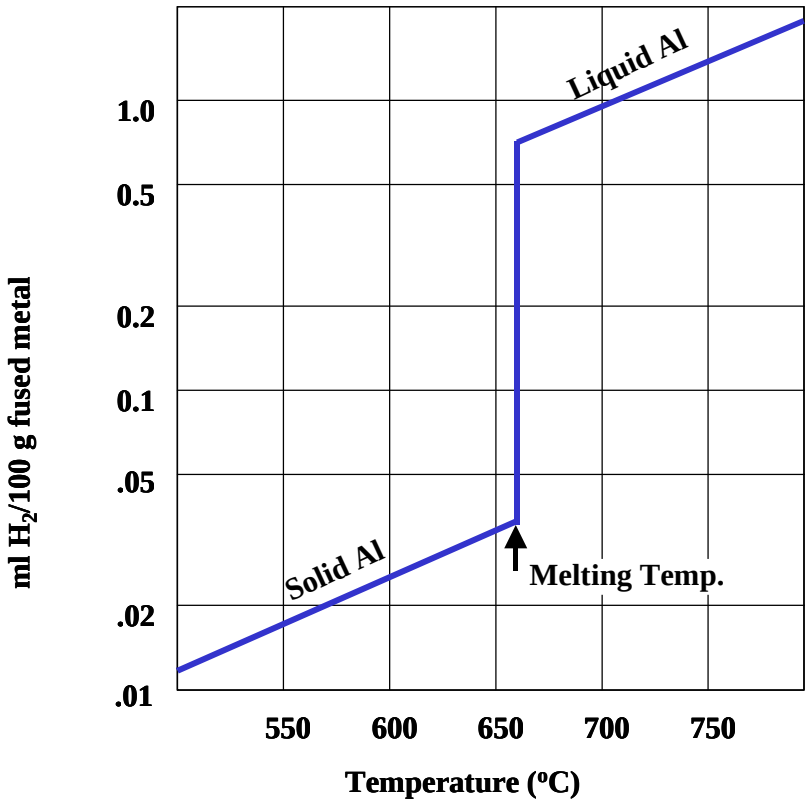

Fig. 2.1 Solubility of hydrogen in aluminum at various temperatures [5]

2.1.2 Procedures

The exact procedure for GMA welding of aluminum is dependent upon three key factors: the equipment available, material thicknesses, and alloy content. Typical procedures for conventional GMA welding of aluminum sheet and plate, for a variety of joints are given in Table 2.1, Table 2.2, and Table 2.3 [5]. The joints investigated during this research effort are similar to those

described in Table 2.2 and Table 2.3, but the geometries differ in the fact that the bevels or chamfer angles on the base plates are designed for ballistic reasons. This means that the weld joints are designed such that the joint will have the greatest strength to withstand impacts by certain rounds of ammunition, the specification of which is not relevant to this research. The precise joint dimensions used for this research will be presented concurrent with the results.

Table 2.1 Procedures for GMAW of Aluminum (Semiautomatic)

Process: Gas Metal-Arc **Type of Joint: Butt** **Plate Thickness: 1/8 - 3/4** **Position: Flat** **Welded from: Two Sides** **Polarity: DCEP**	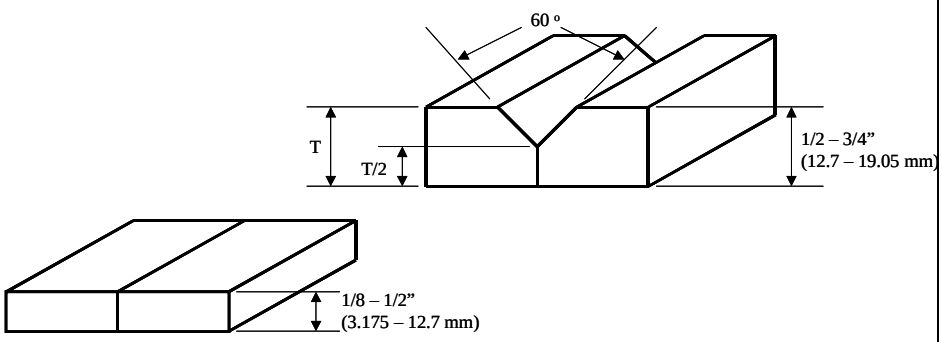							
Plate Thickness, T, in (mm)	1/8 (3.125)	3/16 (4.763)	1/4 (6.35)	3/8 (9.525)	1/2 (12.7)	1/2 (12.7)	5/8 (15.875)	3/4 (19.05)
Pass Face	1	1	1	1	1	1	1	1
Pass Back		1	1	1	1	1	1	1
Electrode Size, in (mm)	3/64 (1.191)	3/64 or 1/16 (1.191) or (1.587)	1/16 (1.587)	1/16 (1.587)	1/16 (1.587)	1/16 (1.587)	1/16 (1.587)	1/16 (1.587)
Current (amp)	90-120	120-150	180-220	220-260	240-280	260-320	260-320	300-400
Volts	19-21	22-24	27-29	28-30	28-30	29-31	29-31	33-37
Arc Speed, ipm (mm/s)	30-34 (12.7 - 14.4)	25-29 (10.6 - 12.3)	20-24 (8.5 - 10.2)	16-20 (6.8 - 8.5)	14-18 (5.9 - 7.6)	12-16 (5.1 - 6.8)	10-14 (4.2 - 5.9)	10-14 (4.2 - 5.9)
Argon Gas, cfh	30-40	30-40	30-40	40-60	40-60	40-60	60-80	60-80
Gas Cup Opening, in (mm)	1/2 (12.7)	1/2 (12.7)	1/2 (12.7)	1/2 (12.7)	1/2 (12.7)	1/2 (12.7)	1/2 (12.7)	1/2 (12.7)
Total Time (hr/ft of weld)	.00625	.0148	.0182	.0222	.0250	.0286	.0333	.0333

Table 2.2 Procedures for GMAW of Aluminum (Semiautomatic)

Process: Gas Metal-Arc **Type of Joint: Butt** **Plate Thickness: 1/2 - 1 1/2** **Position: Flat** **Welded from: Two Sides** **Polarity: DCEP**	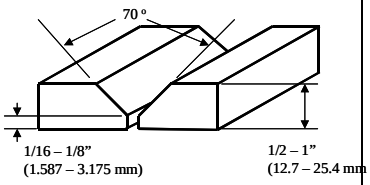			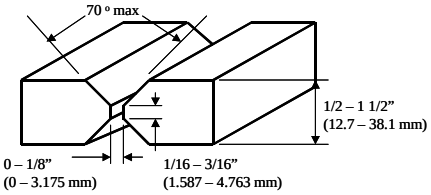				
Plate Thickness, T, in (mm)	1/2 (12.7)	3/4 (19.05)	1 (25.4)	1/2 (12.7)	3/4 (19.05)	1 (25.4)	1 1/4 (31.75)	1 1/2 (38.1)
Pass Face	4	5	7	1	2	3	3	4
Pass Back	1	1	1	1	2	3	3	4
Electrode Size, in (mm)	1/16 (1.587)	3/32 (2.38)	3/32 (2.38)	1/16 (1.587)	1/16 (1.587)	1/16 (1.587)	1/16 (1.587)	1/16 (1.587)
Current (amp)	200-230	260-280	260-300	220-250	240-280	240-280	240-280	240-280
Volts	27-29	27-29	27-29	28-30	28-30	28-30	28-30	28-30
Arc Speed, ipm (mm/s)	16-20 (6.8 - 8.5)	12-16 (5.1 - 6.8)	10-14 (4.2 - 5.9)	16-20 (6.8 - 8.5)	16-20 (6.8 - 8.5)	14-20 (5.9 - 8.5)	14-20 (5.9 - 8.5)	14-20 (5.9 - 8.5)
Argon Gas, cfh	40-60	40-60	40-60	40-60	40-60	60-80	60-80	60-80
Gas Cup Opening, in (mm)	1/2 (12.7)	5/8 (15.875)	5/8 (15.875)	5/8 (15.875)	5/8 (15.875)	5/8 (15.875)	5/8 (15.875)	5/8 (15.875)
Total Time (hr/ft of weld)	.0555	.0858	.133	.0222	.0444	.0708	.0708	.0944

Table 2.3 Procedures for GMAW of Aluminum (Semiautomatic)

Process: Gas Metal-Arc **Weld Size, in (mm): 1/4 - 1/2 (6.35-12.7)** **Type of Joint: Fillet Positions: Horizontal, Vertical, and Overhead Polarity: DCEP**	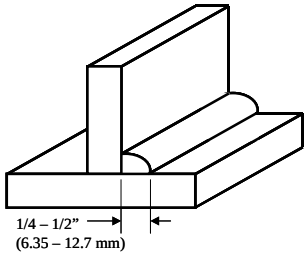			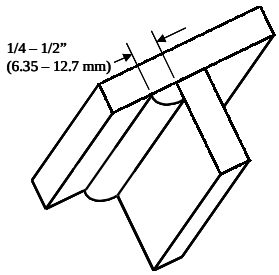			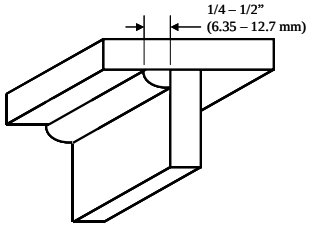		
Fillet Size, L, in (mm)	1/4 (6.35)	3/8 (9.525)	1/2 (12.7)	1/4 (6.35)	3/8 (9.525)	1/2 (12.7)	1/4 (6.35)	3/8 (9.525)	1/2 (12.7)
Pass	1	1	3	1	2	3	1	2	3
Electrode Size, in (mm)	1/16 (1.587)	1/16 (1.587)	3/32 (2.38)	1/16 (1.587)	1/16 (1.587)	1/16 (1.587)	1/16 (1.587)	1/16 (1.587)	1/16 (1.587)
Current (amp)	160 - 180	200 - 230	240 - 280	160 - 180	180 - 200	180 - 220	160 - 180	180 - 200	180 - 220
Volts	24 - 26	27-29	26 - 28	24 - 26	27 - 29	27 - 29	23 - 25	27 - 29	27 - 29
Arc Speed, ipm (mm/s)	24 - 28 (10.2 - 11.9)	20 - 24 (8.5 - 10.2)	16 - 20 (6.8 - 8.5)	16 - 20 (6.8 - 8.5)	14 - 18 (5.9 - 7.6)	12 - 16 (5.1 - 6.8)	18 - 22 (7.6 - 9.3)	18 - 22 (7.6 - 9.3)	16 - 20 (6.8 - 8.5)
Argon Gas, cfh	30 - 40	30 - 40	40 - 60	30 - 40	40 - 60	40 - 60	40 - 60	40 - 60	60 - 80
Gas Cup Opening, in (mm)	1/2 (12.7)	1/2 (12.7)	5/8 (15.875)	1/2 (12.7)	1/2 (12.7)	5/8 (15.875)	1/2 (12.7)	1/2 (12.7)	5/8 (15.875)
Total Time (hr/ft of weld)	.00769	.00909	.0333	.0111	.0250	.0429	.0100	.0200	.0333

2.1.3 Weld Residual Stresses

Residual stresses are stresses that remain in a body after all external loads have been removed from that body. Residual stresses resulting from the intense thermal cycling imposed during welding reduce joint strength. Welding induced residual stresses can significantly increase the fracture driving force in a weldment and also contribute to brittle fracture [7]. If the structure is unable to support these stresses, it will either distort or crack. Residual stresses also combine with

"in service" loads to create stress fields often very different from those expected [8]. Hence, weld joint strength plays a crucial role in the survivability of welded military vehicles.

Residual stresses due to welding are caused by the application of intense heat or thermal loading at the weld joint, which causes plasticity of the material underneath and immediately surrounding the weld arc, but the nearby cooler material remains elastic and acts to constrain the heated material. The thermal cycle imposed on any welded object causes thermal expansions and contractions to occur which vary with time and location. Because this expansion is not uniform, stresses appear when hot regions near the weld are restrained by cooler regions further away. Plastic deformations, occurring as a result of these stresses lead to residual stresses in the object after the temperatures have returned to ambient levels. In the FZ and HAZ, and extending out some distance into the unaffected base material is a region of tensile residual stresses. These residual stresses are usually of magnitude of the yield strength [2]. Dong, et al. [9] found that in Al-Li alloy repair welds, highly tensile longitudinal residual stresses were present in a region spanning a few weld widths to either side of the weld and that under mismatched yield strength conditions, these maximum longitudinal stresses can reach beyond their respective yield strengths.

Residual stresses are produced by an uneven distribution of nonelastic strains, including plastic and thermal strains. Large local plastic strains in the solidified weld metal and the HAZ originate from the very non-uniform temperature field around the weld pool [10]. During the welding thermal cycle, complex transient thermal stresses are produced in the weldment and the surrounding joint. Beneath the welding arc, stresses are close to zero because molten metal does not support shear loading. Adjacent to the welding arc, and moving away from the welding arc, stresses become compressive because the expansion of metal surrounding the weld pool is

restrained by the base metal. These compressive stresses are as high as the yield strength of the base metal at corresponding temperatures. The temperatures of the metal surrounding the weld pool are very high and therefore cause the yield strength of the material to become quite low. Stresses occurring in regions farther away from the welding arc are tensile and balance with these compressive stresses near the weld pool. As the weld-metal and base metal regions cool and shrink, the regions in and adjacent to the weld experience tensile stresses. As the distance from the weld increases, the stresses become compressive. High tensile residual stresses in areas near the weld can cause premature failures of welded structures under certain conditions. Compressive residual stresses in the base plate can reduce the buckling strength of a structural member subjected to compressive loading. A typical residual stress distribution in welded tee joint is shown in Figure 2.2 [4].

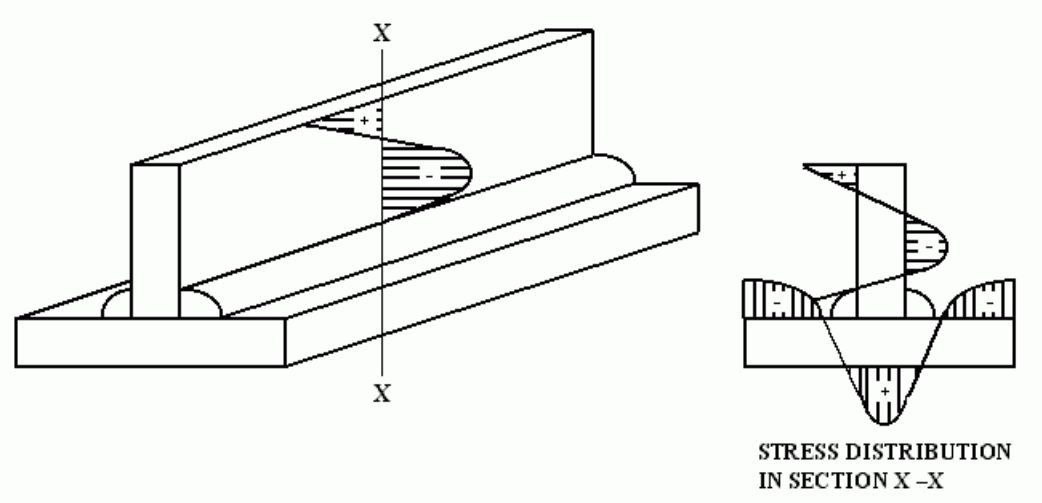

Fig. 2.2 Residual stresses in a welded tee joint [4]

2.2 Precipitation Hardening of Aluminum

The high strength of Aluminum 2519-T87 is due to the heat treatment process of precipitation hardening or age hardening. Precipitation hardening is the formation of extremely small, uniformly dispersed particles of a second phase within the original phase matrix, accomplished by heat treatment. The term age hardening is used because the strength develops with time, or as the alloy ages. Precipitation hardening is the result of two successive heat treatments: Solution heat treatment and Precipitation heat treatment, as shown in Figure 2.3 [3].

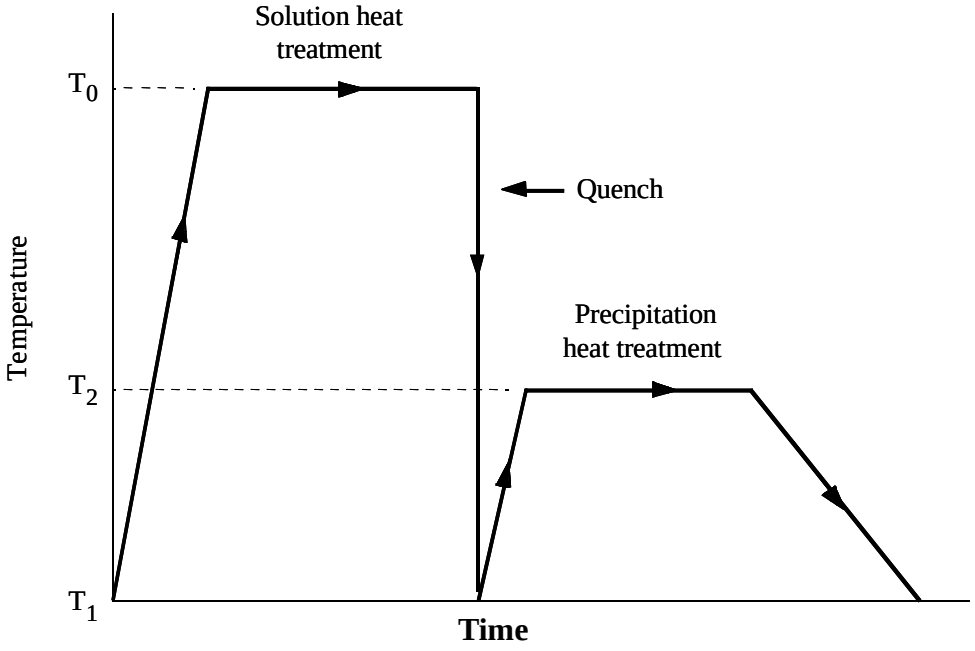

Fig. 2.3 Two Stages of Precipitation Hardening [3]

2.2.4 Solution Heat Treatment

The first stage of the precipitation hardening process is solution heat treatment. The aluminum-copper solution is heated to an elevated temperature, T_0, within the α phase (Cu in Al) and held until all the θ phase ($CuAl_2$) is completely dissolved. The α-phase is substitutional solid solution of copper in aluminum, and the θ-phase is intermetallic compound. This heat treatment is shown on the Aluminum-Copper Phase diagram in Figure 2.4. The solution is then quenched to temperature T_1 (room temp.) to prevent any diffusion and accompanying formation of the θ phase ($CuAl_2$). The alloy after quenching is said to be supersaturated with respect to solute θ in solvent α, and the alloy in this condition is relatively soft and weak [3].

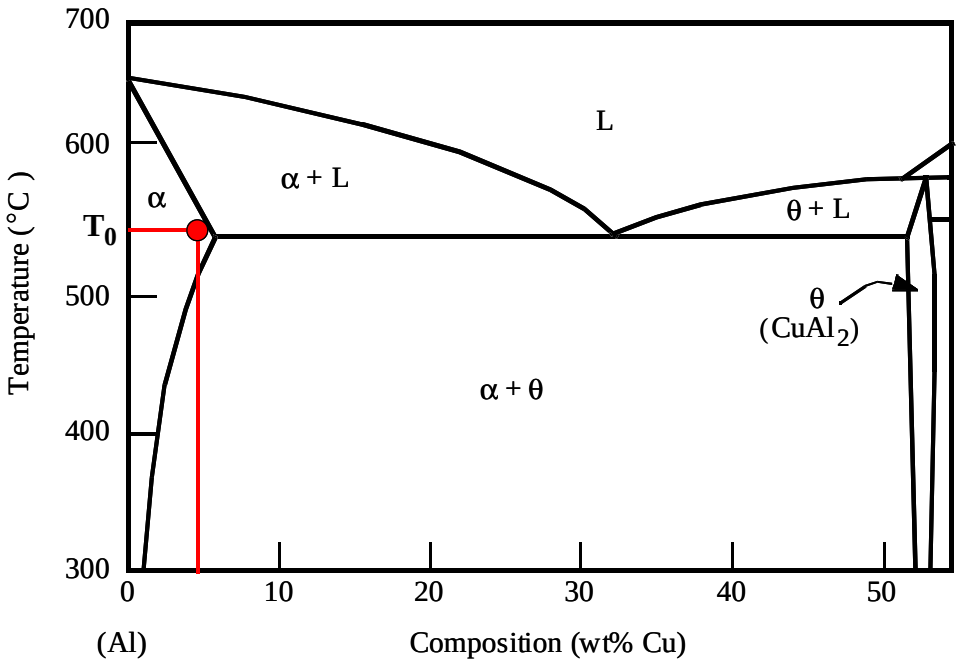

Fig. 2.4 Aluminum-Copper Phase Diagram with Solution Heat Treatment Temperature T_0 [3]

2.2.5 Precipitation Heat Treatment

The next stage in the precipitation hardening process is precipitation heat treatment. In this stage, the supersaturated α phase solution is heated to an intermediate temperature, T_2, within the $\alpha + \theta$ phase region as shown on the Aluminum-Copper Phase Diagram in Figure 2.5 on page 24 [3].

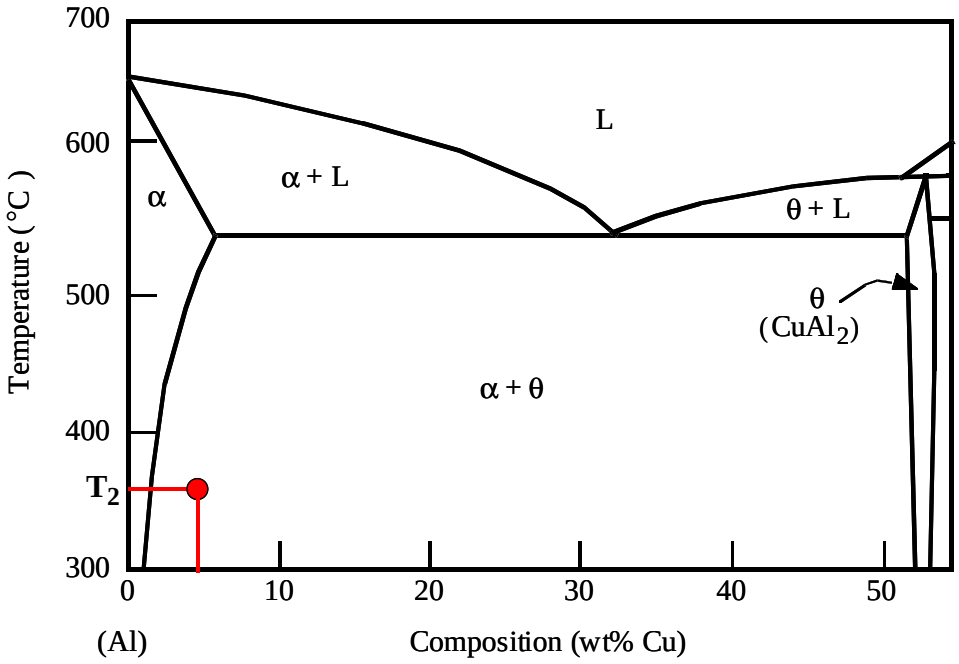

Fig. 2.5 Aluminum-Copper Phase Diagram with Precipitation Heat Treatment Temperature T_2 [3]

During the initial time, minute clusters, or zones, of copper atoms form at countless positions within the α phase, as is shown on the strength-aging diagram in Figure 2.6 on page 25 [3]. These zones of copper atoms are so minute that they are not regarded as distinct precipitates. With

increasing time, the continued diffusion of copper atoms results in the zones increasing in size to form precipitate particles. These precipitate particles pass through two transition phases, denoted θ’ and θ’’, before the equilibrium phase θ forms as finely dispersed particles of $CuAl_2$. The maximum strength coincides with the θ’’ phase, which may be preserved upon cooling to room temperature at the appropriate aging time.

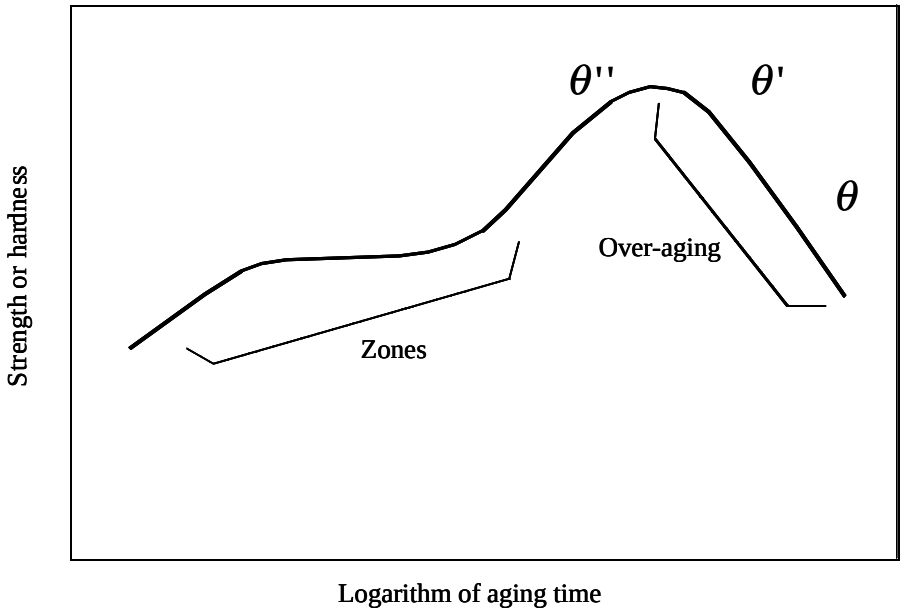

Fig. 2.6 Strength vs. Age Hardening Time [3]

2.2.6 Hardening Mechanism

In precipitation hardened aluminum-copper alloys, there is a distortion of the crystal lattice structure around and within the vicinity of particles of the transition phase (θ'') as shown in Figure 2.7. During plastic deformation, dislocation motions are impeded as a result of these distortions and consequently the alloy becomes harder and stronger. As the θ phase forms, the resultant over-aging (softening and weakening) is due to the decreased resistance to slip offered by the now uniform crystal lattice. The strength and hardness of the alloy depend on the precipitation temperature T_2 and the aging time at this temperature [3]. The welding process imposes temperatures as high as T_0 in the local weld area, therefore the alloy reverts to the intermediate supersaturated α-phase solvent with θ-phase solute. This local effect results in the Heat Affected Zone (HAZ), and the alloy is relatively soft and weak in this area.

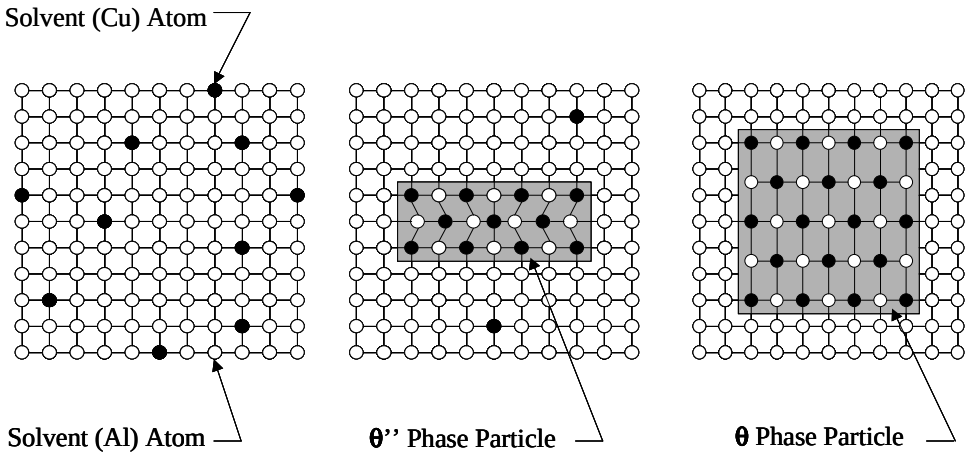

Fig. 2.7 Stages in formation of the equilibrium precipitate θ phase [3]

2.2.7 SYSWELD Metallurgical Model for Precipitate Dissolution Kinetics

With the knowledge that the heat treatment and strength of aluminum 2519-T87 is adversely affected by the thermal cycles imposed during welding, it is desired to take this effect into account when analyzing welded structures. The SYSWELD finite element code provides such a metallurgical model for the computation of the phase transformations for aluminum 2000, 6000, and 7000 series alloys. The equation that is used in the code is

$$x = \left(\frac{t}{t_r}\right)^n \exp\left[\left(\frac{Q_s}{R} + \frac{nQ_d}{R}\right)\left(\frac{1}{T_r} + \frac{1}{T}\right)\right] \qquad (2.1)$$

where

x: dissolute fraction of precipitates
t: time
T: temperature in Kelvin
R: constant of perfect gas
t_r: time for total dissolution of precipitates at given temperature T_r
Q_s: enthalpy of metastable solvus
Q_d: energy for activation of diffusion process of one of alloy elements (the less mobile)
n: parameter which can be dependent on x: $n(x) = 0.5 - a\ x^b$

Therefore when analyzing aluminum 2519, Equation (2.1) governs precipitate dissolution kinetics or the process during the heating cycle where base metal precipitates ($CuAl_2$) form in the aluminum matrix. Proper understanding of the Aluminum-Copper Phase diagram is necessary to determine the parameters involved in Equation (2.1). The solvus line is the solid solubility limit line separating α and $\alpha + \theta$ phase regions. The boundary between α and $\alpha + L$ is termed the

solidus line and the boundary between α + L and L is termed the liquidus line as shown in Figure 2.8 on page 29 [3]. Age hardening is accomplished through the precipitation of a metastable, or non-equilibrium variant, transition phase θ'' instead of the equilibrium phase θ. The enthalpy of metastable solvus, Q_s, is defined as the enthalpy or sum of internal energy plus the pressure of the solution times its volume, when the non-equilibrium precipitates (θ'') form [35]. The energy for activation of the diffusion process of the less mobile alloy elements, Q_d, refers to copper Cu in this instance. The parameter n is typically estimated through a series of metallurgical experiments and for lack of experimental data, the default values for similar aluminum alloys were used for this research. The values used can be found in Chapter 5, Section 5.7 on page 87.

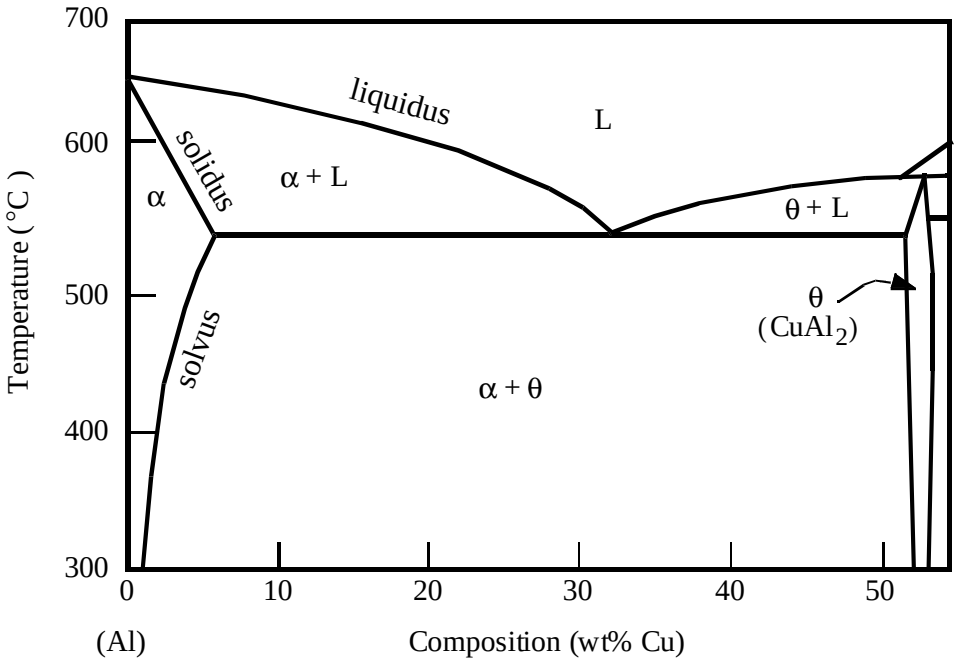

Fig. 2.8 Aluminum-Copper Phase Diagram [3]

The chemical composition of Aluminum 2519 is 93% Al, 6% Cu, and 1% Misc. Precise data to satisfy Equation (2.1) is unavailable from the aluminum manufacturer. Therefore, published binary aluminum-copper (94% Al and 6% Cu) alloy data is used to estimate the parameters needed for the metallurgy model.

CHAPTER 3

Finite Element Analyses of Welding

The prediction of weld residual stress has been the subject of many investigators. Finite element analysis (FEA) has been used by many authors [7-10][12-29] to perform welding simulations and to predict weld residual stresses in different types of joints and materials. Prediction is very difficult due to the complex variations of temperature, thermal contraction and expansion, and variation of material properties with time and space. Furthermore, modeling of the weld process must account for the specialized effects of the moving weld arc, material deposit, and metallurgical transformations. Many authors have utilized the commercial finite element code ABAQUS, enhanced with user subroutines, to model weld simulations with great success [8][9][18][22][26][27]. The finite element code ADINAT was used by Karlsson and Josefson [10], while other authors [20][21][23], have utilized SYSWELD to perform these weld simulations.

3.1 2-D versus 3-D Finite Element Models

Prediction of weld residual stresses foremost relies on accurate prediction of the weld thermal cycle. Oddy et al. [13] state that prediction of the temperature field requires a nonlinear, transient, 3-D analysis. Studies by Chao and Qi [12] propose that 3-D modeling of the weld process is essential for practical problems and can provide accurate residual stress and distortion results that cannot be obtained from 2-D simulations. McDill et al. [17] support this argument, stating that some 2-D predictions of residual stresses for materials exhibiting phase transformations show extremely large differences with experimental measurements. This discrepancy is attributed to the use of the plane strain condition in which plane sections remain planar. Implicit in plane strain analyses are the assumptions that the out-of-plane shear strains and the out-of-plane normal strain vanish. Considering longitudinal stresses, the 2-D plane strain condition corresponds to rigid end constraints where the 3-D reality is closer to the elastic condition [17]. Longitudinal stresses in this case refer to in-plane stresses or stresses in the direction of the weld deposition. Michaleris et al. [14] state that a 2-D model full penetration weld can become unstable due to the decrease of stiffness at high temperatures, where as 3-D models can accurately predict the welding distortion when a moving heat source is used to simulate the welding heat input. In the case of aluminum, the high thermal conductivity (over three times that of steel) causes material movement perpendicular to the weld arc, therefore requiring 3-D analysis to accurately model the residual stress state. As the weld electrode travels along the weld path, two previously independent parts are coupled by the newly deposited weld material, thereby changing the response of the structure to the ensuing deposition of weld material further down the weld path. The full effect of this behavior can only be captured through the use of 3-D models [22]. Feng et

al. [27] report that the strong spatial dependency of the residual stresses near the weld demonstrates that 2-D cross-section models should not be used for repair welding analysis.

Dong et al. [9] have used both shell/plate models and 2-D cross-sectional models to study 3-D weld residual stress characteristics but note that transverse residual stresses in welds may exhibit significant variation along the weld direction and these variations must be taken into account in order to correctly interpret results from a 2-D model. Transverse stresses refers to those stresses perpendicular to the direction of the weld deposition. Dubois et al. [23] have utilized 2-D models, recognizing that the 3-D effect of the movement of the electrode has been neglected. Hong et al. [18] dispute the need for 3-D weld models, suggesting that a 2-D analysis can be carried out with appropriate simplifying assumptions depending on the nature of the problem. To include the effect of a 3-D moving arc on the 2-D cross-section model, a ramped heat input procedure was developed. The ramp function accounts for the out-of-plane heat transfer effects as the arc approaches, travels across, and departs from the specified 2-D cross-section.

Another simplification technique is lump pass modeling. Lump pass modeling is used to reduce computational time and simplify analyses for multi-pass welds, by grouping several welds or passes into one layer. The equivalent heat contents associated with lump passes must be carefully defined to obtain reasonable residual stress prediction [18].

3.2 Thermal, Mechanical, and Metallurgical Analyses

To simplify the welding simulation, it is computationally efficient to perform the thermal and mechanical analyses separately. Physically, it is assumed that changes in the mechanical state do

no cause a change in the thermal state. That is, a change in stress and strain do not cause a change in temperature. However, a change in the thermal state causes a change in the mechanical state. Computation of the temperature history during welding and subsequent cooling is completed first, and then this temperature field is applied to the mechanical model to perform the residual stress analysis. Most of the authors investigated have reported the use of this one-way coupling approach [8][10][12][13][15][20-23][25-28]. One way coupled thermal and mechanical analyses are valid when the relative displacements within the welding portions of the structure are small, assuring that the displacements do not shift the welding electrode and consequently the location of heat flux applied to the model [22]. Oddy et al. [13][25] state that the heat generated by the plastic deformation is much less than the heat introduced by the weld arc itself. Therefore, the thermal analysis may be performed separately from the mechanical analysis.

An important aspect of welding, which has been getting more and more attention by many authors performing finite element simulations, is metallurgical transformations or phase transformations [10][13][17][20-23][25][28][29]. The goal of the metallurgical calculation is to determine the percentages of individual phases in the heat affected zone (HAZ). The influence of the metallurgical history is evident in the following four factors [20]: 1) The mechanical properties of the HAZ are derived from the mechanical properties of the individual phases. 2) The impact on the final residual stress distribution caused by the expansion and contraction of the different phases formed as a result of different temperature dependent properties during transformation. The thermal strains are calculated from the phase and temperature dependent thermal expansion coefficients. 3) During metallurgical transformations the level of plastic deformations decrease because of the movement of dislocations. Each phase of the material has a different strain hardness character. 4) The impact of transformation plasticity.

Irreversible plastic deformation which occurs during a phase transformation in the presence of stress is known as transformation plasticity. This deformation is irreversible because transformation back to the original phase does not undo the deformation, it may in fact increase the deformation. The primary mechanism responsible for transformation plasticity is driven by the volume change which occurs during the phase transformation. When a volume of material transforms, stresses are generated within the transformed volume and the surrounding untransformed material. The stresses can be sizable enough to cause plastic deformation in the weaker phase [13]. These stresses have been called microscopic stresses [30][31] because the stress field varies over distances less than the grain size. If macroscopic or external stresses are not present, the plastic strains are randomly oriented and only the volume change is observed. Interaction of the macroscopic and microscopic stresses orients the plastic strains such that deformation occurs beyond the volume change resulting in transformation plasticity [13]. This has been called the Greenwood-Johnson mechanism [32].

Oddy et al. [13] states that the irreversible plastic deformation, known as transformation plasticity, which occurs during a phase transformation, can affect the magnitude and sign of the residual stresses predicted in the fusion and heat-affected zones. Dubois et al. [23] calculated residual stresses for a steel weld with and without the effect of transformation plasticity, and the results evidenced the considerable influence (up to 400 MPa) of transformation plasticity on the residual stresses. It is therefore important to include this phenomenon in residual stress calculations. L. Karlsson et al. [28] and R. I. Karlsson and Josefson [10] accounted for volume changes due to phase transformation but did not include the effect of transformation plasticity specifically, due to lack of available experimental data. McDill et al. [17] have investigated the role of phase transformations in the development of residual stress in steels and concluded that the

result is significant, particularly in the heat affected zone (HAZ). Welding simulations using materials which exhibit phase transformations must include the effect of transformation plasticity [13].

Another result of a phase transformation is the release or absorption of energy upon solidification or melting known as the latent heat affect. The latent heat affect associated with a solid-solid phase change is much smaller than that associated with a solid-liquid phase change [22]. Dubois et al. [23] in their study of a steel weld included the latent heats for all the phase transformations: fusion, solidification, austenitic, ferritic, bainitic, and martensitic. Also, the phase dependencies of the heat capacity and conductibility were included. Junek et al. [20] modified the heat conduction equation in the commercial code SYSWELD by including both the transformation latent heat and the latent heat at the change of state. Vincent et al. [21] evaluated the commercial codes SYSWELD and CODE_ASTER in the prediction of residual stresses in steel with metallurgical transformations. In SYSWELD the metallurgical and thermal calculations are coupled so at each temperature the phase proportions are calculated. The thermal characteristics are determined using a linear mixture law of the amount of each phase present. The enthalpy of each phase includes the latent heat of transformation and inertia effects. In CODE_ASTER the metallurgical and thermal calculations are de-coupled and the phase proportions are determined in post-treatment of the thermal simulation. The enthalpy and conductivity are considered separately for the heating and cooling of the HAZ to take into account the metallurgical transformation effect. The latent heats of transformation are included through the use of different enthalpic curves for heating and cooling. Furthermore, each code used constitutive equations to account for transformation plasticity [21].

3.3 Modeling the Weld Arc

For modeling of the heat source, many authors [14][15][27], utilize the 3-dimensional double ellipsoid proposed by Goldak et al. [19] as shown in Figure 3.1 on page 37. The double ellipsoid geometry is used so that the size and shape of the heat source can be easily changed to model both the shallow penetration arc welding processes and the deeper penetration laser and electron beam processes. The power or heat flux distribution is Gaussian along the longitudinal axis. The front half of the source is the quadrant of one ellipsoidal source while the rear half is the quadrant of another ellipsoidal source. Four characteristic lengths must be determined which physically correspond to the radial dimensions of the molten zone. If the cross-section of the molten zone is known from experiment, this information can be used to set the heat source dimensions. If precise data does not exist, Goldak et al. [19] suggest that is reasonable to take the distance in front of the source equal to one half the weld width and the distance behind the source equal to two times the weld width.

Chao and Qi [12], as well as Dong et al. [26], concur with the use of a Gaussian distribution to model the gas metal arc but do not include further details of the geometry of the heat source. Hong et al. [18] state the equivalent heat input to simulate arc heating effects, can be assumed as the combination of both surface and body heat flux components, where the surface heat flux was of Gaussian thermal distribution and the body heat flux, input as an internal heat generation per unit volume, was assumed constant. For Tungsten Inert Gas (TIG) welding, Preston et al. [8] simulate the arc as a moveable body flux power source, and decided a more complex heat source model was not needed due to the high thermal conductivity of aluminum, over three times that of steel. Brown and Song [22] also model the heat transfer from the electrode arc to the base metal as a surface heat flux with a Gaussian distribution. Karlsson and

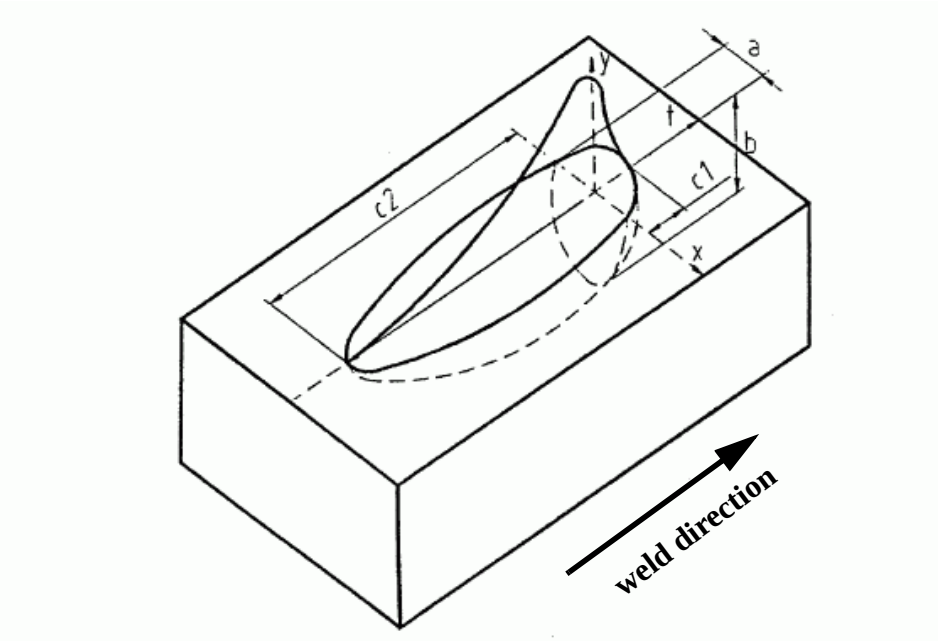

Fig. 3.1 Goldak Double Ellipsoid Heat Source Model [19]

Josefson [10] applied heat as consistent nodal heat flow corresponding to a volume of internal heat generation or power, where the volume had a cross-section and length corresponding to the assumed fusion zone generated by Metal Inert Gas (MIG) welding. In addition, 60 percent of the heat was generated in the outer weld elements while 40 percent was generated by the inner elements. The power was given a spatial variation such that the power increased linearly in the axial direction and radially inwards to ensure the outer most points of the fusion zone reached the melting point.

3.4 Weld Metal Deposition

Material deposit is another important aspect of finite element modeling of the weld process. Typically the finite element model of the weld joint contains the base plates and all passes of the weld in a single mesh. Welding of each pass is simulated in separate steps or sub-analyses. To simulate the first pass of a multi-pass weld the future weld passes are removed using a feature available within the finite element code. Hong et al. [18] employ the element "rebirth" technique to include multipass weld metal deposition effects. With this technique, the elements are grouped to represent each weld pass, then removed and reactivated at a specified moment to simulate a given sequence of weld passes. As a group of weld elements are activated, all of the nodes associated with these elements are specified to have the same initial temperatures. Typically for Gas Metal Arc Welding (GMAW) processes the weld metal is assumed to be deposited at the melting temperature of the filler material. Michaleris et al. [14] employ a similar method but also specify that it is necessary to reactivate the weld elements prior to the analysis of that step. To avoid generating false plastic deformations a low value of Young's modulus and a low yield strength are assigned to the reactivated elements. As the temperature begins to drop the actual material data set for the filler metal is used. Also, for peak temperatures exceeding the melting point of the material, all strains (including the plastic strains) are eliminated to simulate annealing. Annealing in this case refers to the heat treatment of a previously strain hardened metal causing it to recrystallize and soften. Strain hardening is the plastic deformation of a metal at a temperature below the melting temperature at which it recrystallizes [3].

Brown and Song [22] also utilize the element "birth" procedure by reactivating elements which have been deactivated at the start of the mechanical analysis. The activation procedure in the mechanical or stress/strain analysis deforms the deactivated element from its original position

such that it will be compatible with the remaining structure and be in a force equilibrium state. This procedure creates a stress/strain field in the newly activated element, but the high temperatures of the element reduce the effect of this stress on the structure [22]. Karlsson and Josefson [10] utilize the element "birth" facility in the commercial code ADINAT to keep weld elements in front of the weld arc inactive until the front of the heat source enters the element in the thermal analysis. In the mechanical analysis the elements are kept inactive until the front of the source has passed the inactive element by about one element length. Feng et al. [27] use a special user material property subroutine within ABAQUS where elements representing the weld metal are assigned the rigidity of air during the thermal analysis. The weld bead elements always exist during the thermal analysis, but the thermal conductivity and the heat capacity of these elements are assigned small values to represent air, but then switched to the actual metal properties when the element enters the moving weld pool. For the mechanical analysis, a similar approach is used where the elements to be welded are first assigned a set of artificial, very soft properties. As the elements solidify from the weld pool the actual properties of the metal are reassigned.

3.5 Material Model

Different material laws have been utilized in weld simulations. The available material laws typically include an elastic-perfectly plastic model or a plasticity model which takes into account strain hardening, either kinematic or isotropic [33]. Callister [3] defines strain hardening as the increase in hardness or yield strength of a ductile metal as it is plastically deformed. Before discussing kinematic and isotropic hardening it is necessary to define the yield surface. For any element of material in a given state of stress (following some stress history) there exists a region

in the stress space such that the behavior is elastic and path independent if the stress point lies within this region. The elastic region is bounded by a yield surface in the stress space, as shown in Figure 3.2. The von Mises yield surface is the most common yield surface.

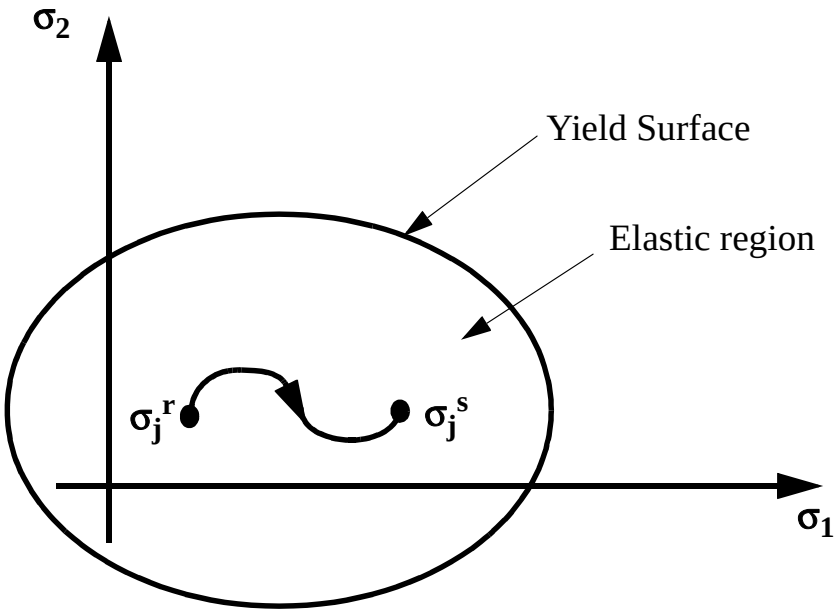

Fig. 3.2 Yield surface in stress space [34]

The points where this yield surface intersects the σ_1 axis, for example, give the yield stresses for the case when σ_1 is the only nonzero component of stress. Isotropic hardening describes the behavior of subsequent yield surfaces associated with monotonic tension loading, where the yield surface retains the same shape as the initial yield surface but merely increases in size following any path loading. Kinematic hardening describes the behavior of subsequent yield surfaces associated with monotonic loading in shear in which the shape and size of the yield

surface remain constant, but the yield surface is displaced along the shear axis without rotation [34]. This discussion is only cursory and the reader is directed to reference [34] for a complete discussion on plasticity.

Karlsson and Josefson [10] utilize a thermo-elastoplastic material model with von Mises' yield criterion and an associated flow rule. No kinematic nonlinearities are taken into account, or equivalently small strains and displacements are assumed. In regions far from the weld the material behaves elastically, otherwise the material in the model is assumed to behave elastic-perfectly plastic, i.e., the analysis does not explicitly consider hardening. The authors recognize that from a physical point of view, considering the thermal loading and large strains that develop, a kinematic hardening rule would be more appropriate. Defending the elastic-perfectly plastic model, Karlsson and Josefson [10] argue that the plastic strains accumulated before the final solid-state phase transformation are relieved to a great extent during the transformation. Also, as mentioned previously the material model should account for the considerable volume change which occurs during phase transformation. Furthermore, all mechanical properties were taken to be temperature dependent.

Kinematic hardening is well suited for simulating multi-pass welds due to the reversal of plasticity within the region where multiple weld passes introduce repetitive thermal cycles [26]. Dong et al. [26] used a von Mises based kinematic hardening law with an associated flow rule. Chao and Qi [12] utilized a rate independent plasticity model with kinematic hardening to model the reverse plasticity associated with the unloading due to a second or future weld pass. Also used was von Mises yield criterion and an associated flow rule to determine the onset of yielding and the incremental plastic strain. Feng et al. [27] assumed the mechanical constitutive behavior to be

rate-independent and elasto-plastic governed by von Mises yield criteria and associated flow rules.

Strain hardening due to a dislocation structure in the material may be affected by atomic motion during metallurgical or phase change. The new phase may have partial memory or no memory of the previous hardening. To describe the hardening recovery due to metallurgical change, parameters associated with isotropic hardening are defined for each phase. Hardening due to plastic strain and hardening recovery due to metallurgical transformations are included in the evolution laws [21]. Michaleris et al. [14] utilized isotropic hardening plasticity but stated that this assumption may be inadequate and that the model may become excessively stiff during a second or future weld pass when examining a 2-D model. Hong et al. [18] used isotropic strain hardening for the analysis of a steel multi-pass weld. Preston et al. [8] used a von Mises yield surface with isotropic hardening behavior for the mechanical model. Brown and Song [22] also used a thermo-elastic-plastic material model with isotropic strain hardening, as well as temperature dependent material properties.

3.6 Boundary Heat Loss/Radiation and Convection

To model heat transfer through the external boundaries of a finite element model, surface or skin elements are typically used [10][33]. Through the use of these elements heat convection and radiation can be modelled. Michaleris et al. [14] used radiation and convection boundary conditions for all free surfaces in the thermal analyses through the use of a temperature dependent free convection coefficient to model both heat transfer processes. Hong et al. [18] use a similar approach by specifying a single heat loss coefficient for all surfaces. Brown and Song [22] incorporate convective heat transfer through the use of a coefficient which is assumed to depend

both on temperature and orientation of the boundary. Radiation is modeled by the standard Boltzman relation and it is assumed to be from the free surfaces to ambient air only. The effect of radiation is typically smaller than the effect of convection except near the melting temperature. Preston et al. [8] take a different approach stating that heat losses to the atmosphere were ignored because the values quoted by other investigators were much smaller than the conduction into the backing plate when it is used. Furthermore, radiative losses were neglected because these only become significant at the high temperatures close to the weld arc and can be incorporated into the arc efficiency factor.

CHAPTER 4

Energy and Constitutive Equations in Welding Simulations

4.1 Heat Flow in Welding

Welding metallurgy involves the application of metallurgical principles for assessment of chemical and physical reactions occurring during welding. In welding the reactions are forced to occur within seconds in a small volume of metal where the thermal conditions are characterized by [36]:

- High peak temperatures, up to several thousand ^{o}C
- High temperature gradients, locally of the order of 10^3 ^{o}C/mm
- Rapid temperature fluctuations, locally of the order of 10^3 ^{o}C/s

4.1.1 Conservation of Energy

To perform a quantitative analysis of metallurgical reactions in welding, a detailed weld thermal history is required. The law of conservation of energy, or first law of thermodynamics, is the physical principle used to begin the mathematical description of the

weld thermal history. Consider a closed, continuum system of particles not interchanging matter with its surroundings. That is, there is no mass flux across the boundary surface of the system, and the boundary surface of the system moves with the flow of matter. Using the Lagrangian formulation, the reference configuration of the system is defined as the configuration of the system at time $t = 0$. The volume of the reference configuration is denoted by V_0 with a bounding surface denoted by S_0. A particle in the reference configuration is located in a rectangular Cartesian system by coordinates X_I, where the usual index notation is used so index I has the range of one to three. At an instant in time $t > 0$ the system occupies a volume V having a boundary surface S, and the particle is at position x_i with respect to the same rectangular Cartesian system. The first law of thermodynamics states the rate of change of the total energy in the system is equal to the input power plus the rate of heat input. The total energy of the system is considered to be the sum of the kinetic energy and internal energy. The input power is the rate at which the external surface tractions per unit area and the body force per unit mass are doing work on the mass of the system. The rate of heat input consists of conduction through the surface S and the strength per unit mass of a distributed internal heat source. As shown by Malvern [37], the energy equation at each point of the continuum reduces to

$$\rho\frac{du}{dt} = \sigma_{ij}D_{ij} + \rho r - \frac{\partial q_j}{\partial x_j} \qquad (4.1)$$

where ρ is the mass density of the particle at time t, ρu is the internal energy per unit volume, σ_{ij} are the Cauchy stress components, D_{ij} are components of the rate of deformation tensor, ρr is the internal supply of heat per unit volume, and q_j are the components of the heat flux vector.

Note that the negative sign for the gradient of the heat flux term on the right-hand side of Equation (4.1) is due to the fact that $\int_S q_j n_j dS$, where n_j are the components of the outward unit normal vector to S, is defined as the outward heat flux. Equation (4.1) written in the reference configuration is

$$\rho_0 \frac{\partial u}{\partial t} = S_{IJ} \frac{\partial E_{IJ}}{\partial t} + \rho_0 r - \frac{\partial q_J}{\partial X_J} \tag{4.2}$$

where ρ_0 is the mass density of the particle in the reference configuration, S_{IJ} are components of the second Piola-Kirchhoff stress tensor, E_{IJ} are the Lagrangian strain components, $\rho_0 r$ is the distributed internal heat source per unit volume in the reference configuration, and components of the heat flux vector in the reference configuration are defined by

$$q_J \equiv (\rho_0 / \rho) \frac{\partial X_J}{\partial x_k} q_k \tag{4.3}$$

For infinitesimal displacement gradients, or infinitesimal strain and rotations, the infinitesimal strains ε_{IJ} are approximately equal to the Lagrangian strains; i.e., $\varepsilon_{IJ} \approx E_{IJ}$. Also, $\sigma_{ij} \approx S_{IJ}$, $\rho_0 \approx \rho$, $q_J \approx q_j$, and there is no distinction between the reference configuration and deformed configuration. Hence for infinitesimal displacement gradients, Equation (4.2) reduces to

$$\rho \frac{\partial u}{\partial t} = \sigma_{IJ} \frac{\partial \varepsilon_{IJ}}{\partial t} + Q - \frac{\partial q_J}{\partial X_J} \tag{4.4}$$

where $Q = \rho_0 r$

Equation (4.4) represents the energy equation for two-way coupling. The term $\sigma_{IJ}(\partial\varepsilon_{IJ}/\partial t)$ is called the stress power (per unit volume), and represents that part of the external input power not contributing to the kinetic energy of the system. The stress power couples the mechanical state to the thermal state; i.e., stress and strain cause heating. Also in the two-way coupling, the internal energy per unit volume may be postulated as a function of the strains and temperature T; i.e, $u = u(\varepsilon_{IJ}, T)$ [38]. Note that the temperature is a function of time and position. A specific internal energy considered only a function of the mechanical state variables of strains, and the thermal state variable of temperature, would be one of the constitutive equations of an ideal thermoelastic solid. Malvern [37], points out that this particular form of the constitutive equation for an ideal thermoelastic solid is too simple to represent, for example, the change in internal energy of a bar that was stretched inelastically to twice its initial length, pushed back to its initial length, and then cooled to its original temperature.

In one way coupling, the stress power term is assumed negligible compared to the heat input terms on the right-hand side of Equation (4.4), and it is also assumed that the internal energy is only a function of the temperature. The internal energy per unit volume is written as

$$\rho u = \rho C_p(T)\frac{\partial T}{\partial t} \qquad (4.5)$$

where C_p denote the specific heat of the material, and it, in general, is a function of the temperature. Thus, the energy equation for one-way coupling is

$$\rho C_p(T)\frac{\partial T}{\partial t} = Q - \frac{\partial q_J}{\partial X_J} \qquad (4.6)$$

Equation (4.6) is a field equation for energy balance that only contains dependent variables associated with the thermal state. Once a thermal constitutive equation relating the heat flux components to the temperature is postulated, Equation (4.6) can be solved independent of the variables of stress and strain associated with the mechanical state. However, the thermal strains are included in the formulation of the constitutive laws for the mechanical state. So the thermal state affects the mechanical state but not visa versa.

The electric arc in gas metal arc welding applies a large heat flux per unit area over a small area of the workpiece, which is on the order of 5×10^{6} to 5×10^{8} W/m^2 [6]. As a consequence of this intense local heat flux, there are large temperature gradients in the vicinity of the weld pool. Therefore, it is assumed that the stress power term is small with respect to the heat input terms of the energy equation, and that modeling the welding process as one-way coupling is reasonable.

4.1.2 Fourier Law of Heat Conduction

Heat is a form of energy that is transferred across the boundary between systems due to a difference in temperature between the two systems. The amount of heat to be conducted is proportional to the area of the surface, the difference in temperature, and the duration for which the temperature difference is maintained. However, the amount of heat is inversely proportional to the distance between the two terminals [39]. The classical thermal constitutive law which relates the heat flux components to the temperature distribution is Fourier's law. The mathematical formulation of the Fourier law for an anisotropic material is

$$q_I = -k_{IJ}\frac{\partial T}{\partial X_J} \qquad (4.7)$$

where k_{IJ} is the thermal-conductivity tensor of the material, which is shown to be symmetric in continuum texts as cited by Thornton [38]. For an orthotropic material the thermal-conductivity tensor is diagonal, so that only the temperature gradient along the X_I-axis influences the heat flux in the direction of that axis. For an isotropic material there is only one independent thermal conductivity, k, and then Equation (4.7) simplifies to

$$q_I = -k\frac{\partial T}{\partial X_I} \tag{4.8}$$

4.1.3 Heat Conduction Equation

Substitute Fourier's law, Equation (4.7), for the heat flux components in the energy equation, Equation (4.6), to get the heat conduction equation. The heat conduction equation is

$$\rho C_p(T)\frac{\partial T}{\partial t} = Q + \frac{\partial}{\partial X_I}\left(k_{IJ}\frac{\partial T}{\partial X_J}\right) \tag{4.9}$$

in which $Q = Q(X_I, t)$ is a specified internal heat generation function per unit volume.

4.1.4 Initial and Boundary Conditions

The solution of the heat conduction equation, Equation (4.9), involves a number of arbitrary constants to be determined by specified initial and boundary conditions. These conditions are necessary to translate the real physical conditions into mathematical expressions [39].

Initial conditions are required only when dealing with transient heat transfer problems in which the temperature field in the material changes with time. The common initial condition in a material can be expressed mathematically as

$$T(X_I, 0) = T_0(X_I) \qquad (4.10)$$

where the temperature field T_0 is a specified function of spatial coordinates only [39].

Specified boundary conditions are required in the analysis of all transient or steady-state problems. Five types of boundary conditions which are commonly used are [40]:

a) *Prescribed surface temperature, $T_S(t)$.* It is often necessary to prescribe an initial surface temperature for a structure. The mathematical expression takes the form:

$$T(X_I, t)\big|_{X_I(S_0)} = T_S(t) \qquad (4.11)$$

where $X_I(S_0)$ are the coordinates evaluated on the external surface S_0 where the temperatures are specified to be $T_S(t)$.

b) *Prescribed surface heat flux, $q_s(t)$.* Many structures, particularly in the case of welding, have the boundary surface exposed to a heat source or heat sink. Let N_I denote the unit out ward normal to the external surface S_0 whose coordinates are given by $X_I(S_0)$, then the mathematical formulation for the heat flux across a solid boundary surface is

$$N_I \left.\frac{\partial T}{\partial X_I}\right|_{X_I(S_0)} = q_S[X_I(S_0), t]/k \qquad (4.12)$$

where q_S is the specified surface heat flux, positive into the surface.

c) *Adiabatic boundary condition (No heat flow).* When the rate of heat flow across a boundary is zero, Fourier's Law leads to

$$N_I \left.\frac{\partial T}{\partial X_I}\right|_{X_I(S_0)} = 0 \qquad (4.13)$$

d) *Convective boundary conditions.* Most structures have boundary surfaces which are in contact with fluids, either gases or liquids. The mathematical formulation for this type of boundary condition can be derived as follows: A structure with an unknown temperature field $T(X_I, t)$ has its surface S_0 in contact with a fluid, ambient air for instance, at temperature T_0. The heat flux that reaches the specified boundary at S_0 from the solid can be expressed as [40]

$$q_S = -kN_I \left.\frac{\partial T}{\partial X_I}\right|_{X_I(S_0)} \qquad (4.14)$$

where q_S denotes the heat flux leaving S_0 into the fluid at temperature T_0. The heat flux leaving the body through surface S_0 is equal to the heat flux q_f transferred to the boundary layer of the fluid, assuming no heat is stored at the interface. The heat flux q_f is represented by Newton's law of surface heat transfer, which is

$$q_f = h\{T[X_I(S_0), t] - T_0\} \tag{4.15}$$

where h is the convection coefficient, which, in general, can be a function of temperature. Hence, the convection boundary condition is

$$-kN_I \left.\frac{\partial T}{\partial X_I}\right|_{X_I(S_0)} = h\{T[X_I(S_0), t] - T_0\} \tag{4.16}$$

e) *Radiation heat exchange.* When the rate of heat flow across a boundary is specified in terms of the emitted energy from the surface and the incident radiant thermal energy, emitted and reflected from other solids and/or fluids, the boundary condition is:

$$-kN_I \left.\frac{\partial T}{\partial X_I}\right|_{X_I(S_0)} = \sigma\varepsilon T_S^4 - \alpha q_i \tag{4.17}$$

where σ is the Stefan-Boltzmann constant, ε is the surface emissivity, and T_S is the surface temperature, α is the surface absorptivity, and q_i is the incident radiant thermal energy. The first term on the right-hand side of the equation is the emitted energy from the surface, and the second term on the right-hand side is the absorbed incident radiant energy.

If the body at temperature T is within an enclosed space whose walls have a uniform temperature T_e, and the walls are assumed to emit and absorb energy perfectly with $\varepsilon = \alpha = 1$, then the radiant energy emitted from the body per unit time and per unit area is $\varepsilon\sigma T^4$, while the corresponding absorbed radiant energy from the walls is $\alpha\sigma T_e^4$. Therefore, the net rate of heat flow per unit area from the body surface can be expressed as

$$q = \varepsilon\sigma T^4 - \alpha\sigma T_e^4 \qquad (4.18)$$

By Kirchhoff's law $\varepsilon = \alpha$, so the net rate of heat flow per unit area from the body surface to its surroundings can be expressed in the familiar form [40]

$$q = \varepsilon\sigma(T^4 - T_e^4) \qquad (4.19)$$

4.1.5 Moving Heat Sources and Pseudo-Steady State

Heat generation in welding is based on the concept of instantaneous heat sources. The heat source model developed by Goldak [19] is used in this research, which distributes the heat throughout the volume of the molten zone. The Goldak heat source model is defined spatially by a double-ellipsoid as is shown in Figure 4.1. The front half of the source is the quadrant of one ellipsoidal source, and the rear half is the quadrant of a second ellipsoidal source. The power density distribution is assumed to be Gaussian along the weld path, or the z-axis on the workpiece in Ref. [19]. It is convenient to introduce a coordinate, ξ, fixed on the heat source and moving with it. The moving reference frame on the heat source is related to the coordinate fixed on the work piece by

$$\xi = z + v(\tau - t) \qquad (4.20)$$

where v is the welding speed, τ is a lag time necessary to define the position of the heat source at time $t = 0$. In the double ellipsoid model, the fractions of heat deposited in the front and rear of heat source are denoted by f_f and f_r, respectively, and these fractions are specified to satisfy $f_f + f_r = 2$. Let q denote the power density in W/m^3 within the ellipsoid, and let a, b, and c

denote the semi-axes of the ellipsoid parallel to the x, y, ξ axes. Then the power density distribution inside the front quadrant is specified by

$$q(x, y, z, t) = \left(\frac{6\sqrt{3}f_f Q}{abc_1\pi\sqrt{\pi}}\right)e^{-3(x^2/a^2)}e^{-3(y^2/b^2)}e^{-3(\xi^2/c_1^2)} \qquad (4.21)$$

and the power density in the rear quadrant is specified by

$$q(x, y, z, t) = \left(\frac{6\sqrt{3}f_f Q}{abc_2\pi\sqrt{\pi}}\right)e^{-3(x^2/a^2)}e^{-3(y^2/b^2)}e^{-3(\xi^2/c_2^2)} \qquad (4.22)$$

In Equation (4.21) and Equation (4.22), Q is the heat available at the source. For an electric arc the heat available is

$$Q = \eta VI \qquad (4.23)$$

where η is the heat source efficiency, $0 \le \eta \le 1$, V is the arc voltage, and I is the arc current.The parameters a, b, c_1, and c_2 are independent, and can take on different values for the front and rear quadrants of the source to properly model the weld arc.

Using the SYSWELD software it is possible to account for the moving heat source in two distinct manners. The first method involves the typical transient formulation where the heat source is “marched” along the part with time. In this manner, the start and stop effects of the heat source can be taken into account. The second method involves a “moving reference frame” or pseudo-steady state computation. The metallurgical and mechanical steady state induced by the moving heat source are determined by solving the governing equations in the moving reference

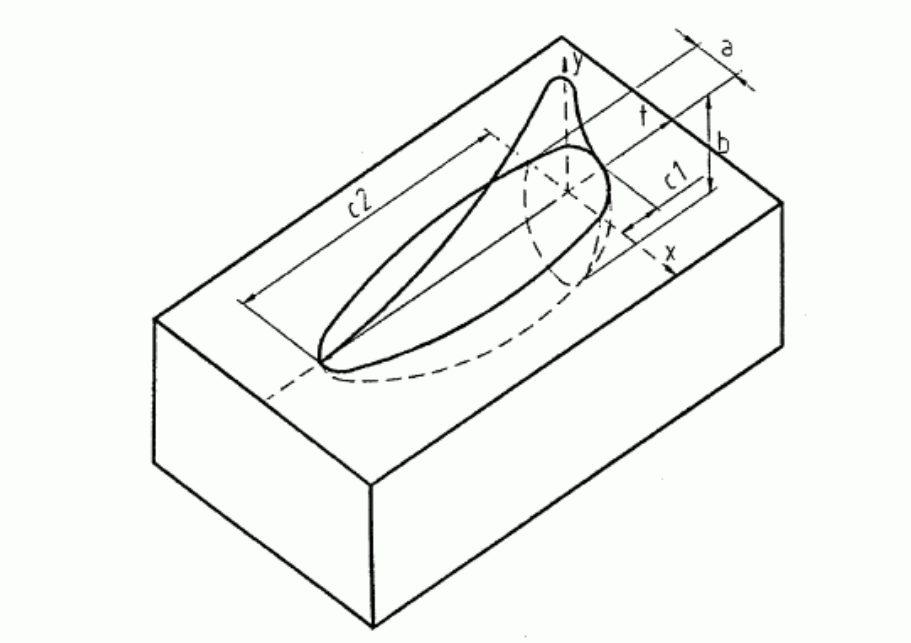

Fig. 4.1 Goldak Double Ellipsoid Heat Source Model [19]

frame (x, y, ξ), instead of the stationary reference frame (x, y, z). Since this method calculates a steady or quasi-steady state, the method is less time consuming than a transient calculation. The procedure is based on the definition of element trajectories and therefore integration point trajectories. These trajectories are parallel to the rate of the loading or heat source, such that the thermal-metallurgical and mechanical history undergone by each point of the structure can be determined. A schematic of the procedure is depicted in Figure 4.2 [33].

Besides substantial savings in computation time, the steady-state computation is helpful in this research. As described in Chapter 1, the goal of this research is to compute representative

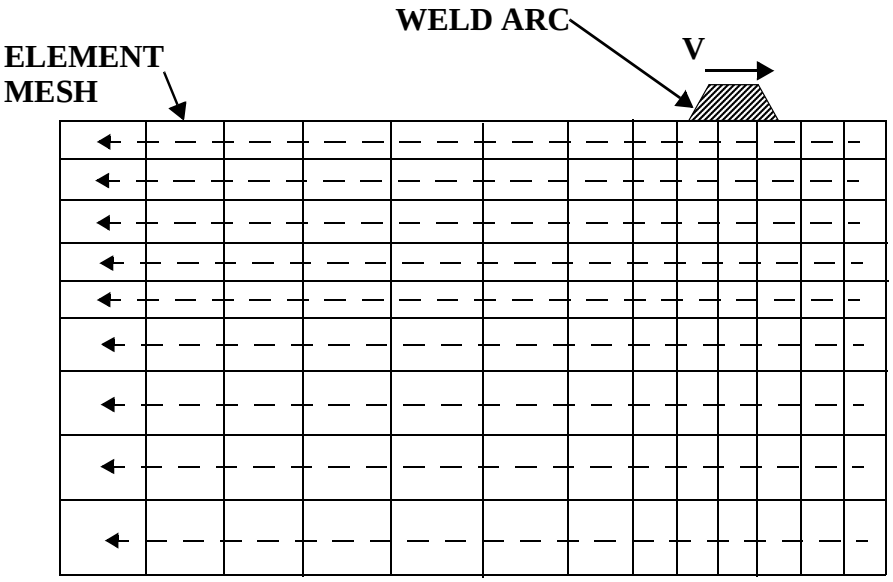

Fig. 4.2 "Moving Reference Frame" Schematic [33]

residual stress states for a tee joint and butt joint for possible implementation in the global/local optimization scheme. Since the heat source moves at a constant speed along a straight line, and the heat input Q from the source is constant, experience shows that such conditions lead to a fused zone of constant width. Moreover, zones of temperatures below the melting point also remain at constant width [33]. The residual stresses and weld zone size attained in the steady state, where end effects are not important, are those to be used in design.

4.2 Thermoelastic-Plastic Stress Analysis

Some of the plasticity constitutive laws for metals are discussed in this section. Thermal effects are accounted for in the mechanical analysis by including thermal strains and temperature dependent material properties. Also, the thermal state effects the plastic yield criterion. The constitutive laws relating stresses, strains, and temperature are nonlinear in the theory of plastic deformation of solids [34].

4.2.1 Fundamental Assumptions

The following assumptions apply to the formulations that follow [39]:

1. The material is treated as a continuous medium or a continuum.
2. The material is isotropic, with its properties independent of direction.
3. The material has no “memory” such that the effect on the material in previous events does not impact the current event.

4.2.2 Fundamental difference between elastic and plastic deformation of solids

The following outlines some of the fundamental differences between elastic and plastic material behavior [39].

a. *Elastic deformation*

1. Very small deformation with the strain up to about 0.1%
2. Usually a linear relationship between the stress and strain.
3. Completely recoverable strain or deformation after the applied load is removed.

b. *Plastic deformation*

1. Larger deformation.
2. Nonlinear relationship between the stress and strain.

3. Results in permanent deformation after the removal of the applied load.
4. No volumetric change in the solid during plastic deformation, often modeled with Poisson's ratio of 0.5. Deformation is caused by shear actions on the material. Only shape changes can be observed.
5. The total strain, ε_T, is the sum of the elastic components ε_e and the plastic component ε_p as shown in Figure 4.3 on page 58.

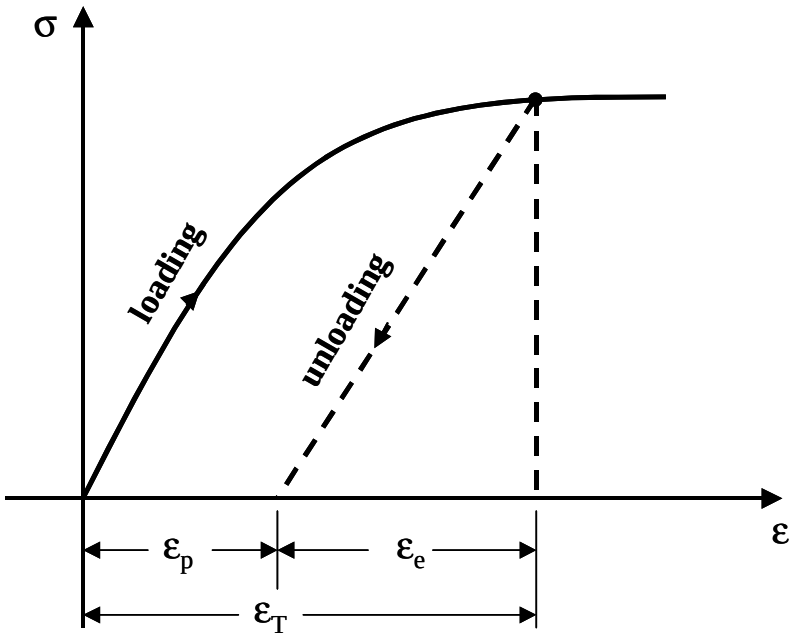

Fig. 4.3 Uniaxial elastic-plastic loading and elastic unloading of a material [39]

4.2.3 Idealized uniaxial stress-strain curves

Three idealized stress-strain curves for a prismatic, metal bar subjected to uniaxial tension are shown in Figure 4.4 on page 59. Rigid, perfectly plastic, elastic, perfectly plastic, and elastic,

strain-hardening behaviors are shown in parts (a), (b), and (c), respectively, of the figure. The yield strength of the material is denoted by σ_y in the plots. The rigid, perfectly plastic idealization neglects elastic strains and hardening. The elastic, perfectly plastic curve includes elastic strains but neglects hardening. The elastic, strain hardening curve includes elastic strains and assumes linear hardening. When large deformations are prevented, say, by a surrounding elastic material, then plastic deformation is contained. For contained plastic deformation, neglecting strain-hardening, or work-hardening, is a reasonable assumption. Large deformations by cold-working occur in metal-forming processes such as drawing, rolling, and extrusion. Cold-working involves hardening and the plastic deformations in these processes are much larger than elastic deformations, so that neglecting elastic deformation is a reasonable assumption.

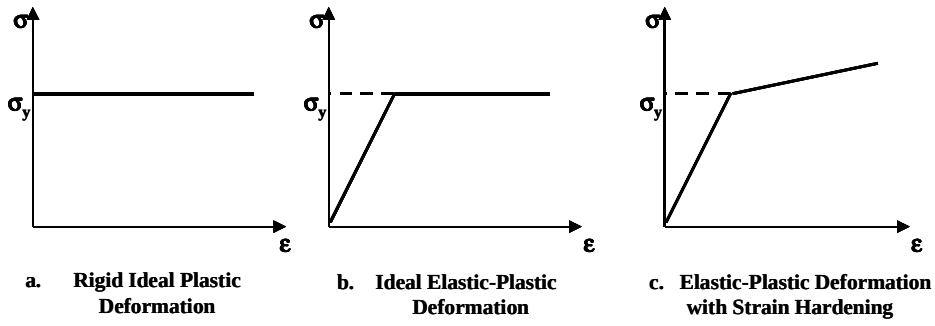

Fig. 4.4 Idealized flow curves from uniaxial tension test [39]

The yield strength of a metal is measured in the tension test, which is a uniaxial state of stress. The question of what governs yielding in a multi-axial state of stress is determined from

experiments, since there is no theoretical way to correlate yielding in a three-dimensional stress state with yielding in the uniaxial tensile test. The yield condition now can only be defined by the "yield criterion" [39].

4.2.4 von Mises Yield Criterion

The von Mises yield criterion was first derived from the distortion energy theory. Let $\bar{\sigma}$ denote the Mises effective stress defined by

$$\bar{\sigma} \equiv \frac{1}{\sqrt{2}}[(\sigma_{XX}-\sigma_{YY})^2 + (\sigma_{YY}-\sigma_{ZZ})^2 + (\sigma_{XX}-\sigma_{ZZ})^2 + 6(\sigma_{XY}^2 + \sigma_{YZ}^2 + \sigma_{XZ}^2)]^{1/2} \qquad (4.24)$$

where $\sigma_{XX}, \sigma_{YY}, \ldots, \sigma_{XZ}$ are the Cartesian stress components at a point in the material. Mises criterion states that yielding initiates in a three-dimensional state of stress when the effective stress equals the yield strength of the material determined from the uniaxial tensile test. Expressed mathematically the criterion is simply

$$\bar{\sigma} = \sigma_y \qquad \text{at the initiation of yielding} \qquad (4.25)$$

For the uniaxial state of stress where $\sigma_{XX} \neq 0$ and all other stresses components are equal to zero, Mises criterion predicts yield initiation when $\sigma_{XX} = \pm\sigma_y$. For the state of pure shear where $\sigma_{XY} \neq 0$ and all other stress components are equal to zero, Mises criterion predicts the initiation of yielding when $\sigma_{XY} = \pm\sigma_y/(\sqrt{3})$. Thus, Mises criterion implies that the yield stress in tension is $\sqrt{3}$ times the yield stress in shear. This relationship between the yield stresses in tension and pure shear closely approximates many tests of polycrystalline metals [37]. Mises criterion can be

visualized in principal stress space, where the principal stresses are denoted $(\sigma_1, \sigma_2, \sigma_3)$. The criterion plots as right circular cylindrical surface of radius $\sqrt{2/3}\sigma_y$, with the axis of the cylinder equally inclined with respect to the positive principal stress axes. For $\sigma_3 = 0$, Mises criterion plots as an ellipse in the σ_1-σ_2 plane as is shown in Figure 4.5.

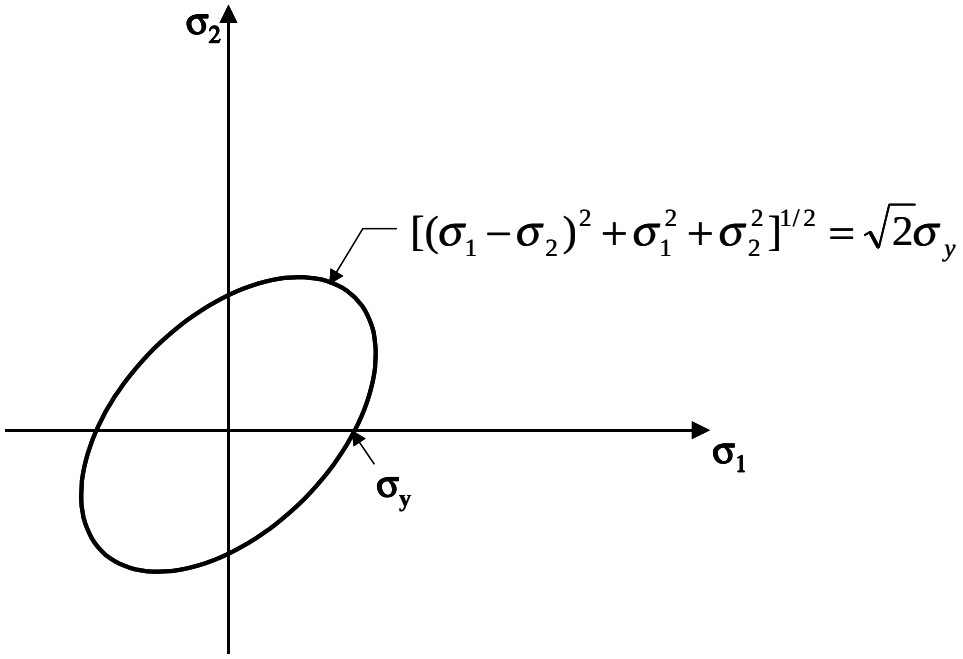

Fig. 4.5 Two-dimensional von Mises yield surface [39]

4.2.5 Strain Hardening

Strain hardening is defined as the increase in hardness and strength of a metal as it is plastically deformed [3]. Initial plastic yielding takes place when a material is loaded beyond its elastic limit. Theoretically, the material starts to "flow" without any additional load as depicted in Figure 4.4 (b). However, in reality most materials retain some of their original stiffness after yielding. Additional loading is required to further plastically deform the material as shown in Figure 4.4 (c). The material also becomes "harder" after some plastic deformation as a higher applied load is required to cause the same material to deform plastically again after the completion of one previous loading cycle [39]. Two types of strain-hardening schemes are typically used in finite element analysis: (1) isotropic hardening; (2) kinematic hardening.

(1) *Isotropic hardening.*

Figure 4.6 illustrates the principle of isotropic hardening of a material. First the material is loaded beyond its initial yield strength σ_y to an instantaneous strain ε_1 and then unloaded upon reaching point A. A permanent strain ε_2 is introduced in the material after unloading. If the solid is loaded again, the material is found to yield at a higher strength σ_y' which coincides with the stress σ_A at the last load point.

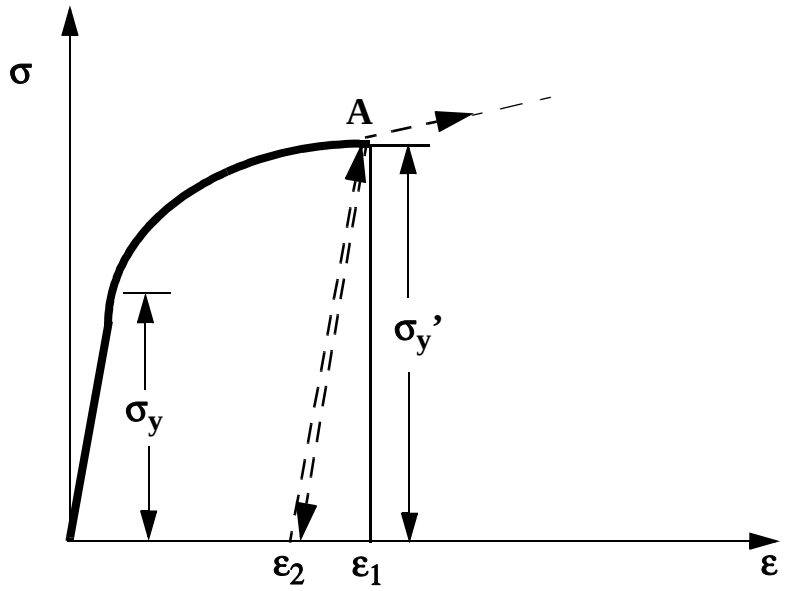

Fig. 4.6 Paths for loading, unloading and reloading for an isotropic hardening solid [39]

The biaxial stress states for the isotropic strain-hardening behavior can be graphically represented by the uniform expansion of the initial yield surface of Figure 4.5, or as shown in Figure 4.7 [39]. The yield surface maintains its shape and does not translate, while its size increase is controlled by a single parameter depending on the plastic deformation.

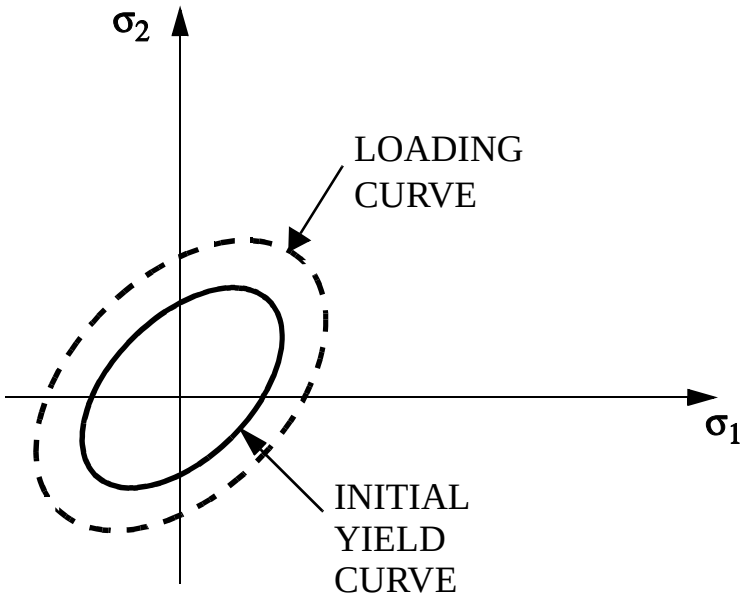

Fig. 4.7 Biaxial loading surfaces for isotropic hardening solids [39]

(2) *Kinematic hardening.*

A material which exhibits kinematic hardening has the characteristic that when the material is plastically deformed in tension followed by loading in the reverse direction, the compressive yield strength in reverse loading is reduced in the same amount as the tensile yield strength is increased during the initial loading. The lowering of the compression yield following a first loading in tension is called the Bauschinger effect. The isotropic hardening model would predict a compression yield strength at $\sigma_{zz} = -(\sigma_y + \alpha_{zz})$ in Figure 4.8. Thus, the isotropic hardening

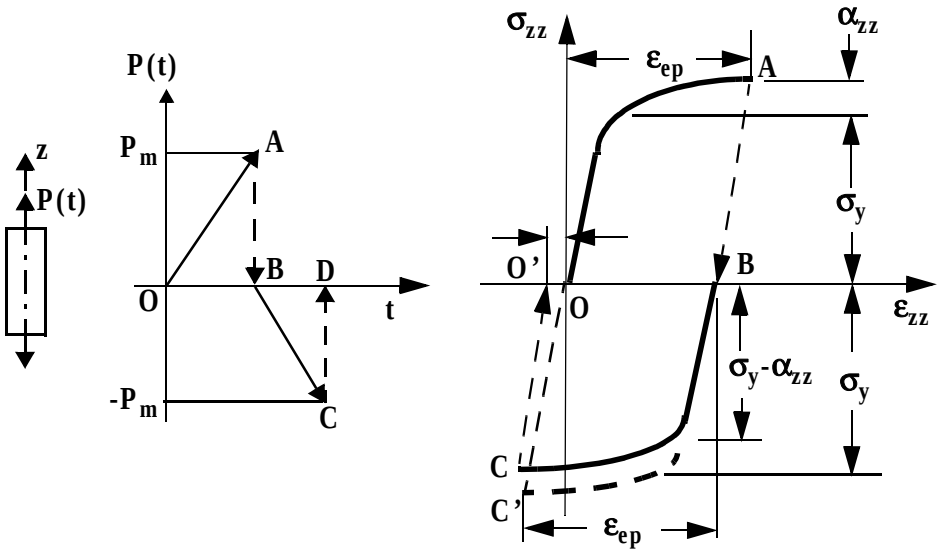

Fig. 4.8 Paths for a uniaxially loaded bar under kinematic hardening plastic deformation [39]

model cannot predict the Bauschinger effect, but the kinematic model can predict it. Kinematic hardening results in the strain hysteresis observed after a complete tension-compression load cycle, as shown in Figure 4.8. For the multiaxial loading situation, the size and shape of the yield surface does not change, but it merely translates in stress space as is shown in Figure 4.9 [39]. The translation is in a direction of the plastic-deformation-increment vector.

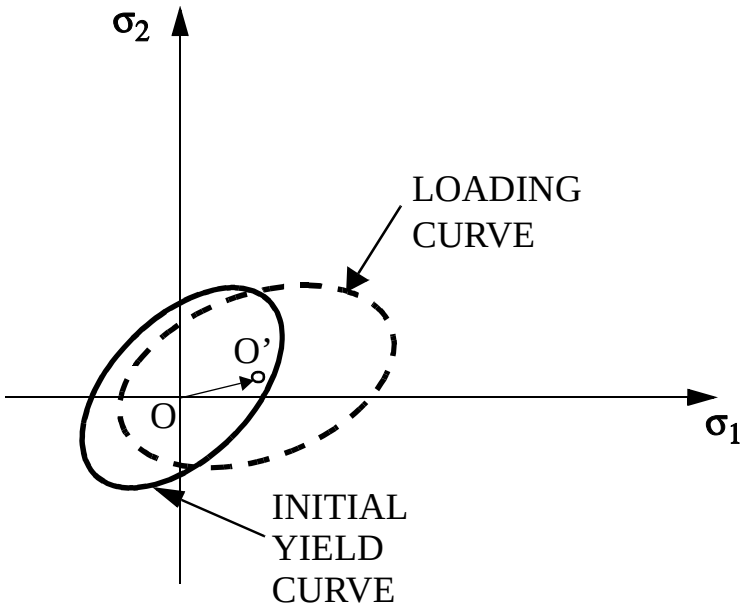

Fig. 4.9 Translation of the yield surface with kinematic hardening rule under biaxial loading condition [39]

CHAPTER 5

SYSWELD Models of the Butt and Tee Joints

5.1 SYSWELD Capabilities

After a review of the limited number of commercial finite element codes capable of weld simulations, the SYSWELD finite element code was chosen for use in this research due to the extensive capabilities and dedicated tools for the simulation of welding. These tools include material deposit via element activation/de-activation and pre-defined moving heat sources including but not limited to the Goldak Double Ellipsoid model described in Chapter 2. Another key feature of the SYSWELD code which sets it apart from other commercial finite element software, is the ability to model metallurgical transformations. Metallurgical transformations include volume changes due to phase transformations as well as the change of mechanical properties due to the phase transformations. Also included is a library of metallurgical models for both steel and aluminum. The other more general capabilities include the option to use either 2-D or 3-D models, the ability to perform multiple weld passes, availability of a large range of material behavior laws including elastic-perfectly plastic,

isotropic strain hardening, kinematic strain hardening, and finally the use of temperature dependent material properties. The SYSWELD code has many other capabilities, but those presented here are the only ones of concern for this research.

5.2 SYSWELD Analysis Procedure

Assuming a one-way coupling between the thermal and mechanical analyses, it is necessary to perform either the transient or the steady state thermal analysis first. The thermal data for each element determined from the thermal analysis is then used in the subsequent mechanical analysis. These analyses are completed in stages in SYSWELD, and therefore require separate input decks for each stage. The interaction of the different stages and files required for a complete welding simulation are shown in the flow chart in Figure 5.1.

The boxes with the yellow background in Figure 5.1 represent the thermal analysis and mechanical analysis input files for one weld pass. As described in Chapter 4, it is possible to account for the moving heat source in two separate methods. The first method “marches” the weld arc along the part with time. This is referred to as a “step by step” computation, and one weld pass requires only one input file. The second method involves the “moving reference frame” computation. The governing equations for the metallurgical and mechanical state induced by the moving heat source are solved in a moving reference frame instead of the stationary reference frame. In this second method, a single time is specified, and the computation is performed assuming the steady state has been reached at this time, and all time steps up until this time. To complete the first weld pass using this moving reference frame method, a “step by step” computation must be performed to account for the end boundary of the workpiece. After the heat source leaves the end boundary, the step-by-step transient thermal analysis continues until the

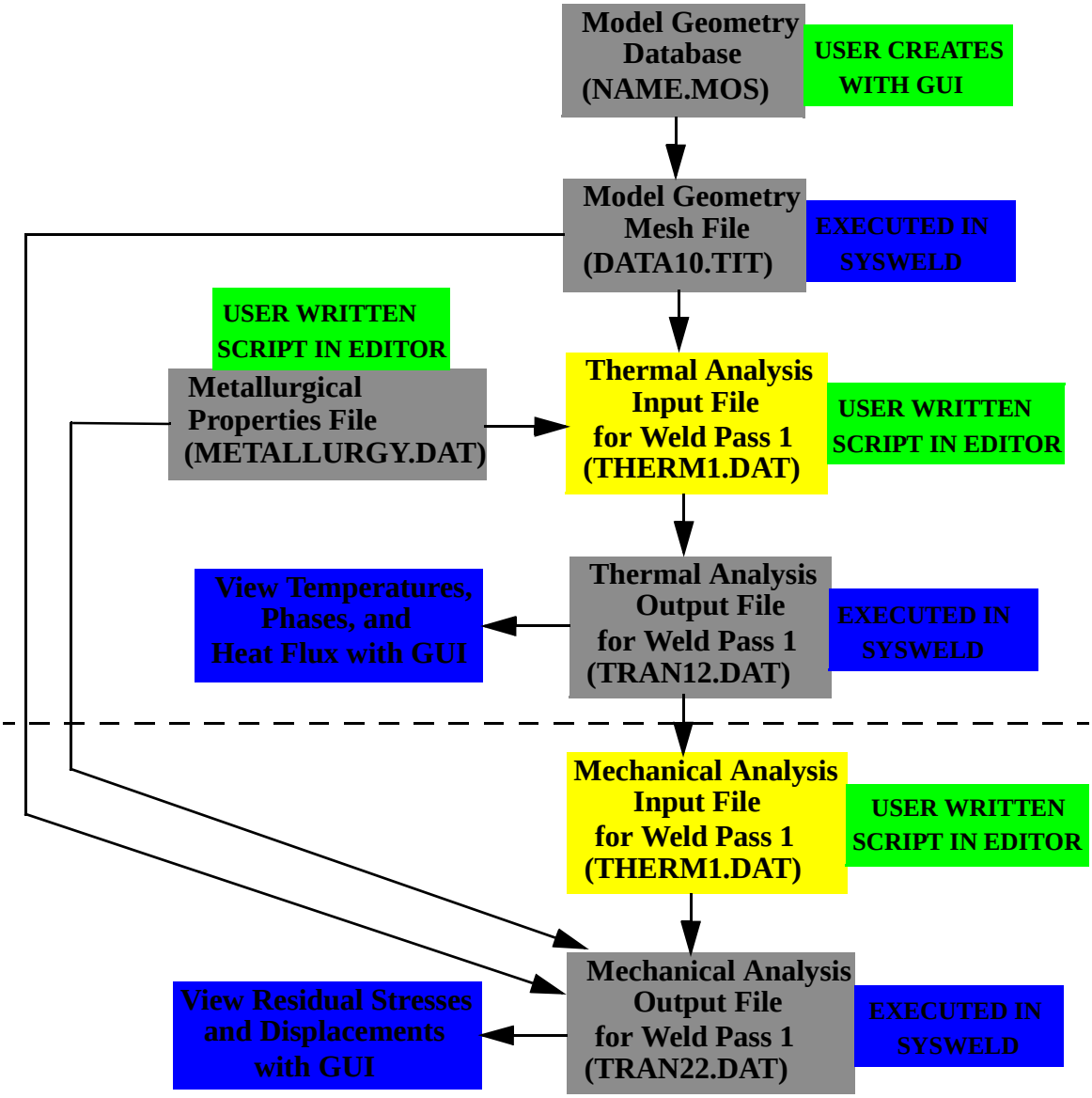

Fig. 5.1 Flow Chart for SYSWELD Analysis

workpiece is cooled to ambient temperature. Therefore, two thermal analysis and two mechanical analysis input files are required for one weld pass if the moving reference frame procedure is used. The input files for a butt-weld moving reference frame analysis and a tee joint transient analysis can be found in the appendices.

5.2.1 SYSWELD Analysis Preparation

As with any finite element analysis, the first step in a weld analysis is the creation of the finite element mesh. After the mesh is created, it is then necessary to apply material properties, choose a material behavior law, choose a metallurgical model, and apply thermal and mechanical boundary conditions. Where welding simulations differ from other analyses is in the specification of the heat source parameters and the parameters for the activation and de-activation of the deposited weld bead elements.

5.3 Finite Element Meshes for the Butt and Tee Joints

The butt joint simulation models the joining of two identical plates with rectangular planform and uniform thickness. The dimensions of one of the two plates of the butt joint are shown in Figure 5.2. Since the plate thicknesses are greater than 13 mm for this butt joint model, it is a design recommendation that the plates be chamfered in a double V-groove configuration along the joint as can be seen in Figure 5.2. The basis for the weld-groove design is to provide a shape and size of opening that enables a sound deposition of filler material. Also, a root gap or offset of the faying face of each part is maintained such that the filler material penetrates the gap to create a complete bond between the two parts. Since the two plates to be joined are identical, only one plate is modeled in the finite element analysis. The mid-plane of the root gap is assumed to be the

plane of symmetry in the analysis. The finite element model with only the first weld bead deposited is depicted in Figure 5.3. The actual joining process consists of six weld passes as shown in Figure 5.4, yet only the residual stress state due to the first weld pass is investigated. This butt joint model is based on the one studied by Michaleris et. al. [14], except for the elimination of the run-off tabs. Michaleris et. al. [14] investigated the six pass aluminum weld joint to determine the effects of restraint in the formation of welding distortion. The focus of this research is to determine the residual stress state in the part where the “steady state” of the welding process has been attained. Satisfactorily, the model examined by Michaleris et. al. [14] is of sufficient length to reach approximately a “steady state” of the welding process at the mid-plane of the part.

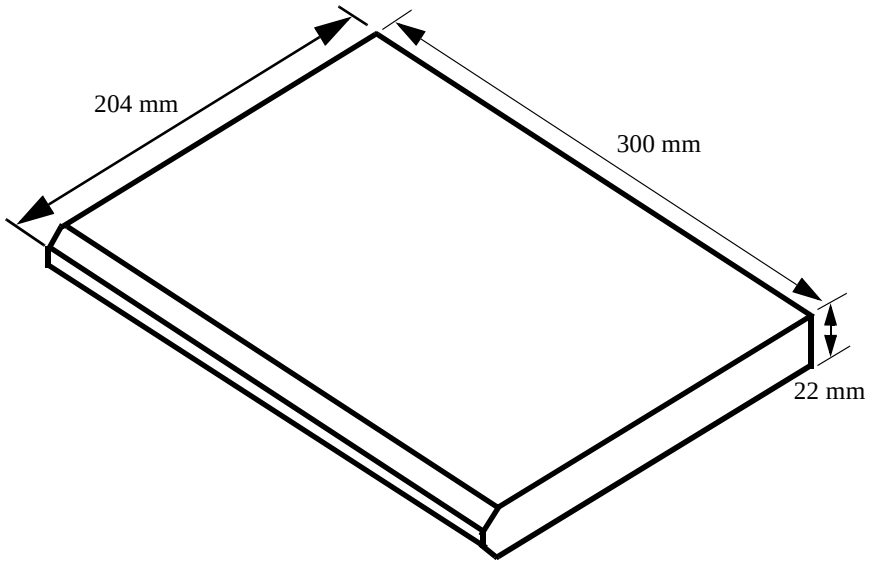

Fig. 5.2 Butt-weld Plate Dimensions

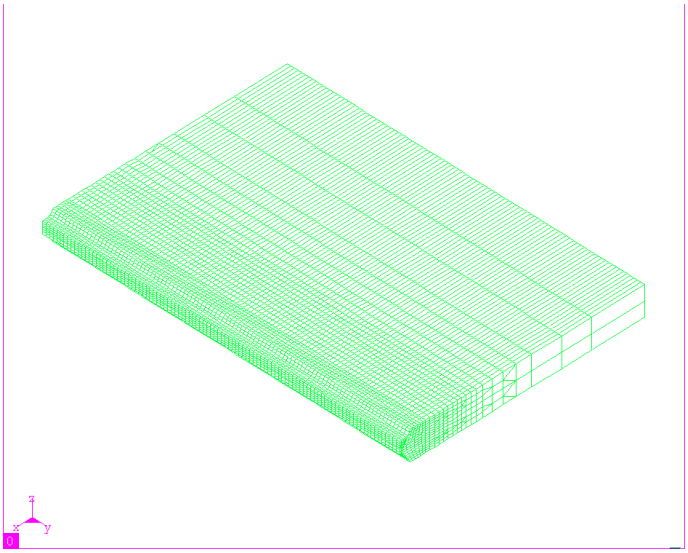

Fig. 5.3 Butt-weld Finite Element Mesh

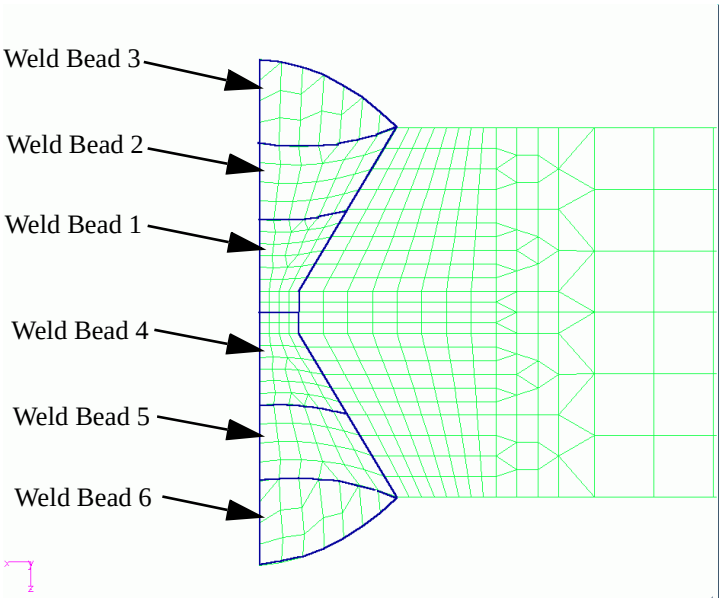

Fig. 5.4 Butt-weld Finite Element Mesh

The dimensions of the configuration for the tee joint are depicted in Figure 5.5. A view of the cross-sectional plane, or the *x-z* plane, shown in Figure 5.6 shows the double bevel fillet used for the joint. The two beads are modeled as two separate weld passes. Two different finite element meshes were developed to analyze the tee joint. The first mesh consists entirely of solid elements and is shown in Figure 5.7.

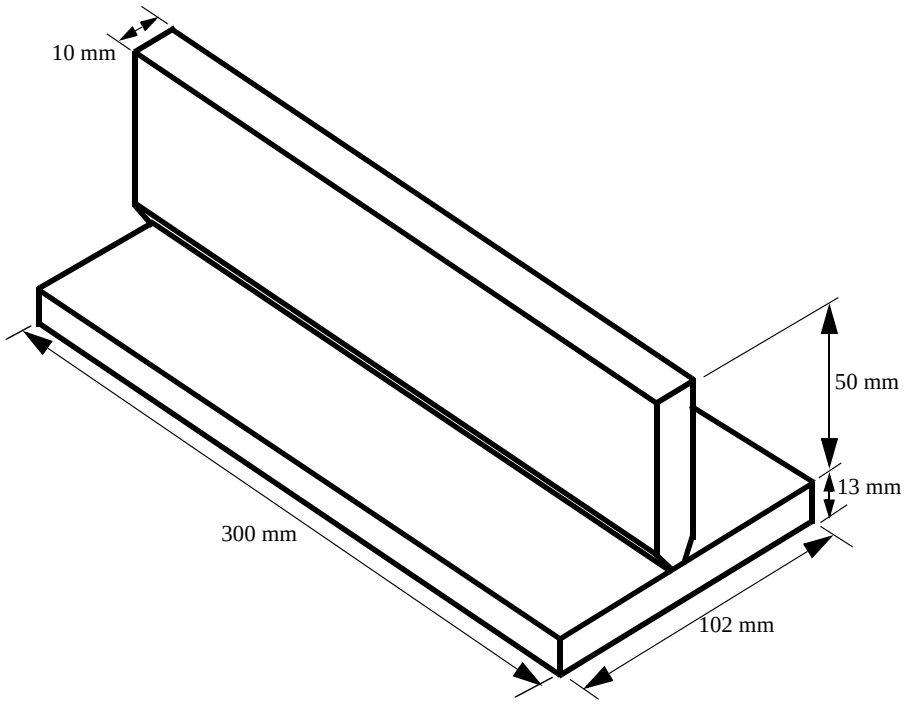

Fig. 5.5 Tee Joint Configuration

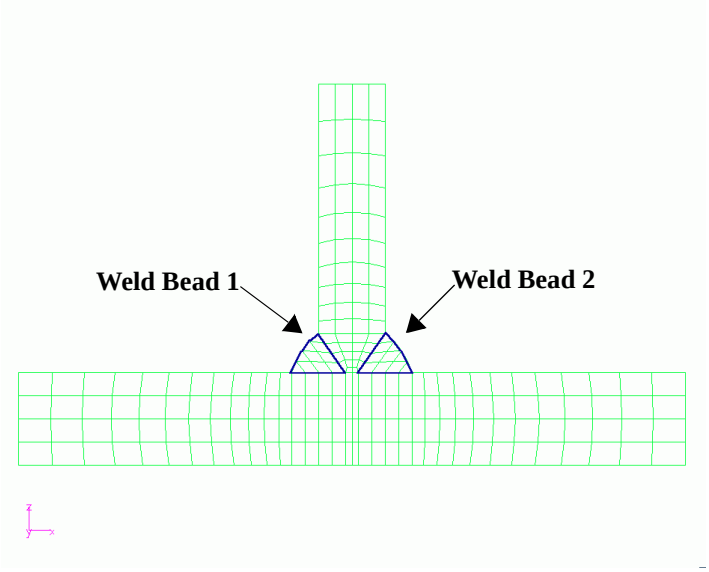

Fig. 5.6 Cross Section of the Tee Joint Finite Element Mesh

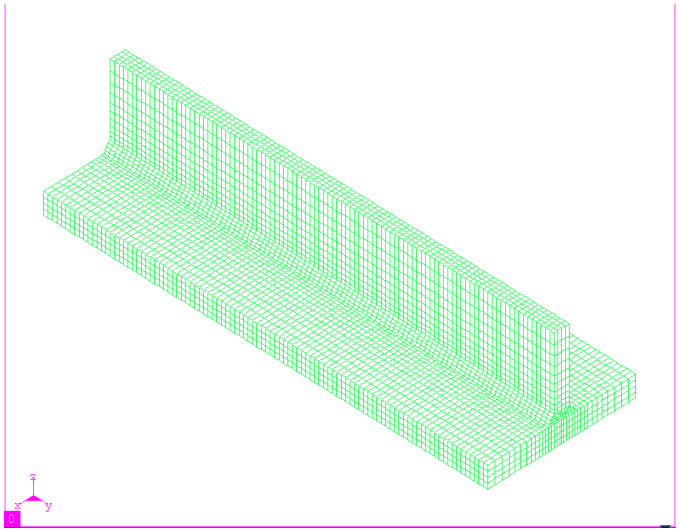

Fig. 5.7 Tee Joint Finite Element Mesh

Due to the large number of elements required for the solid element model, and therefore prohibitive computational times and data storage, a simplified tee joint model was created. The mesh, shown in Figure 5.8, utilizes solid elements and shell elements that are connected by interface elements between solid and shell element boundaries. To reduce the number of solid elements, shell elements are used in the flange and web outside the expected heat affected zone (HAZ). Solid elements are required to calculate three-dimensional effects in the weld zone including metallurgical changes and the micromechanical variables. Insight into the accuracy of the solid-shell model is important for handling larger and more complex geometries containing multiple weld joints.

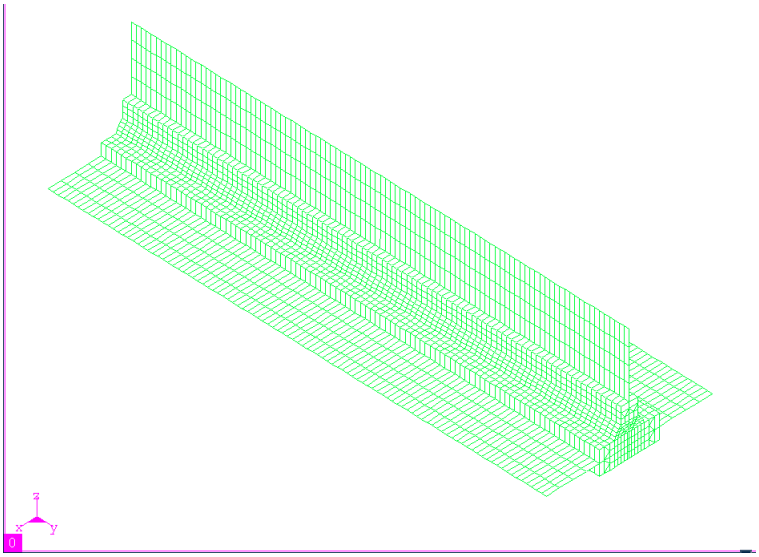

Fig. 5.8 Solid-Shell Tee Joint Finite Element Model

5.3.2 Mesh Size and Time Step Relationship

Due to high peak temperatures, large spatial temperature gradients, and rapid temporal temperature fluctuations imposed by the weld heat source, it is necessary to have very small element sizes and consistent time steps. A fine mesh to capture the spatial gradients implies a small time step. That is, it is necessary to choose a time step which is small enough to resolve these large temperature variations for a given mesh. An approximation to the relationship of mesh density to the time step is developed from the heat conduction equation.

Consider the heat conduction equation, Equation (4.9), for an isotropic material with a temperature independent thermal conductivity, no internal heat generation, and heat transfer in one dimension only, say, the x-direction. Then, Equation (4.9) reduces to

$$\rho C_p \frac{\partial T}{\partial t} = k \frac{\partial^2 T}{\partial X^2} \qquad (5.1)$$

For the same change in temperature, Equation (5.1) can be used to estimate the relationship between the spatial and time increments as

$$\Delta t = (\Delta X)^2 / \kappa \qquad (5.2)$$

where the thermal diffusivity $\kappa = k/(\rho C_p)$. Utilizing the data for Aluminum 2519 at $400°C$; $k = 145 W/(m°C)$, $\rho = 2823 \text{kg/m}^3$, $C_p = 1065 \text{J/(kg}°C)$, the thermal diffusivity $\kappa = 48.23 \times 10^{-6} \text{m}^2/\text{s}$. Assuming a characteristic mesh size of 3 mm, the estimate of the time step is

$$\Delta t = \frac{(3mm)^2}{48.23\times10^{-6}\mathrm{m}^2/\mathrm{s}}\left(\frac{m}{1000mm}\right)^2 = 0.19\mathrm{s} \qquad (5.3)$$

Therefore, for a characteristic mesh size of 3 mm, a time step of about 0.19 seconds should be sufficient to properly capture the temporal thermal variations in the weld model. Convergence studies utilizing the 3 mm mesh also confirmed a time step of 0.1 seconds yields numerically acceptable results. These studies were performed using convergence tolerance criteria of 0.10 on displacement and 1.0 on the force. These values are relative between two successive iterations. Analyses using a time step of 0.1s proved too time consuming such that the convergence criteria were relaxed to 1.0 on displacement, and 10.0 on force, such that a time step of 0.5 seconds could be used.

5.4 Aluminum 2519 and 2319 Material Properties

After creation of the finite element mesh it is necessary to specify the material properties as a function of temperature. The physical data used to model the plate material, Aluminum Alloy 2519-T87 and the filler material, Aluminum Alloy 2319, are plotted versus temperature in Figure 5.9 to Figure 5.19 [14]. The mass density of both materials is $2823\mathrm{kg/m}^3$. The melting range for Al 2519-T87 is $555°C$ - $668°C$, and the melting range for Al 2319 is $543°C$ - $643°C$. Since the chemical compositions of Al 2519 and Al 2319 are very similar, where data was available for one alloy and not the other, the other alloy data was substituted.

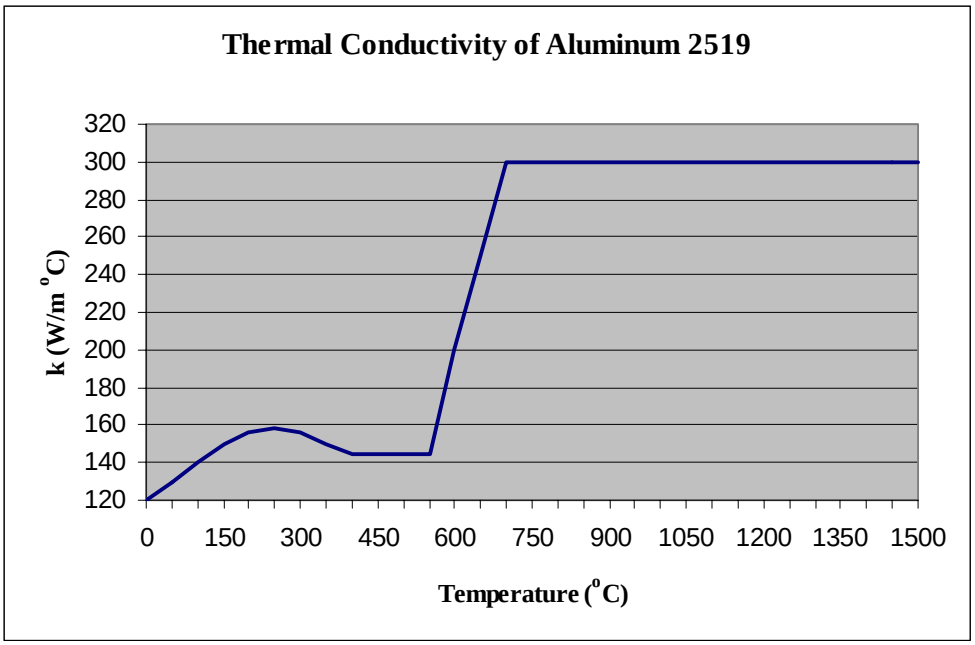

Fig. 5.9 Thermal Conductivity of Aluminum 2519

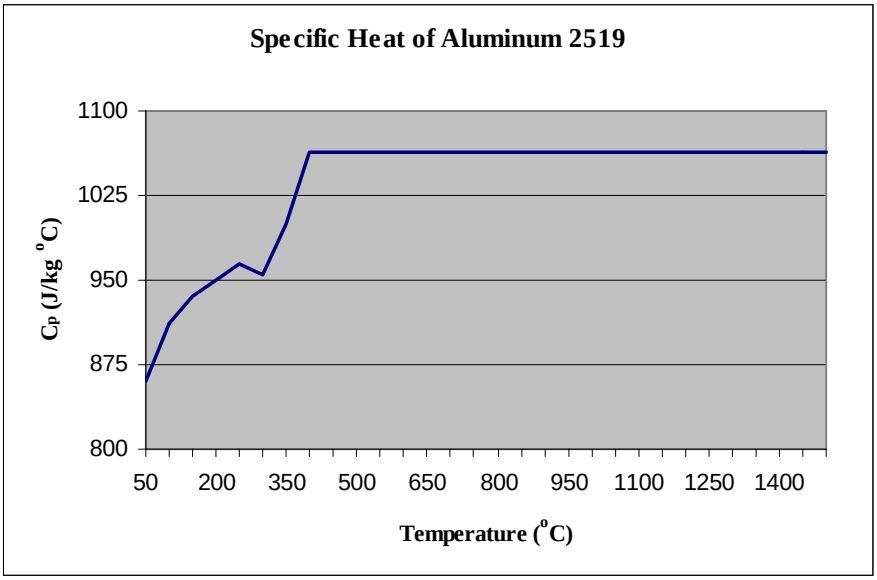

Fig. 5.10 Specific Heat of Aluminum 2519

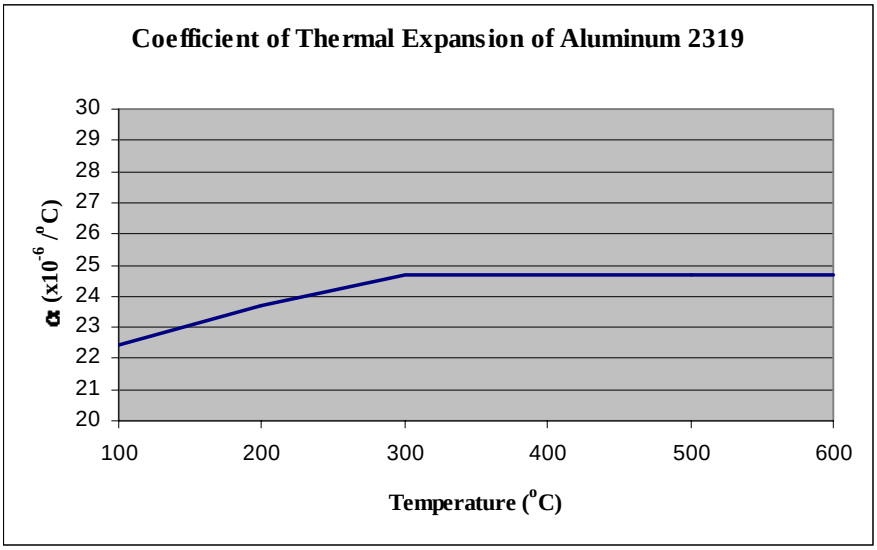

Fig. 5.11 Coefficient of Thermal Expansion of Aluminum 2319

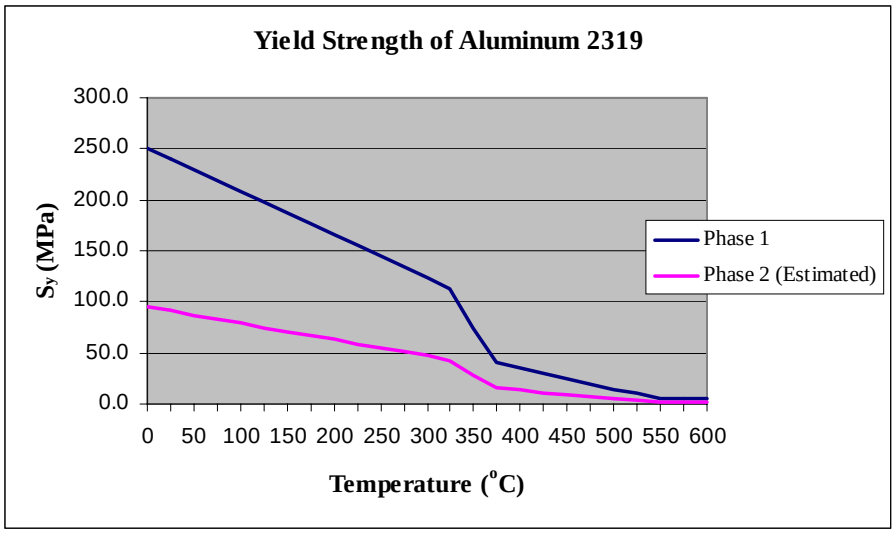

Fig. 5.12 Yield Strength of Aluminum 2319

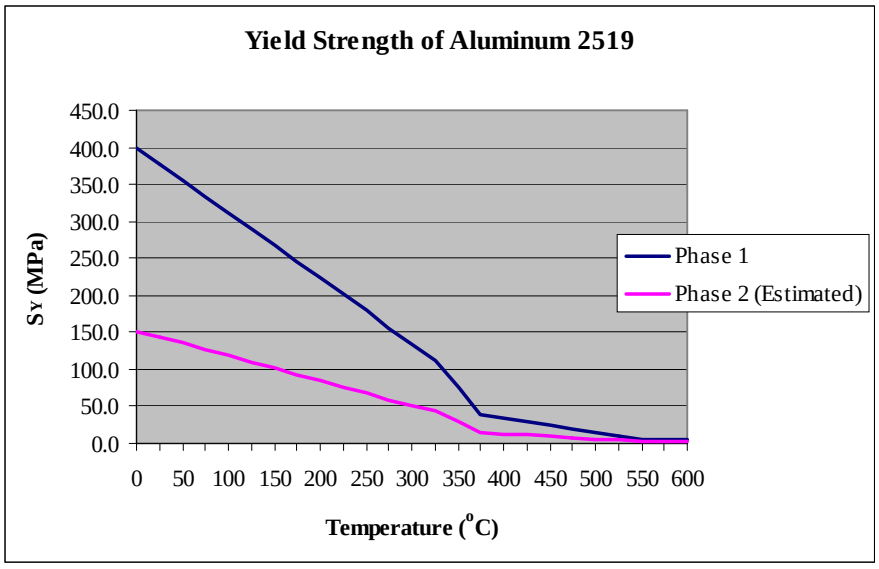

Fig. 5.13 Yield Strength of Aluminum 2519

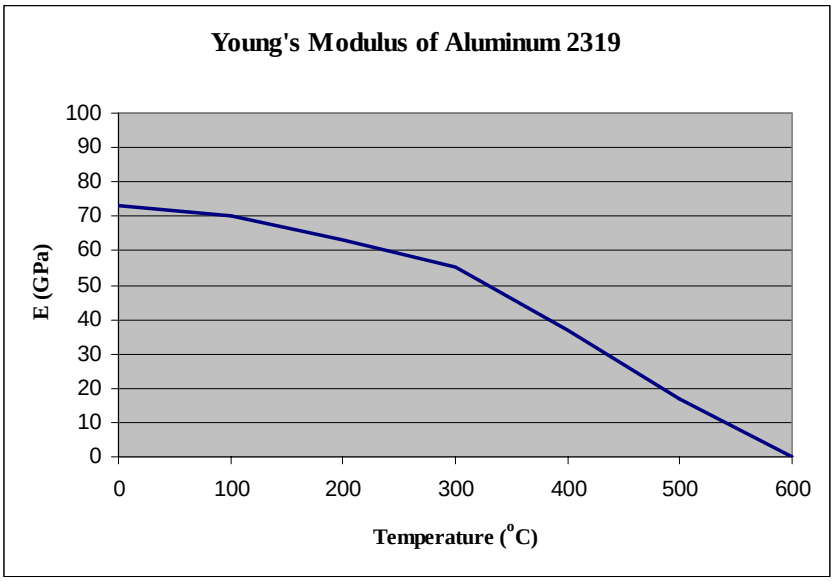

Fig. 5.14 Young's Modulus of Aluminum 2319

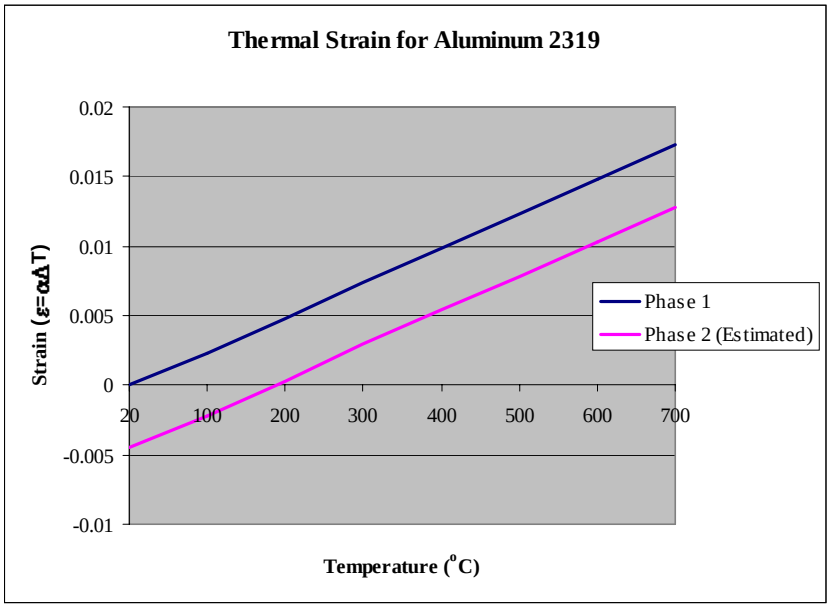

Fig. 5.15 Thermal Strain for Aluminum 2319

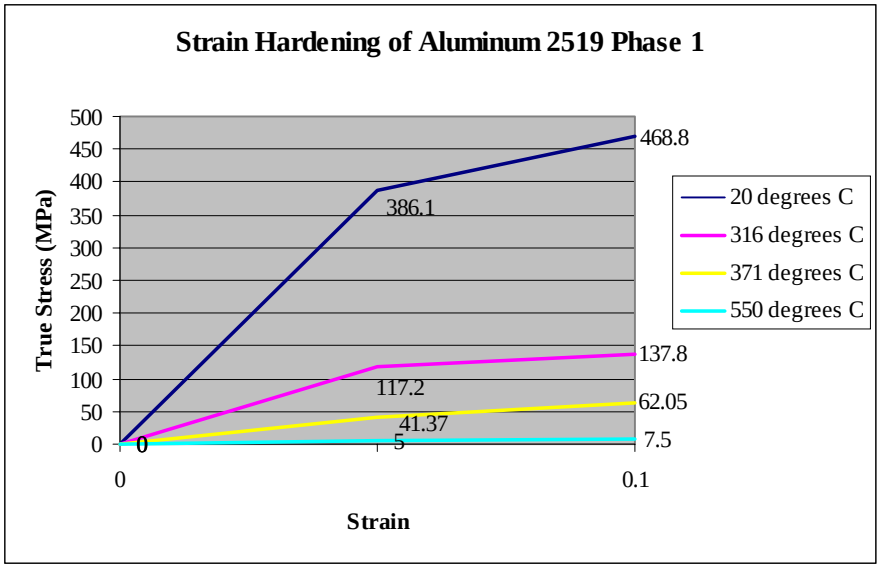

Fig. 5.16 Strain Hardening of Aluminum 2519 Phase 1

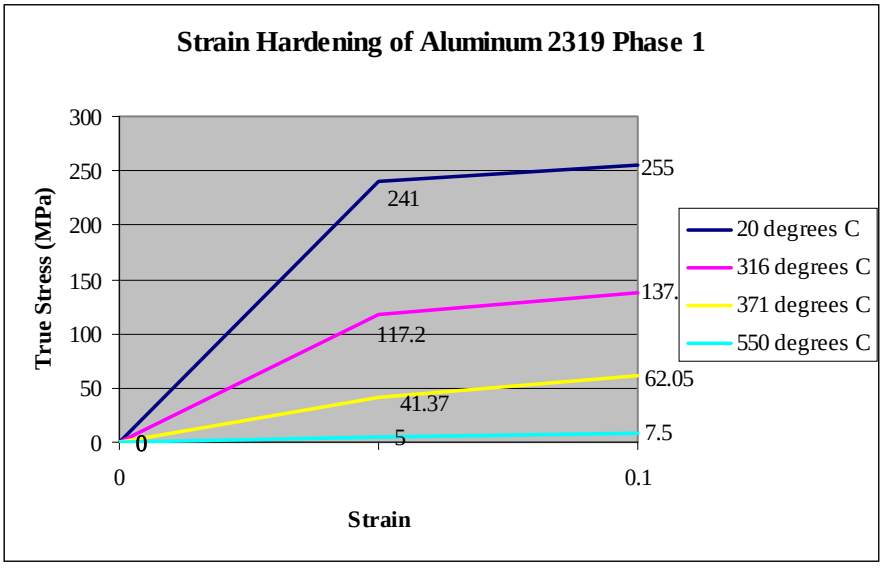

Fig. 5.17 Strain Hardening of Aluminum 2319 Phase 1

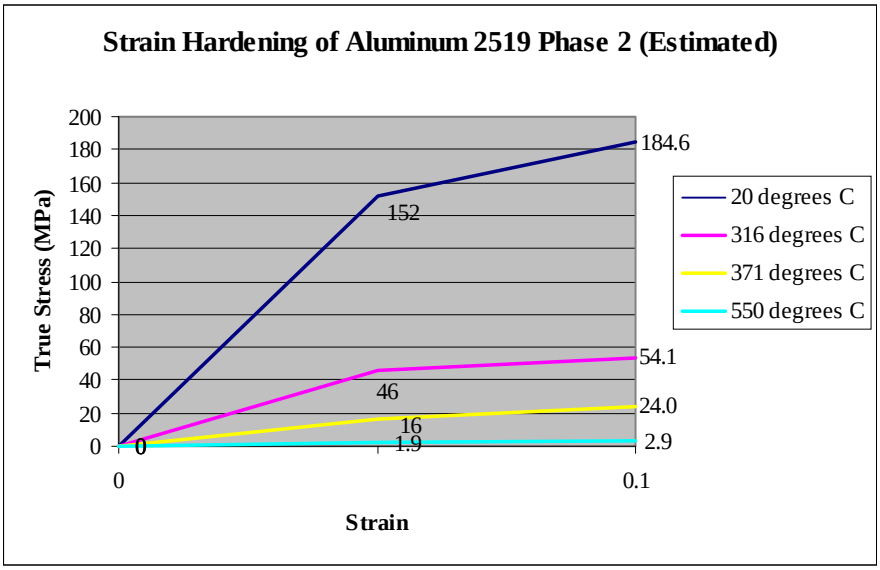

Fig. 5.18 Strain Hardening of Aluminum 2519 Phase 2

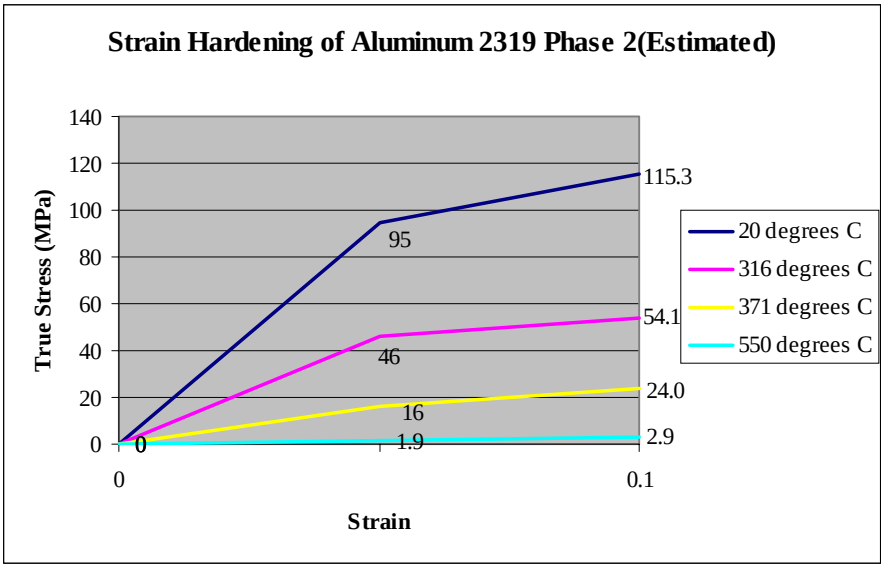

Fig. 5.19 Strain Hardening of Aluminum 2519 Phase 2

In the previous material data figures, Figure 5.15 through Figure 5.19, the designations Phase 1 and Phase 2 are used. Phase 1 refers to the age hardened condition of the material, or θ'' condition as discussed in Chapter 4. Phase 2 refers to the weaker intermediate supersaturated α-phase solvent with θ-phase solute. After consulting two manufacturers of Aluminum 2519, and the failure to obtain precise Phase 2 data, the data was estimated based on published binary aluminum-copper alloy data.

The material model used for this research is a plasticity model utilizing von Mises criterion with isotropic strain hardening. A strain hardening model is more appropriate than an elastic-perfectly plastic model, due to the thermal loading and large strains which develop. The hardening curves used are depicted in Figure 5.16 and Figure 5.17 on page 82.

5.5 Thermal Boundary Conditions

Convective boundary conditions, Equation (4.16), are represented in the numerical model by skin elements. The heat flux transferred to the boundary layer of the gas or fluid is given by Equation (4.15), which is repeated below as Equation (5.4).

$$q_f = h(T)\{T[X_I(S_0), t] - T_0\} \qquad (5.4)$$

The unknown temperature on the external face of the solid, or wall, in contact with the air is $T[X_I(S_0), t]$, and the ambient air temperature T_0 is specified as $20°C$. The convection coefficient, h, in W/(m^2°C) is specified as a function of the wall temperature by the plot shown in Figure 5.20.

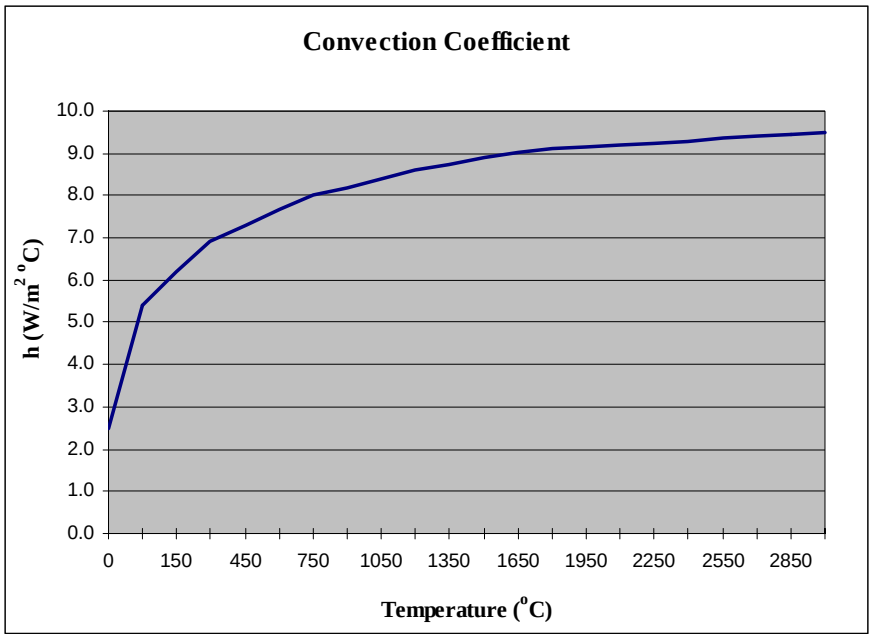

Fig. 5.20 Convection Coefficient

5.6 Mechanical Boundary Conditions

The specified mechanical boundary conditions are those just sufficient to prevent rigid body motion of the model. Figure 5.21 depicts the specified zero displacement conditions for the butt joint and Figure 5.22 depicts the specified zero displacement conditions for the tee joint. As mentioned earlier, the mid-plane of the root gap of the butt joint is assumed to be a plane of symmetry in the analysis, which is parallel to the y-z plane in Figure 5.21.

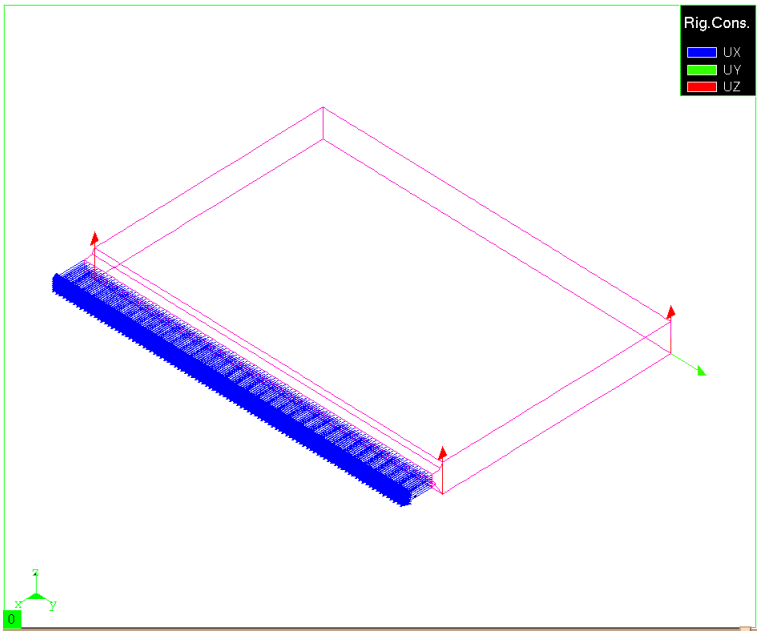

Fig. 5.21 Mechanical Constraints for Butt Joint

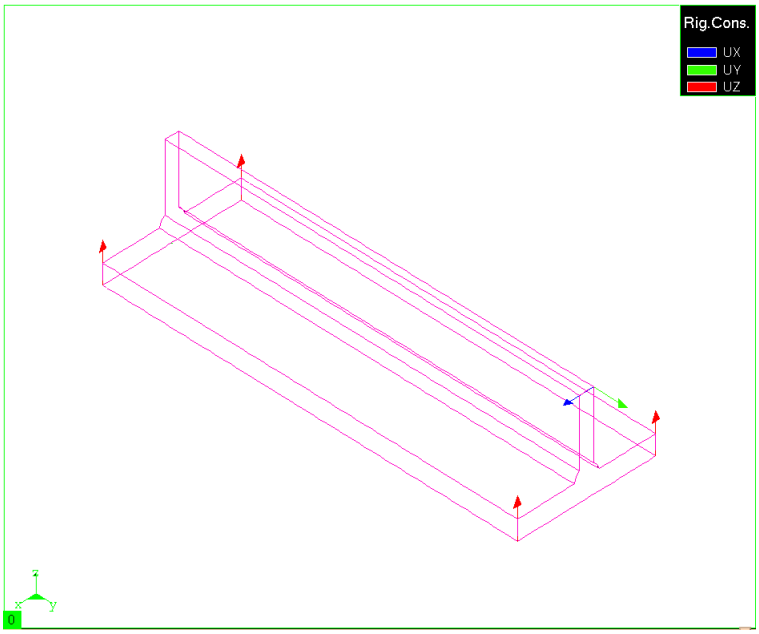

Fig. 5.22 Mechanical Constraints for Tee Joint

5.7 Specified Metallurgical Parameters

As described in Chapter 3, the SYSWELD metallurgical model for precipitate dissolution kinetics was given by Equation (2.1), which is repeated here for convenience in Equation (5.5) below.

$$x = \left(\frac{t}{t_r}\right)^n \exp\left[\left(\frac{Q_s}{R} + \frac{nQ_d}{R}\right)\left(\frac{1}{T_r} + \frac{1}{T}\right)\right] \qquad (5.5)$$

Published binary aluminum-copper alloy data having a composition of 94% Al and 6% Cu is used to estimate the parameters needed for the metallurgy model defined by Equation (5.5). The specified parameters in Equation (5.5) are as follows:

R: constant of perfect gas: 8.31 J/mol ^{o}K [3]

Aluminum 2519

t_r: time for total dissolution of precipitates at given temperature T_r: 3000 s [41][42]

T_r: 545 ^{o}C [43]

Q_s: enthalpy of metastable solvus: 30 kJ/mol [44]

Q_d: energy for activation: 130 kJ/mol [44]

n: parameter which can be dependent on x: $n(x)=0.5-a\ x^b$

a: 0 [44]

b: 0 [44]

Aluminum 2319

t_r: time for total dissolution of precipitates at given temperature T_r: 3000 s [41][42]

T_r: 545^{o}C [43]

Q_s: enthalpy of metastable solvus: 30 kJ/mol [44]

Q_d: energy for activation: 130 kJ/mol [44]

n: parameter which can be dependent on x: $n(x)=0.5-a\ x^b$

a: 0 [44]

b: 0 [44]

5.8 Specified Weld Arc Model Parameters

As described previously in Section 4.1.5, the Goldak heat source model, Eqs.(4.21-4.23), is used to simulate the weld arc. The heat source parameters are shown in Figure 5.23, while the values used are given in Table 5.1.

Table 5.1 Goldak Heat Source Parameters

Finite Element Model	**a, mm**	**b, mm**	**c_1, mm**	**c_2, mm**	**Q, kW**	***Weld speed v*, mm/s**
Butt-weld joint	30	30	24	80	5.35	6
T-section joint	30	30	24	80	11.5	6

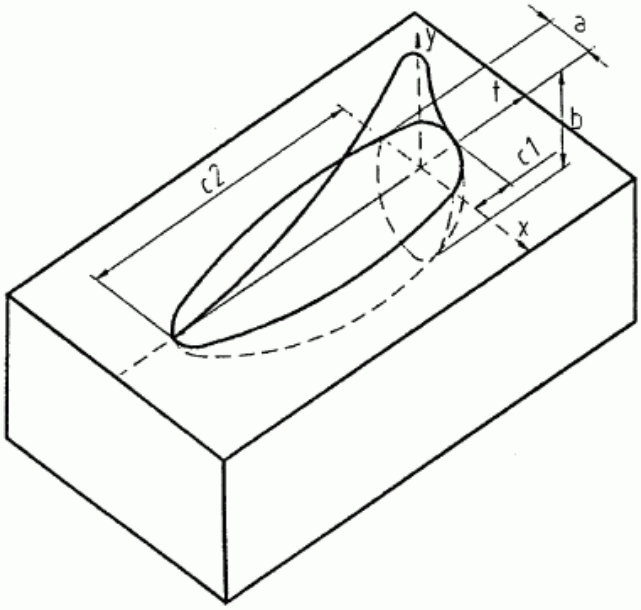

Fig. 5.23 Goldak Double Ellipsoid Heat Source Model [19]

The first thing to note is the correlation of the heat source parameters to the molten zone size is not one to one, and therefore the values are oversized to produce the correct molten zone. This is due primarily to the interaction between the heat source power which is Gaussian along the longitudinal weld arc axis and the volume specified by the double ellipsoid dimensions as shown in Figure 5.23. In order to get temperatures above 545 ^{o}C, the molten temperature of the filler material Aluminum 2319, throughout a volume equivalent to the actual weld pool size, it was necessary to increase the ellipsoid dimensions of the heat source. A secondary reason for the over-sized heat source parameters is due to the interaction between the heat source and the element activation/de-activation function. Depending upon the number of elements activated in front of the weld heat source center, these elements are within the front half of the ellipsoid and are heated. If more elements are activated in front of the heat source then are encompassed by the heat source volume, these elements are still heated by conduction. Therefore, in the cases where element activation/de-activation was not used, the heat source is applied to the elements within the specified volume, but conduction effects transfer the heat to a large number of weld bead elements.

The molten zone is sized to emulate the molten zone produced by the weld arc during the actual welding operation as shown in Figure 5.24. Based on manufacturing experience a molten pool length of approximately 23 mm was used, while the cross-section was chosen to encompass the weld bead cross-section.

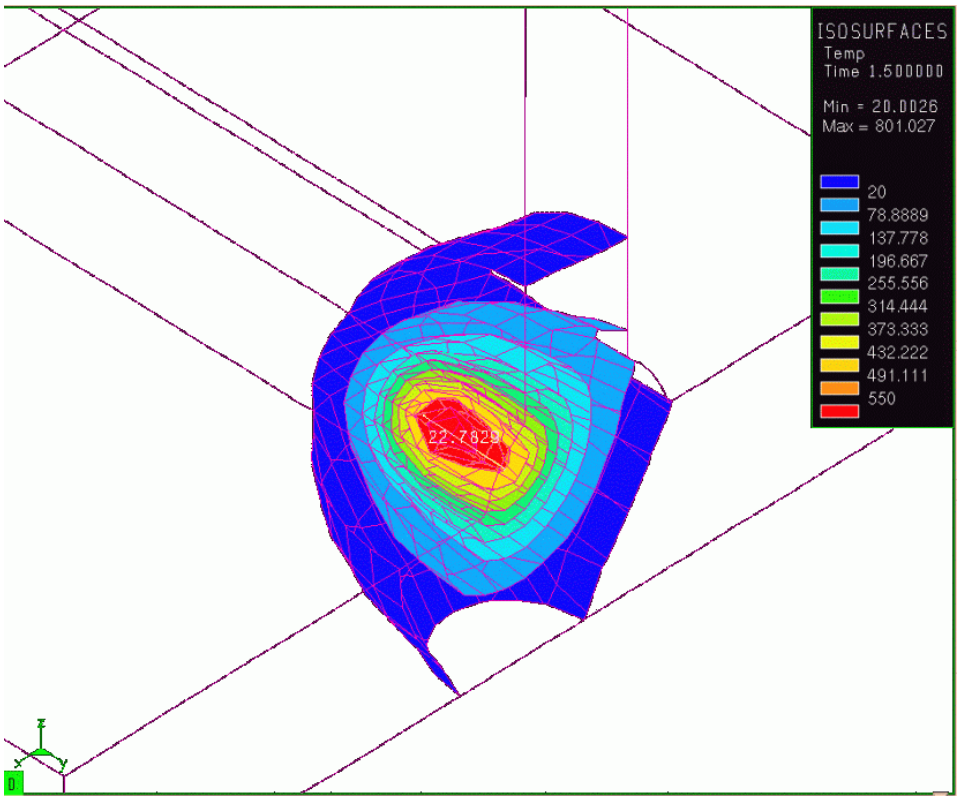

Fig. 5.24 Weld Pool Size Measurement

The second thing to note is due to the symmetry in the butt-weld model, and therefore a smaller weld bead cross-section, a reduced heat source strength is required. The manufacturing data provided by General Dynamics [45] is: average heat input per weld pass = 25.3 kJ per inch of weld length (~1 kJ/mm), average weld bead cross-sectional area per weld pass = 0.05 in^2 (~32 mm^2), and typical travel speed of 15 in/min. (~6 mm/s). This data was used to estimate the heat source strength. The power is typically computed as follows (also see Eq. 4.23):

$$Q = \eta VI \tag{5.6}$$

where η is the arc efficiency, V is the voltage, and I is the amperage of the arc. Lacking voltage and amperage information, the power input was computed by:

$$Q = q_p v \tag{5.7}$$

where q_p is the heat input per weld pass and v is the weld velocity. So,

$$Q = 1.0\text{kJ/mm} \times 6\text{mm/s} = 6.0\text{kW} \tag{5.8}$$

This information was used as a starting point for the heat input. As was mentioned previously, the resulting molten zone governs what value to actually use for the heat input. The molten zone cross-section is taken to be the weld bead cross-section plus a small amount of base material. The molten zone length is approximated at 20 mm long, or equivalent to an actual molten pool based on manufacturing experience. Michaleris et al. [14] used a value of 5.35 kW for the first weld pass of the butt-weld analysis, therefore this value was used for the butt-weld analyses. Due to the larger weld bead required for the tee section analyses, a value of 11.5 kW was used for the power input.

5.9 Element Activation/De-activation

To simulate weld deposit, a simplified FORTRAN program provided within the SYSWELD code is used to specify the activation and de-activation of the proper elements. This is accomplished through specifying an offset parameter, in the direction of the weld arc, which activates elements as the weld arc approaches. When this function was used, the parameter was adjusted to activate

elements 3 mm or 12 mm in front of the heat source as recommended by the SYSWELD manual [33] and other authors[10][14].

CHAPTER 6

Results and Discussion

6.1 Butt-weld Analysis

In order to gain confidence in using the SYSWELD code it was desired to match the results for the 3-D butt-weld analysis published by Michaleris et al. [14]. Two separate analyses were completed to investigate the different capabilities of SYSWELD. The first analysis utilized the time saving technique called the “moving reference frame” calculation in which a quasi-steady state is computed for the first part of the analysis and then the weld simulation is completed utilizing a traditional transient calculation. The second analysis utilized a fully transient computation to complete the entire weld simulation.

6.1.1 “Moving Reference Frame” Analysis

It was determined that using the element activation/de-activation capability of the software in conjunction with the “moving reference frame” computation provided incorrect residual stress distributions when compared to results published by Michaleris et al. [14], as well as by other

authors [4][8][18]. Therefore, element activation/de-activation was not utilized for the “moving reference frame” part of the simulation. This first part of the simulation begins at a time step of 45s with a weld arc velocity specified as 6 mm/s, which locates the arc 270 mm along the 300 mm plate. In this manner, the software performs the thermal analysis from 0 to 45s in one computational step. It is implied that the welding process has reached a steady state by 45s and that the starting, or transient, conditions for welding at the beginning of the plate are neglected. The temperature distribution at 45s is shown Figure 6.1.

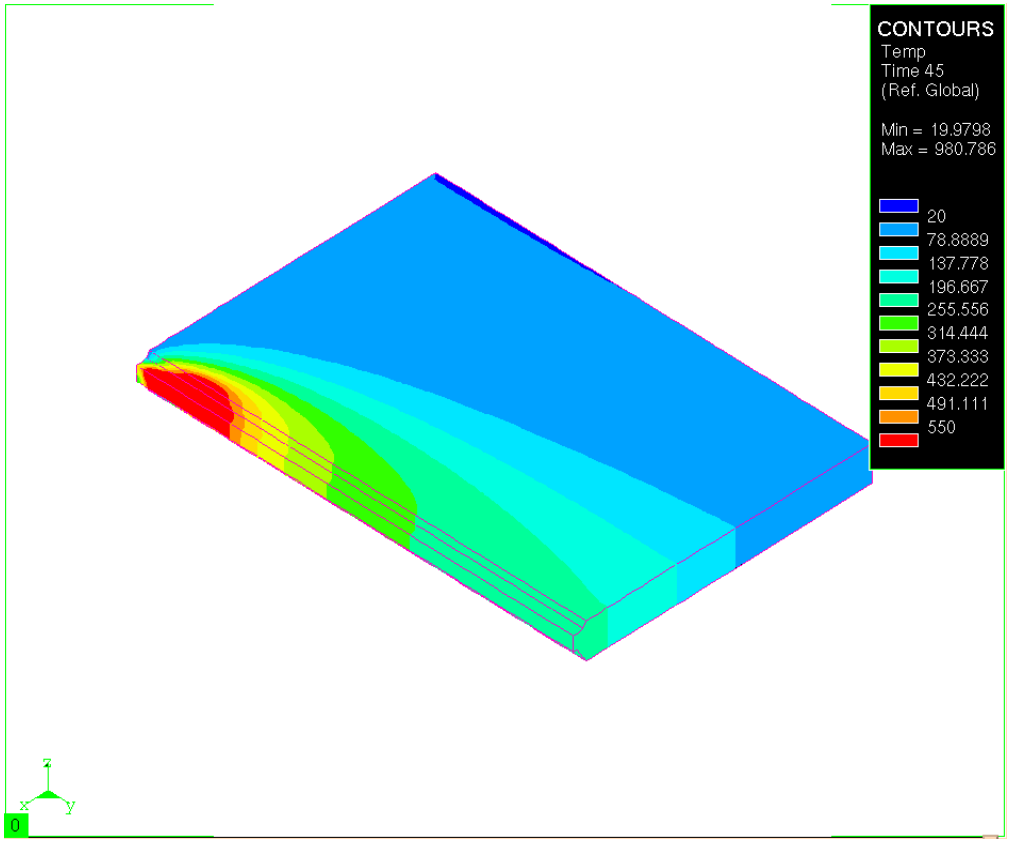

Fig. 6.1 Surface temperature distribution during the first weld pass of the butt joint model at t = 45s.

The next part of the simulation involved a fully transient calculation in which the weld arc is stepped along the remainder of the plate using a time step of 0.5s until a time of 50s. Element activation/de-activation was implemented for this part of the simulation. One element was activated ahead of the heat source, which corresponds to 3 mm ahead of the source. A transient analysis is required to capture the end effects of the weld arc leaving the plate. The temperature distribution at a time of 50s is shown in Figure 6.2. From t = 50s until 5000s, the heat source is

removed from the plate and the plate is allowed to cool. Ideally, the plate should cool to the ambient temperature of 20^{o}C after a time of 5000s, yet using the convection coefficient reported by Michaleris et al. [14], the final temperature was 53^{o}C. Other authors have reported higher convection coefficients by factors of 2-10 times those used here [46]. The final temperature upon cool-down is shown in Figure 6.3.

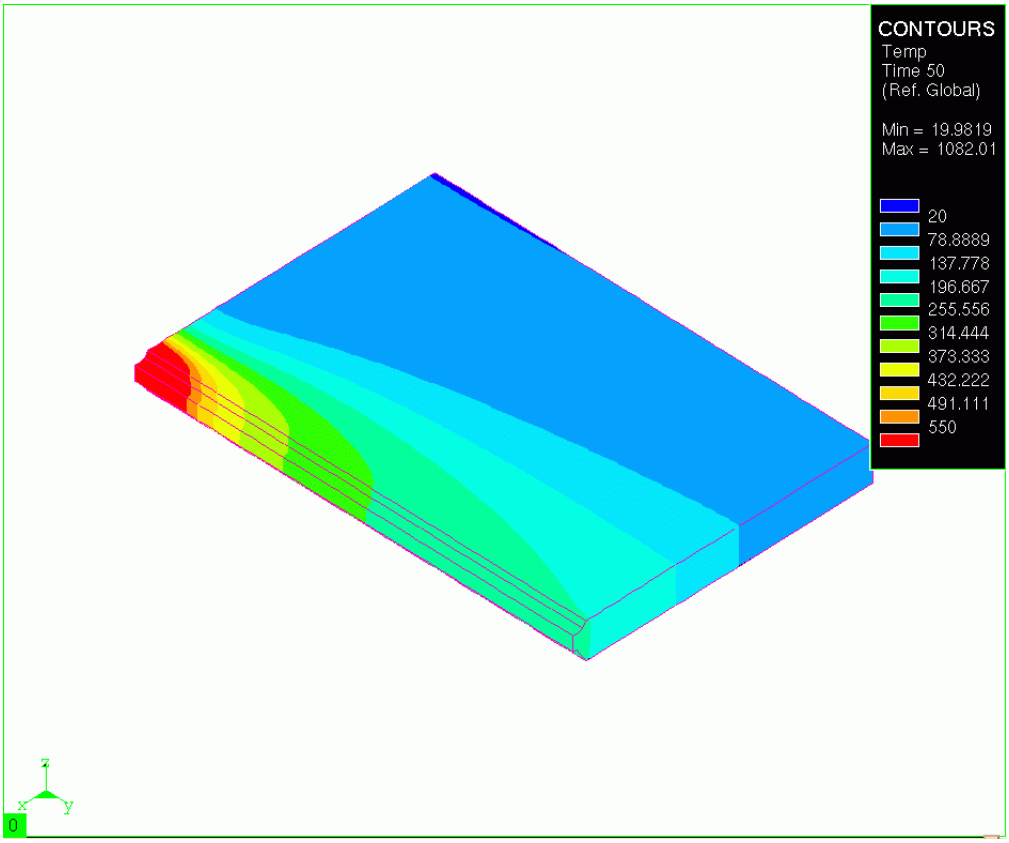

Fig. 6.2 Surface temperature distribution during the first weld pass of the butt joint model at t = 50s.

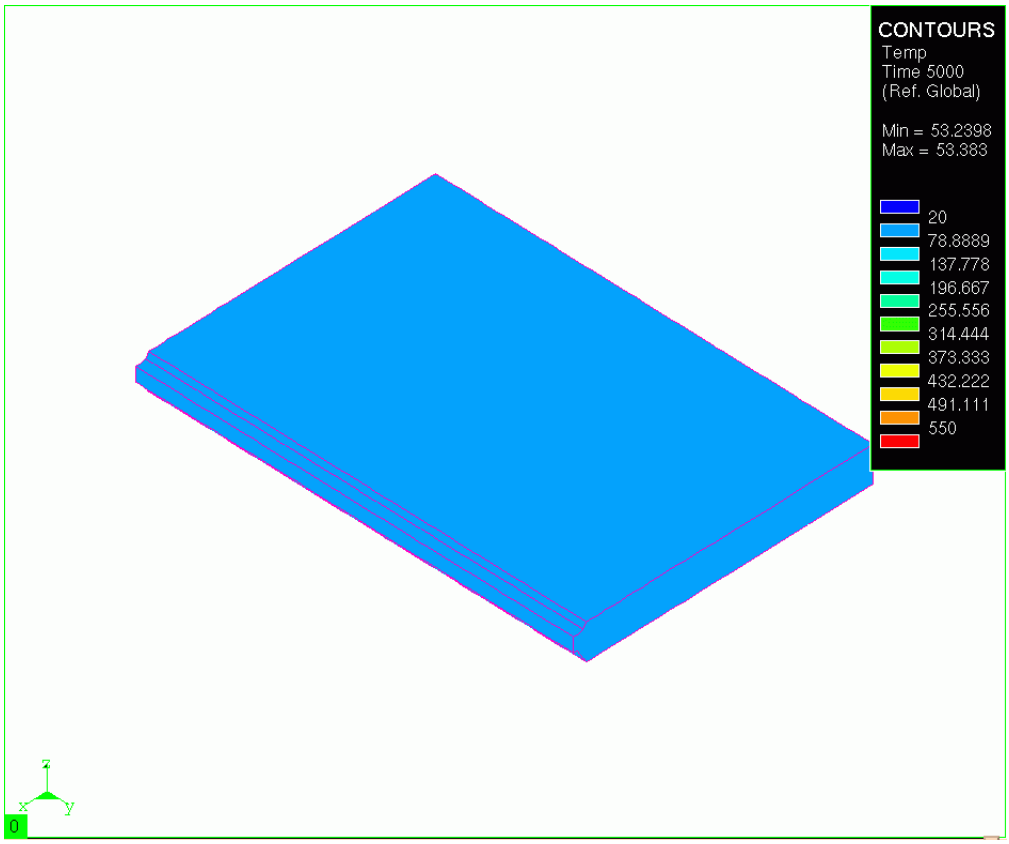

Fig. 6.3 Surface temperature distribution after the first weld pass of the butt joint model at t = 5000s.

Now that the thermal history has been determined, the residual stress distribution is calculated. As described in Chapter 5, a mechanical analysis stage corresponding to each thermal analysis stage is completed. The final von Mises residual stress state after cool-down is shown in Figure 6.4. It is interesting to note that on the majority of the external surfaces the residual stresses are minimal, and it is not until after the part is sectioned are the highest residual stresses

evident as shown in Figure 6.5. Also, it can be seen in Figure 6.5 that the von Mises stress distribution reaches a steady-state condition near the middle of the plate.

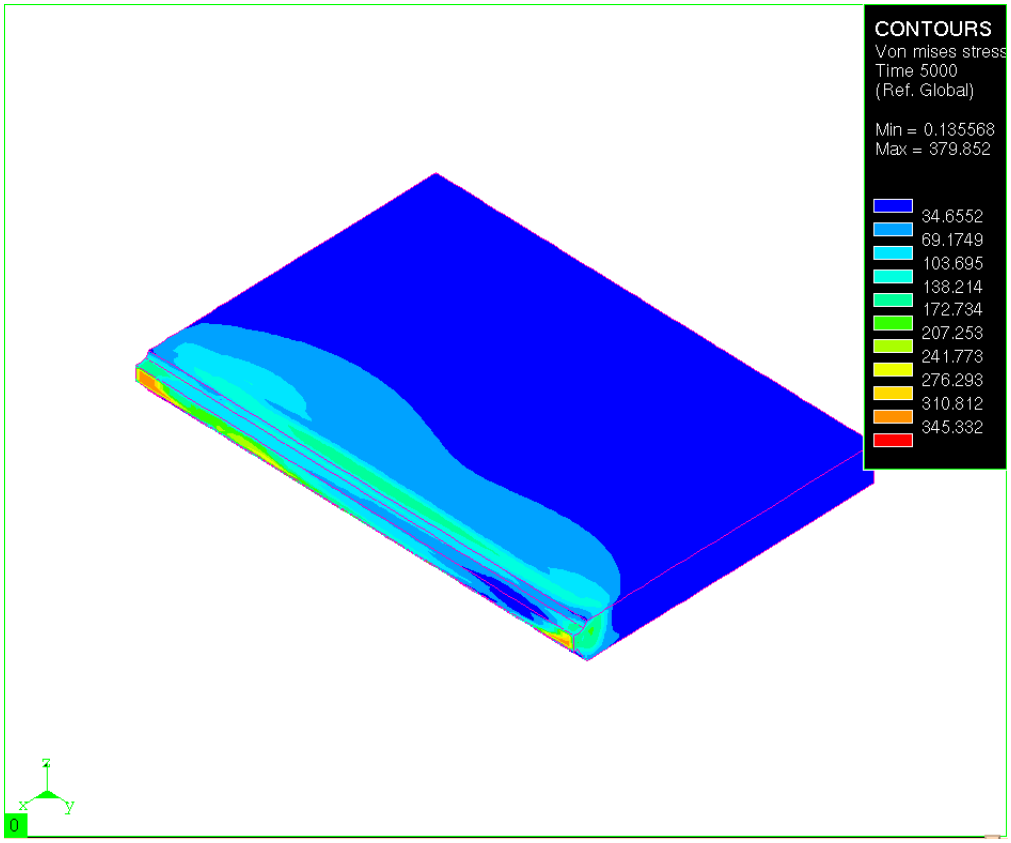

Fig. 6.4 Surface contours of the von Mises stress after the first weld pass of the butt joint model at t = 5000s.

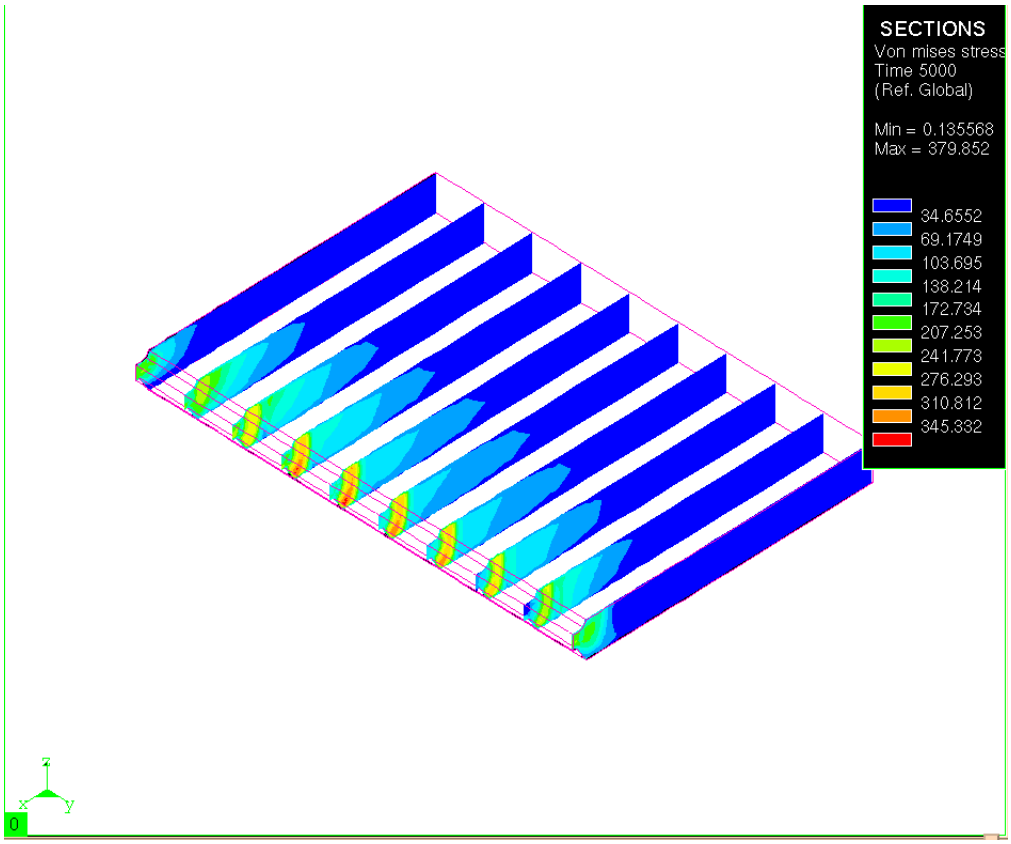

Fig. 6.5 Contours of the von Mises stress in several cross sections of the plate from Fig. 6.4.

It is interesting to see the evolution of the longitudinal normal stress, σ_{yy}, in cross sections of the plate normal to the welding direction. These stress distributions are shown in Figure 6.6, where the longitudinal normal stress is denoted as σ_{22} in the legend. Contours of σ_{yy} in the central cross section of the plate are shown in Figure 6.7. The stress distribution shown in

Figure 6.6 is similar to the distribution determined by Michaleris et al.[14], which is shown in Figure 6.8. The maximum value of σ_{yy} is within 3.6% of the maximum reported in Ref.[14].

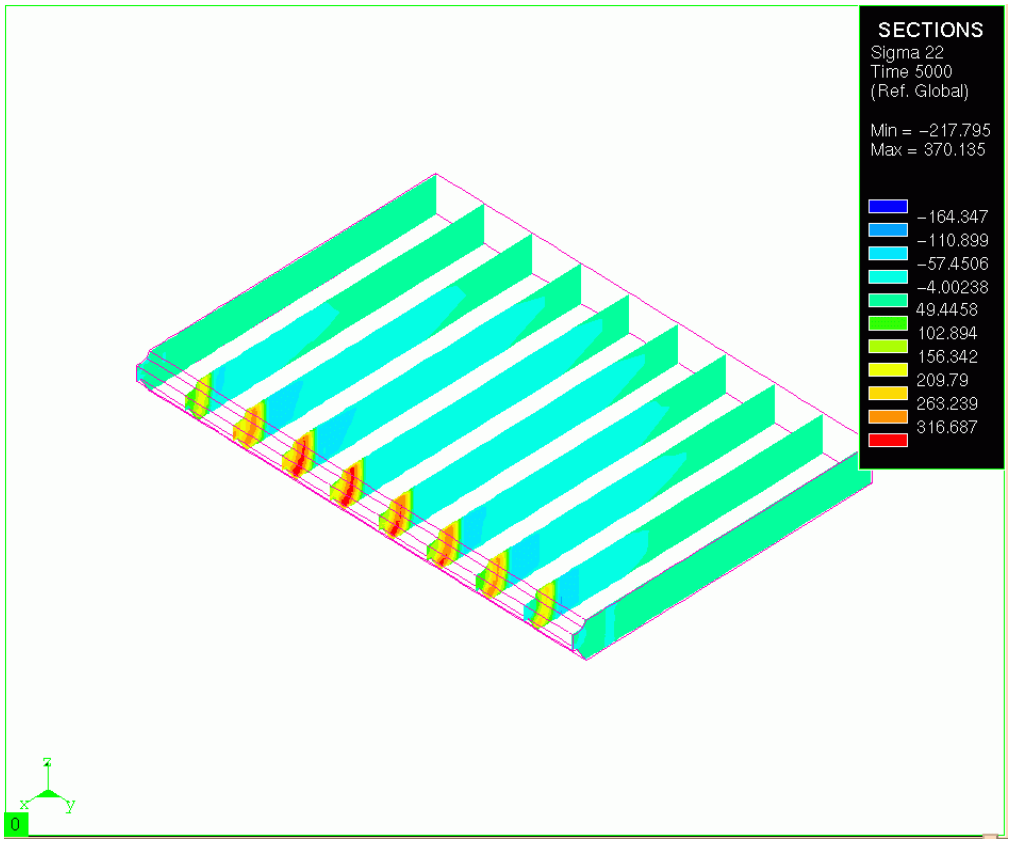

Fig. 6.6 Contours of the longitudinal normal stress in several cross sections of the plate after first weld pass at t = 5000s.

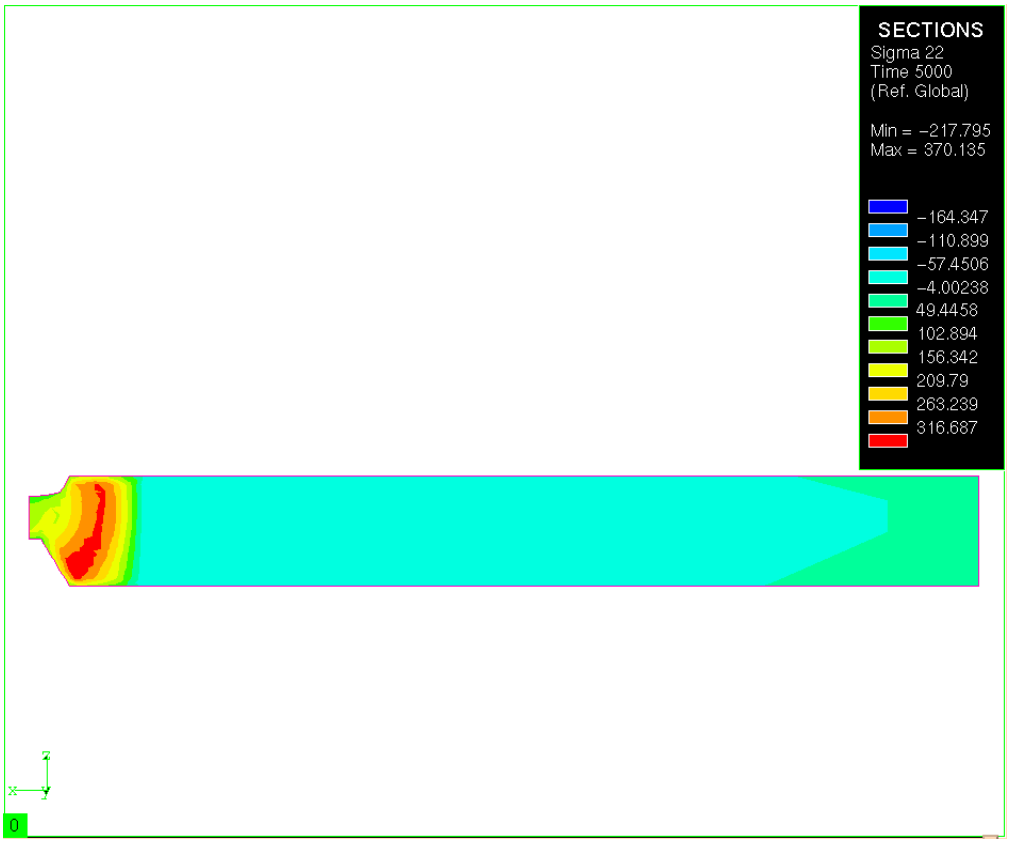

Fig. 6.7 Distributions of the longitudinal normal stress in the central cross section of the plate from Fig. 6.6

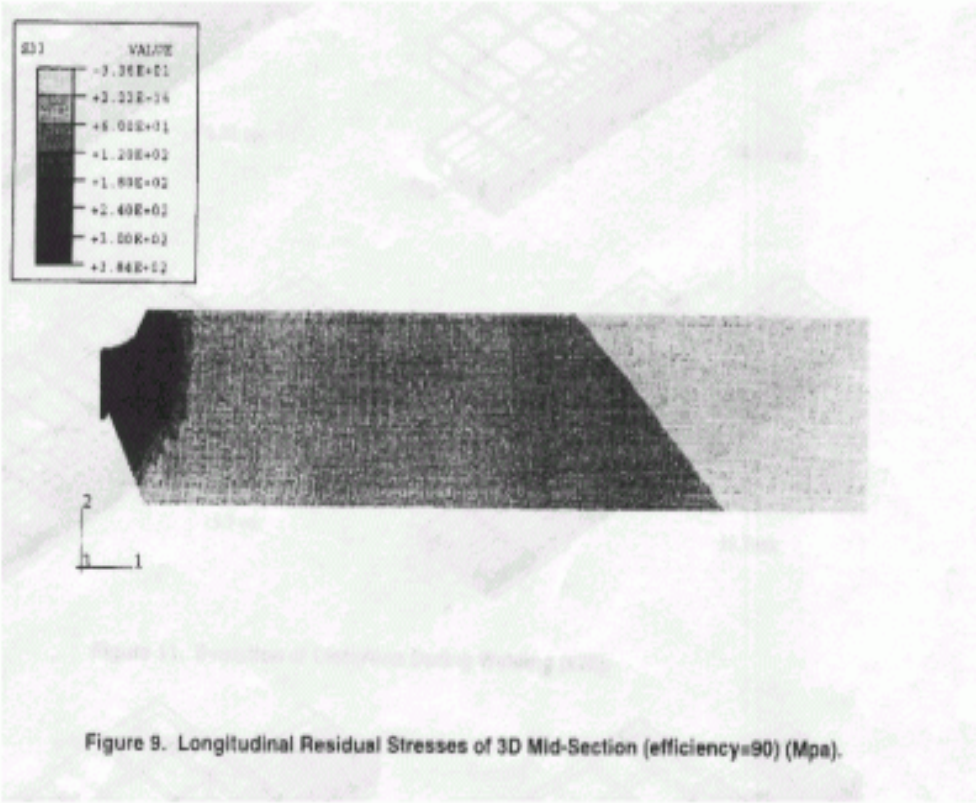

Fig. 6.8 Distribution of the longitudinal residual stress from Michaleris et al. [14]

6.1.2 Fully Transient Analysis

The fully transient analysis was performed using the element activation/de-activation option, with activation of 4 elements in front of the heat source. The analysis begins at t = 0 and continues to t = 50s as the weld arc progresses along the part using a time step of 0.5s. The distribution of the surface temperature at t = 45s and t = 50s, are shown in Figure 6.9 and Figure 6.10, respectively.

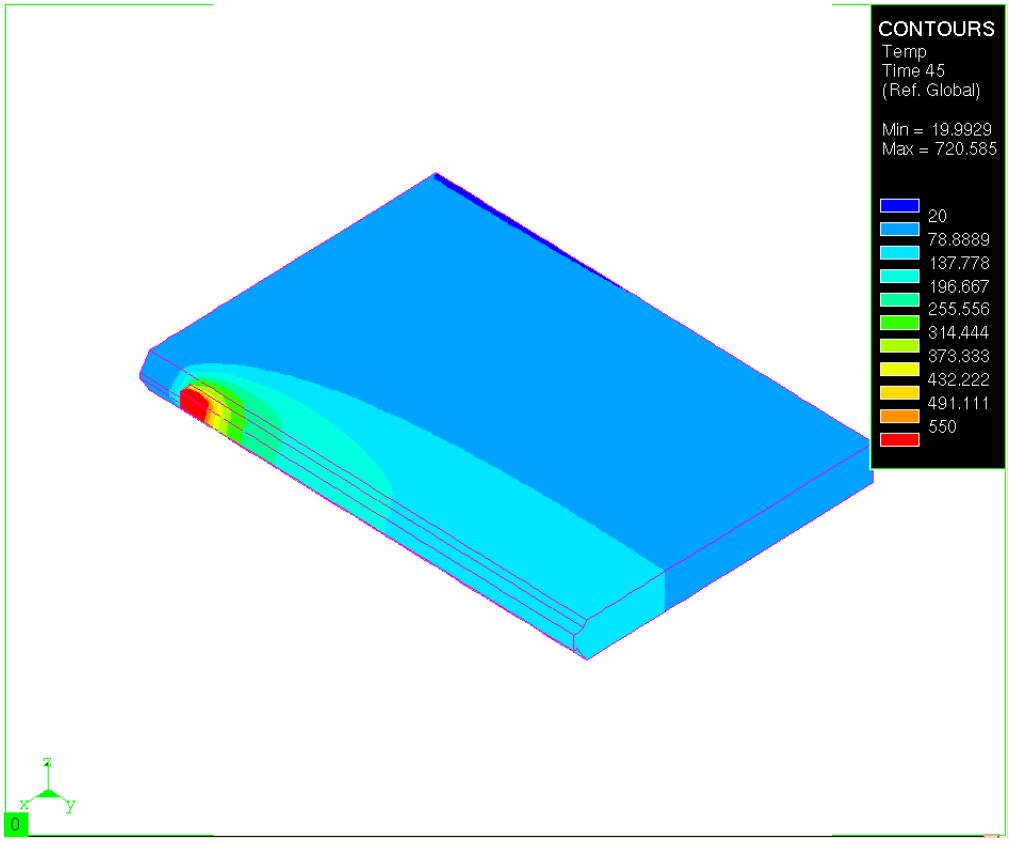

Fig. 6.9 Distribution of the surface temperature for the fully transient analysis of the butt joint at t = 45s.

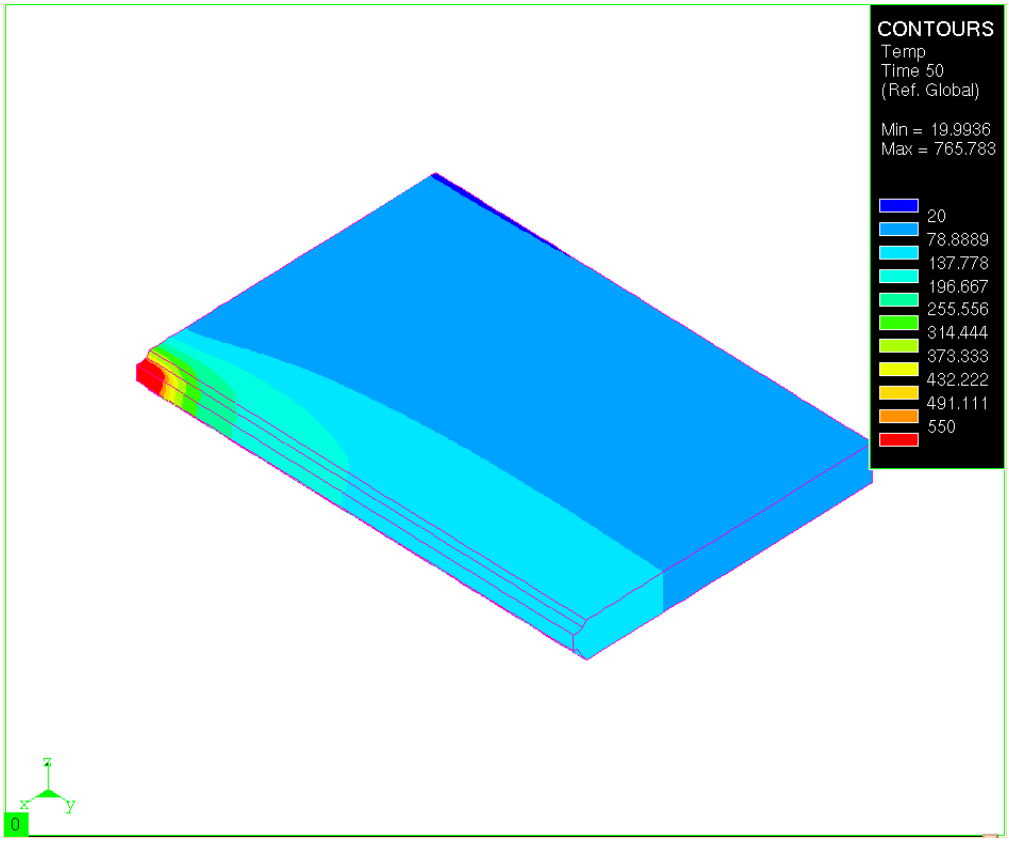

Fig. 6.10 Distribution of the surface temperature for the fully transient analysis of the butt joint at t = 50s.

As in the "moving reference frame" analysis, from t = 50s until 5000s, the weld arc is removed from the part and the part is allowed to cool. The final temperature in this case was 36^{o}C and it is shown in Figure 6.11.

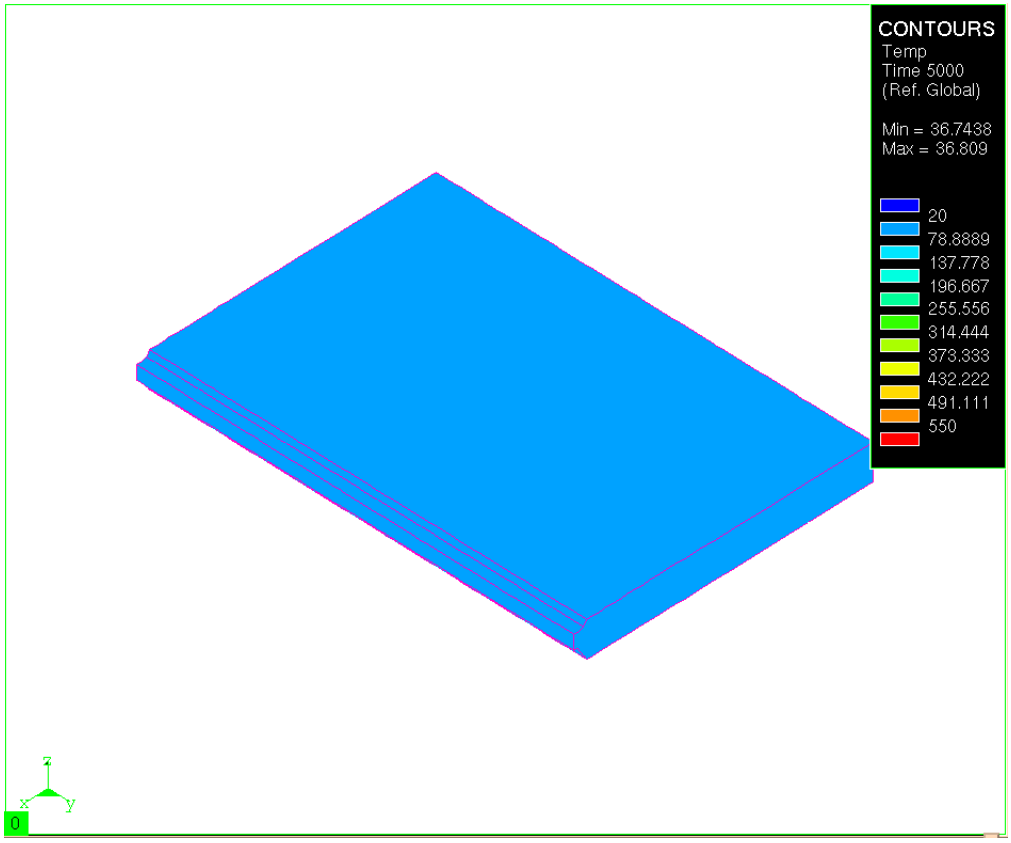

Fig. 6.11 Distribution of the surface temperature for the fully transient analysis of the butt joint at t = 5000s.

The mechanical analysis was performed to determine the final residual stress state after one weld pass. After cool-down, the final von Mises residual stress state is shown in Figure 6.12. Again the residual stresses on the surface do not reveal the highest stress magnitudes, and only after the part is sectioned are the highest residual stresses visible as shown in Figure 6.13. Also, it can be seen in Figure 6.13 that the stress state reaches a steady-state condition at the middle of the part.

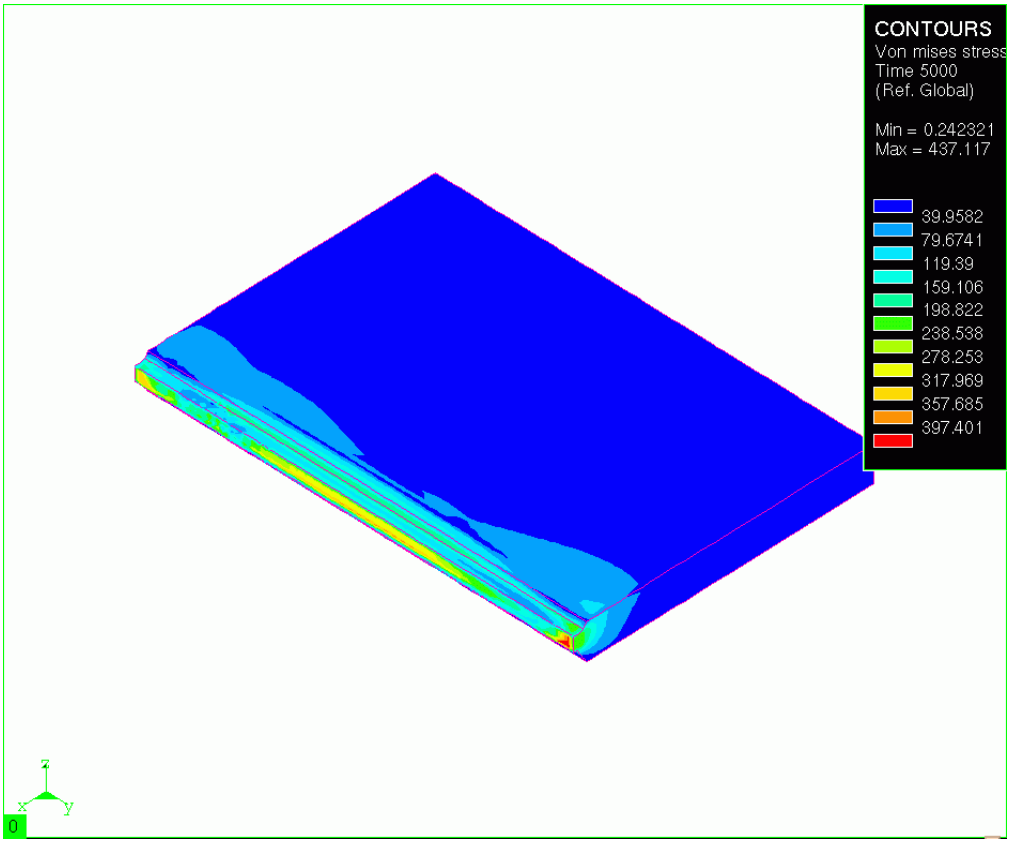

Fig. 6.12 Distribution of the von Mises stress over the plate's surface in the transient analysis of the butt joint at t = 5000s

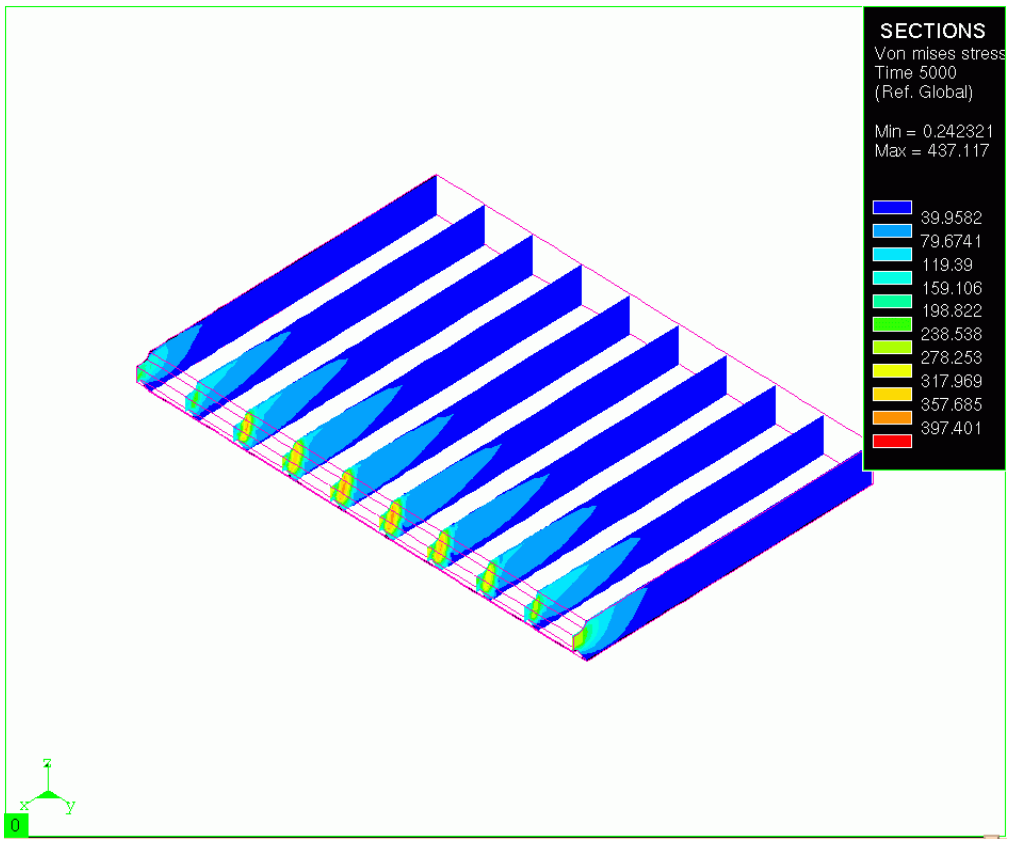

Fig. 6.13 Distribution of the von Mises stress in several cross sections of the plate from Fig. 6.12.

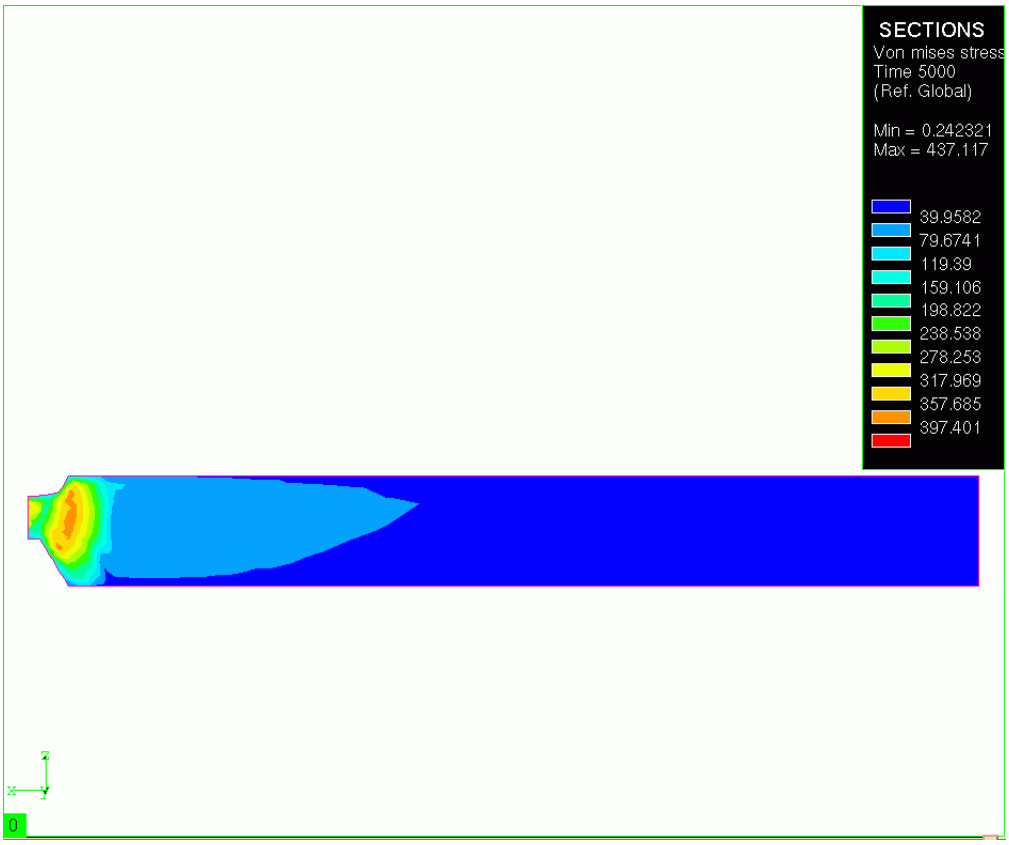

Fig. 6.14 Distribution of the von Mises stress in the central cross section of the plate from Fig. 6.13.

The distribution of the longitudinal normal stress in the fully transient analysis is similar to the distribution from the "moving reference frame" computation. The development of σ_{22} in the y-direction is shown in Figure 6.15, and the distribution of the longitudinal stress in the central cross section of the plate is shown in Figure 6.16. The maximum longitudinal stress value is found

to be 435 MPa, over-predicting the value reported by Michaleris et al. [14] by 13%. The distribution from Ref. [14] is shown in Figure 6.17.

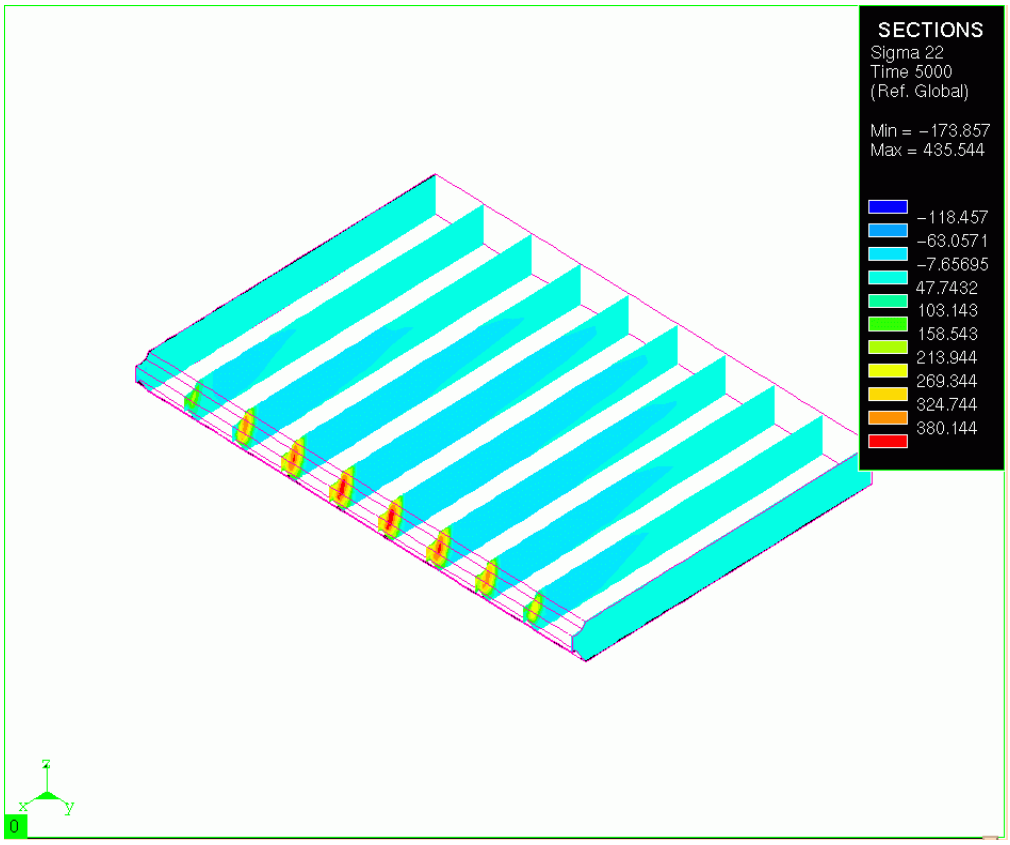

Fig. 6.15 Distribution of the longitudinal normal stress in several cross sections from the transient analysis of the butt joint at t = 5000s.

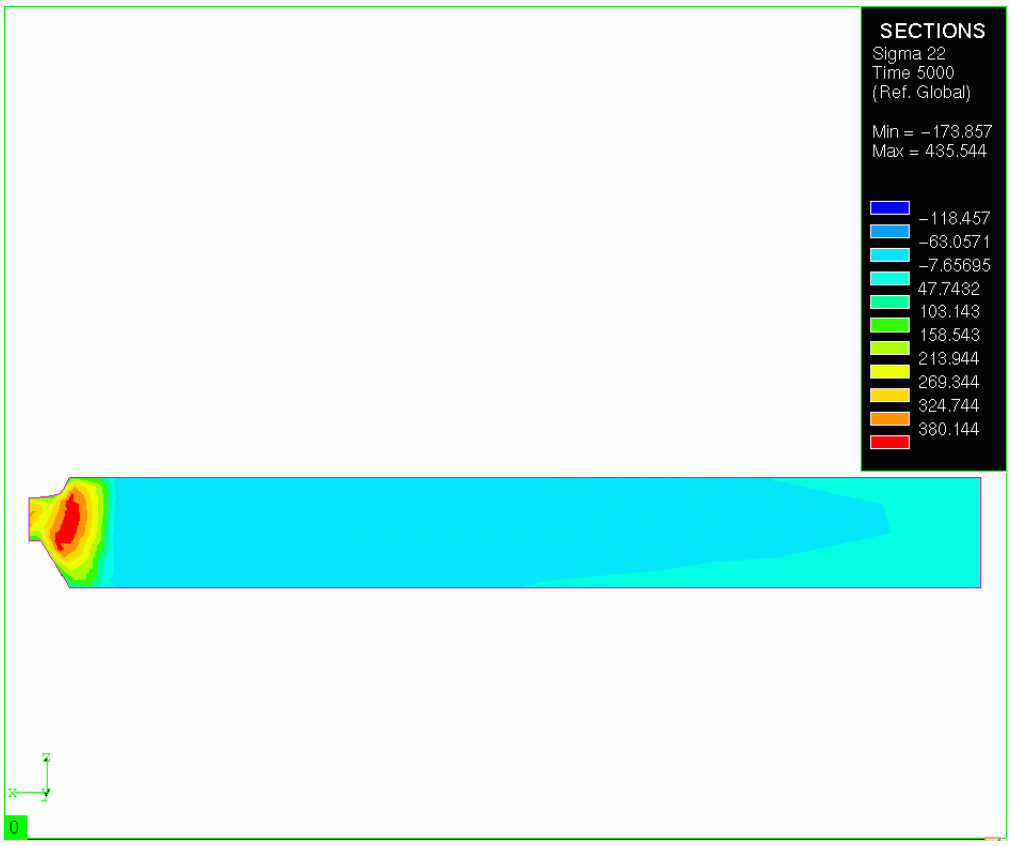

Fig. 6.16 Distribution of the longitudinal normal stress in the central cross section of the plate from Fig. 6.15.

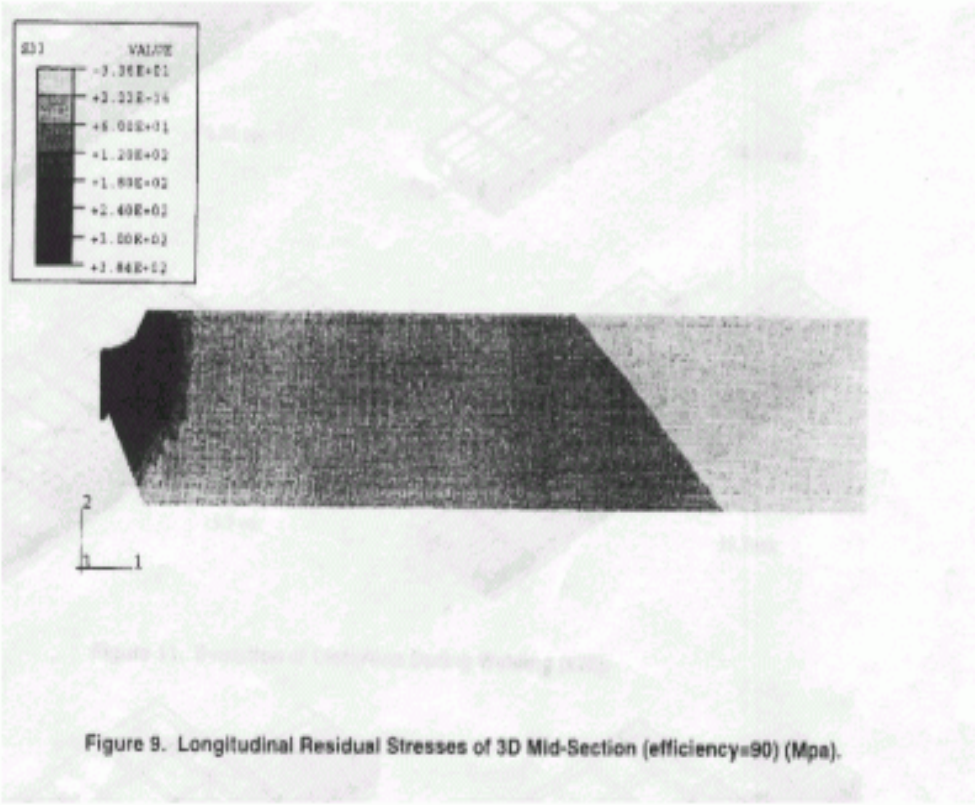

Fig. 6.17 Distribution of the longitudinal residual stress from Ref. [14]

6.2 Tee Section Analysis

After successfully duplicating the residual stress results for the butt-weld analysis, it was now possible to use SYSWELD to analyze the tee section joint. The complexity of the tee section analysis is doubled relative to the butt joint analysis due to the addition of the second weld bead. The solid tee section analysis was completed in three stages. The first stage consisted of the "moving reference frame" analysis, where the majority of the first weld pass from t = 0 to t = 45s

was completed in one computational step. The second stage of the analysis consisted of a transient analysis from t = 45s to 5000s using a time step of 0.5s. In these two stages, the weld arc traverses the work piece and then continues off into space beyond it. This second stage is equivalent to actually removing the arc from the work piece, and has the computational advantage of limiting the number of analysis files in SYSWELD. The third stage is a transient analysis simulating the deposit of the second weld bead from t = 5000s to 10,000s, where the weld arc was stepped along from start to finish. It was decided to allow the first weld bead to cool before depositing the second weld bead. Since the second weld bead is continued from a time after the first weld bead has cooled, only a transient analysis is possible. The transient analyses utilized element activation/de-activation to simulate weld deposit, with an element offset in front of the arc of 1 element. Similarly, the same process was applied to the solid-shell coupled tee section analysis, which will be discussed “Solid-Shell Coupled Tee Section Analysis” on page 143.

6.2.1 Tee Section “Moving Reference Frame” Analysis

As with the “moving reference frame” computation for the butt-weld analysis, element activation/ de-activation was not utilized. The computation begins at a time step of t = 45s, which at a weld arc velocity of 6 mm/s, puts the arc 270 mm along the 300 mm part. Again, the software performs the calculation from t = 0 to 45s in one computational step. The temperature distribution at t = 45s is shown Figure 6.18.

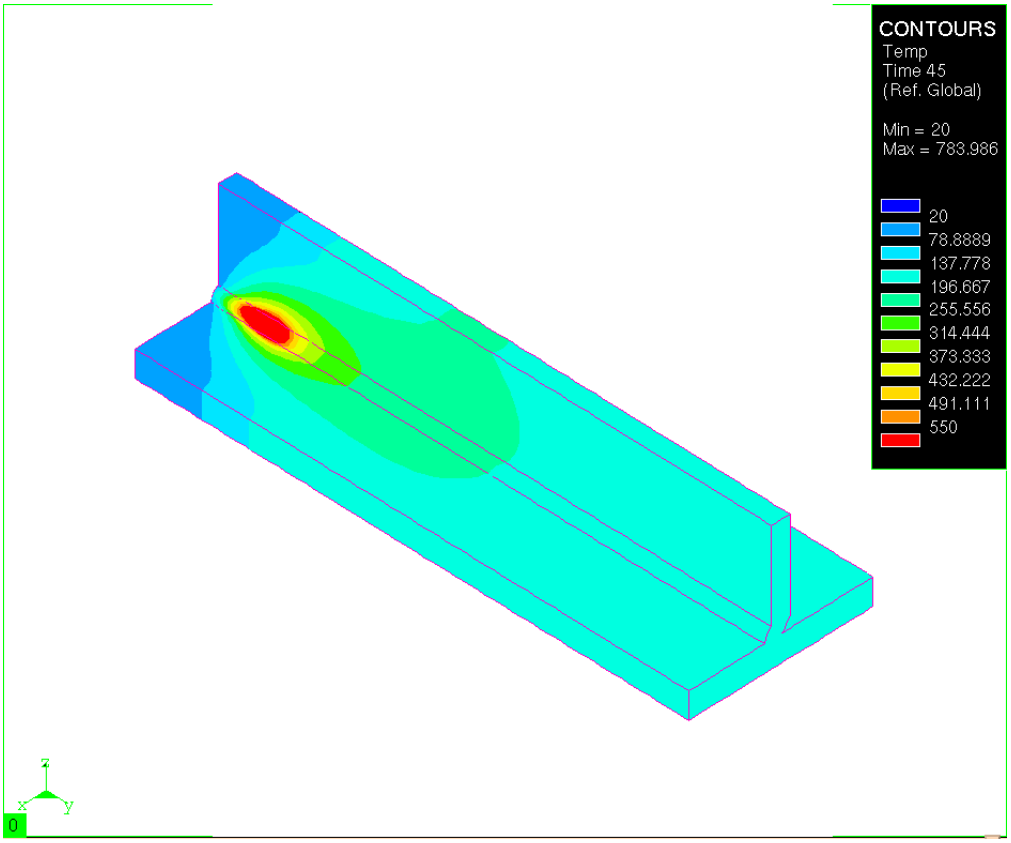

Fig. 6.18 Distribution of the surface temperatures for the first weld pass of the tee joint model at t = 45s.

The next stage of the analysis involves a fully transient calculation in which the weld arc is stepped along the remainder of the part and into space beyond the part using a time step of 0.5 s until t = 5000 s. The temperature distribution at t = 50 s is shown in Figure 6.19. From t = 50 s until 5000 s, the weld arc is beyond the part and the part is allowed to cool. Utilizing the same free

convection coefficient as in the butt-weld analyses, the final temperature was 52^{o}C, as is shown in Figure 6.20

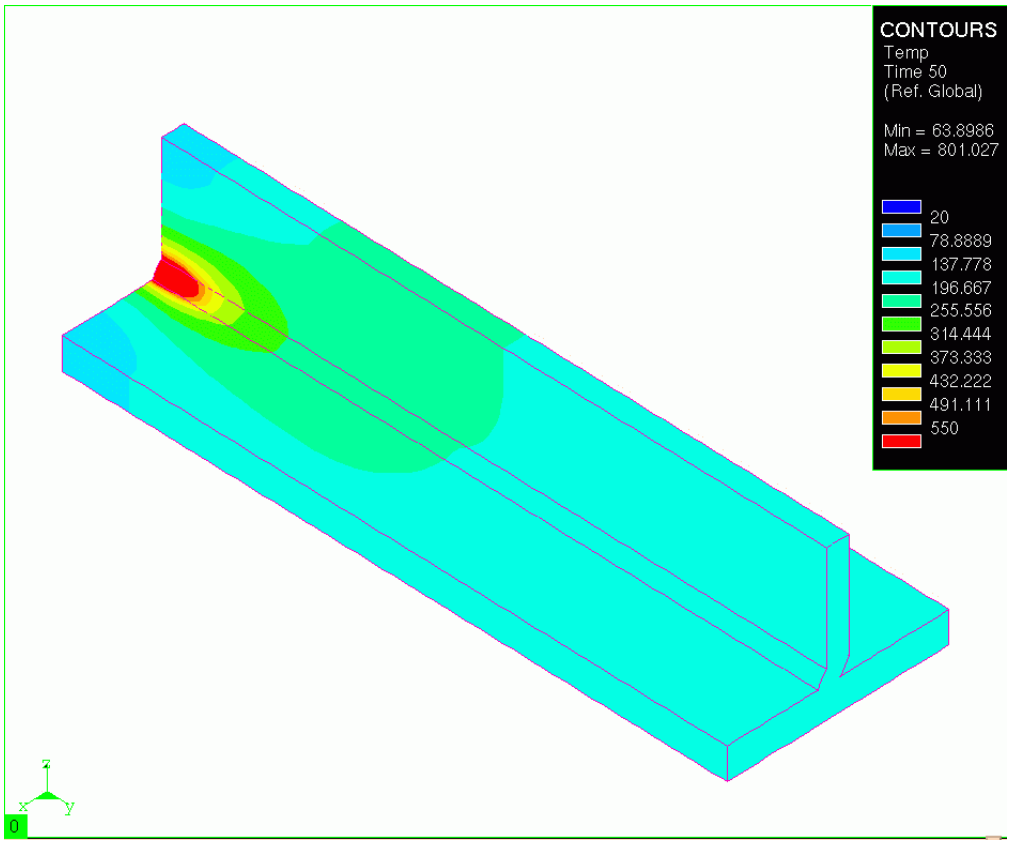

Fig. 6.19 Distribution of the surface temperatures for the first weld pass of the tee joint model at t = 50s.

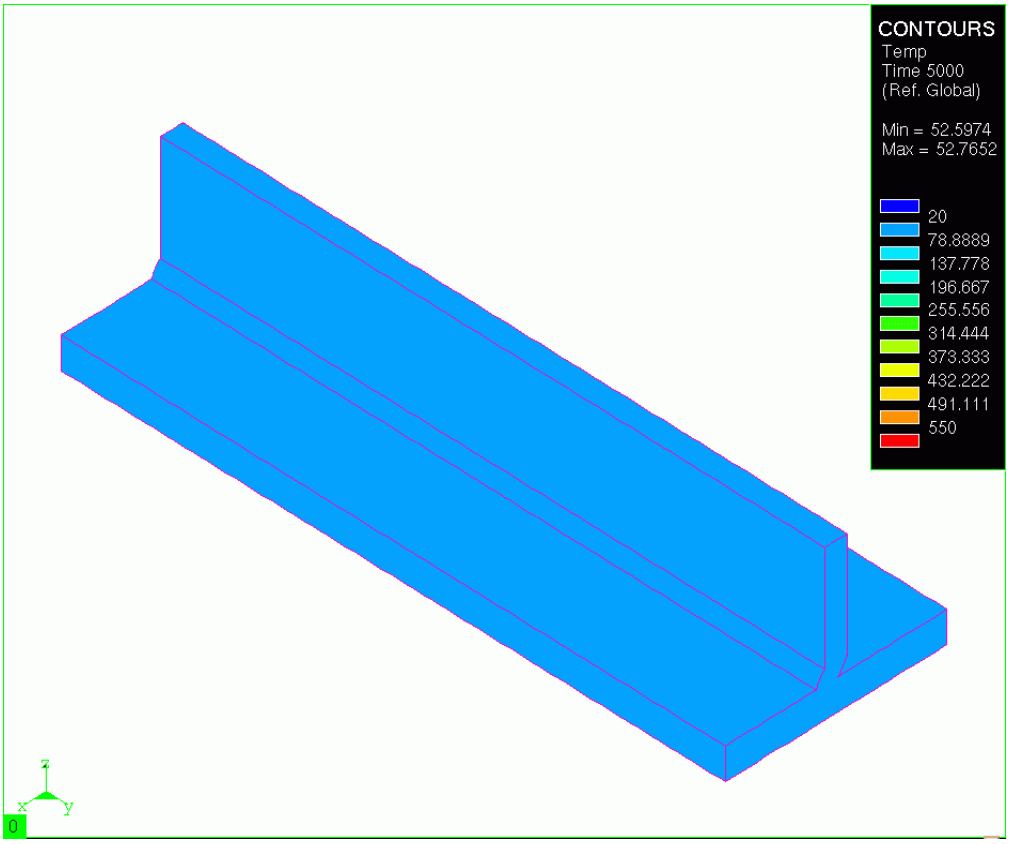

Fig. 6.20 Distribution of the surface temperatures after the first weld pass of the tee joint model at t = 5000s.

To complete the second weld pass, the transient analysis steps the weld arc from t = 5000s to 10000s using a time step of 0.5s. The temperature distributions at t = 5045s, 5050s, and 10000s are shown in Figure 6.21, Figure 6.22, and Figure 6.23, respectively.

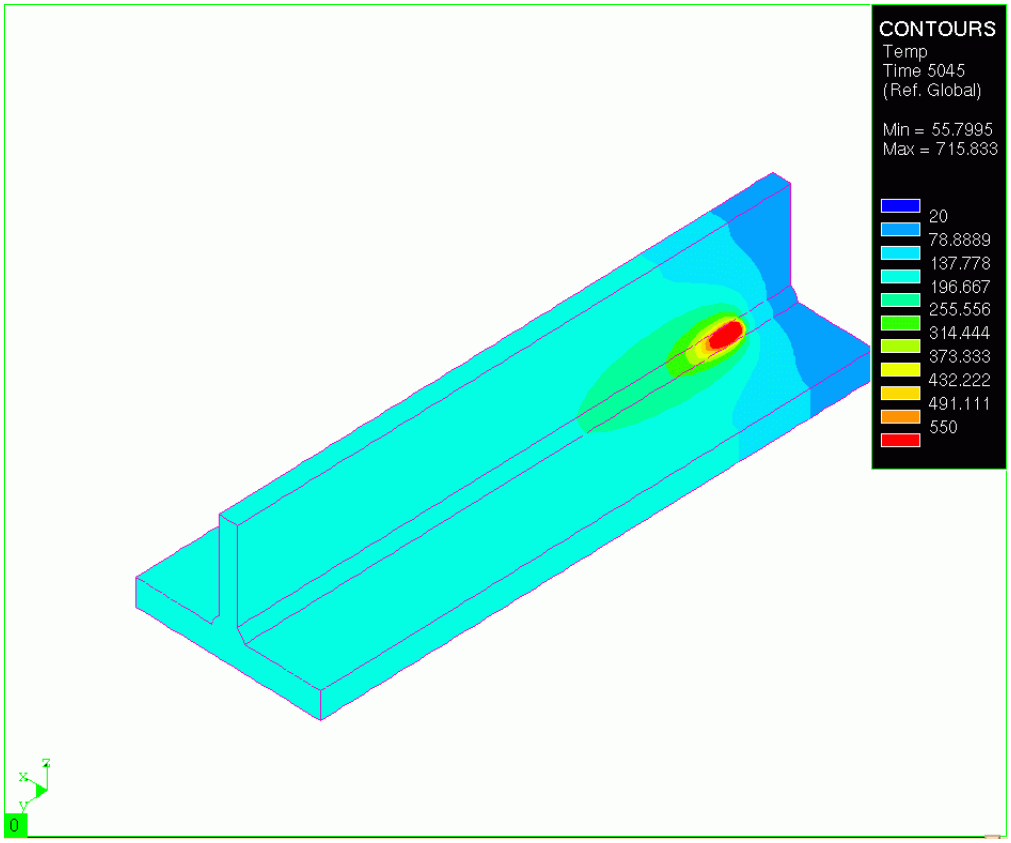

Fig. 6.21 Distribution of the surface temperatures for the second weld pass of the tee joint model at t = 5045s.

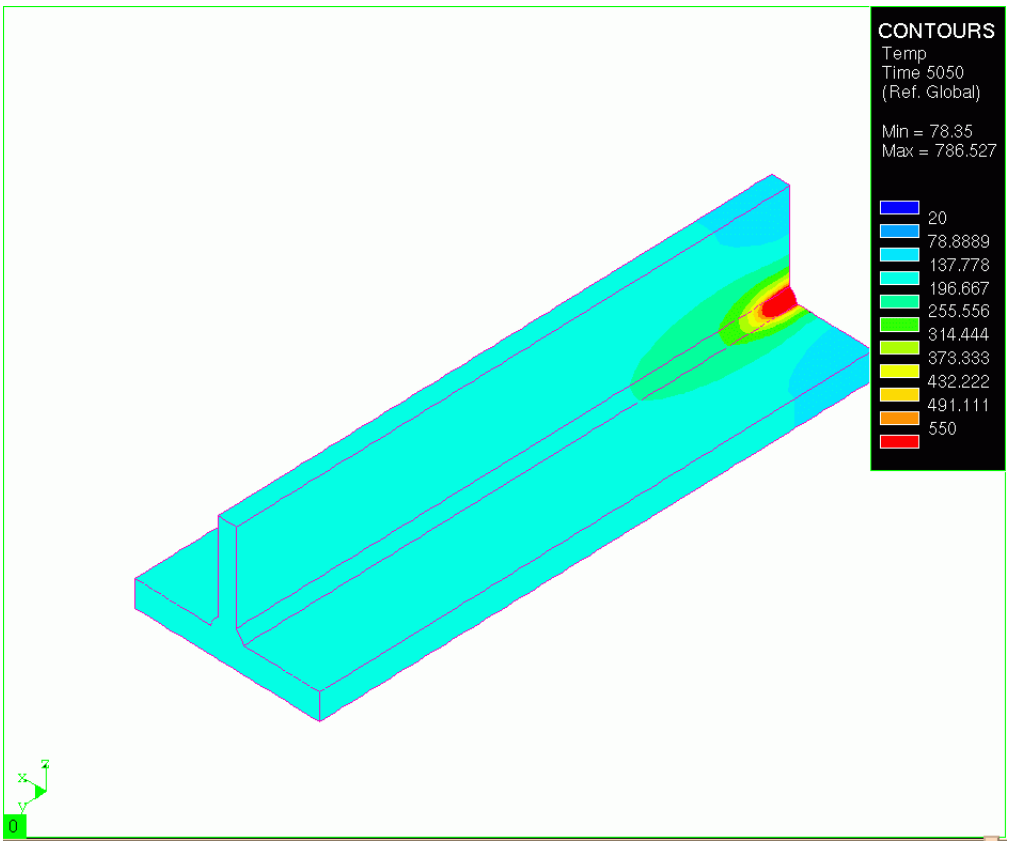

Fig. 6.22 Distribution of the surface temperatures for the second weld pass of the tee joint model at t = 5050s.

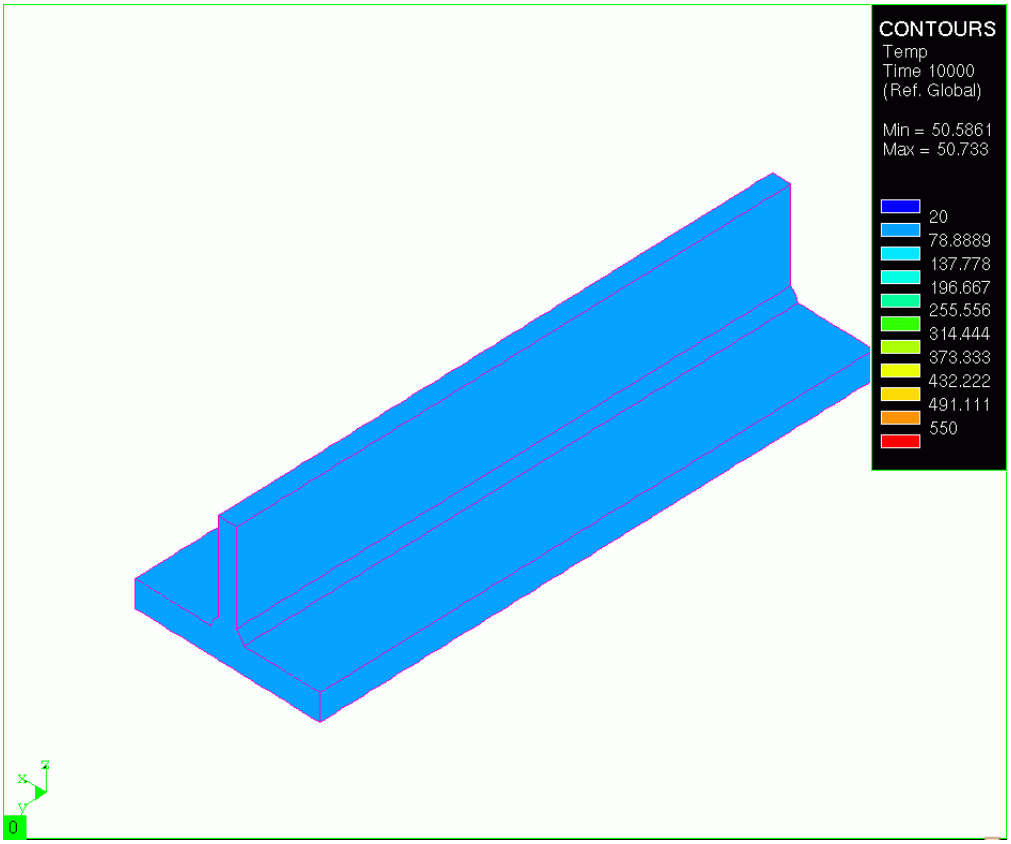

Fig. 6.23 Distribution of the surface temperatures after the second weld pass of the tee joint model at t = 10,000s.

During the thermal computation, the metallurgical composition is calculated. The decimal percentage of the base metal, or phase 1, in the work piece after the first weld pass is shown in the contour plot of the tee joint in Figure 6.24. A contour plot of phase 1 over the cross section is

shown in Figure 6.25, and it can be seen in the figure that composition of phase 1 in the weld zone varies from about 40% to 95%.

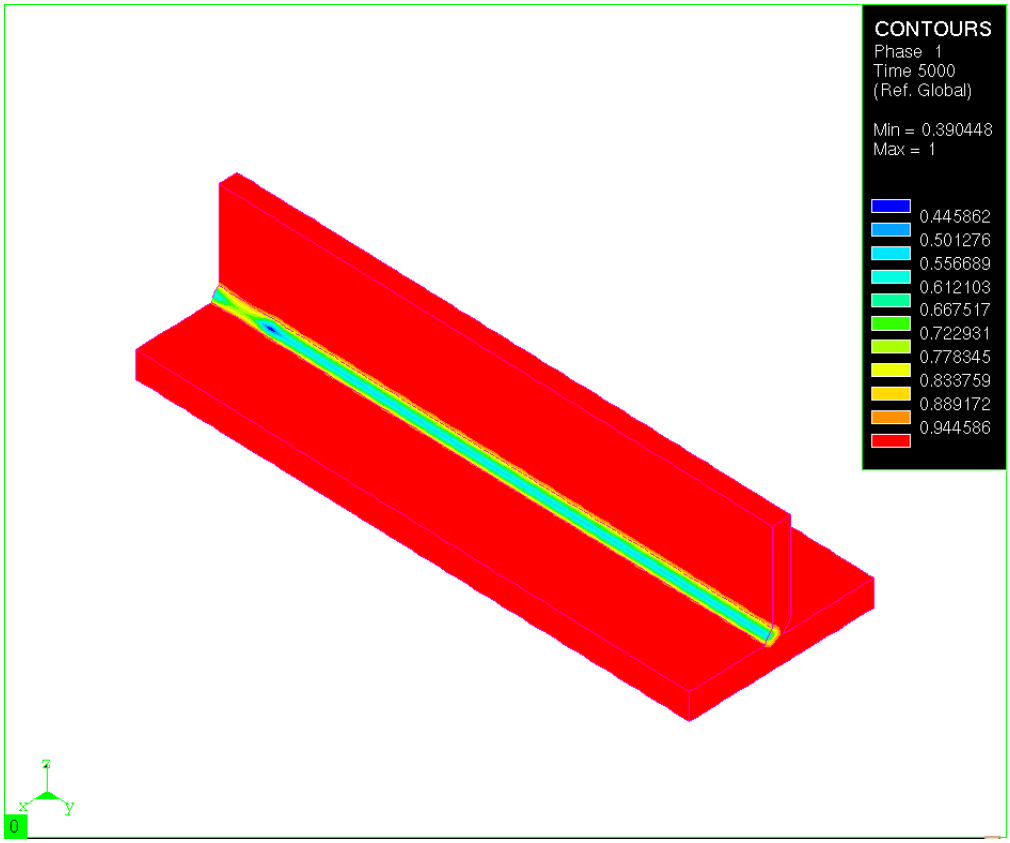

Fig. 6.24 Surface distribution of phase 1 material after the first weld pass of the tee joint at t = 5000s

Fig. 6.25 Distribution of phase 1 material over the cross section after the first weld pass of the tee joint at t = 5000s

The phase 1 constitution after completion of the second weld pass is shown in Figure 6.26 and Figure 6.27. Again the change in phase 1 concentration is from about 40% to 95% in the second weld bead area, but the penetration of the weld zone into the joint from the second bead is not as great as is the penetration of the weld zone from the first pass. This lack of penetration of the second bead weld zone was due to the slightly lower temperatures the work piece experienced

in the transient analysis for the second weld pass. In general, it was expected that the weld zone, and consequently the heat affected zone, would be much larger. This relatively small weld zone may be due to the fact that the metallurgical properties were estimated from the available literature. By adjusting the parameters of dissolution temperature T_r, the time to dissolution t_r, the enthalpy of metastable solvus Q_s, and the energy for activation of the diffusion process of the less mobile of the alloy elements Q_d as described in Equation (2.1) on page 27, a larger heat affected zone could be produced. Unfortunately, the long computation times required for these analyses prevented further investigation into the metallurgical parameters.

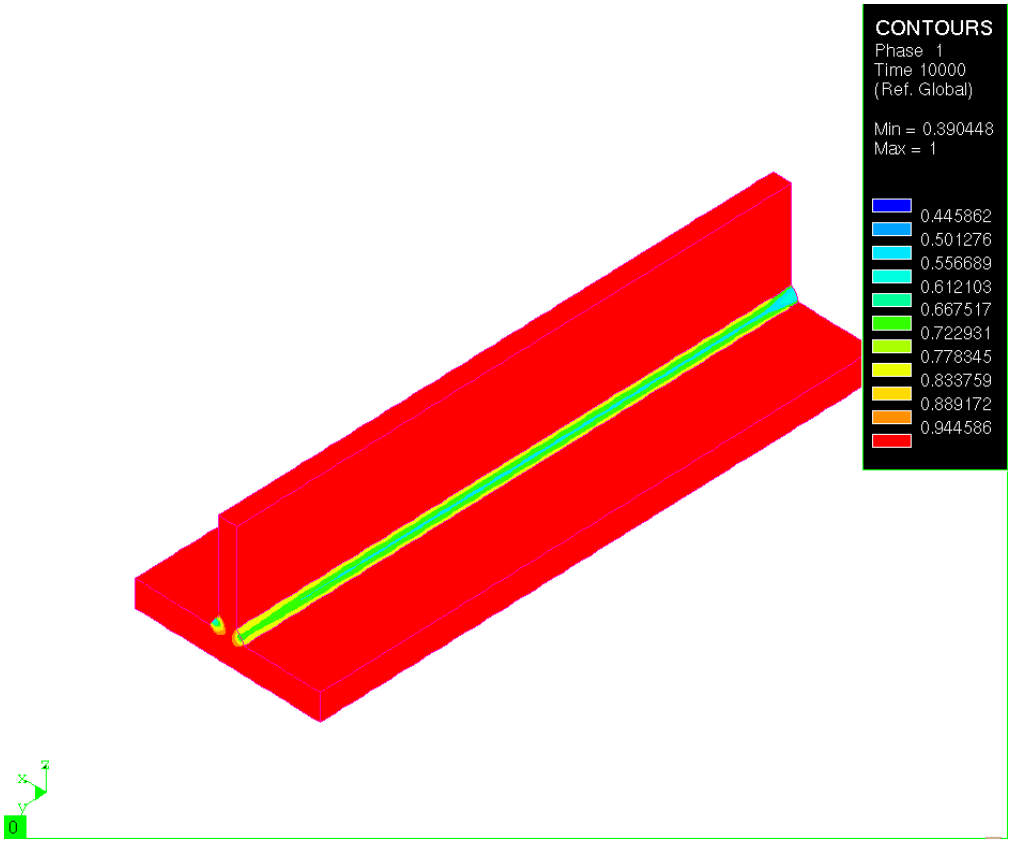

Fig. 6.26 Surface distribution of phase 1 material after the second weld pass of the tee joint at t = 10,000s

Fig. 6.27 Distribution of phase 1 material over the cross section after the second weld pass of the tee joint at t = 10,000s

After completion of the thermal analyses, the mechanical analyses were executed. The residual stress state was computed for the first weld pass and then the second weld pass. After cool-down of the first weld bead at t = 5000s, the von Mises residual stress state is computed and a surface contour plot of it is shown in Figure 6.28. The residual stresses on the surface are low, but the cross-sectional plots of the residual stresses shown in Figure 6.29 indicate that the highest

magnitudes occur on the interior of the work piece. Also, the stress state reaches a steady-state condition at the middle of the part as shown in Figure 6.29.

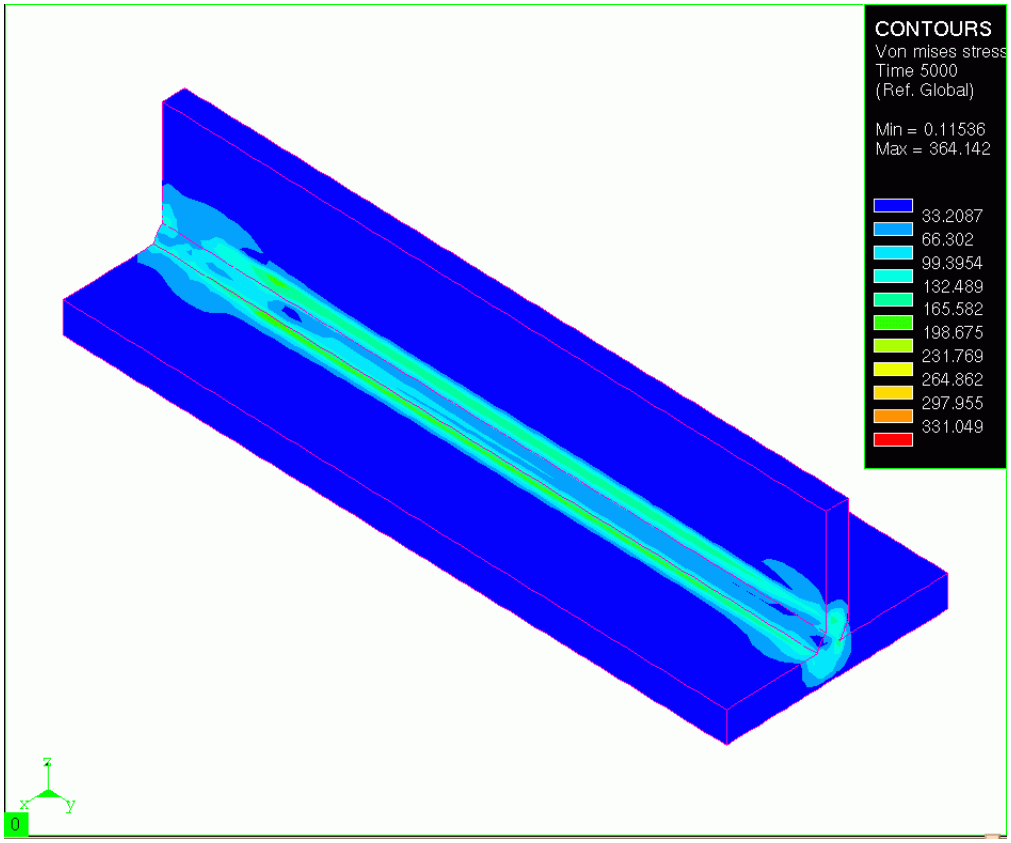

Fig. 6.28 Surface distribution of the von Mises stress after the first weld pass of the tee joint at t = 5000s

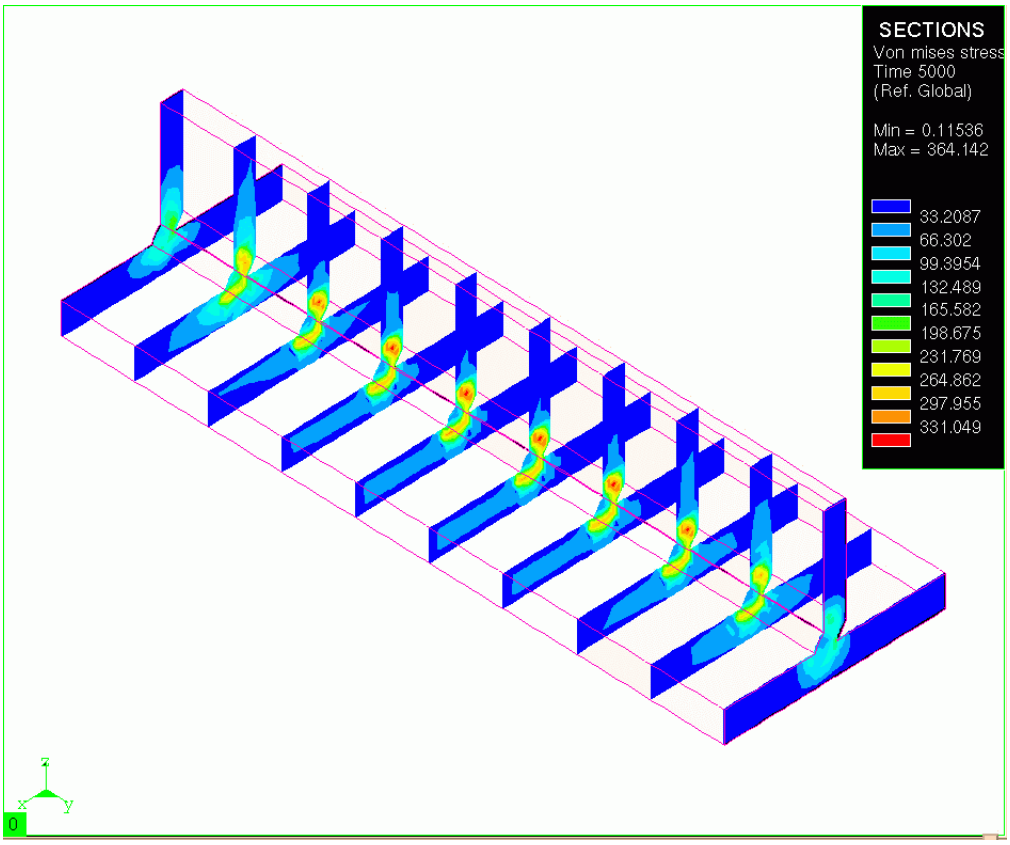

Fig. 6.29 Distribution of the von Mises stress in several cross sections after the first weld pass of the tee joint at t = 5000s

The von Mises stress distribution over the central cross section of the work piece is shown in Figure 6.30. It is interesting to note that the maximum value of the residual stress is 364 MPa, which is nearly equal to the yield strength of 400 MPa.

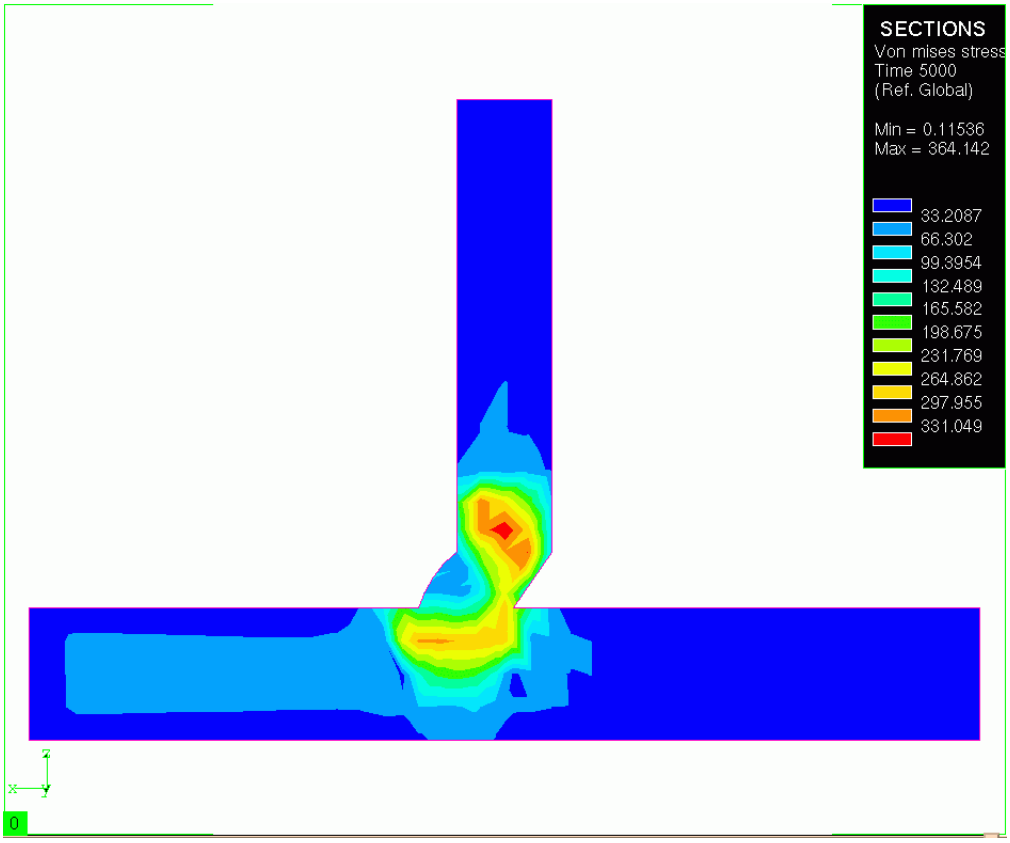

Fig. 6.30 Distribution of the von Mises stress over the central cross section after the first weld pass of the tee joint at t = 5000s

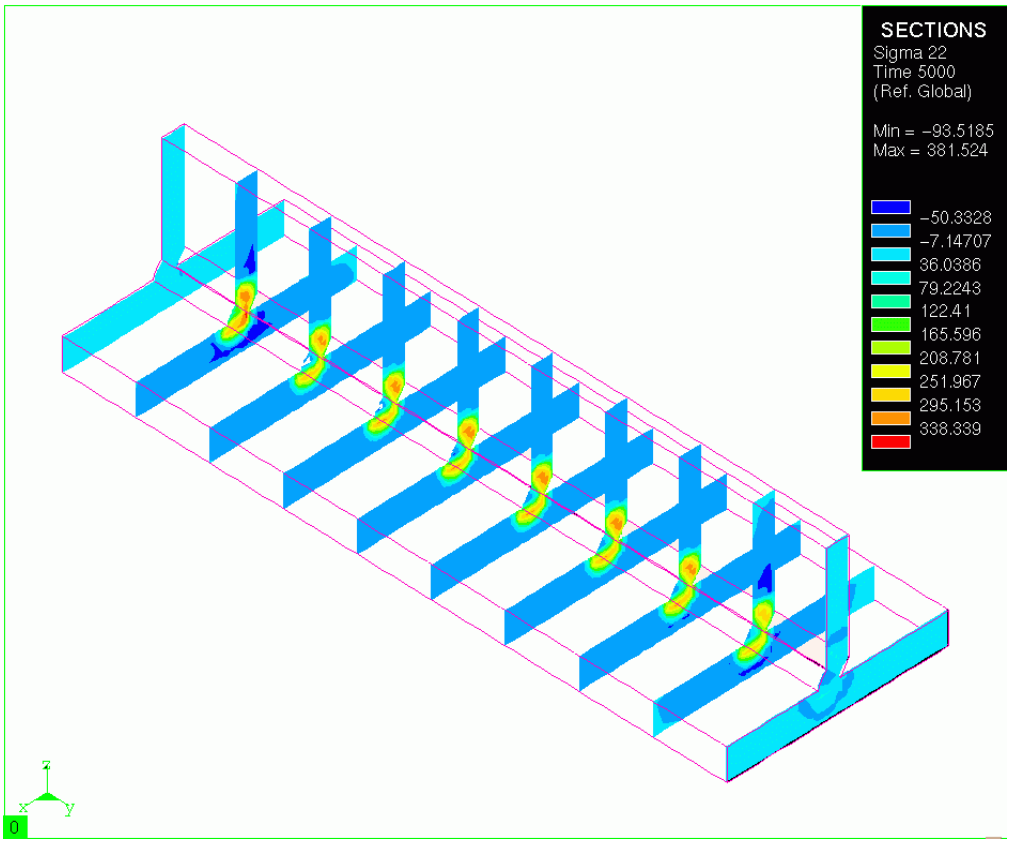

Fig. 6.31 Distribution of the longitudinal normal stress in several cross sections after the first weld pass of the tee joint at t = 5000s

The distribution of the longitudinal normal stress over several cross sections of the tee joint is shown in Figure 6.31. Again, after sectioning it is apparent that a steady-state condition is attained in the central cross sections of the work piece. The distribution of the longitudinal normal stress in a central cross section is shown in Figure 6.32. Examining this stress state we find the longitudinal normal stress is tensile within the base plate material at the juncture of the two plates,

while this stress component is slightly compressive within the first weld bead. The stress state within the weld bead is different than that found within the weld bead of the butt-weld where the longitudinal normal stresses were tensile.

Fig. 6.32 Distribution of the longitudinal normal stress over the central cross section after the first weld pass of the tee joint at t = 5000s

Continuing on to the final stress state after the second weld bead has been deposited, the von Mises stress after cool-down is depicted in Figure 6.33. Sectioning the part as shown in Figure 6.34 again reveals the steady-state reached in the central cross sections of the work piece. The distribution of the residual stress state in the central cross section is shown in Figure 6.35. Examining the stress state in this central cross section, notice that the peak magnitudes are as high as 370 MPa, which is just below the yield strength of 400 MPa.

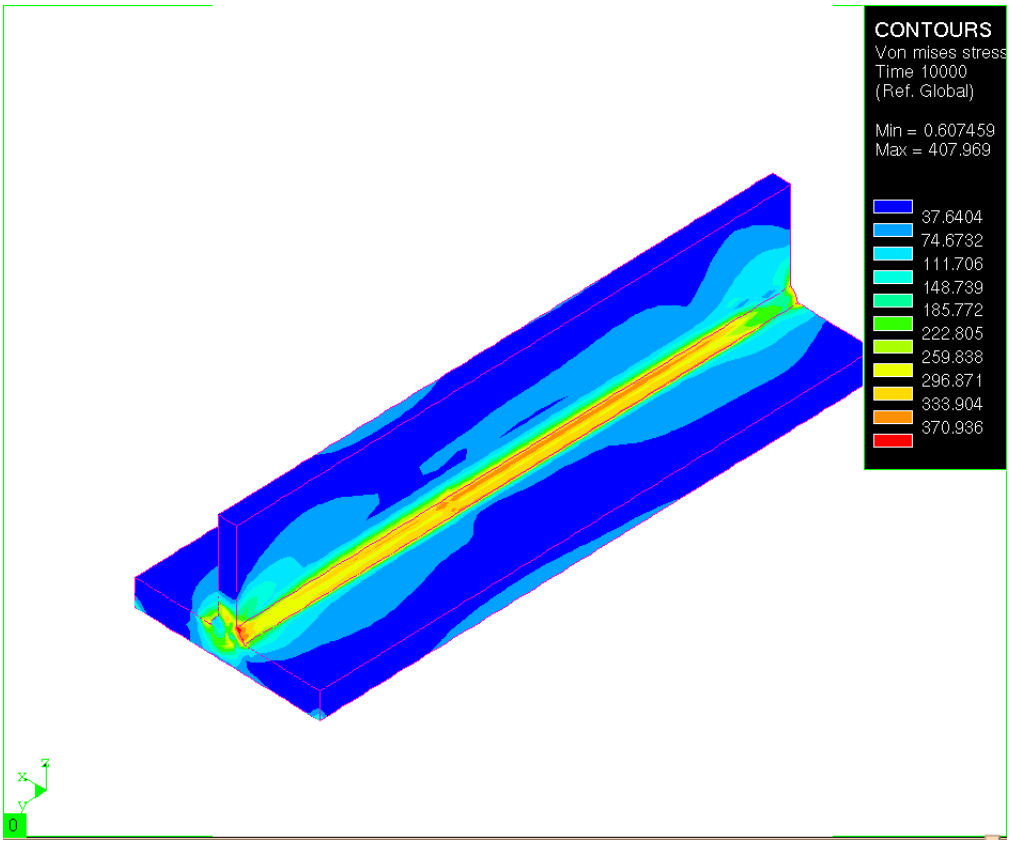

Fig. 6.33 Surface distribution of the von Mises stress after the second weld pass of the tee joint at t = 10,000s

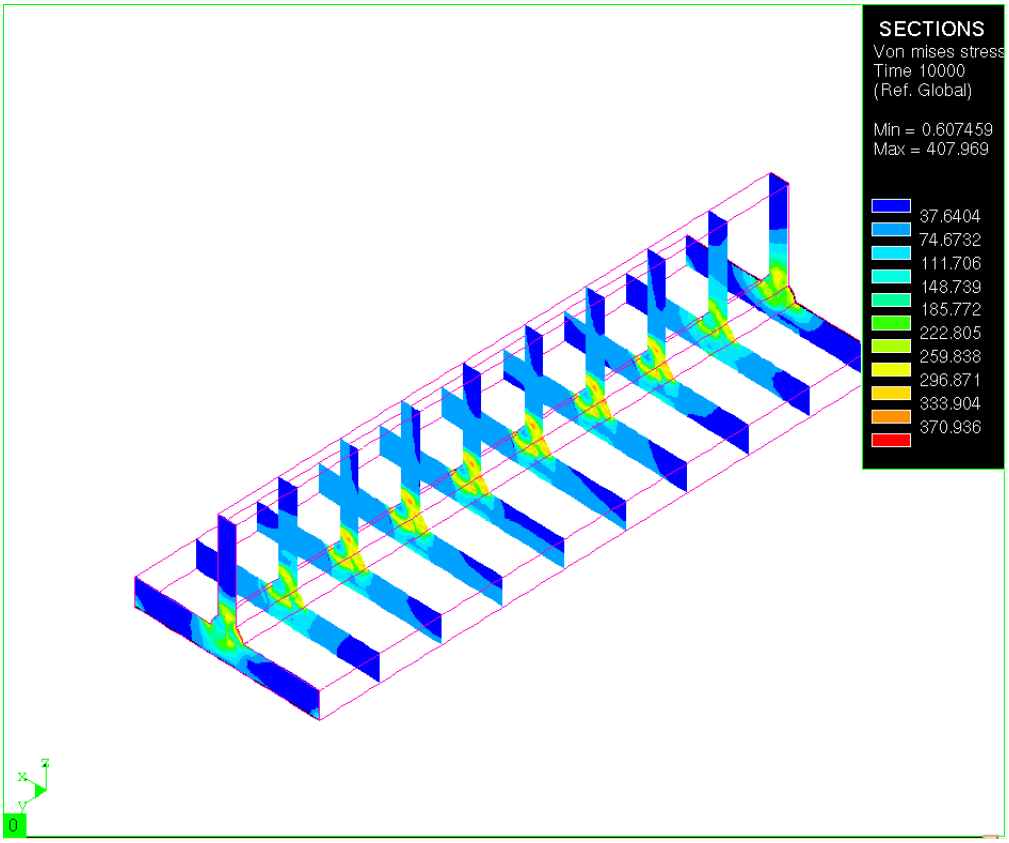

Fig. 6.34 Distribution of the von Mises stress in several cross sections after the second weld pass of the tee joint at t = 10,000s

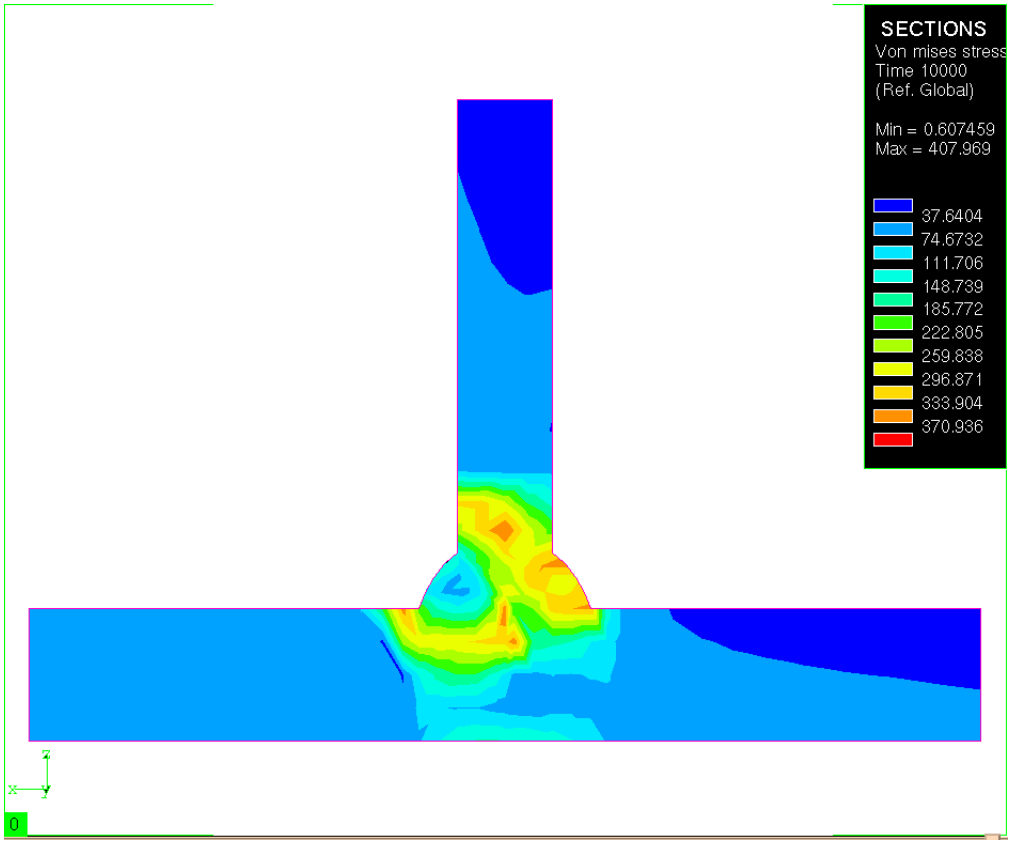

Fig. 6.35 Distribution of the von Mises stress over the central cross section after the second weld pass of the tee joint at t = 10,000s

The longitudinal normal stress state in several cross sections of the work piece is shown in Figure 6.36. The steady-state attained at the central cross section is shown in Figure 6.37. The longitudinal normal stress state within the second weld bead is tensile, reaching 416 MPa. Compared to the low compressive stress within the first weld bead, this was unexpected. Remembering that the first weld bead was deposited using a “moving reference frame” simulation, while the second weld bead was deposited with a fully transient analysis, it was

decided to further investigate the type of analysis on the response by performing a fully transient analysis under which both weld beads are deposited through transient simulations.

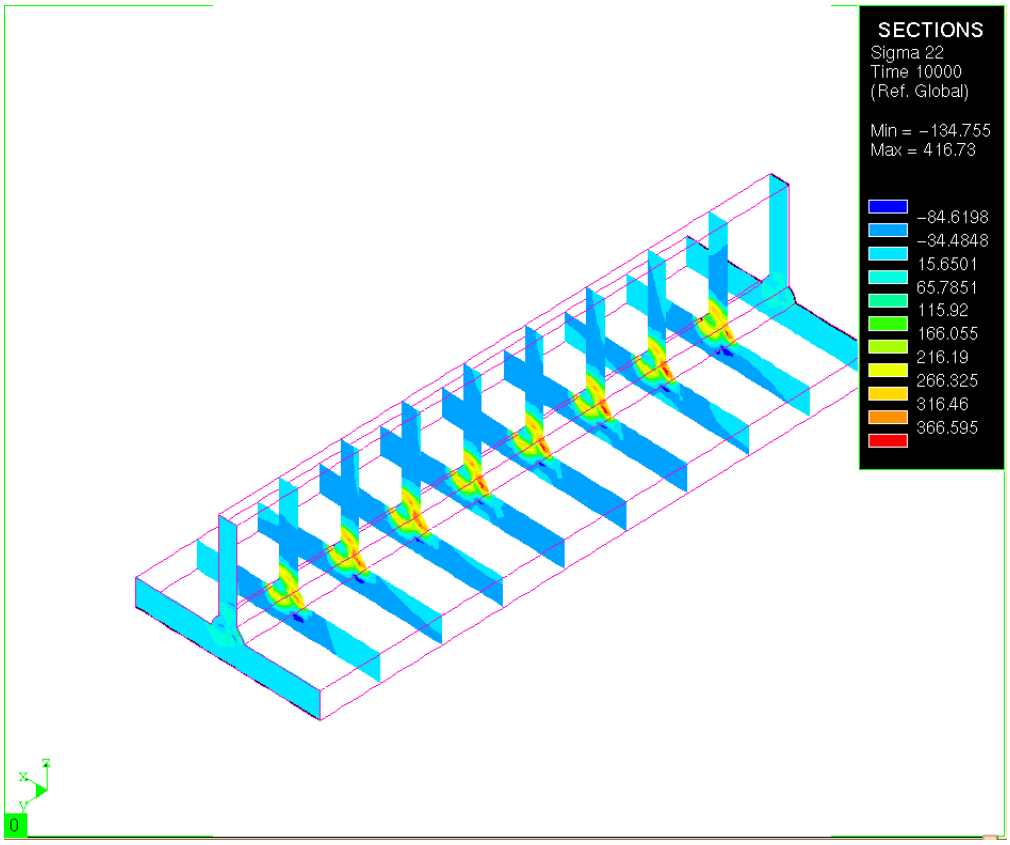

Fig. 6.36 Distribution of the longitudinal normal stress in several cross sections after the second weld pass of the tee joint at t = 10,000s

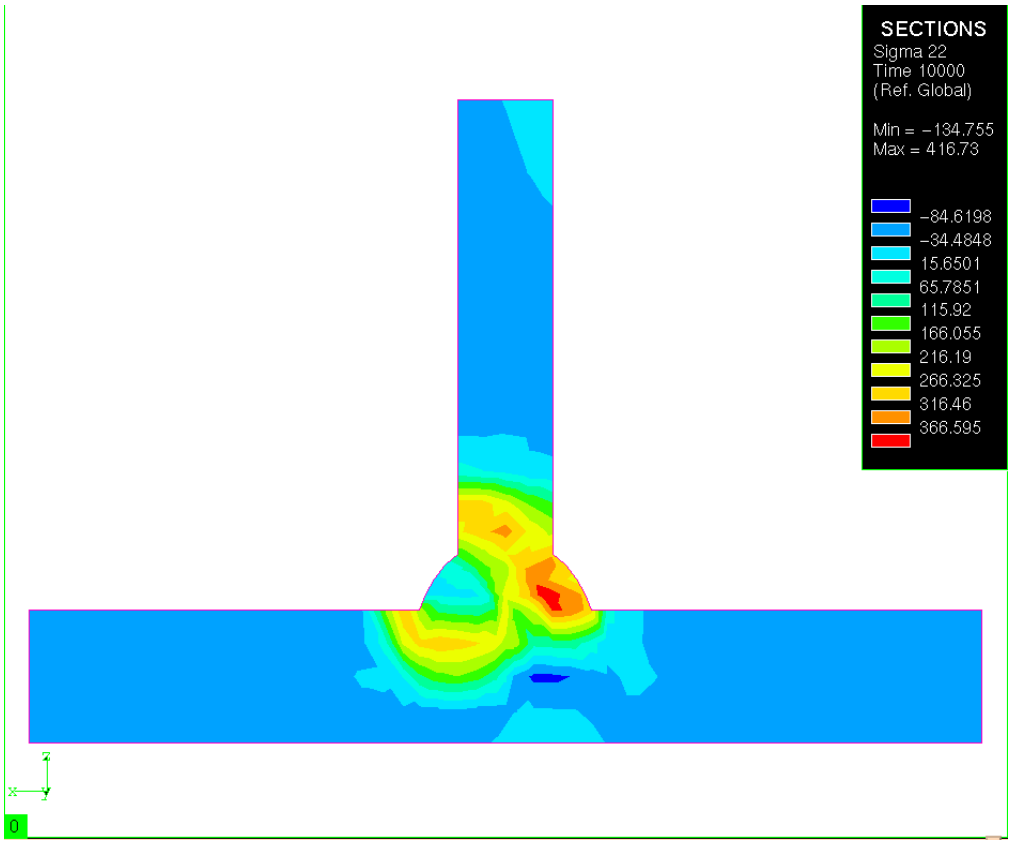

Fig. 6.37 Distribution of the longitudinal normal stress over the central cross section after the second weld pass of the tee joint at t = 10,000s

6.2.2 Tee Section Fully Transient Analysis

The surface temperature distribution at t = 45s during the first weld pass is shown in Figure 6.38. Note that only the activated or newly deposited weld material is visible. The temperature distribution is similar to that found in the “moving reference frame” simulation. The temperature

at t = 50s and then at 5000s, or after cool-down, is shown in Figure 6.39 and Figure 6.40, respectively.

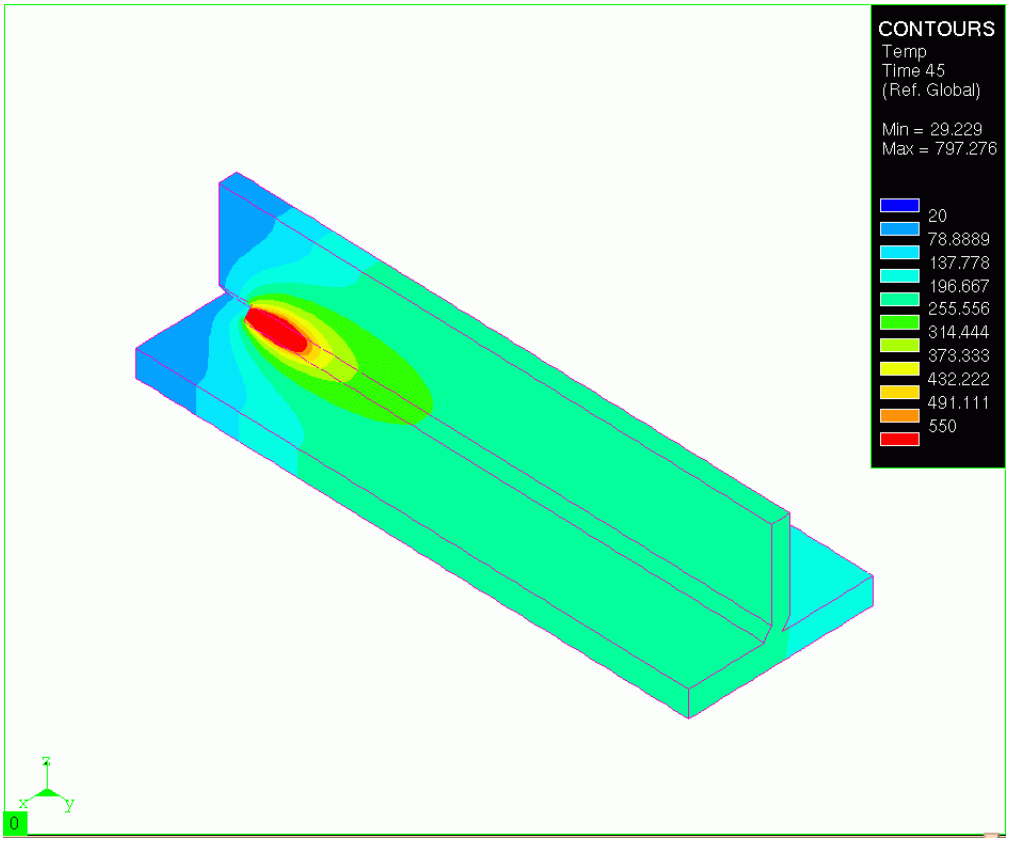

Fig. 6.38 Temperature distribution from the transient analysis of the tee joint during the first weld pass at t = 45s

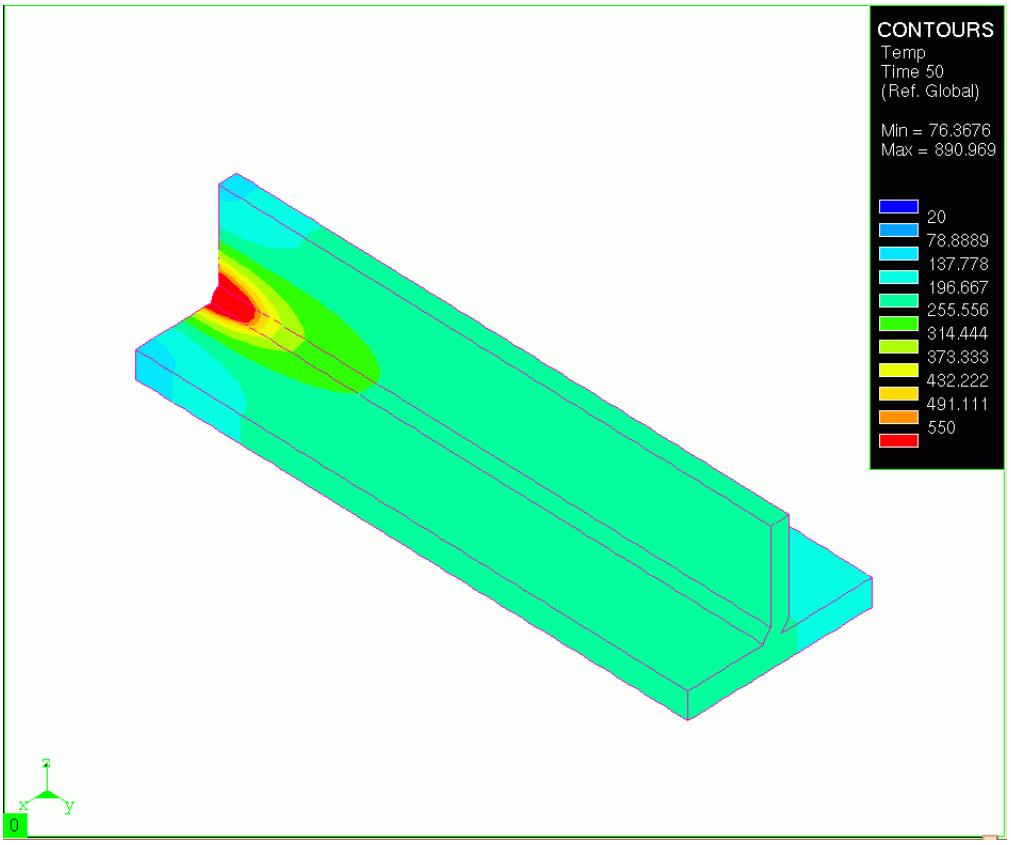

Fig. 6.39 Temperature distribution from the transient analysis of the tee joint during the first weld pass at t = 50s

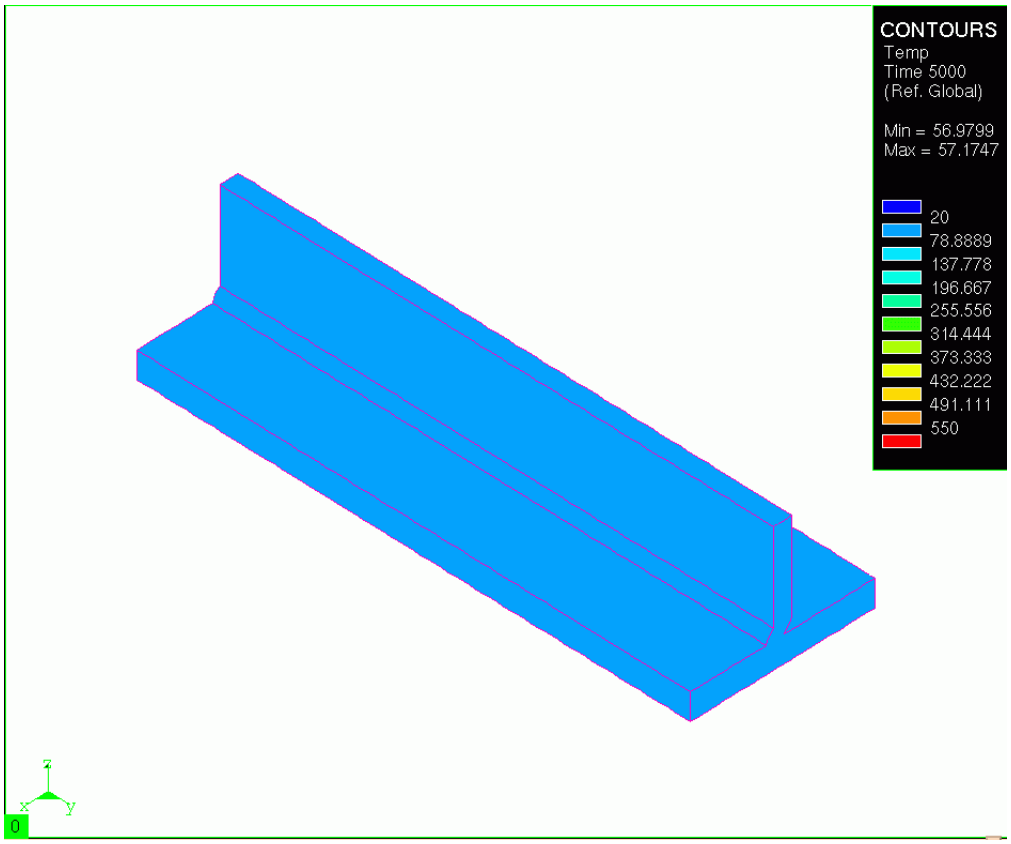

Fig. 6.40 Temperature distribution from the transient analysis of the tee joint after the first weld pass at t = 5,000s

The distribution of the phase 1 material in the cross section after the first weld pass is shown in Figure 6.41. This distribution is similar to that found by the "moving reference frame" analysis, although the "moving reference frame" analysis predicted a greater reduction in the phase 1 content than the transient analysis.

Fig. 6.41 Distribution of the phase 1 material from the transient analysis of the tee joint after the first weld pass at t = 5,000s

The temperature distributions for the second weld bead would be the same as those found during the "moving reference frame" simulation, since they actually are the result of the transient second weld bead deposition. Consequently, the second weld bead analysis was not carried out.

Examining the von Mises stress distribution on the surface of the work piece, which is shown in Figure 6.42, the stress at the interface between the weld bead and base plate is larger than that predicted by the “moving reference frame” computation (refer to Figure 6.28). The von Mises stress distributions in several cross sections of the work piece are shown Figure 6.43. The von Mises stress is as large as 390 MPa within the work piece.

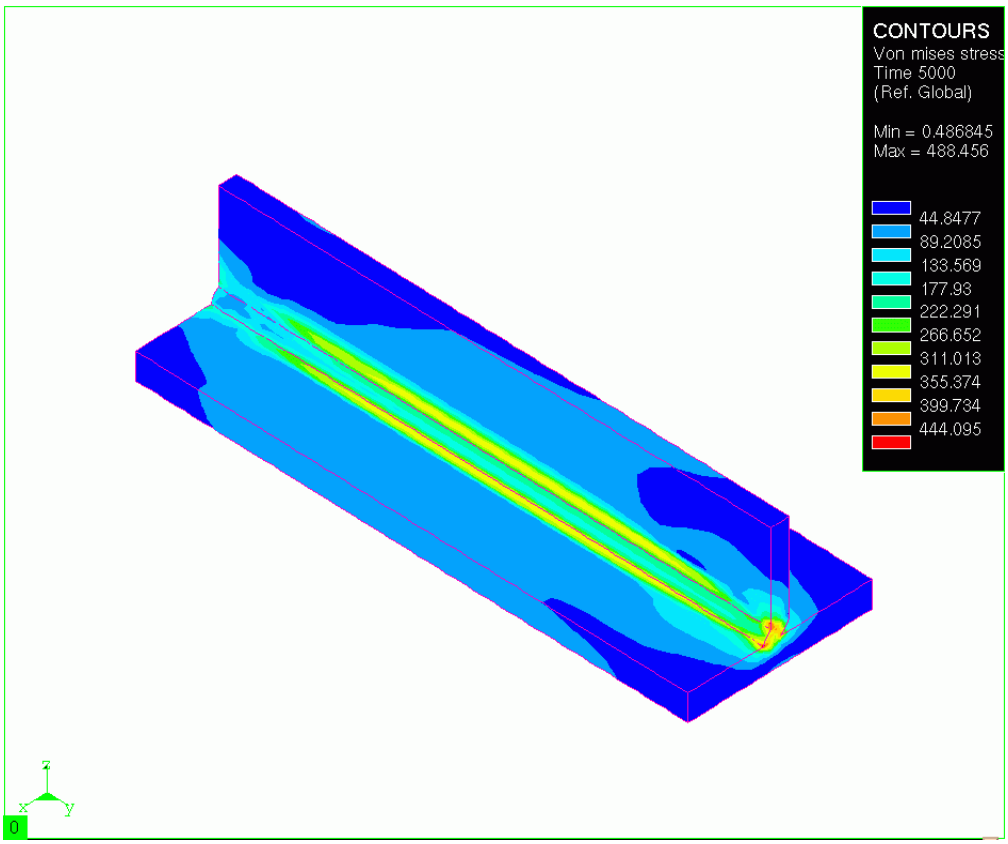

Fig. 6.42 Surface distribution of the von Mises stress from the transient analysis of the tee joint after first weld pass at t=5000s

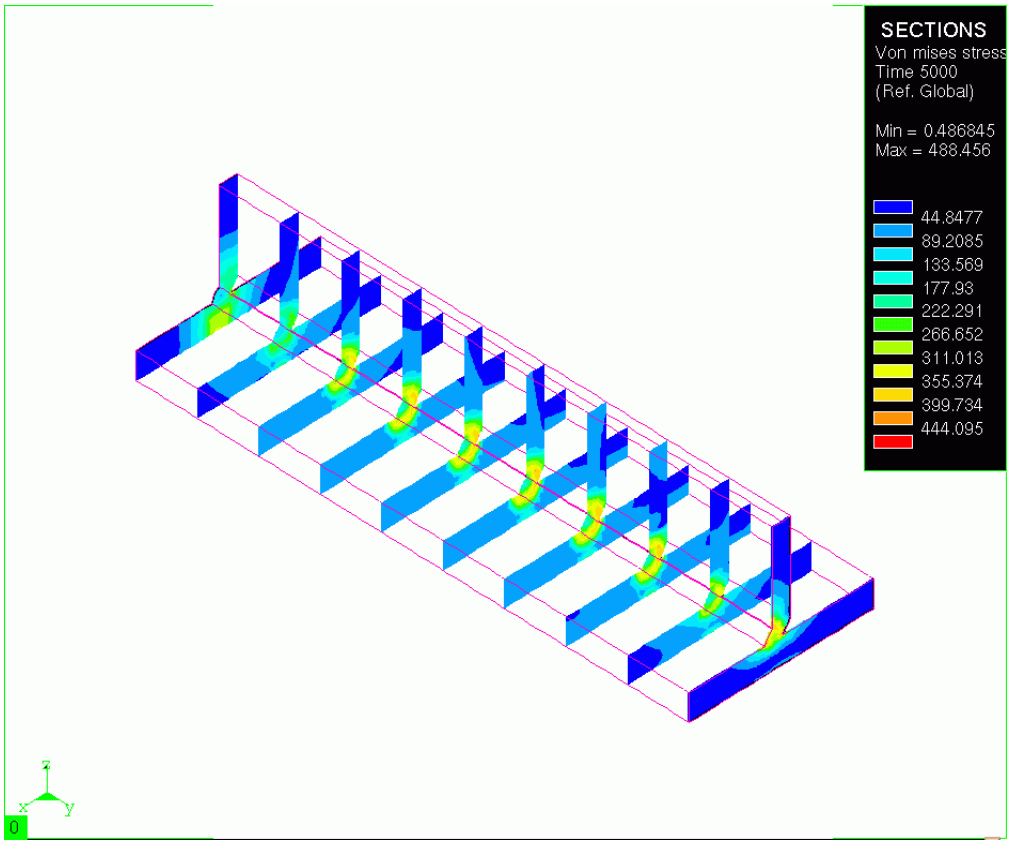

Fig. 6.43 Distributions of the von Mises stress in several cross sections from the transient analysis of the tee joint after first weld pass at t=5000s

The von Mises stress distribution in the central cross section of the work piece is shown in Figure 6.44. The stresses in the weld bead from the transient analysis are again larger than those computed by the "moving reference frame" analysis (refer to Figure 6.30).

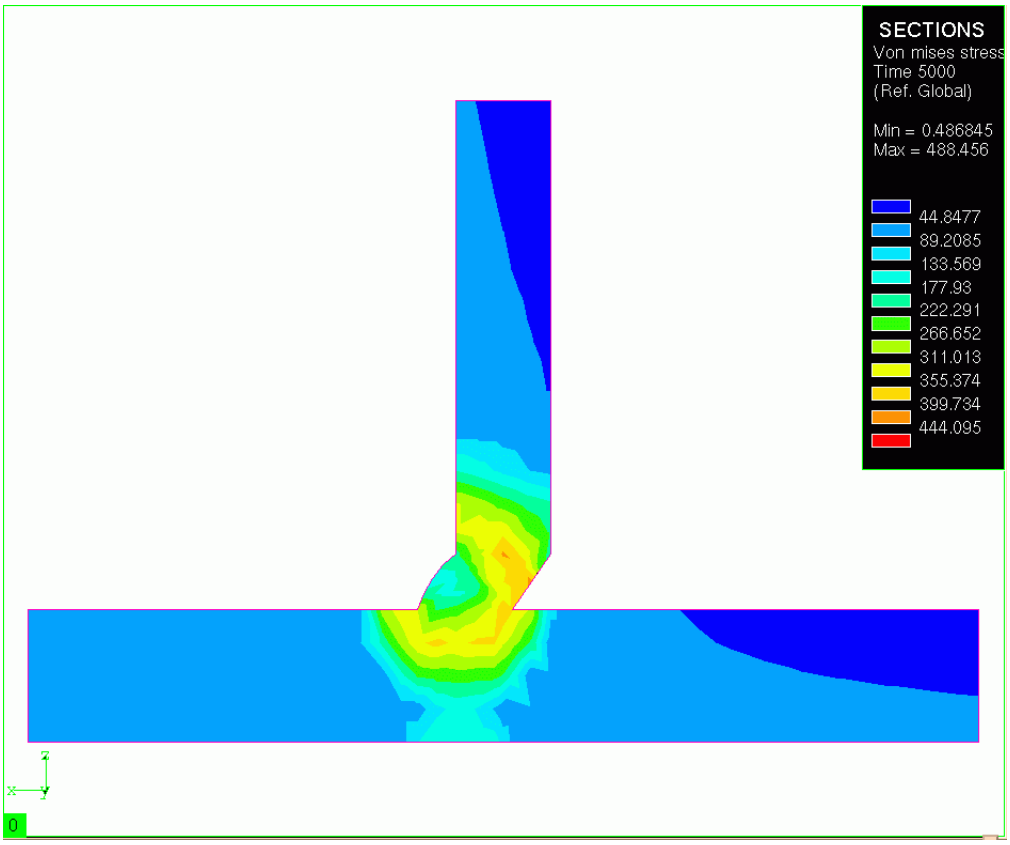

Fig. 6.44 Distribution of the von Mises stress in the central cross section from the transient analysis of the tee joint at t = 5000s

The evolution of the longitudinal normal stress in several cross sections along the work piece is depicted in Figure 6.45. This distribution is much different than that predicted by the "moving reference frame" computation, which was shown Figure 6.31. The longitudinal normal stress distribution in the central cross section of the work piece from the transient analysis after the first weld pass is shown in Figure 6.46. Clearly, the distribution from the transient analysis is

different than predicted by the “moving reference frame” analysis, which was shown in Figure 6.32. The normal stress in the weld bead is tensile compared to the compressive stress predicted by the “moving reference frame” computation.

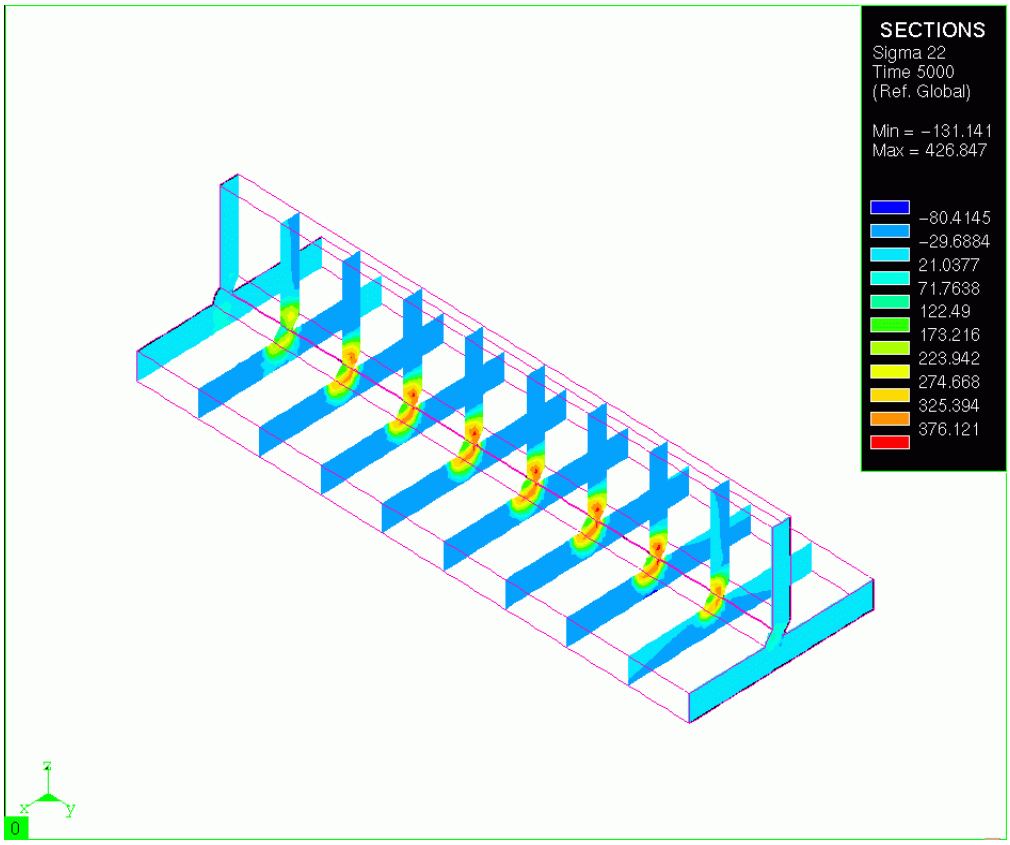

Fig. 6.45 Distribution of the longitudinal normal stress in several cross sections from the transient analysis of the tee joint at t = 5000s

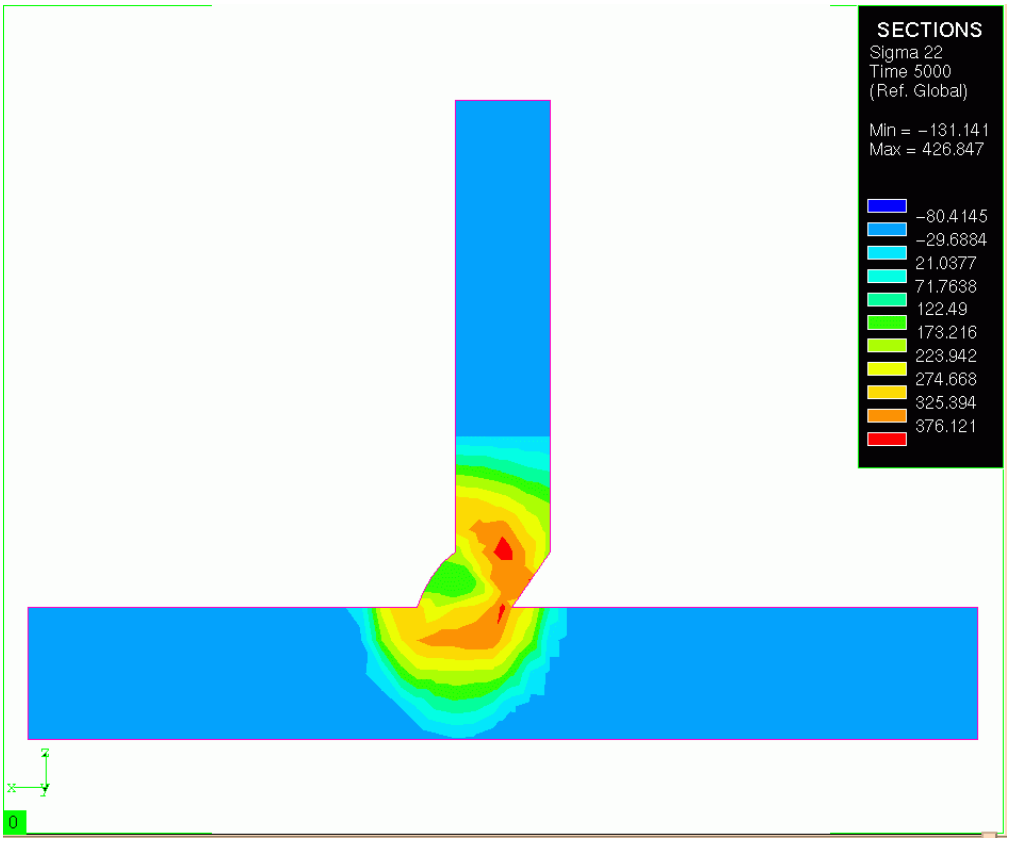

Fig. 6.46 Distribution of the longitudinal normal stress in the central cross section from the transient analysis of the tee joint at t = 5000s

6.3 Solid-Shell Coupled Tee Section Analysis

Since the computation times were very large for the solid tee section model, especially for the fully transient analysis, a solid-shell coupled model was analyzed. The solid-shell model consists of solid elements in the weld zone and shell elements outside the joint. Transition elements are used to connect the solid and shell elements. A “moving reference frame” analysis was used for

the first weld pass, while a transient analysis was required for the second weld pass. The temperature distributions at t = 45s, 50s, and 5000s, are shown in Figure 6.47, Figure 6.48, and Figure 6.49, respectively. The temperature distributions are similar to those found in the solid tee section analyses, yet somewhat different due to the conduction properties of the shell elements and the different convection surfaces.

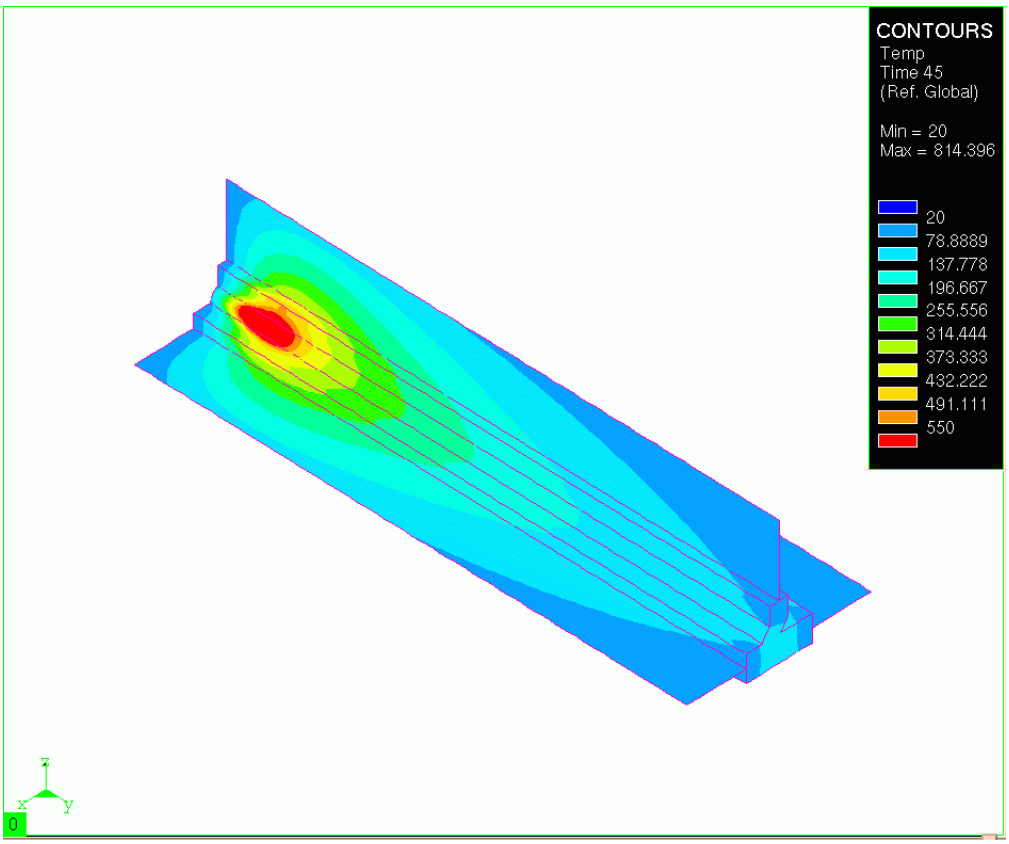

Fig. 6.47 Surface temperature distribution from the moving reference frame analysis of the solid-shell model of the tee joint at t = 45s

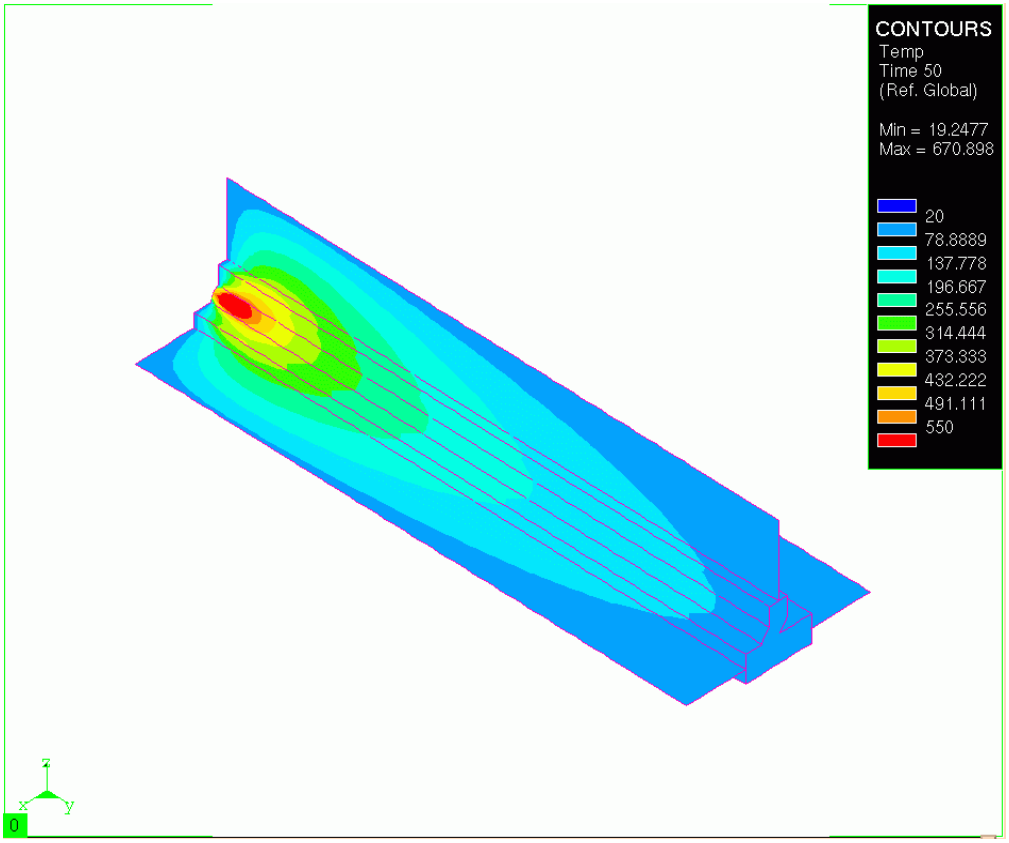

Fig. 6.48 Surface temperature distribution from the analysis of the solid-shell model of the tee joint during the first weld pass at t = 50s

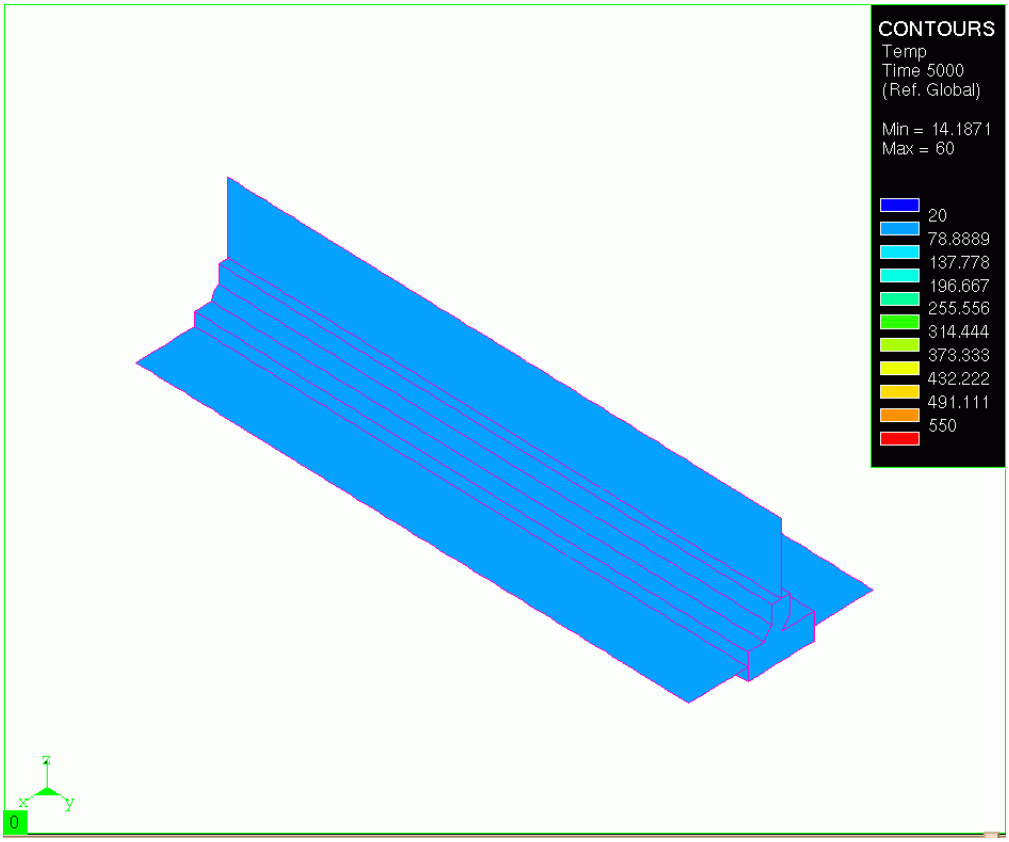

Fig. 6.49 Surface temperature distribution from the analysis of the solid-shell model of the tee joint after the first weld pass at t = 5,000s

The second weld bead deposition was simulated using a fully transient analysis. The temperature distributions at t = 5001s and 5050s, are shown in Figure 6.50 and Figure 6.51, respectively. After cool-down of the second weld pass, the temperature distribution is shown in Figure 6.52.

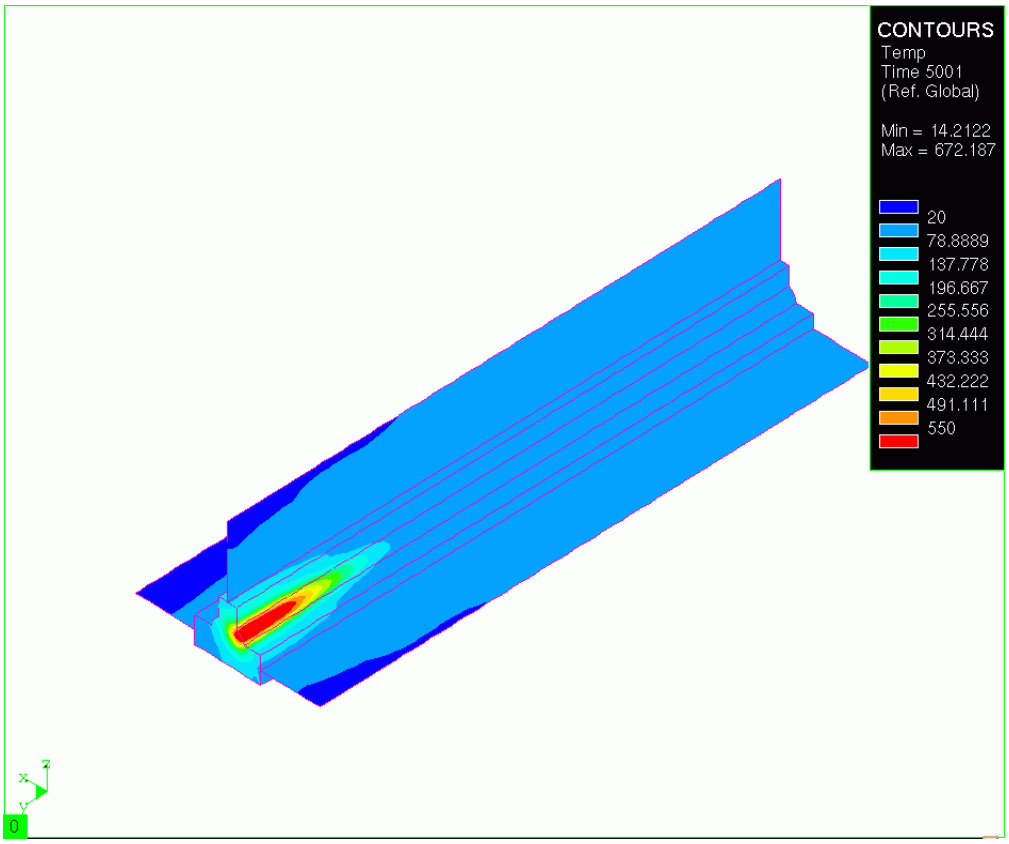

Fig. 6.50 Surface temperature distribution from the solid-shell coupled model of the tee joint during the second weld pass at t = 5001s

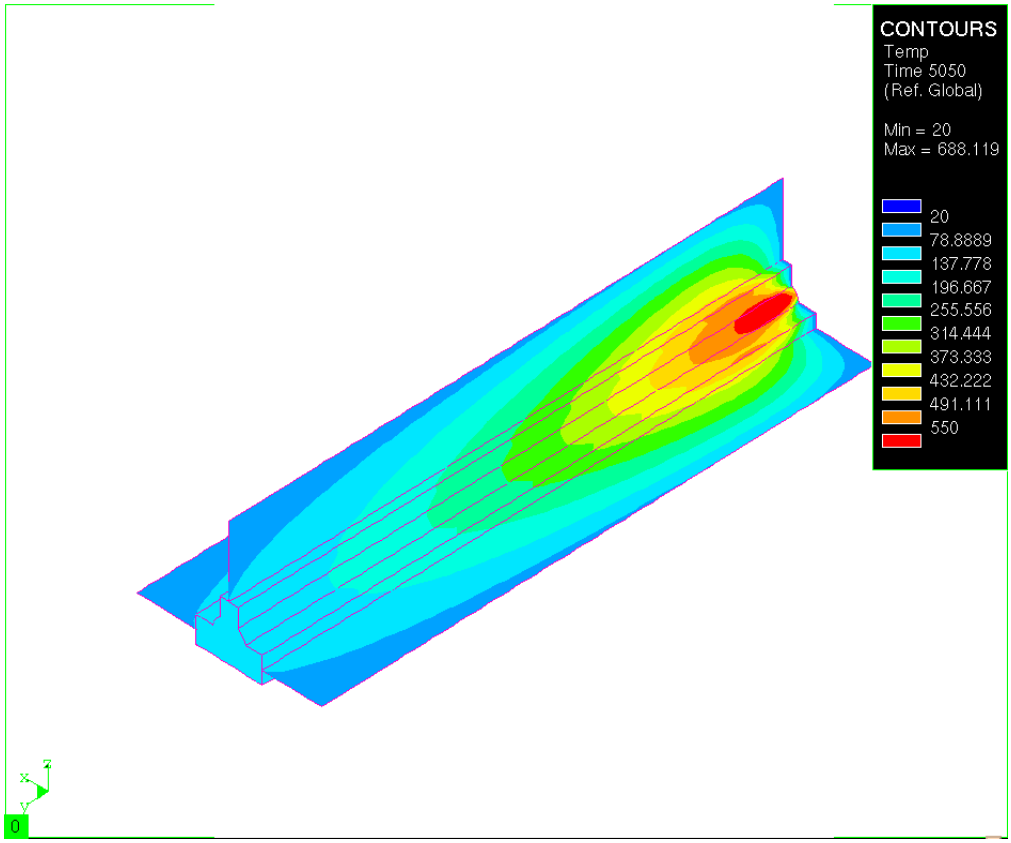

Fig. 6.51 Surface temperature distribution from the solid-shell coupled model of the tee joint during the second weld pass at t = 5050s

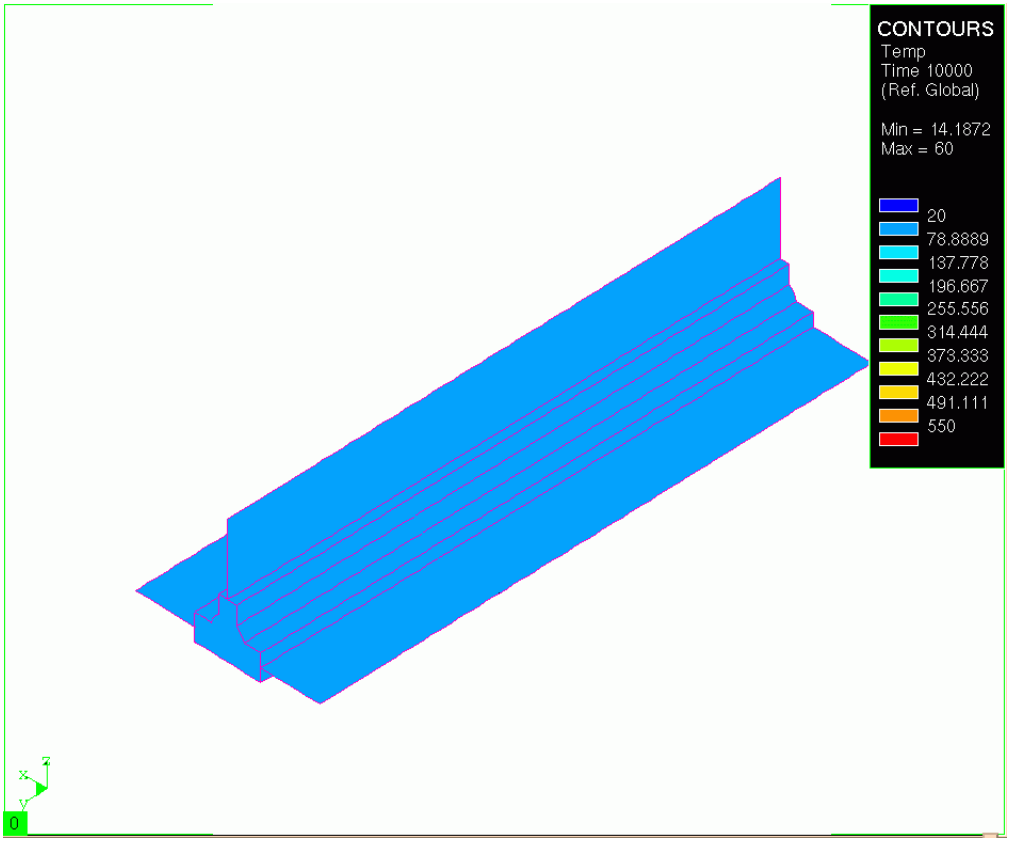

Fig. 6.52 Surface temperature distribution from the solid-shell coupled model of the tee joint after the second weld pass at t = 10,000s

In creating the solid-shell coupled model, transition elements are necessary between the solid and shell elements for the mechanical analysis. These transition elements link the varying degrees of freedom between the solid and shell elements. The transition elements are given a stiffness coefficient which is recommended in the Sysweld manuals [33] to be $E\times10^{3}$, where E is Young's Modulus of the material. This stiffness value, and also other values of $E\times10^{-1}$ and $E\times10^{0}$ were investigated for the mechanical analysis, yet convergence could not be obtained.

Convergence in this case is defined by the residual force components at each node being less than a specified error tolerance.

CHAPTER 7

Concluding Remarks

7.1 Summary

The motivation for this work was to explore the possibility of using results from finite element analyses of the welding process of structural joints in a global-local design optimization methodology. The global-local design methodology discussed in Chapter 1 was proposed as a rational approach to reduce the structural weight of the Advanced Amphibious Assault Vehicle (AAAV). The AAAV, which is shown in Figure 1.1 on page 2, contains many welded aluminum tee joints connecting stiffeners to the skin of the vehicle. Detailed welding simulations performed in this study were for both a butt joint and a tee joint configuration. To gain confidence in performing welding simulations, it was necessary to replicate as closely as possible the residual stress results for an aluminum butt-weld analysis published by Michaleris et al. [14]. The tee joint configuration is representative of a generic skin-stiffener joint as found in the AAAV. The welds for both joint configurations are continuous and use the gas metal-arc welding (GMAW) process. The base metal is aluminum alloy 2519-T87, and

the filler metal is aluminum alloy 2319. GMAW of aluminum was discussed in Chapter 2. Also, the phase diagram for binary aluminum-copper (94% Al and 6% Cu) alloy is discussed in Chapter 2 since the heat treatment and strength of aluminum 2519 is adversely affected by the thermal cycles imposed during welding,

In the initial effort to demonstrate the potential of the global-local methodology, which was called Phase I [2], a simplified finite element model of the skin-stiffener joint was developed. The cross section of the finite element model of the simplified skin-stiffener joint is shown in Figure 7.1. For a given weld size, the heat affected zone (HAZ) was approximated based on engineering experience, and the yield strength of the material in the HAZ was degraded to a value of 152 MPa to account for the adverse effects of welding on the strength. As reviewed in Chapter 3, there has been significant advancement in the finite element simulation of the welding process. The SYSWELD+[1] software was selected to assess if a welding simulation can replace, and/or verify, the approximation of the reduction in joint strength as used in the Phase I effort.

1. SYSWELD+ is the registered trademark of ESI Group, ESI North America, 13399 West Star, Shelby Township MI 48315-2701.

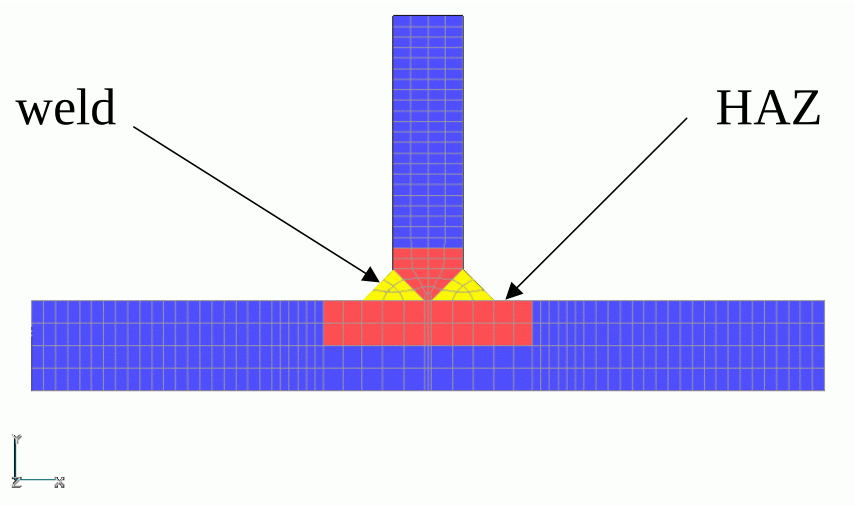

Fig. 7.1 Simplified finite element model of the welded tee joint used in the Phase I work [2]

The energy and constitutive equations governing a welding simulation were discussed in Chapter 4. Since the electric arc in GMAW applies a large heat flux per unit area over a small area of the work piece, there are large temperature gradients in the vicinity of the weld pool. As a consequence, one-way coupling between the thermal state and mechanical state was assumed in the welding simulations performed in this research. That is, it was assumed that the stress power term in the first law of thermodynamics is small with respect to the heat flux input, and that the internal energy is a function of the temperature only. Using the heat conduction law of Fourier combined with the approximations in the first law, the thermal state is de-coupled from the mechanical state. However, the thermal strains are included in the constitutive law for the mechanical state, so that the thermal state affects the mechanical state.

As described in Chapter 5, the capabilities of the SYSWELD+® software used in the welding simulations in this research include material deposit via element activation/de-activation, the Goldak Double Ellipsoid model of the moving weld arc, and the equation for precipitate dissolution kinetics to model metallurgical phase transformations of binary aluminum. Assuming one-way coupling between the thermal and mechanical states, either a transient or steady state thermal analysis is performed prior to the mechanical analysis, as is shown in the flow chart of the analysis procedure using this software in Figure 5.1 on page 69. The finite element meshes for the butt and tee joint geometries were presented in Section 5.3. For the transient thermal analyses, the finite element mesh size was related to the time step size using the heat conduction equation (see Section 5.3.2 on page 76). Thermal and mechanical boundary conditions, thermal and mechanical properties of aluminum alloys 2519 and 2319, metallurgical parameters, and weld arc parameters were specified in Sections 5.5 to 5.8. The following data was used to estimate the heat source strength: average heat input per weld pass = 25.3 kJ per inch of weld length (~1 kJ/mm), average weld bead cross-sectional area per weld pass = 0.05 in^2 (~32 mm^2), and typical travel speed of 15 in/min. (~6 mm/s). Finally, the thermal and mechanical results for the welding simulations of the butt and tee joints were reported in Chapter 6.

7.2 Butt-weld Analysis Results

The butt joint simulation models the joining of two identical plates with rectangular planform and uniform thickness. The dimensions of one of the two plates of the butt joint model are shown in Figure 5.2 on page 71. The plates are chamfered in a double V-groove configuration along the joint. Since the two plates to be joined are identical, only one plate is modeled in the finite element analysis. The mid-plane of the root gap is assumed to be the plane of symmetry in the

analysis. A root gap is an offset of the faying faces of each part which is maintained so filler material penetrates the gap, forming a complete bond. The finite element mesh is shown in Figure 5.3 on page 72.

Two separate analyses were completed. The first analysis used what is called the moving reference frame procedure in SYSWELD, which is a steady state, or time independent, analysis (Section 6.1.1 on page 94). In the moving reference frame analysis, the governing equations for the metallurgical and thermal-mechanical state induced by the moving heat source are solved in a reference frame moving with the constant speed torch, instead of an analysis using a stationary reference frame in the work piece. Transient conditions at the beginning and end of the work piece are ignored in the moving reference frame analysis. The second analysis is a transient analysis in the reference frame of the work piece, in which the weld arc moves along the work piece in time (Section 6.1.2 on page 102). This transient analysis is referred to as a step-by-step computation in SYSWELD.

The distribution of the longitudinal normal stress in the central cross section of the work piece from the moving reference frame analysis is shown in Figure 7.2 and that found by the transient analysis is shown in Figure 7.3. The results found by Michaleris et al. [14] are shown in Figure 7.4.

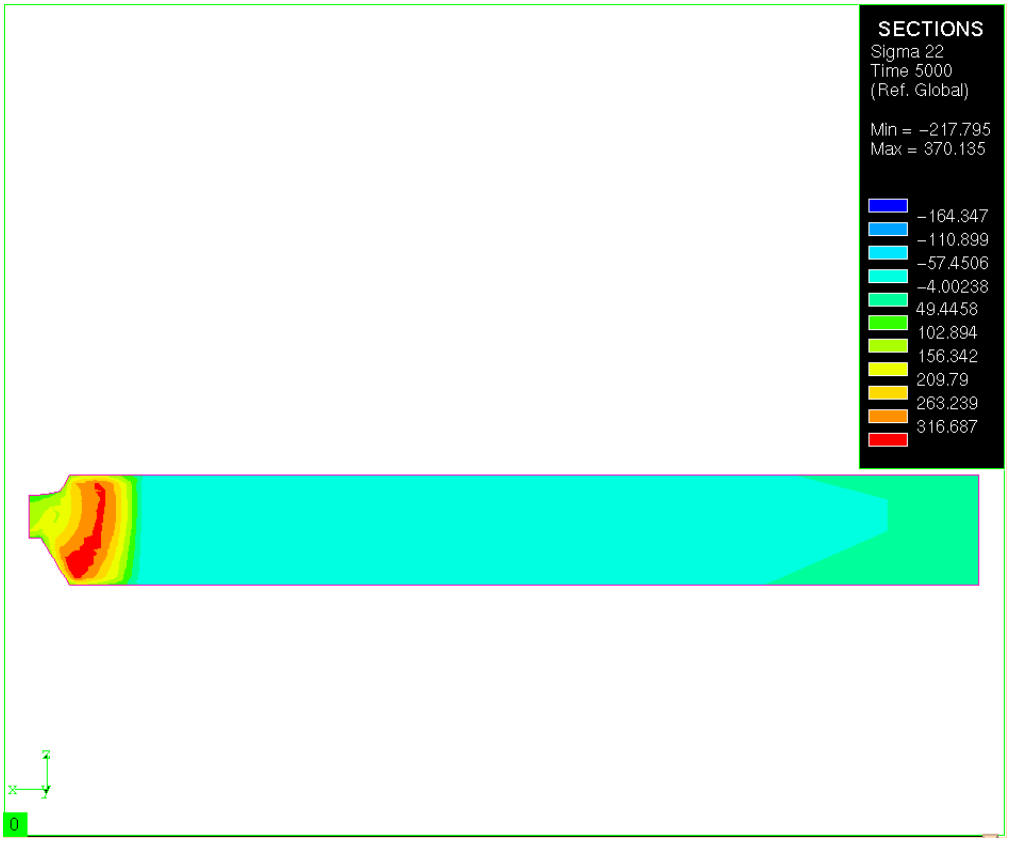

Fig. 7.2 Distribution of the longitudinal normal stress in the central cross section of the butt joint from moving ref. frame analysis at t = 5000s

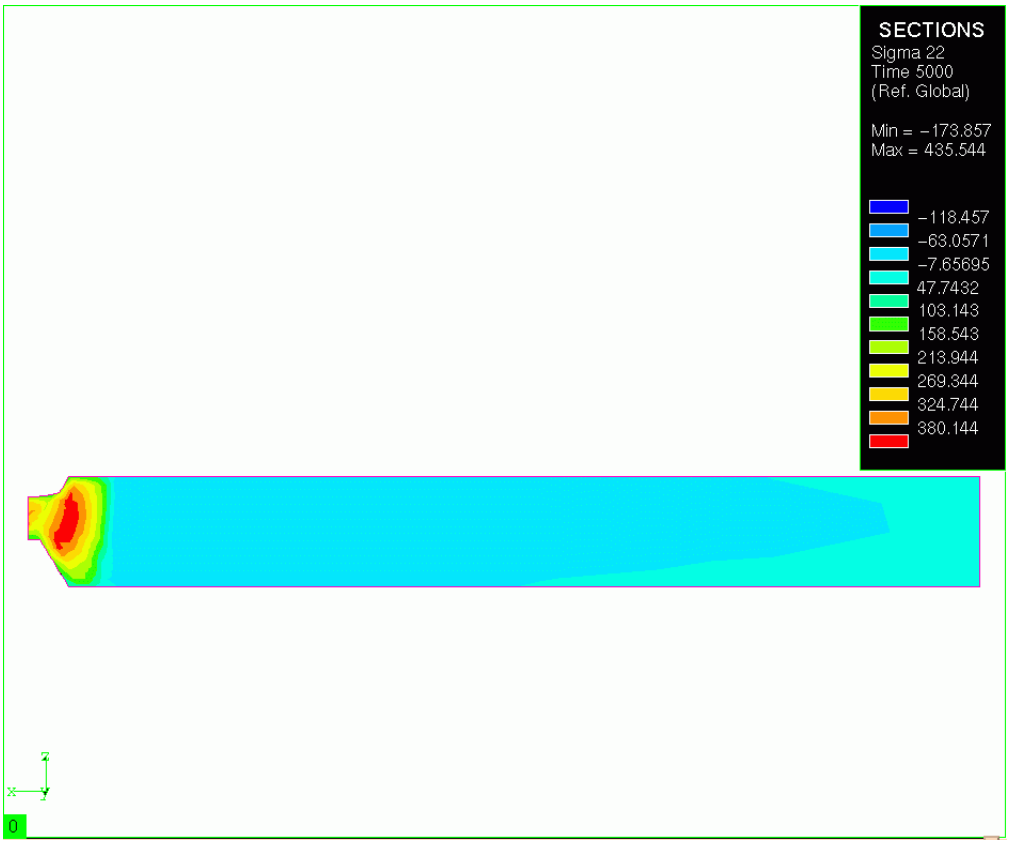

Fig. 7.3 Distribution of the longitudinal normal stress in the central cross section of the butt joint from the transient analysis at t = 5000s

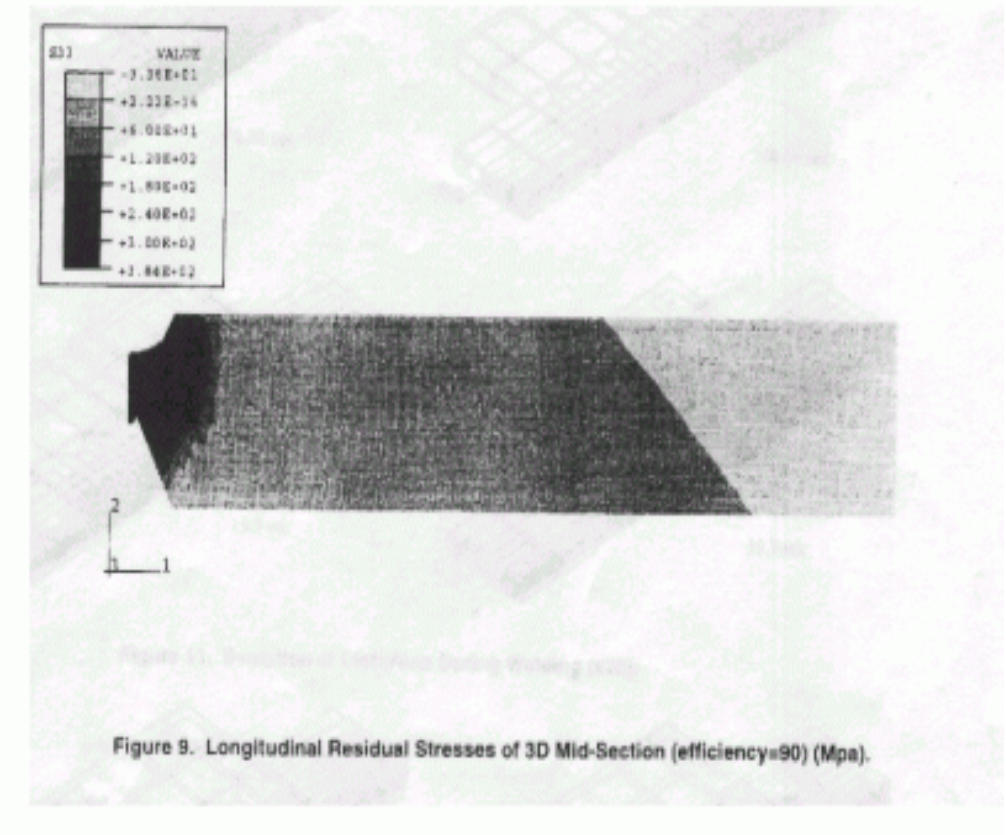

Fig. 7.4 Distribution of the longitudinal residual stress from Ref. [14].

The longitudinal residual stress resulting from the moving reference frame analysis was similar in distribution and within 3.6% of that predicted by Michaleris et al. [14]. The longitudinal stress distribution resulting from the transient analysis was again similar in distribution to that predicted by Michaleris et al. [14] but the maximum was over-predicted by 13%.

The reason for undertaking the second analysis was that the element activation/de-activation function could not be utilized for the moving reference frame analysis. Bead deposit is an important aspect of welding, and therefore plays an important part in a finite element simulation of welding. Though the maximum longitudinal residual stress value was over-predicted by 13%, this could be caused by many factors. Michaleris et al. [14] used run-off tabs or extra material at the start and stop of the welded part to eliminate start and stop effects. Also, the mechanical boundary conditions could have varied since these were not published by Michaleris et al. [14]. Concluding, both analysis methods, moving reference frame and transient, provided results close to published results and confidence in using the SYSWELD software.

A summary of the butt-weld results for the “moving reference frame” analysis and fully transient analysis using SYSWELD, compared to the results published by Michaleris et al. [14], are listed in Table 7.1.

Table 7.1 Butt-weld Results

Analysis	Maximum Longitudinal Normal Stress
“Moving Ref. Frame”	370 MPa
Fully Transient	435 MPa
Michaleris et al. [14]	384 MPa

7.3 Tee Section Analysis Results

The goal of this research was to determine the heat affected zone and the residual stress state of the tee joint configuration shown in Figure 5.5 on page 73. The tee joint has a double bevel fillet weld, and the two beads were modeled as two separate weld passes.The finite element mesh is shown in Figure 5.7 on page 74.

The first simulation of the tee joint was completed in three analysis stages as discussed in Section 6.2.1 on page 113. The first stage consisted of the moving reference frame analysis, where the majority of the first weld pass from t = 0 to t = 45s was completed in one computational step. The second stage of the analysis consisted of a transient analysis from t = 45s to 5000s using a time step of 0.5s. In these two stages, the weld arc traverses the work piece and then continues off into space beyond it. The third stage is a transient analysis simulating the deposit of the second weld bead from t = 5000s to 10,000s, where the weld arc was stepped along from start to finish. The decimal percentage of the base metal, or phase 1, after the first pass is shown in Figure 7.5 as a contour plot over the cross section. It can be seen in the figure that the composition of phase 1 in the weld zone, or heat affected zone, varies from about 40% to 95%. The von Mises stress distribution is shown in Figure 7.6. The computed heat affected zone and von Mises stress distribution after the second weld pass analysis are shown in Figure 7.7 and Figure 7.8, respectively.

Fig. 7.5 Distribution of the phase 1 material over the cross section after the first weld pass of the tee joint at t = 5000s

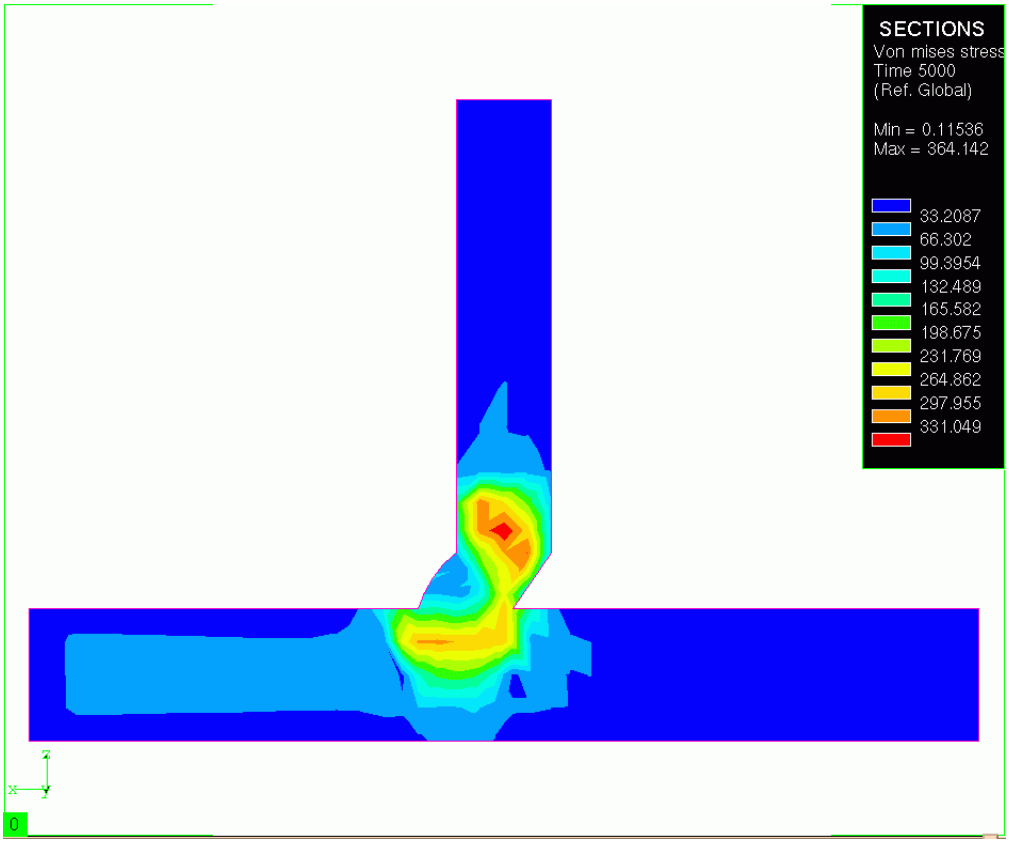

Fig. 7.6 Distribution of the von Mises stress over the central cross section after the first weld pass of the tee joint at t = 5000s

Fig. 7.7 Distribution of the phase 1 material over the cross section after the second weld pass of the tee joint at t = 10,000s

Examining the heat affected zone (Figure 7.7), the material composition maintains 80% of the base metal properties as depicted by the orange region on the contour plot. This relatively small heat affected zone could be due to the fact that the metallurgical properties were estimated as found in the available literature. Unfortunately, the long computation times required for these analyses prevented further investigation into the metallurgical parameters and more attention was

focused on computing the final residual stress state. Examining the final von Mises residual stress state as shown in Figure 7.8, stresses as large as 370 MPa occur, which are close to the 400 MPa yield strength of the base metal. The zone of high residual stresses, or yellow region on the contour plot, provides more insight into an actual heat affected zone as expected.

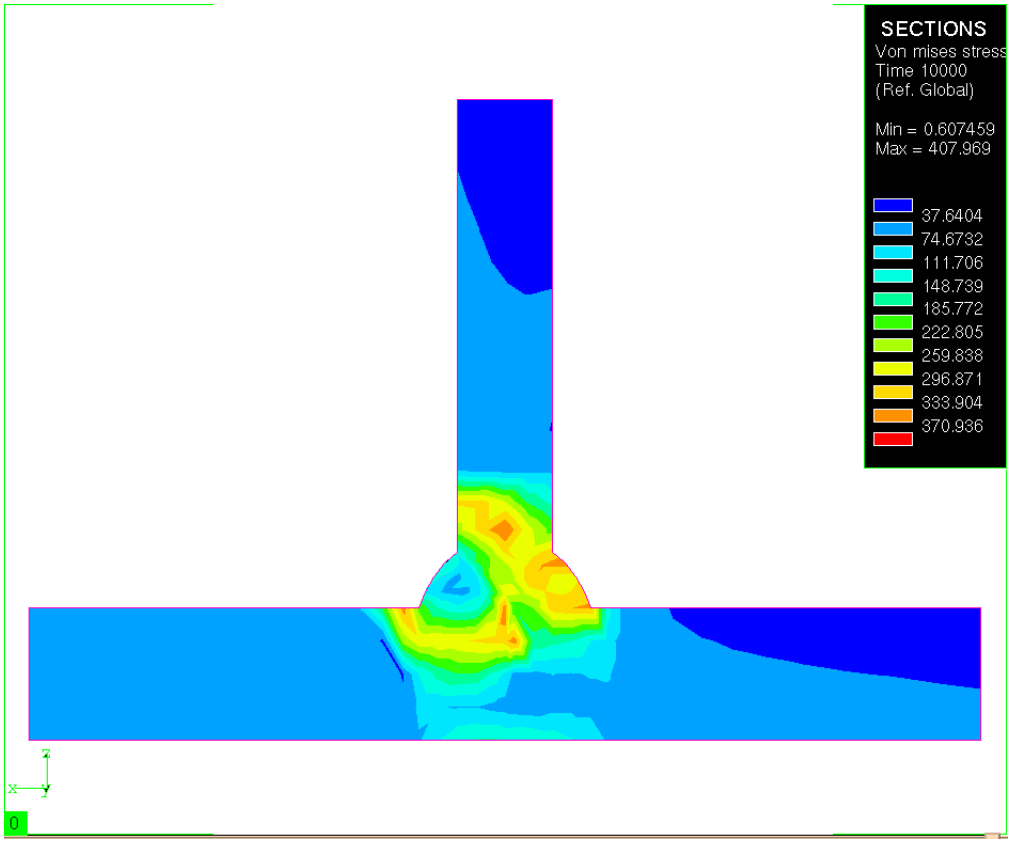

Fig. 7.8 Distribution of the von Mises stress over the central cross section after the second weld pass of the tee joint at t = 10,000s

The assumptions made in Phase I of the project for the size of the HAZ and using a reduced yield strength of 152 MPa in the HAZ, as depicted in Figure 7.1, are in close agreement with the zone of residual stresses shown in Figure 7.8.

The longitudinal normal stress state in the central cross section after the first weld pass is shown in Figure 6.32 on page 129, and the same stress after the second weld pass is shown in Figure 6.37 on page 134. The longitudinal normal stress state within the first weld bead was compressive, while within the second weld bead this normal stress was tensile attaining a value of 416 MPa. Compared to the low compressive stress within the first weld bead, this was unexpected. Since the first weld bead was deposited using a "moving reference frame" simulation, while the second weld bead was deposited with a fully transient analysis, it was decided to further investigate the type of analysis on the response by performing a fully transient analysis under which both weld beads are deposited through transient simulations.

A second simulation using a fully transient analysis for both weld beads was undertaken (Section 6.2.2 on page 134). The results from the fully transient analysis are similar to those found from the first simulation, which utilized the moving reference frame analysis for part of the first pass, except for the longitudinal normal stress. Due to the large computation times only the first weld pass was completed for this fully transient analysis. The second weld pass would be identical to that found by the first simulation, since it would also be a transient computation. As shown in Figure 7.9, the heat affected zone computed by the transient analysis under-predicts the material transformation when compared to that predicted by the "moving reference frame" analysis. The longitudinal normal stress distribution in the central cross section of the work piece from the transient analysis after the first weld pass is shown in Figure 6.46 on page 143, and this

distribution is much different that the moving reference frame results shown in Figure 6.32 on page 129. The normal stress in the weld bead is tensile compared to the compressive stress predicted by the “moving reference frame” computation.

Fig. 7.9 Distribution of the phase 1 material from the transient analysis of the tee joint after the first weld pass at t = 5,000s

Examining the von Mises stress state after the first weld pass of the transient analysis, Figure 7.10, the maximum value within the cross-section is found to be 390 MPa, which is again

close to the material yield strength of 400 MPa. The maximum von Mises residual stresses for the

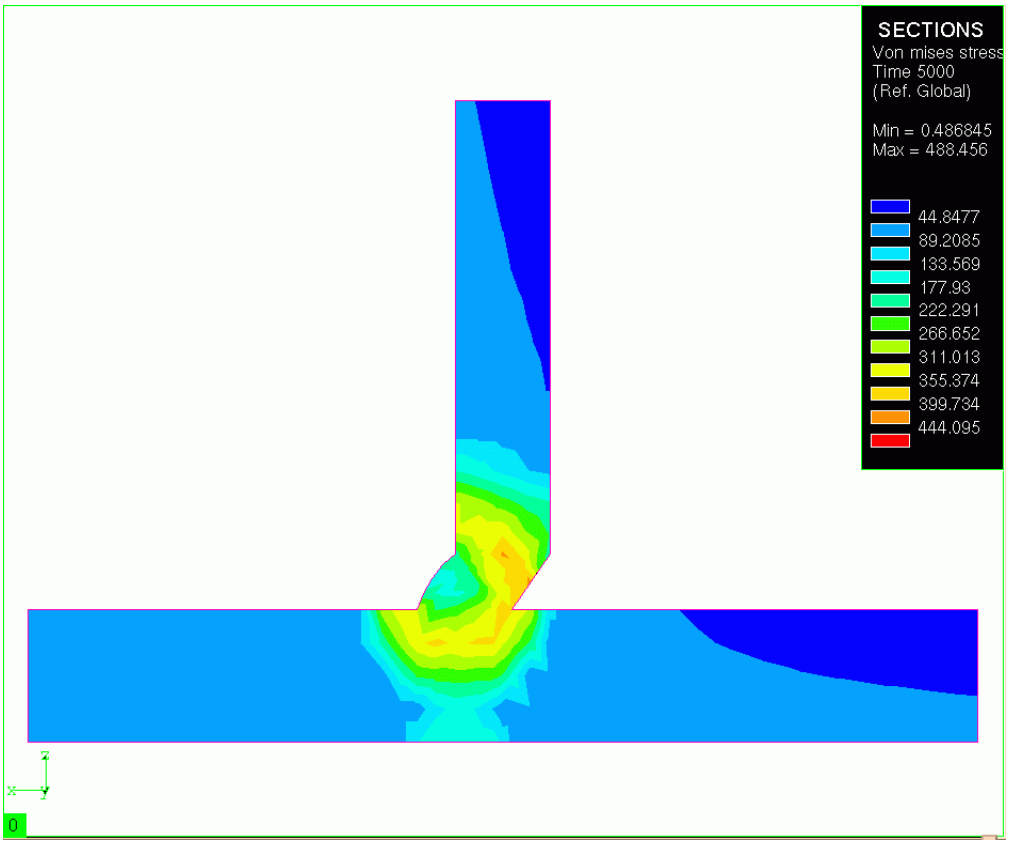

Fig. 7.10 Distribution of the von Mises stress over the central cross section of the tee joint after the first weld pass from the transient analysis at t = 5000s

tee section from first and second simulations are listed in Table 7.2. In this table, the first simulation is labeled as moving reference frame analysis and the second simulation is labeled as the fully transient analysis.

Table 7.2 Tee section Results

Analysis	Maximum von Mises Stress
“Moving Ref. Frame” 1st weld pass	364 MPa
“Moving Ref. Frame” 2nd weld pass	408 MPa
Fully Transient 1st weld pass	488 MPa

7.4 Computation Times and Disk Storage

Welding simulations utilizing finite element analyses are computationally intensive. The computation time and disk storage space required for each analysis is summarized in Table 7.3. Though steps can be taken to reduce computation times, such as performing “moving reference frame” calculations or utilizing solid-shell coupled models (Section 6.3 on page 143), a fully transient analysis is required to capture the complex effects of the welding thermal cycle on a structure.

Table 7.3 Computation Times and Disk Storage

Analysis	Computation time	Disk Storage
Butt-weld moving ref. frame analysis:		
Thermal Analysis	16 hours	.2 Gigabytes
Mechanical Analysis	5.5 hours	.8 Gigabytes
Butt-weld fully transient analysis:		
Thermal Analysis	101hours	2 Gigabytes
Mechanical Analysis	24.5 hours	4 Gigabytes
Tee joint moving ref. frame analysis:		
Thermal Analysis	109 hours	2 Gigabytes
Mechanical Analysis	19 hours	4 Gigabytes
Tee joint fully transient analysis:		
Thermal Analysis	180 hours	3 Gigabytes
Mechanical Analysis	40 hours	5 Gigabytes
Tee joint solid-shell moving ref. frame analysis:		
Thermal Analysis	26 hours	1 Gigabyte
Mechanical Analysis	N/A hours	N/A Gigabytes

7.5 Conclusions

This research effort was successful in determining the weld heat affected zone and final residual stress state for a tee section joint and a butt-weld joint using finite element simulations. The butt-weld joint was the first simulation to be completed since results published by other authors [14] were readily accessible. After successful completion of butt-weld simulations which consisted of a single weld pass, the two weld pass tee section weld simulations were undertaken. The complexity of the tee section weld simulations were increased compared to the single pass butt-weld simulations due to the addition of the second weld pass. Multiple weld pass simulations

require fully transient analyses which are computationally expensive and which prohibit quasi-steady state analyses.

The research was also successful in validating the assumptions made in the local model of the Phase 1 global/local optimization methodology as described in Chapter 1. The assumption that a given weld size will produce a proportionate heat affected zone, HAZ, based on engineering intuition, proved surprisingly accurate. The metallurgical heat affected zone found during the weld simulations, combined with the resulting residual stress distribution closely matched the Phase 1 assumptions.

This effort was unsuccessful in examining the weld heat affected zone and residual stress states for a variety of tee section joint dimensions due to the large computation times required for the analyses. It was not possible to examine a range of geometries or even geometries generated by the minimum and maximum design variable values, within the time constraints for the research.

Bibliography

[1]General Dynamics Land Systems Programs. Advanced Amphibious Assault Vehicle [Online]. Available: http://www.gdls.com [2001, January].

[2]Ragon, S., Nikolaidis, E., Kapania, R., Johnson, E., and Gurdal, Z., 1999, "Global/Local Methodology for Optimum Design of AAAV Structures: Final Report", Department of Navy Contract: N00014-99-M-0253, pp. 1-37.

[3]Callister, W., Jr., 1995, *Materials Science and Engineering*, John Wiley & Sons, Inc., New York, NY, pp.236-243,142,558,560.

[4]Masubuchi, K., 1980, *Analysis of Welded Structures-Residual Stresses, Distortion, and Their Consequences*, Pergamon Press, New York, NY, pp. 205.

[5]The Lincoln Electric Company, 1994, *The Procedure Handbook of Arc Welding*, The Lincoln Electric Company, Cleveland, OH, pp. 9.1-1 -9.4-12.

[6]Messler, R., W., Jr., 1999, *Principles of Welding: Processes, Physics, Chemistry, and Metallurgy*, John Wiley & Sons, Inc. New York, NY, pp. 23-25, 131.

[7] Zhang, J., Dong, P., and Brust, F, 1999, "Residual Stress Analysis and Fracture Assessment of Weld Joints in Moment Frames," ASME *PVP- Fracture, Fatigue and Weld Residual Stress*, **393**, pp. 201-207.

[8] Preston, R., Smith, S., Shercliff, H., and Withers, P., 1999, "An Investigation into the Residual Stresses in an Aluminum 2024 Test Weld," ASME *PVP- Fracture, Fatigue and Weld Residual Stress*, **393**, pp. 265-277.

[9] Dong, P., Hong, J., Bynum, J., and Rogers, P.,1997, "Analysis of Residual Stresses in Al-Li Alloy Repair Welds," ASME *PVP- Approximate Methods in the Design and Analysis of Pressure Vessels and Piping Components*, **347**, pp. 61-75.

[10]Karlsson, R.I., and Josefson, B.L., 1990, "Three-Dimensional Finite Element Analysis of Temperatures and Stresses in a Single-Pass Butt-Welded Pipe," ASME *Journal of Pressure Vessel Technology*, **112**, pp. 76-84.

[11]Boyles, L.G., 1989, "Computer Analysis of Failure Modes in Welded Joints," ASME *PVP-Weld Residual Stress and Plastic Deformation*, **173**, pp. 1-4.

[12] Chao, Y., and Qi, X., 1999, "Thermo-mechanical Modeling of Residual Stress and Distortion During Welding Process," ASME *PVP- Fracture, Fatigue and Weld Residual Stress,* **393**, pp. 209-213.

[13]Oddy, A. S., Goldak, J.A., and McDill, J. M. J., 1989, "Transformation Plasticity and Residual Stresses in Single-Pass Repair Welds," ASME *PVP- Weld Residual Stresses and Plastic Deformation,* **173**, pp. 13-18.

[14]Michaleris, P., Feng, Z., and Campbell, G., 1997, "Evaluation of 2D and 3D FEA Models for Predicting Residual Stress and Distortion," ASME *PVP- Approximate Methods in the Design and Analysis of Pressure Vessels and Piping Components*, **347**, pp. 91-102.

[15]Michaleris, P., Dantzig, J., and Tortorelli, D., 1999, "Minimization of Welding Residual Stress and Distortion in Large Structures," *Welding Journal, Welding Research Supplement,* pp. 361s-366s.

[16]Tsai, C. L., Park, S. C., and Cheng, W. T., 1999, "Welding Distortion of a Thin-Plate Panel Structure," *Welding Journal, Welding Research Supplement*, pp. 156s - 165s.

[17]McDill, J. M. J., Oddy, A. S., and Goldak, J. A., 1993, "Comparing 2-D Plane Strain and 3-D Analyses of Residual Stresses in Welds," *International Trends in Welding Science and Technology, Proceedings of the 3rd International Conference on Trends in Welding Research,* ASM International, Materials Park, OH, pp.105-108.

[18]Hong, J. K., Tsai, C. L., and Dong, P., 1998, "Assessment of Numerical Procedures for Residual Stress Analysis of Multipass Welds," *Welding Journal, Welding Research Supplement*, pp. 372s - 382s.

[19]Goldak, J., Chakravarti, A., and Bibby, M., 1984, "A New Finite Element Model for Welding Heat Sources," *Metallurgical Transactions B*, **15B**, pp. 299-305.

[20]Junek, L., Slovacek, M., Magula, V., and Ochodek, V., 1999, "Residual Stress Simulation Incorporating Weld HAZ Microstructure," ASME *PVP- Fracture, Fatigue and Weld Residual Stress*, **393**, pp. 179-192.

[21]Vincent, Y., Jullien, JF., Cavallo, N., Taleb, L., Cano, V., Taheri, S., and Gilles, Ph., 1999, "On the Validation of the Models Related to the Prevision of the HAZ Behaviour," ASME *PVP-Fracture, Fatigue and Weld Residual Stress*, **393**, pp. 193-200.

[22]Brown, S. and Song, H., 1992, "Finite Element Simulation of Welding of Large Structures," ASME *Journal of Engineering for Industry*, **114**, pp. 441-451.

[23] Dubois, D., Devaux, J., and Leblond, J. B.,1984, "Numerical Simulation of a Welding Operation: Calculation of Residual Stresses and Hydrogen Diffusion," ASME *Fifth International Conference on Pressure Vessel Technology, Materials and Manufacturing*, **II,** San Francisco, CA, pp. 1210 - 1238.

[24]Goldak, J. and Gu, M., 1995, "Computational Weld Mechanics of the Steady State", *Mathematical Modelling of Weld Phenomena 2*, The Institute of Materials, London, pp. 207 - 225.

[25]Oddy, A. S., McDill, J. M. J., and Goldak, J. A., 1990, "Consistent Strain Fields in 3D Finite Element Analysis of Welds," ASME *Journal of Pressure Vessel Technology, Technical Briefs*, **112**, pp. 309-311.

[26]Dong, P., Ghadiali, P. N., and Brust, F. W., 1998, "Residual Stress Analysis of a Multi-pass Girth Weld," ASME *PVP- Fatigue, Fracture, and Residual Stresses*, **373**, pp. 421-431.

[27]Feng, Z., Wang, X. L., Spooner, S., Goodwin, G. M., Maziasz, P. J., Hubbard, C. R., and Zacharia, T., 1996, "A Finite Element Model for Residual Stress in Repair Welds," ASME *PVP-Residual Stresses in Design, Fabrication, Assessment and Repair*, **327**, pp. 119-125.

[28]Karlsson, L., Jonsson, M., Lindgren, L. E., Nasstrom, M., and Troive, L., 1989, "Residual Stresses and Deformations in a Welded Thin-walled Pipe," ASME *PVP- Weld Residual Stress and Plastic Deformation*, **173**, pp. 7-10.

[29]Grong, O., and Myhr, O. R., 1993, "Modelling of the Strength Distribution in the Heat Affected Zone of 6082-T6 Aluminum Weldments", *Mathematical Modelling of Weld Phenomena*, The Institute of Materials, London, pp. 300-311.

[30]Leblond, J. B., Mottet, G., and Devaux, J. C., 1986, “A Theoretical and Numerical Approach to the Plastic Behaviour of Steels During Phase Transformations - I. Derivation of General Relations”, *J. Mech. Phys. Solids*, **34**, pp. 395-409.

[31]Leblond, J. B., Mottet, G., and Devaux, J. C., 1986, “A Theoretical and Numerical Approach to the Plastic Behaviour of Steels During Phase Transformations - II. Study of Classical Plasticity for Ideal-Plastic Phases”, *J. Mech. Phys. Solids*, **34**, pp. 411-432.

[32]Greenwood, G. W., and Johnson, R. H., 1965, “The Deformation of Metals Under Small Stresses During Phase Transformations”, *Proceedings of the Royal Society of London. Series A, Mathematical and Physical Sciences,* **283**, pp. 403-422.

[33] ESI Group, 2000, *SYSTUS 2000 Analysis Reference Manuals*, ESI North America, 13399 West Star, Shelby Township, MI.

[34]Martin, J. B., 1975, *Plasticity: Fundamentals and General Results*, The MIT Press, Cambridge, MA, pp. 63-65.

[35]Hatch, J. E., 1984, *Aluminum: Properties and Physical Metallurgy,* American Society for Metals, Metals Park, OH, pp. 42.

[36] Grong, O, 1997, *Metallurgical Modelling of Welding*, Second Edition, Materials Modelling Series, 1997, The Institute of Materials, London, pp. 1-4.

[37]Malvern, L. E., 1969, *Introduction to the Mechanics of a Continuous Medium*, Prentice-Hall, Inc., Englewood Cliffs, NJ, pp. 233, 338.

[38]Thornton, E. A., 1996, *Thermal structures for aerospace applications*, American Institute of Aeronautics and Astronautics, Reston, VA, pp. 54, 58.

[39]Hsu, T. R., 1986, *The Finite Element Method in Thermomechanics*, Allen & Unwin, Inc., Winchester, MA, pp. 24 - 76.

[40]Huebner, K. H., Thornton, E. A., and Byrom, T. G., 1995, *The Finite Element Method for Engineers*, John Wiley & Sons, Inc., New York, NY, pp. 600.

[41]Beck, G., Denis, S., and Simon, A., 1988, "The Influence of Thermomechanical Treatment on Residual Elastic Microstrain in an Aluminium Alloy", *2nd International Conference on Residual Stresses*, Nancy, France, pp. 765-770.

[42]Wyss, R. K., and Sanders, Jr., R. E., 1988, "Microstructure-Property Relationship in a 2XXX Aluminum Alloy with Mg Addition", *Metallurgical Transactions A*, **19A**, pp. 2523-2530.

[43]Thiery, J., Archambault, P., and Moreaux, F., 1989, "Influence of a Traction Stress on the Hardening Kinetics of Aluminium Alloys", *2nd International Conference on Residual Stresses*, Nancy, France, pp. 771-776.

[44]Myhr, O. R. and Grong, O., 1991, “Process Modelling Applied to 6082-T6 Aluminium Weldments-I. Reaction Kinetics”, *Acta. metall. mater.*, **39**, pp. 2693-2702.

[45]Stoumbos, T., E-mail Communication, General Dynamics Amphibious Systems, 2000.

[46]Incropera, F. P., and De Witt, D. P., 1990, *Fundamentals of Heat and Mass Transfer*, John Wiley & Sons, Inc., New York, NY, pp. 9,14.

Appendix A

1.0 Butt-weld Moving Reference Frame Analysis Input Files

1.1 THERM1.DAT

```
SEARCH DATA 10

DEFINITION
 3D ALUMINUM BUTT MOVING REF FRAME
OPTION THERMAL METALLURGY SPATIAL CONVECTION
RESTART GEOMETRY
MATERIAL PROPERTIES
;
; MATERIAL 1 IS ALUMINUM 2519 AND MATERIAL 2 IS ALUMINUM 2319
;
; DENSITY RHO (kg/mm^3)
;
 ELEM GROUP $PLATE$/ KX KY KZ -10 RHO 2.82*-6 C -11 MATERIAL 1 VY=6
 ELEM GROUP $BEAD1$/ KX KY KZ -10 RHO 2.82*-6 C -11 MATERIAL 2 VY=6
 ELEM GROUP $BEAD1SKIN$/ TYPE 5
;
CONSTRAINT
;
; CONVECTION (H = KT*TABLE 3 = W/mm^2 C)

 ELEMENTS GROUP $SKIN$/ KT=1*-6 VARIABLE=3
 ELEMENTS GROUP $BEAD1SKIN$/ KT=1*-6 VARIABLE=3
```

```
 NODES GROUP $PLANY-50$/ TT
;
LOADINGS
;
1 WELDING / NOTHING
;
 ELEM GROUP $BEAD1$/ QR=5.35 VARI -4
;
 ELEM GROUP $SKIN$/ TT=20
 ELEM GROUP $BEAD1SKIN$/ TT=20
 NODES GROUP $PLANY-50$/ TT=20
;
MEDIUM
 TRANSLATION / VELOCITY 6
;
TABLES
;
; THERMAL CONDUCTIVITY K (W/mm^2 C)
 10 / 1 (0 0.120) (50 0.130) (100 0.140) (150 0.150) (200 0.156) --
       (250 0.158) (300 0.156) (350 0.150) (400 0.145) (450 0.145) --
       (500 0.145) (550 0.145) (600 0.200) (650 0.250) (700 0.300) --
       (750 0.300) (800 0.300) (850 0.300) (900 0.300) (950 0.300) --
       (1000 0.300) (1100 0.300) (1200 0.300) (1300 0.300) (1500 0.300) --

; SPECIFIC HEAT Cp (J/kg C)
 11 / 1 (0 850) (50 860) (100 912) (150 935) (200 950) (250 965) --
       (300 955) (350 1000) (400 1063) (450 1063) (500 1063) (600 1063) --
       (700 1063) (800 1063) (900 1063) (1000 1063) (1200 1063) (1500 1063) --

; CONVECTION COEFFICIENT H (W/m^2 C) AFTER *KT UNITS ARE (W/mm^2 C)
;
 3 / 1 (0 2.5) (100 5.40) (150 6.20) (300 6.90) (450 7.30) (600 7.70) --
      (750 8.00) (900 8.20) (1050 8.40) (1200 8.60) (1350 8.75) (1500 8.90) --
      (1650 9.05) (1800 9.10) (1950 9.15) (2100 9.20) (2250 9.25) --
      (2400 9.30) (2550 9.35) (2700 9.40) (2850 9.45) (3000 9.50) --
;
; GOLDAK DOUBLE ELLIPSOID MOVING HEAT SOURCE

;     Heat source definition
 4 / FORTRAN
      FUNCTION F(X)
      DIMENSION X(5)
C HEAT SOURCE MOVING ON Z AXIS
C
C  VARIABLES
C
       X1=X(1)
       X2=X(2)
       X3=X(3)
```

```
      TT=X(4)
C VELOCITY VY
      VY  = -6.
C
    M1 = -1
    PI = acos (M1)
C CONSTANTS OF THE SOURCE
C
      A      = 30;DEPTH OF THE MOLTEN ZONE ALONG LOCAL X AXIS
      ALIMIT  = 30
      A2LIMIT = -ALIMIT
      B      = 30;WIDTH OF THE MOLTEN ZONE ALONG LOCAL Y AXIS
      BLIMIT  = 30
      B2LIMIT = -BLIMIT
      C1      = 24;LENGTH OF THE MOLTEN ZONE ALONG LOCAL T AXIS
      C2      = 80
      C1LIMIT  = 24
      C2LIMIT  = 80
      C1LIMIT = -C1LIMIT
      C2LIMIT = -C2LIMIT
C
C INITIAL POSITION OF THE SOURCE IN LOCAL FRAME
C
       DX = 0.7
       DY = 300.
       DZ = 5.0
C
C ANGLE OF ROTATION OF FRAME ABOUT Y AXIS
C
      TETA = 90. 180. / pi *
C CALCULATION OF SINE AND COSINE OF TETA
C
     CTETA = COS(TETA)
     STETA = SIN(TETA)
C
C CALCULATION OF THE COORDINATES OF THE GAUSS POINT IN THE MOVING
C FRAME
C CALCULATION OF THE POSITION OF THE SOURCE
C
C CALCULATION OF COORDINATES IN THE LOCAL MOVING FRAME
C
     XA = X1 - DX
     YA = X2 - DY
     ZA = X3 - DZ
C
     D1     = CTETA * XA
     D2     = STETA * ZA
     XLOCAL  = D1 + D2
     D3     = STETA * XA
```

```
      D4      = CTETA * ZA
      ZLOCAL  = D4 - D3
      YLOCAL  = X2 DY VY TT * + -
C
            C COMPUTING THE GOLDAK SOURCE
C
      XX = XLOCAL * XLOCAL
      YY = YLOCAL * YLOCAL
      ZZ = ZLOCAL * ZLOCAL
     EXP1 = 3 * XX
     AA   = A * A
     EXP1 = EXP1 / AA
     EXP1 = -EXP1
     EXP1 = EXP(EXP1)
     EXP2 = 3 * ZZ
     BB   = B * B
     EXP2 = EXP2 / BB
     EXP2 = -EXP2
     EXP2 = EXP(EXP2)
     EXP3 = 3 * YY
     IF (YLOCAL.GE.0) CC=C1*C1
     IF (YLOCAL.LE.0) CC=C2*C2
     EXP3 = EXP3 / CC
     EXP3 = -EXP3
     EXP3 = EXP(EXP3)
     COEF = EXP1 * EXP2
     COEF = COEF * EXP3
     IF (XLOCAL.GT.ALIMIT)  COEF=0
     IF (XLOCAL.LT.A2LIMIT) COEF=0
     IF (ZLOCAL.GT.BLIMIT)  COEF=0
     IF (ZLOCAL.LT.B2LIMIT) COEF=0
      F = COEF
C     CONTINUE
     RETURN
     END
;
RETURN
;
SAVE DATA 11

SEARCH DATA 11

MEDIUM

TRANSIENT NON-LINEAR STATIC
BEHAVIOUR METALLURGY 2
ALGORITHM BFGS IMPLICIT 1 ITERATION 100
PRECISION ABSOLUTE NORM 0 DISPLACEMENT 5
METHOD DIRECT NONSYMMETRIC SGI ORDER 1
```

```
INITIAL CONDITION
  NODES / TT 20
  ELEMENTS GROUP $PLATE$/ P 1 0
  ELEMENTS GROUP $BEAD1$/ P 1 0
  ELEMENTS GROUP $BEAD1SKIN$/ P 1 0
TIME INITIAL 45
 45  / STORE 1
RETURN

SAVE DATA TRAN 12
DEASSIGN 19
```

1.2 THERM2.DAT

```
SEARCH DATA 11
;
DEFINITION
;
 3D ALUMINUM BUTT
;
;
OPTION THERMAL METALLURGY SPATIAL
;
RESTART GEOMETRY
;
;
MATERIAL PROPERTIES
;
; MATERIAL 1 IS ALUMINUM 2519 AND MATERIAL 2 IS ALUMINUM 2319
;
; DENSITY RO (kg/mm^3)
;
 ELEM GROUP $PLATE$/ KX KY KZ -10 RO 2.82*-6 C -11 MATERIAL 1
 ELEM GROUP $BEAD1$/ KX KY KZ -10 RO 2.82*-6 C -11 MATERIAL 2
 ELEM GROUP $BEAD1SKIN$/ KX KY KZ -10 RO 2.82*-6 C -11 MATERIAL 2
;
CONSTRAINT
;
; CONVECTION (H = KT*TABLE 3 = W/mm^2 C)
;
 ELEMENTS GROUP $SKIN$/ KT=1*-6 VARIABLE=3
 ELEMENTS GROUP $BEAD1SKIN$/ KT=1*-6 VARIABLE=3
;
LOADINGS
;
1 WELDING / NOTHING
;
 ELEM GROUP $BEAD1$/ QR=5.35 VARI -4
;
```

```
 ELEM GROUP $SKIN$/ TT=20
 ELEM GROUP $BEAD1SKIN$/ TT=20
;
TABLES
;
; THERMAL CONDUCTIVITY K (W/mm^2 C)
 10 / 1 (0 0.120) (50 0.130) (100 0.140) (150 0.150) (200 0.156) --
       (250 0.158) (300 0.156) (350 0.150) (400 0.145) (450 0.145) --
       (500 0.145) (550 0.145) (600 0.200) (650 0.250) (700 0.300) --
       (750 0.300) (800 0.300) (850 0.300) (900 0.300) (950 0.300) --
       (1000 0.300) (1100 0.300) (1200 0.300) (1300 0.300) (1500 0.300) --
;
; SPECIFIC HEAT Cp (J/kg C)
 11 / 1 (0 850) (50 860) (100 912) (150 935) (200 950) (250 965) --
       (300 955) (350 1000) (400 1063) (450 1063) (500 1063) (600 1063) --
       (700 1063) (800 1063) (900 1063) (1000 1063) (1200 1063) (1500 1063) --
;
; CONVECTION COEFFICIENT H (W/m^2 C) AFTER *KT UNITS ARE (W/mm^2 C)
;
 3 / 1 (0 2.5) (100 5.40) (150 6.20) (300 6.90) (450 7.30) (600 7.70) --
      (750 8.00) (900 8.20) (1050 8.40) (1200 8.60) (1350 8.75) (1500 8.90) --
      (1650 9.05) (1800 9.10) (1950 9.15) (2100 9.20) (2250 9.25) --
      (2400 9.30) (2550 9.35) (2700 9.40) (2850 9.45) (3000 9.50) --
;
; GOLDAK DOUBLE ELLIPSOID MOVING HEAT SOURCE
;
;    Heat source definition
 4 / FORTRAN
      FUNCTION F(X)
      DIMENSION X(5)
C HEAT SOURCE MOVING ON Z AXIS
C
C  VARIABLES
C
       X1=X(1)
       X2=X(2)
       X3=X(3)
       TT=X(4)
C
C VELOCITY VY
       VY  = -6.
C
     M1 = -1
     PI = acos (M1)
C CONSTANTS OF THE SOURCE
C
       A      = 30; DEPTH OF THE MOLTEN ZONE ALONG LOCAL X AXIS
       ALIMIT  = 30
       A2LIMIT = -ALIMIT
```

```
C
      B      = 30;WIDTH OF THE MOLTEN ZONE ALONG LOCAL Y AXIS
      BLIMIT  = 30
      B2LIMIT = -BLIMIT
C
      C1      = 24;LENGTH OF THE MOLTEN ZONE ALONG LOCAL Z AXIS
      C2      = 80
      C1LIMIT  = 24
      C2LIMIT  = 80
      C1LIMIT = -C1LIMIT
      C2LIMIT = -C2LIMIT
C
C INITIAL POSITION OF THE SOURCE IN LOCAL FRAME
C
       DX = 0.7
       DY = 300.
       DZ = 5.0
C
C
C ANGLE OF ROTATION OF FRAME ABOUT Y AXIS
C
      TETA = 90. 180. / pi *
C CALCULATION OF SINE AND COSINE OF TETA
C
     CTETA = COS(TETA)
     STETA = SIN(TETA)
C
C CALCULATION OF THE COORDINATES OF THE GAUSS POINT IN THE MOVING FRAME
C CALCUALTION OF THE POSITION OF THE SOURCE
C
C CALCULATION OF COORDINATES IN THE LOCAL MOVING FRAME
C
     XA = X1 - DX
     YA = X2 - DY
     ZA = X3 - DZ
C
     D1     = CTETA * XA
     D2     = STETA * ZA
     XLOCAL  = D1 + D2
C
C
     D3     = STETA * XA
     D4     = CTETA * ZA
     ZLOCAL  = D4 - D3
C
c
     YLOCAL  = X2 DY VY TT * + -

C COMPUTING THE GOLDAK SOURCE
```

```
C
      XX = XLOCAL * XLOCAL
      YY = YLOCAL * YLOCAL
      ZZ = ZLOCAL * ZLOCAL
C
     EXP1 = 3 * XX
     AA   = A * A
     EXP1 = EXP1 / AA
     EXP1 = -EXP1
     EXP1 = EXP(EXP1)
     EXP2 = 3 * ZZ
     BB   = B * B
     EXP2 = EXP2 / BB
     EXP2 = -EXP2
     EXP2 = EXP(EXP2)
     EXP3 = 3 * YY
     IF (YLOCAL.GE.0) CC=C1*C1
     IF (YLOCAL.LE.0) CC=C2*C2
     EXP3 = EXP3 / CC
     EXP3 = -EXP3
     EXP3 = EXP(EXP3)
     COEF = EXP1 * EXP2
     COEF = COEF * EXP3
     IF (XLOCAL.GT.ALIMIT)  COEF=0
     IF (XLOCAL.LT.A2LIMIT) COEF=0
     IF (ZLOCAL.GT.BLIMIT)  COEF=0
     IF (ZLOCAL.LT.B2LIMIT) COEF=0
      F = COEF
     CONTINUE
     RETURN
     END

 5 /  FORTRAN
      FUNCTION F(X)
      DIMENSION X(5)
C ACTIVATION
C
C  VARIABLES
C
       X1=X(1)
       X2=X(2)
       X3=X(3)
       TT=X(4)
C
C VELOCITY VY=-6.
       VY  = -6.
C
     M1 = -1
     PI = acos (M1)
```

```
C CONSTANTS OF THE SOURCE
C
      A      = 30;DEPTH OF THE MOLTEN ZONE ALONG X AXIS
      ALIMIT  = 30
      A2LIMIT = -ALIMIT
      B      = 30;WIDTH OF THE MOLTEN ZONE ALONG Y AXIS
      BLIMIT  = 30
      B2LIMIT = -BLIMIT
      C1     = 24;LENGTH OF THE MOLTEN ZONE ALONG Z AXIS
      C2     = 80
      C1LIMIT  = 24
      C2LIMIT  = 80
      C1LIMIT = -C1LIMIT
      C2LIMIT = -C2LIMIT
C
C INITIAL POSITION OF THE SOURCE IN LOCAL FRAME
C
       DX = 0.7
       DY = 300.
       DZ = 5.0
C
C
C ANGLE OF ROTATION OF FRAME ABOUT Y AXIS
C
      TETA = 90. 180. / pi *
C CALCULATION OF SINE AND COSINE OF TETA
C
     CTETA = COS(TETA)
     STETA = SIN(TETA)
C
C CALCULATION OF THE COORDINATES OF THE GAUSS POINT IN THE MOVING FRAME
C CALCUALTION OF THE POSITION OF THE SOURCE
C
C CALCULATION OF COORDINATES IN THE LOCAL MOVING FRAME
C
     XA = X1 - DX
     YA = X2 - DY
     ZA = X3 - DZ
     D1     = CTETA * XA
     D2     = STETA * ZA
     XLOCAL  = D1 + D2
     D3     = STETA * XA
     D4     = CTETA * ZA
     ZLOCAL  = D4 - D3
     YLOCAL  = X2 DY VY TT * + -
C
C COMPUTING THE GOLDAK SOURCE
C
     XX = XLOCAL * XLOCAL
```

```
      YY = YLOCAL * YLOCAL
      ZZ = ZLOCAL * ZLOCAL
     AA = YY YY *
     BB = ZZ ZZ *
     AA = AA BB +
     AA = SQRT (AA)
     DIST = YY - 3.
C
C F Computation
C
    F = 0
    IF(YLOCAL.GE. 0.0) F = 1
    IF(YLOCAL.GE. DIST) F = 1
C
     RETURN
     END
 6/ FORTRAN
     FUNCTION F(X)
C
C F= 1 ACTIVATION OF ELEMENT
C F= -1 DEACTIVATION OF ELEMENT
C F=0 N0 EFFECT
C
     F=-1
     RETURN
     END
;
RETURN
;
SAVE DATA 13

SEARCH DATA 13

ASSIGN 19 TRAN12.TIT BINARY
TRANSIENT NON LINEAR EXTRACT 0
BEHAVIOUR METAL 2
ALGO BFGS IMPLICIT 1 ITER 40
PRECISION ABSOLUTE NORM 0 DISPLACMENT 1 FORCE 1*-1
METHOD DIRECT NONSYMMETRIC SGI ORDER 1
INITIAL CONDITION RESTART CARD LAST
TIME INITIAL 45
  50 STEP 0.5 / STORE 1
RETURN
SAVE DATA 12
DEASSIGN 19
```

1.3 COOL.DAT

```
SEARCH DATA 13
```

```
;
DEFINITION
;
 3D ALUMINUM BUTT
;
OPTION THERMAL METALLURGY SPATIAL
;
RESTART GEOMETRY
;
MATERIAL PROPERTIES
;
; MATERIAL 1 IS ALUMINUM 2519 AND MATERIAL 2 IS ALUMINUM 2319
;
; DENSITY RO (kg/mm^3)
;
 ELEM GROUP $PLATE$/ KX KY KZ -10 RO 2.82*-6 C -11 MATERIAL 1
 ELEM GROUP $BEAD1$/ KX KY KZ -10 RO 2.82*-6 C -11 MATERIAL 2
 ELEM GROUP $BEAD1SKIN$/ KX KY KZ -10 RO 2.82*-6 C -11 MATERIAL 2
;
CONSTRAINT
;
; CONVECTION (H = KT*TABLE 3 = W/mm^2 C)
;
 ELEMENTS GROUP $SKIN$/ KT=1*-6 VARIABLE=3
 ELEMENTS GROUP $BEAD1SKIN$/ KT=1*-6 VARIABLE=3
;
LOADINGS
;
1 WELDING / NOTHING
;
 ELEM GROUP $SKIN$/ TT=20
 ELEM GROUP $BEAD1SKIN$/ TT=20
;
TABLES
;
; THERMAL CONDUCTIVITY K (W/mm^2 C)
 10 / 1 (0 0.120) (50 0.130) (100 0.140) (150 0.150) (200 0.156) --
       (250 0.158) (300 0.156) (350 0.150) (400 0.145) (450 0.145) --
       (500 0.145) (550 0.145) (600 0.200) (650 0.250) (700 0.300) --
       (750 0.300) (800 0.300) (850 0.300) (900 0.300) (950 0.300) --
       (1000 0.300) (1100 0.300) (1200 0.300) (1300 0.300) (1500 0.300) --

; SPECIFIC HEAT Cp (J/kg C)
 11 / 1 (0 850) (50 860) (100 912) (150 935) (200 950) (250 965) --
       (300 955) (350 1000) (400 1063) (450 1063) (500 1063) (600 1063) --
       (700 1063) (800 1063) (900 1063) (1000 1063) (1200 1063) (1500 1063) --

; CONVECTION COEFFICIENT H (W/m^2 C) AFTER *KT UNITS ARE (W/mm^2 C)
;
```

```
 3 / 1 (0 2.5) (100 5.40) (150 6.20) (300 6.90) (450 7.30) (600 7.70) --
      (750 8.00) (900 8.20) (1050 8.40) (1200 8.60) (1350 8.75) (1500 8.90) --
      (1650 9.05) (1800 9.10) (1950 9.15) (2100 9.20) (2250 9.25) --
      (2400 9.30) (2550 9.35) (2700 9.40) (2850 9.45) (3000 9.50) --
;
RETURN
;
SAVE DATA 14

SEARCH DATA 14

ASSIGN 19 TRAN12.TIT BINARY
TRANSIENT NON LINEAR EXTRACT 0
BEHAVIOUR METAL 2
ALGO BFGS IMPLICIT 1 ITER 40
PRECISION ABSOLUTE NORM 0 DISPLACMENT 1 FORCE 1*-1
METHOD DIRECT NONSYMMETRIC SGI ORDER 1
INITIAL CONDITION RESTART CARD LAST
TIME INITIAL 50
   60 STEP 1.0   / STORE 10
  100 STEP 10.0  / STORE 10
 1000 STEP 100.0 / STORE 10
 5000 STEP 500.0 / STORE 10
RETURN

SAVE DATA 12
DEASSIGN 19
```

1.4 MECH1.DAT

```
SEARCH DATA 10
;
DEFINITION
;
 3D ALUMINUM BUTT
;
OPTION THERMOMECHANICAL THREE DIMENSION
;
RESTART GEOMETRY
;
MATERIAL
;
;
 ELEMENTS GROUP $PLATE$/ E=-10 YIELD=-20 LX=LY=LZ=-30--
  MODEL=3 NU=0.34 SLOPE=-40 PHAS=2 TF 550 KY -1
;
 ELEMENTS GROUP $BEAD1$/ E=-10 YIELD=-23 LX=LY=LZ=-30--
  MODEL=3 NU=0.34 SLOPE=-60 PHAS=2 TF 550 KY -1
;
```

```
 ELEMENTS GROUP $BEAD1SKIN$/ TYPE 5
;
MEDIUM
 TRANSLATION / VELOCITY 6
;
CONSTRAINTS
;
;NODES   10  INTER /  UX UY UZ
 NODES   481  INTER / UY UZ
 NODES   18906   INTER /  UZ
 NODES   82   INTER /  UZ
 NODES GROUP $SYMX$/ UX
;
LOAD
;
1 WELDING / NOTHING
;
TABLE
  4 /  FORTRAN
       FUNCTION F(X)
       DIMENSION X(5)
C ACTIVATION
C
C  VARIABLES
C
        X1=X(1)
        X2=X(2)
        X3=X(3)
        TT=X(4)
C
C VELOCITY VY=-6.
        VY  = -6.
C
      M1 = -1
      PI = acos (M1)
C CONSTANTS OF THE SOURCE
C
        A       = 30;DEPTH OF THE MOLTEN ZONE ALONG X AXIS
        ALIMIT  = 30
        A2LIMIT = -ALIMIT
        B       = 30;WIDTH OF THE MOLTEN ZONE ALONG Y AXIS
        BLIMIT  = 30
        B2LIMIT = -BLIMIT
        C1      = 24;LENGTH OF THE MOLTEN ZONE ALONG Z AXIS
        C2      = 80
        C1LIMIT  = 24
        C2LIMIT  = 80
        C1LIMIT = -C1LIMIT
        C2LIMIT = -C2LIMIT
```

```
C
C INITIAL POSITION OF THE SOURCE IN LOCAL FRAME
C
       DX = 0.7
       DY = 300.
       DZ = 5
C
C ANGLE OF ROTATION OF FRAME ABOUT Y AXIS
C
      TETA = 90. 180. / pi *
C CALCULATION OF SINE AND COSINE OF TETA
C
     CTETA = COS(TETA)
     STETA = SIN(TETA)
C
C CALCULATION OF THE COORDINATES OF THE GAUSS POINT IN THE MOVING FRAME
C CALCULATION OF THE POSITION OF THE SOURCE
C
C CALCULATION OF COORDINATES IN THE LOCAL MOVING FRAME
C
     XA = X1 - DX
     YA = X2 - DY
     ZA = X3 - DZ
     D1     = CTETA * XA
     D2     = STETA * ZA
     XLOCAL  = D1 + D2
     D3     = STETA * XA
     D4     = CTETA * ZA
     ZLOCAL  = D4 - D3
     YLOCAL  = X2 DY VY TT * + -
C COMPUTING THE GOLDAK SOURCE
C
     XX = XLOCAL * XLOCAL
     YY = YLOCAL * YLOCAL
     ZZ = ZLOCAL * ZLOCAL
    AA = YY YY *
    BB = ZZ ZZ *
    AA = AA BB +
    AA = SQRT (AA)
    DIST = YY - 3.
C
C F Computation
C
   F = 0
   IF(YLOCAL.GE. 0.0) F = 1
   IF(YLOCAL.GE. DIST) F = 1
C
     RETURN
     END
```

```
 5/ FORTRAN
      FUNCTION F(X)
C
C F= 1 ACTIVATION OF ELEMENT
C F= -1 DEACTIVATION OF ELEMENT
C F=0 NO EFFECT
C
      F=-1
      RETURN
      END

; Y0UNGS MODULUS E (N/mm^2) FOR ALUMINUM
;
 10 / 1 (0, 73000) (20, 73000) (100, 70000) (200, 63000) --
     (300, 55000) (400, 37000) (500, 15000) (600, 100) --
     (700, 10)

; YIELD STRENGTH (N/mm^2) FOR ALUMINUM 2519
 20 / -21 -24
 21 / 1 (0, 400) (20, 400) (25, 378) (50, 356) (75, 334) --
      (100, 312) (125, 289) (150, 267) (175, 245) --
      (200, 223) (225, 201) (250, 179) (275, 157) --
      (300, 135) (325, 112) (350, 75) (375, 40) (400, 35) --
      (425, 30) (450, 25) (475, 20) (500, 15) (525, 10) --
      (550, 5) (575, 3) (600, 2) (700, 1)

; YIELD STRENGTH (N/mm^2) FOR ALUMINUM 2319
 23 / -24 -24
 24 / 1 (0, 250) (20, 250) (25, 239) (50, 229) (75, 218) --
      (100, 208) (125, 197) (150, 186) (175, 176) --
      (200, 165) (225, 155) (250, 144) (275, 134) --
      (300, 123) (325, 112) (350, 75) (375, 40) (400, 35) --
      (425, 30) (450, 25) (475, 20) (500, 15) (525, 10) --
      (550, 5) (575, 3) (600, 2) (700, 1)

; THERMAL STRAINS FOR ALUMINUM
 30 / -31 -31
 31 / 1 (20, 0) (100, 0.00224) (200, 0.00474) --
       (300, 0.00741) (400, 0.00988) (500, 0.01235) --
       (600, 0.01482) (700, 0.01729)

; ISOTROPIC STRAIN HARDENING FOR ALUMINUM 2519
 40 / -41 -51
 41 / 7 (20, 45) (316, 46) (371, 47) (550, 48)
 45 / 1 (0, 386.1) (.1, 468.8)
 46 / 1 (0, 117.2) (.1, 137.8)
 47 / 1 (0, 41.37) (.1, 62.05)
 48 / 1 (0, 5) (.1, 7.5)
```

```
 51 / 7 (20, 55) (316, 56) (371, 57) (550, 58)
 55 / 1 (0, 152) (.1, 185)
 56 / 1 (0, 46) (.1, 54)
 57 / 1 (0, 16) (.1, 24)
 58 / 1 (0, 1.9) (.1, 2.9)

; ISOTROPIC STRAIN HARDENING FOR ALUMINUM 2319
 60 / -61 -71
 61 / 7 (20, 65) (316, 66) (371, 67) (550, 68)
 65 / 1 (0, 241) (.1, 255)
 66 / 1 (0, 117.2) (.1, 137.8)
 67 / 1 (0, 41.37) (.1, 62.05)
 68 / 1 (0, 5) (.1, 7.5)
 71 / 7 (20, 75) (316, 76) (371, 77) (550, 78)
 75 / 1 (0, 95) (.1, 115)
 76 / 1 (0, 46) (.1, 54)
 77 / 1 (0, 16) (.1, 24)
 78 / 1 (0, 1.9) (.1, 2.9)

RETURN
SAVE DATA 21

SEARCH DATA 21

MEDIUM

ASSIGN 19 TRAN12.TIT BINARY
TEMPERATURE METALLURGY TRANSIENT CARD 1
DEASSIGN 19

TRANSIENT NON-LINEAR STATIC
BEHAVIOUR METALLURGY 2 PLASTIC
METHOD DIRECT SGI ORDER 1
ALGORITHM BFGS ITERATION 80
PRECISION ABSOLUTE DISPLACEMENT 1 FORCE 10
;INITIAL CONDITION
; ELEMENTS GROUP $BEAD1$ /  IS -1
TIME INITIAL 45.
  45.  / STORE 1
RETURN

SAVE DATA TRAN 22
DEASSIGN 19
```

1.5 MECH2.DAT

```
SEARCH DATA 10
;
DEFINITION
```

```
;
 3D ALUMINUM BUTT
;
OPTION THERMOMECHANICAL THREE DIMENSION
;
RESTART GEOMETRY
;
MATERIAL
;
 ELEMENTS GROUP $PLATE$/ E=-10 YIELD=-20 LX=LY=LZ=-30--
  MODEL=3 NU=0.34 SLOPE=-40 PHAS=2
;
 ELEMENTS GROUP $BEAD1$/ E=-10 YIELD=-23 LX=LY=LZ=-30--
  MODEL=3 NU=0.34 SLOPE=-60 PHAS=2
;
 ELEMENTS GROUP $BEAD1SKIN$/ E=-10 YIELD=-23 LX=LY=LZ=-30--
  MODEL=3 NU=0.34 SLOPE=-60 PHAS=2
;
CONSTRAINTS
;
; NODES   10  INTER /  UX UY UZ
 NODES   481  INTER /  UY UZ
 NODES   18906   INTER /  UZ
 NODES   82   INTER /  UZ
 NODES GROUP $SYMX$/ UX

LOAD
;
1 WELDING / NOTHING
;
TABLE
  4 /  FORTRAN
       FUNCTION F(X)
       DIMENSION X(5)
C ACTIVATION
C
C  VARIABLES
C
        X1=X(1)
        X2=X(2)
        X3=X(3)
        TT=X(4)
C
C VELOCITY VY=-6.
        VY  = -6.
C
      M1 = -1
      PI = acos (M1)
C CONSTANTS OF THE SOURCE
```

```
C
      A      = 30;DEPTH OF THE MOLTEN ZONE ALONG X AXIS
      ALIMIT  = 30
      A2LIMIT = -ALIMIT
      B      = 30;WIDTH OF THE MOLTEN ZONE ALONG Y AXIS
      BLIMIT  = 30
      B2LIMIT = -BLIMIT
      C1      = 24;LENGTH OF THE MOLTEN ZONE ALONG Z AXIS
      C2      = 80
      C1LIMIT  = 24
      C2LIMIT  = 80
      C1LIMIT = -C1LIMIT
      C2LIMIT = -C2LIMIT
C
C INITIAL POSITION OF THE SOURCE IN LOCAL FRAME
C
       DX = 0.7
       DY = 300.
       DZ = 5.
C
C ANGLE OF ROTATION OF FRAME ABOUT Y AXIS
C
      TETA = 90. 180. / pi *
C CALCULATION OF SINE AND COSINE OF TETA
C
     CTETA = COS(TETA)
     STETA = SIN(TETA)
C
C CALCULATION OF THE COORDINATES OF THE GAUSS POINT IN THE MOVING FRAME
C CALCULATION OF THE POSITION OF THE SOURCE
C
C CALCULATION OF COORDINATES IN THE LOCAL MOVING FRAME
C
     XA = X1 - DX
     YA = X2 - DY
     ZA = X3 - DZ
     D1     = CTETA * XA
     D2     = STETA * ZA
     XLOCAL  = D1 + D2
     D3     = STETA * XA
     D4     = CTETA * ZA
     ZLOCAL  = D4 - D3
     YLOCAL  = X2 DY VY TT * + -
C
C COMPUTING THE GOLDAK SOURCE
C
     XX = XLOCAL * XLOCAL
     YY = YLOCAL * YLOCAL
     ZZ = ZLOCAL * ZLOCAL
```

```
      AA = YY YY*
      BB = ZZ ZZ *
      AA = AA BB +
      AA = SQRT (AA)
      DIST = YY - 3.
C
C F Computation
C
     F = 0
      IF(YLOCAL.GE. 0.0) F = 1
      IF(YLOCAL.GE. DIST) F = 1
      RETURN
      END

 5/ FORTRAN
      FUNCTION F(X)
C
C F= 1 ACTIVATION OF ELEMENT
C F= -1 DEACTIVATION OF ELEMENT
C F=0 NO EFFECT
C
      F=-1
      RETURN
      END

; Y0UNGS MODULUS E (N/mm^2) FOR ALUMINUM
;
 10 / 1 (0, 73000) (20, 73000) (100, 70000) (200, 63000) --
    (300, 55000) (400, 37000) (500, 15000) (600, 100) --
    (700, 10)

; YIELD STRENGTH (N/mm^2) FOR ALUMINUM 2519
 20 / -21 -24
 21 / 1 (0, 400) (20, 400) (25, 378) (50, 356) (75, 334) --
      (100, 312) (125, 289) (150, 267) (175, 245) --
      (200, 223) (225, 201) (250, 179) (275, 157) --
      (300, 135) (325, 112) (350, 75) (375, 40) (400, 35) --
      (425, 30) (450, 25) (475, 20) (500, 15) (525, 10) --
      (550, 5) (575, 3) (600, 2) (700, 1)

; YIELD STRENGTH (N/mm^2) FOR ALUMINUM 2319
 23 / -24 -24
 24 / 1 (0, 250) (20, 250) (25, 239) (50, 229) (75, 218) --
      (100, 208) (125, 197) (150, 186) (175, 176) --
      (200, 165) (225, 155) (250, 144) (275, 134) --
      (300, 123) (325, 112) (350, 75) (375, 40) (400, 35) --
      (425, 30) (450, 25) (475, 20) (500, 15) (525, 10) --
      (550, 5) (575, 3) (600, 2) (700, 1)
```

```
; THERMAL STRAINS FOR ALUMINUM
 30 / -31 -31
 31 / 1 (20, 0) (100, 0.00224) (200, 0.00474) --
      (300, 0.00741) (400, 0.00988) (500, 0.01235) --
      (600, 0.01482) (700, 0.01729)

; ISOTROPIC STRAIN HARDENING FOR ALUMINUM 2519
 40 / -41 -51
 41 / 7 (20, 45) (316, 46) (371, 47) (550, 48)
 45 / 1 (0, 386.1) (.1, 468.8)
 46 / 1 (0, 117.2) (.1, 137.8)
 47 / 1 (0, 41.37) (.1, 62.05)
 48 / 1 (0, 5) (.1, 7.5)
 51 / 7 (20, 55) (316, 56) (371, 57) (550, 58)
 55 / 1 (0, 152) (.1, 185)
 56 / 1 (0, 46) (.1, 54)
 57 / 1 (0, 16) (.1, 24)
 58 / 1 (0, 1.9) (.1, 2.9)

; ISOTROPIC STRAIN HARDENING FOR ALUMINUM 2319
 60 / -61 -71
 61 / 7 (20, 65) (316, 66) (371, 67) (550, 68)
 65 / 1 (0, 241) (.1, 255)
 66 / 1 (0, 117.2) (.1, 137.8)
 67 / 1 (0, 41.37) (.1, 62.05)
 68 / 1 (0, 5) (.1, 7.5)
 71 / 7 (20, 75) (316, 76) (371, 77) (550, 78)
 75 / 1 (0, 95) (.1, 115)
 76 / 1 (0, 46) (.1, 54)
 77 / 1 (0, 16) (.1, 24)
 78 / 1 (0, 1.9) (.1, 2.9)

RETURN
SAVE DATA 23

SEARCH DATA 23

; THERMAL LOAD

ASSIGN 19 TRAN12.TIT BINARY
TEMPERATURE TRANSIENT METALLURGY CARD
DEASSIGN 19

ASSIGN 19 TRAN22.TIT BINARY

TRANSIENT NON LINEAR STATIC
BEHAVIOR METALLURGY 2 PLASTIC
METHOD DIRECT SGI ORDER 1
ALGORITHM BFGS ITERATION 80
```

```
PRECISION ABSOLUTE DISPLACEMENT 1*-1 FORCE 1
INITIAL CONDITION RESTART CARD LAST
TIME INITIAL 45.
  50 STEP 0.5 / STORE 1
RETURN

SAVE DATA 22
DEASSIGN 19
```

1.6 MECH3.DAT

```
SEARCH DATA 10
;
DEFINITION
;
 3D ALUMINUM BUTT
;
OPTION THERMOMECHANICAL THREE DIMENSION
;
RESTART GEOMETRY
;
MATERIAL
;
 ELEMENTS GROUP $PLATE$/ E=-10 YIELD=-20 LX=LY=LZ=-30--
  MODEL=3 NU=0.34 SLOPE=-40 PHAS=2
;
 ELEMENTS GROUP $BEAD1$/ E=-10 YIELD=-23 LX=LY=LZ=-30--
  MODEL=3 NU=0.34 SLOPE=-60 PHAS=2
;
 ELEMENTS GROUP $BEAD1SKIN$/ E=-10 YIELD=-23 LX=LY=LZ=-30--
  MODEL=3 NU=0.34 SLOPE=-60 PHAS=2
;
CONSTRAINTS
;
; NODES   10  INTER /  UX UY UZ
 NODES   481  INTER /  UY UZ
 NODES   18906   INTER /  UZ
 NODES   82   INTER /  UZ
 NODES GROUP $SYMX$/ UX

LOAD
;
1 WELDING / NOTHING

TABLES
;
; Y0UNGS MODULUS E (N/mm^2) FOR ALUMINUM
;
 10 / 1 (0, 73000) (20, 73000) (100, 70000) (200, 63000) --
    (300, 55000) (400, 37000) (500, 15000) (600, 100) --
```

```
    (700, 10)

; YIELD STRENGTH (N/mm^2) FOR ALUMINUM 2519
 20 / -21 -24
 21 / 1 (0, 400) (20, 400) (25, 378) (50, 356) (75, 334) --
      (100, 312) (125, 289) (150, 267) (175, 245) --
      (200, 223) (225, 201) (250, 179) (275, 157) --
      (300, 135) (325, 112) (350, 75) (375, 40) (400, 35) --
      (425, 30) (450, 25) (475, 20) (500, 15) (525, 10) --
      (550, 5) (575, 3) (600, 2) (700, 1)

; YIELD STRENGTH (N/mm^2) FOR ALUMINUM 2319
 23 / -24 -24
 24 / 1 (0, 250) (20, 250) (25, 239) (50, 229) (75, 218) --
      (100, 208) (125, 197) (150, 186) (175, 176) --
      (200, 165) (225, 155) (250, 144) (275, 134) --
      (300, 123) (325, 112) (350, 75) (375, 40) (400, 35) --
      (425, 30) (450, 25) (475, 20) (500, 15) (525, 10) --
      (550, 5) (575, 3) (600, 2) (700, 1)

; THERMAL STRAINS FOR ALUMINUM
 30 / -31 -31
 31 / 1 (20, 0) (100, 0.00224) (200, 0.00474) --
       (300, 0.00741) (400, 0.00988) (500, 0.01235) --
       (600, 0.01482) (700, 0.01729)

; ISOTROPIC STRAIN HARDENING FOR ALUMINUM 2519
 40 / -41 -51
 41 / 7 (20, 45) (316, 46) (371, 47) (550, 48)
 45 / 1 (0, 386.1) (.1, 468.8)
 46 / 1 (0, 117.2) (.1, 137.8)
 47 / 1 (0, 41.37) (.1, 62.05)
 48 / 1 (0, 5) (.1, 7.5)
 51 / 7 (20, 55) (316, 56) (371, 57) (550, 58)
 55 / 1 (0, 152) (.1, 185)
 56 / 1 (0, 46) (.1, 54)
 57 / 1 (0, 16) (.1, 24)
 58 / 1 (0, 1.9) (.1, 2.9)

; ISOTROPIC STRAIN HARDENING FOR ALUMINUM 2319
 60 / -61 -71
 61 / 7 (20, 65) (316, 66) (371, 67) (550, 68)
 65 / 1 (0, 241) (.1, 255)
 66 / 1 (0, 117.2) (.1, 137.8)
 67 / 1 (0, 41.37) (.1, 62.05)
 68 / 1 (0, 5) (.1, 7.5)
 71 / 7 (20, 75) (316, 76) (371, 77) (550, 78)
 75 / 1 (0, 95) (.1, 115)
 76 / 1 (0, 46) (.1, 54)
```

```
 77 / 1 (0, 16) (.1, 24)
 78 / 1 (0, 1.9) (.1, 2.9)

RETURN
SAVE DATA 24

SEARCH DATA 24

; THERMAL LOAD

ASSIGN 19 TRAN12.TIT BINARY
TEMPERATURE TRANSIENT METALLURGY CARD
DEASSIGN 19

ASSIGN 19 TRAN22.TIT BINARY

TRANSIENT NON LINEAR STATIC
BEHAVIOR METALLURGY 2 PLASTIC
METHOD DIRECT SGI ORDER 1
ALGORITHM BFGS ITERATION 80
PRECISION ABSOLUTE DISPLACEMENT 1*-1 FORCE 1
INITIAL CONDITION RESTART CARD LAST
TIME INITIAL 50
   60 STEP 1.0   / STORE 10
  100 STEP 10.0  / STORE 10
 1000 STEP 100.0 / STORE 10
 5000 STEP 500.0 / STORE 10
RETURN

SAVE DATA 22
DEASSIGN 19
```

1.7 METALLURGY.DAT

```
MATERIAL 1 PHASE 2
REACTION
 1 2 DISSOLUTION TABLE 10 N TABLE 11
TABLE
 10 / 3610 15644 3000 545
 11 / 0 0
MATERIAL 2 PHASE 2
REACTION
 1 2 DISSOLUTION TABLE 12 N TABLE 13
TABLE
 12 / 3610 15644 3000 545
 13 / 0 0
END
```

Appendix B

1.0 Tee Section Transient Analysis Input Files

1.1 THERM1.DAT

```
SEARCH DATA 10
;
DEFINITION
 T-WELD MOVING REF FRAME
OPTION THERMAL METALLURGY SPATIAL
RESTART GEOMETRY
MATERIAL PROPERTIES
; MATERIAL 1 IS ALUMINUM 2519, MATERIAL 2 IS ALUMINUM 2319
; DENSITY RHO (kg/mm^3)
 ELEM GROUP $PLATES$ / KX KY KZ -10 RHO 2.82*-6 C -11 MATERIAL 1
 ELEM GROUP $BEAD1$ / KX KY KZ -10 RHO 2.82*-6 C -11 MATERIAL 2 STATE=-5
 ELEM GROUP $BEAD1SKIN$ / KX KY KZ -10 RHO 2.82*-6 C -11 MATERIAL 2 STATE=-5
 ELEM GROUP $BEAD2$ / KX KY KZ -10 RHO 2.82*-6 C -11 MATERIAL 2 STATE=-6
 ELEM GROUP $BEAD2SKIN$ / KX KY KZ -10 RHO 2.82*-6 C -11 MATERIAL 2 STATE=-6
;
CONSTRAINT
;
; CONVECTION (H = KT*TABLE 3 = W/mm^2 C)
;
 ELEMENTS GROUP $SKIN$ / KT=1*-6 VARIABLE=3
 ELEMENTS GROUP $BEAD1SKIN$ / KT=1*-6 VARIABLE=3
 ELEMENTS GROUP $BEAD2SKIN$ / KT=1*-6 VARIABLE=3
```

```
;
LOADINGS
;
1 WELDING / NOTHING
;
 ELEM GROUP $BEAD1$ / QR=11.5 VARI -4
;
 ELEM GROUP $SKIN$ / TT=20
 ELEM GROUP $BEAD1SKIN$ / TT=20
 ELEM GROUP $BEAD2SKIN$ / TT=20
;
TABLES
;
; THERMAL CONDUCTIVITY K (W/mm^2 C)
 10 / 1 (0 0.120) (50 0.130) (100 0.140) (150 0.150) (200 0.156) --
       (250 0.158) (300 0.156) (350 0.150) (400 0.145) (450 0.145) --
       (500 0.145) (550 0.145) (600 0.200) (650 0.250) (700 0.300) --
       (750 0.300) (800 0.300) (850 0.300) (900 0.300) (950 0.300) --
       (1000 0.300) (1100 0.300) (1200 0.300) (1300 0.300) (1500 0.300) --

; SPECIFIC HEAT Cp (J/kg C)
 11 / 1 (0 850) (50 860) (100 912) (150 935) (200 950) (250 965) --
       (300 955) (350 1000) (400 1063) (450 1063) (500 1063) (600 1063) --
       (700 1063) (800 1063) (900 1063) (1000 1063) (1200 1063) (1500 1063) --

; CONVECTION COEFFICIENT H (W/m^2 C) AFTER *KT UNITS ARE (W/mm^2 C)
;
 3 / 1 (0 2.5) (100 5.40) (150 6.20) (300 6.90) (450 7.30) (600 7.70) --
      (750 8.00) (900 8.20) (1050 8.40) (1200 8.60) (1350 8.75) (1500 8.90) --
      (1650 9.05) (1800 9.10) (1950 9.15) (2100 9.20) (2250 9.25) --
      (2400 9.30) (2550 9.35) (2700 9.40) (2850 9.45) (3000 9.50) --
;
; GOLDAK DOUBLE ELLIPSOID MOVING HEAT SOURCE

;    Heat source definition
 4 / FORTRAN
      FUNCTION F(X)
      DIMENSION X(5)
C HEAT SOURCE MOVING ON Z AXIS
C
C  VARIABLES
C
       X1=X(1)
       X2=X(2)
       X3=X(3)
       TT=X(4)

C
C VELOCITY VY
```

```
      VY  = -6.
C
     M1 = -1
     PI = acos ( M1 )
C CONSTANTS OF THE SOURCE
C
      A       = 30 ;DEPTH OF THE MOLTEN ZONE ALONG LOCAL X AXIS
      ALIMIT  = 30
      A2LIMIT = -ALIMIT
      B       = 30 ;WIDTH OF THE MOLTEN ZONE ALONG LOCAL Y AXIS
      BLIMIT  = 30
      B2LIMIT = -BLIMIT
      C1      = 24 ;LENGTH OF THE MOLTEN ZONE ALONG LOCAL T AXIS
      C2      = 80
      C1LIMIT  = 24
      C2LIMIT  = 80
      C1LIMIT = -C1LIMIT
      C2LIMIT = -C2LIMIT
C
C INITIAL POSITION OF THE SOURCE IN LOCAL FRAME
C
       DX = 4.12
       DY = 300.
       DZ = 14.45
C
C ANGLE OF ROTATION OF FRAME ABOUT Y AXIS
C
      TETA = 45. 180. / pi *
C CALCULATION OF SINE AND COSINE OF TETA
C
     CTETA = COS(TETA)
     STETA = SIN(TETA)
C
C CALCULATION OF THE COORDINATES OF THE GAUSS POINT IN THE MOVING FRAME
C CALCUALTION OF THE POSITION OF THE SOURCE
C
C CALCULATION OF COORDINATES IN THE LOCAL MOVING FRAME
C
     XA = X1 - DX
     YA = X2 - DY
     ZA = X3 - DZ
     D1     = CTETA * XA
     D2     = STETA * ZA
     XLOCAL  = D1 + D2
     D3     = STETA * XA
     D4     = CTETA * ZA
     ZLOCAL  = D4 - D3
     YLOCAL  = X2 DY VY TT * + -
C
```

```
C COMPUTING THE GOLDAK SOURCE
C
      XX = XLOCAL * XLOCAL
      YY = YLOCAL * YLOCAL
      ZZ = ZLOCAL * ZLOCAL
     EXP1 = 3 * XX
     AA   = A * A
     EXP1 = EXP1 / AA
     EXP1 = -EXP1
     EXP1 = EXP(EXP1)
     EXP2 = 3 * ZZ
     BB   = B * B
     EXP2 = EXP2 / BB
     EXP2 = -EXP2
     EXP2 = EXP(EXP2)
     EXP3 = 3 * YY
     IF (YLOCAL.GE.0) CC=C1*C1
     IF (YLOCAL.LE.0) CC=C2*C2
     EXP3 = EXP3 / CC
     EXP3 = -EXP3
     EXP3 = EXP(EXP3)
     COEF = EXP1 * EXP2
     COEF = COEF * EXP3
     IF (XLOCAL.GT.ALIMIT)  COEF=0
     IF (XLOCAL.LT.A2LIMIT) COEF=0
     IF (ZLOCAL.GT.BLIMIT)  COEF=0
     IF (ZLOCAL.LT.B2LIMIT) COEF=0
     F = COEF
C      CONTINUE
     RETURN
     END

 5 /  FORTRAN
      FUNCTION F(X)
      DIMENSION X(5)
C ACTIVATION
C
C  VARIABLES
C
       X1=X(1)
       X2=X(2)
       X3=X(3)
       TT=X(4)
C
C VELOCITY VY=-6.
       VY  = -6.
C
     M1 = -1
     PI = acos ( M1 )
```

```
C CONSTANTS OF THE SOURCE
C
      A      = 30 ;DEPTH OF THE MOLTEN ZONE ALONG X AXIS
      ALIMIT  = 30
      A2LIMIT = -ALIMIT
      B      = 30 ;WIDTH OF THE MOLTEN ZONE ALONG Y AXIS
      BLIMIT  = 30
      B2LIMIT = -BLIMIT
      C1     = 24 ;LENGTH OF THE MOLTEN ZONE ALONG Z AXIS
      C2     = 80
      C1LIMIT  = 24
      C2LIMIT  = 80
      C1LIMIT = -C1LIMIT
      C2LIMIT = -C2LIMIT
C
C INITIAL POSITION OF THE SOURCE IN LOCAL FRAME
C
       DX = 4.12
       DY = 300.
       DZ = 14.45
C
C ANGLE OF ROTATION OF FRAME ABOUT Y AXIS
C
      TETA = 45. 180. / pi *
C CALCULATION OF SINE AND COSINE OF TETA
C
     CTETA = COS(TETA)
     STETA = SIN(TETA)
C
C CALCULATION OF THE COORDINATES OF THE GAUSS POINT IN THE MOVING FRAME
C CALCUALTION OF THE POSITION OF THE SOURCE
C
C CALCULATION OF COORDINATES IN THE LOCAL MOVING FRAME
C
     XA = X1 - DX
     YA = X2 - DY
     ZA = X3 - DZ
     D1     = CTETA * XA
     D2     = STETA * ZA
     XLOCAL  = D1 + D2
     D3     = STETA * XA
     D4     = CTETA * ZA
     ZLOCAL  = D4 - D3
     YLOCAL  = X2 DY VY TT * + -
C
C COMPUTING THE GOLDAK SOURCE
C
     XX = XLOCAL * XLOCAL
     YY = YLOCAL * YLOCAL
```

```
      ZZ = ZLOCAL * ZLOCAL
      AA = YY YY *
      BB = ZZ ZZ *
      AA = AA BB +
      AA = SQRT (AA)
      DIST = YY - 144.
C
C F Computation
C
     F = 0
     IF( YLOCAL .GE. 0.0 ) F = 1
     IF( YLOCAL .GE. DIST ) F = 1
C
      RETURN
      END

 6/ FORTRAN
      FUNCTION F(X)
C
C F= 1 ACTIVATION OF ELEMENT
C F= -1 DEACTIVATION OF ELEMENT
C F=0 N0 EFFECT
C
      F=-1
      RETURN
      END
;
RETURN
;
NAME
SAVE DATA 11

SEARCH DATA 11

TRANSIENT NON-LINEAR
BEHAVIOUR METALLURGY 2
ALGORITHM BFGS IMPLICIT 1 ITERATION 40
PRECISION ABSOLUTE NORM 0 DISPLACEMENT 1 FORCE 1*-10
METHOD DIRECT NONSYMMETRIC SGI ORDER 1
INITIAL CONDITION
   NODES   / TT 20
   ELEMENTS GROUP $PLATES$    / P 1 0
   ELEMENTS GROUP $BEAD1$     / P 1 0 IS -1
   ELEMENTS GROUP $BEAD1SKIN$ / P 1 0 IS -1
   ELEMENTS GROUP $BEAD2$     / P 1 0 IS -1
   ELEMENTS GROUP $BEAD2SKIN$ / P 1 0 IS -1
TIME INITIAL 0
   50 STEP 0.5 / STORE 1
   60 STEP 1.0   / STORE 10
```

```
  100 STEP 10.0  / STORE 10
 1000 STEP 100.0 / STORE 10
 5000 STEP 500.0 / STORE 10
RETURN

GROUP CREATE NAME CARD5
ELEMENTS CRITERION ACTIVATED CARD 10
RETURN

GROUP CREATE NAME CARD45
ELEMENTS CRITERION ACTIVATED CARD 90
RETURN

GROUP CREATE NAME CARD50
ELEMENTS CRITERION ACTIVATED CARD 100
RETURN

SAVE DATA TRAN 12
DEASSIGN 19
```

1.2 THERM2.DAT

```
SEARCH DATA 10

DEFINITION
 T-WELD STEP BY STEP
OPTION THERMAL METALLURGY SPATIAL
RESTART GEOMETRY
MATERIAL PROPERTIES
; MATERIAL 1 IS ALUMINUM 2519, MATERIAL 2 IS ALUMINUM 2319
; DENSITY RHO (kg/mm^3)
 ELEM GROUP $PLATES$ / KX KY KZ -10 RHO 2.82*-6 C -11 MATERIAL 1
 ELEM GROUP $BEAD1$ / KX KY KZ -10 RHO 2.82*-6 C -11 MATERIAL 2
 ELEM GROUP $BEAD1SKIN$ / KX KY KZ -10 RHO 2.82*-6 C -11 MATERIAL 2
 ELEM GROUP $BEAD2$ / KX KY KZ -10 RHO 2.82*-6 C -11 MATERIAL 2 STATE=-5
 ELEM GROUP $BEAD2SKIN$ / KX KY KZ -10 RHO 2.82*-6 C -11 MATERIAL 2 STATE=-5
;
CONSTRAINT
;
; CONVECTION (H = KT*TABLE 3 = W/mm^2 C)
;
 ELEMENTS GROUP $SKIN$ / KT=1*-6 VARIABLE=3
 ELEMENTS GROUP $BEAD1SKIN$ / KT=1*-6 VARIABLE=3
 ELEMENTS GROUP $BEAD2SKIN$ / KT=1*-6 VARIABLE=3
;
LOADINGS
;
1 WELDING / NOTHING
;
```

```
 ELEM GROUP $BEAD2$ / QR=11.5 VARI -4
;
 ELEM GROUP $SKIN$ / TT=20
 ELEM GROUP $BEAD1SKIN$ / TT=20
 ELEM GROUP $BEAD2SKIN$ / TT=20
;
TABLES
;
; THERMAL CONDUCTIVITY K (W/mm^2 C)
 10 / 1 (0 0.120) (50 0.130) (100 0.140) (150 0.150) (200 0.156) --
       (250 0.158) (300 0.156) (350 0.150) (400 0.145) (450 0.145) --
       (500 0.145) (550 0.145) (600 0.200) (650 0.250) (700 0.300) --
       (750 0.300) (800 0.300) (850 0.300) (900 0.300) (950 0.300) --
       (1000 0.300) (1100 0.300) (1200 0.300) (1300 0.300) (1500 0.300) --

; SPECIFIC HEAT Cp (J/kg C)
 11 / 1 (0 850) (50 860) (100 912) (150 935) (200 950) (250 965) --
       (300 955) (350 1000) (400 1063) (450 1063) (500 1063) (600 1063) --
       (700 1063) (800 1063) (900 1063) (1000 1063) (1200 1063) (1500 1063) --

; CONVECTION COEFFICIENT H (W/m^2 C) AFTER *KT UNITS ARE (W/mm^2 C)
;
 3 / 1 (0 2.5) (100 5.40) (150 6.20) (300 6.90) (450 7.30) (600 7.70) --
      (750 8.00) (900 8.20) (1050 8.40) (1200 8.60) (1350 8.75) (1500 8.90) --
      (1650 9.05) (1800 9.10) (1950 9.15) (2100 9.20) (2250 9.25) --
      (2400 9.30) (2550 9.35) (2700 9.40) (2850 9.45) (3000 9.50) --
;
; GOLDAK DOUBLE ELLIPSOID MOVING HEAT SOURCE

;    Heat source definition
 4 / FORTRAN
      FUNCTION F(X)
      DIMENSION X(5)
C HEAT SOURCE MOVING ON Z AXIS
C
C  VARIABLES
C
       X1=X(1)
       X2=X(2)
       X3=X(3)
       TT=X(4)
C
C VELOCITY VY
       VY  = -6.
C
     M1 = -1
     PI = acos ( M1 )
C CONSTANTS OF THE SOURCE
C
```

```
      A      = 30 ;DEPTH OF THE MOLTEN ZONE ALONG LOCAL X AXIS
      ALIMIT  = 30
      A2LIMIT = -ALIMIT
      B      = 30 ;WIDTH OF THE MOLTEN ZONE ALONG LOCAL Y AXIS
      BLIMIT  = 30
      B2LIMIT = -BLIMIT
      C1      = 24 ;LENGTH OF THE MOLTEN ZONE ALONG LOCAL T AXIS
      C2      = 80
      C1LIMIT  = 24
      C2LIMIT  = 80
      C1LIMIT = -C1LIMIT
      C2LIMIT = -C2LIMIT
C
C INITIAL POSITION OF THE SOURCE IN LOCAL FRAME
C
       DX = -4.12
       DY = 30300.
       DZ = 14.45
C
C ANGLE OF ROTATION OF FRAME ABOUT Y AXIS
C
      TETA = 135. 180. / pi *
C CALCULATION OF SINE AND COSINE OF TETA
C
     CTETA = COS(TETA)
     STETA = SIN(TETA)
C
C CALCULATION OF THE COORDINATES OF THE GAUSS POINT IN THE MOVING FRAME
C CALCUALTION OF THE POSITION OF THE SOURCE
C
C CALCULATION OF COORDINATES IN THE LOCAL MOVING FRAME
C
     XA = X1 - DX
     YA = X2 - DY
     ZA = X3 - DZ
     D1     = CTETA * XA
     D2     = STETA * ZA
     XLOCAL  = D1 + D2
     D3     = STETA * XA
     D4     = CTETA * ZA
     ZLOCAL  = D4 - D3
     YLOCAL  = X2 DY VY TT * + -
C
C COMPUTING THE GOLDAK SOURCE
C
     XX = XLOCAL * XLOCAL
     YY = YLOCAL * YLOCAL
     ZZ = ZLOCAL * ZLOCAL
    EXP1 = 3 * XX
```

```
      AA   = A * A
      EXP1 = EXP1 / AA
      EXP1 = -EXP1
      EXP1 = EXP(EXP1)
      EXP2 = 3 * ZZ
      BB   = B * B
      EXP2 = EXP2 / BB
      EXP2 = -EXP2
      EXP2 = EXP(EXP2)
      EXP3 = 3 * YY
      IF (YLOCAL.GE.0) CC=C1*C1
      IF (YLOCAL.LE.0) CC=C2*C2
      EXP3 = EXP3 / CC
      EXP3 = -EXP3
      EXP3 = EXP(EXP3)
      COEF = EXP1 * EXP2
      COEF = COEF * EXP3
      IF (XLOCAL.GT.ALIMIT)  COEF=0
      IF (XLOCAL.LT.A2LIMIT) COEF=0
      IF (ZLOCAL.GT.BLIMIT)  COEF=0
      IF (ZLOCAL.LT.B2LIMIT) COEF=0
      F = COEF
C     CONTINUE
      RETURN
      END

 5 /  FORTRAN
       FUNCTION F(X)
       DIMENSION X(5)
C ACTIVATION
C
C  VARIABLES
C
       X1=X(1)
       X2=X(2)
       X3=X(3)
       TT=X(4)
C
C VELOCITY VY=-6.
       VY  = -6.
C
      M1 = -1
      PI = acos ( M1 )
C CONSTANTS OF THE SOURCE
C
       A      = 30 ;DEPTH OF THE MOLTEN ZONE ALONG X AXIS
       ALIMIT  = 30
       A2LIMIT = -ALIMIT
       B      = 30 ;WIDTH OF THE MOLTEN ZONE ALONG Y AXIS
```

```
      BLIMIT  = 30
      B2LIMIT = -BLIMIT
      C1      = 24 ;LENGTH OF THE MOLTEN ZONE ALONG Z AXIS
      C2      = 80
      C1LIMIT  = 24
      C2LIMIT  = 80
      C1LIMIT = -C1LIMIT
      C2LIMIT = -C2LIMIT
C
C INITIAL POSITION OF THE SOURCE IN LOCAL FRAME
C
       DX = -4.12
       DY = 30300.
       DZ = 14.45
C
C ANGLE OF ROTATION OF FRAME ABOUT Y AXIS
C
      TETA = 135. 180. / pi *
C CALCULATION OF SINE AND COSINE OF TETA
C
     CTETA = COS(TETA)
     STETA = SIN(TETA)
C
C CALCULATION OF THE COORDINATES OF THE GAUSS POINT IN THE MOVING FRAME
C CALCULATION OF THE POSITION OF THE SOURCE
C
C CALCULATION OF COORDINATES IN THE LOCAL MOVING FRAME
C
     XA = X1 - DX
     YA = X2 - DY
     ZA = X3 - DZ
     D1     = CTETA * XA
     D2     = STETA * ZA
     XLOCAL  = D1 + D2
     D3     = STETA * XA
     D4     = CTETA * ZA
     ZLOCAL  = D4 - D3
     YLOCAL  = X2 DY VY TT * + -
C
C COMPUTING THE GOLDAK SOURCE
C
     XX = XLOCAL * XLOCAL
     YY = YLOCAL * YLOCAL
     ZZ = ZLOCAL * ZLOCAL
    AA = YY YY *
    BB = ZZ ZZ *
    AA = AA BB +
    AA = SQRT (AA)
    DIST = YY - 144.
```

```
C
C F Computation
C
    F = 0
    IF( YLOCAL .GE. 0.0 ) F = 1
    IF( YLOCAL .GE. DIST ) F = 1
C
     RETURN
     END

 6/ FORTRAN
     FUNCTION F(X)
C
C F= 1 ACTIVATION OF ELEMENT
C F= -1 DEACTIVATION OF ELEMENT
C F=0 N0 EFFECT
C
     F=-1
     RETURN
     END
;
RETURN
;
NAME
SAVE DATA 14

SEARCH DATA 14

ASSIGN 19 TRAN12.TIT BINARY
TRANSIENT NON-LINEAR
BEHAVIOUR METALLURGY 2
ALGORITHM BFGS IMPLICIT 1 ITERATION 40
PRECISION ABSOLUTE NORM 0 DISPLACEMENT 1 FORCE 1*-10
METHOD DIRECT NONSYMMETRIC SGI ORDER 1
INITIAL CONDITION RESTART CARD 42
TIME INITIAL 5000
  5050 STEP 0.5  / STORE 1
  5060 STEP 1.0   / STORE 10
  5100 STEP 10.0  / STORE 10
  6000 STEP 100.0 / STORE 10
 10000 STEP 500.0 / STORE 10
RETURN

GROUP CREATE NAME CARD5000
ELEMENTS CRITERION ACTIVATED CARD 1
RETURN

GROUP CREATE NAME CARD5046
ELEMENTS CRITERION ACTIVATED CARD 3
```

```
RETURN

GROUP CREATE NAME CARD5047
ELEMENTS CRITERION ACTIVATED CARD 5
RETURN

SAVE DATA 12
DEASSIGN 19
```

1.3 MECH1.DAT

```
SEARCH DATA 10
;
DEFINITION
;
 3D ALUMINUM T
;
OPTION THERMOMECHANICAL THREE DIMENSION
;
RESTART GEOMETRY
;
MATERIAL
;
 ELEMENTS GROUP $PLATES$ / E=-10 YIELD=-20 LX=LY=LZ=-30--
  MODEL=3 NU=0.34 PHAS=2 SLOPE=-40
;
 ELEMENTS GROUP $BEAD1$ / E=-10 YIELD=-23 LX=LY=LZ=-30--
  MODEL=3 NU=0.34 PHAS=2 SLOPE=-60
;
 ELEMENTS GROUP $BEAD2$ / STATE=-5 E=-10 YIELD=-23 LX=LY=LZ=-30--
  MODEL=3 NU=0.34 PHAS=2 SLOPE=-60
;
CONSTRAINTS
 NODES   95      INTER /   UZ
 NODES   6623    INTER /   UZ
 NODES   17361   INTER /   UZ
 NODES   7     INTER /   UZ
 NODES   23794   INTER /  UX UY
;
LOAD
;
1 WELDING / NOTHING
;
TABLE
  4 /  FORTRAN
       FUNCTION F(X)
       DIMENSION X(5)
C ACTIVATION
C
```

```
C  VARIABLES
C
      X1=X(1)
      X2=X(2)
      X3=X(3)
      TT=X(4)
C
C VELOCITY VY=-6.
      VY  = -6.
C
    M1 = -1
    PI = acos ( M1 )
C CONSTANTS OF THE SOURCE
C
      A      = 30 ;DEPTH OF THE MOLTEN ZONE ALONG X AXIS
      ALIMIT  = 30
      A2LIMIT = -ALIMIT
      B      = 30 ;WIDTH OF THE MOLTEN ZONE ALONG Y AXIS
      BLIMIT  = 30
      B2LIMIT = -BLIMIT
      C1       = 24 ;LENGTH OF THE MOLTEN ZONE ALONG Z AXIS
      C2       = 80
      C1LIMIT  = 24
      C2LIMIT  = 80
      C1LIMIT = -C1LIMIT
      C2LIMIT = -C2LIMIT
C
C INITIAL POSITION OF THE SOURCE IN LOCAL FRAME
C
       DX = 4.12
       DY = 300.
       DZ = 14.45
C
C ANGLE OF ROTATION OF FRAME ABOUT Y AXIS
C
      TETA = 45. 180. / pi *
C CALCULATION OF SINE AND COSINE OF TETA
C
     CTETA = COS(TETA)
     STETA = SIN(TETA)
C
C CALCULATION OF THE COORDINATES OF THE GAUSS POINT IN THE MOVING FRAME
C CALCUALTION OF THE POSITION OF THE SOURCE
C
C CALCULATION OF COORDINATES IN THE LOCAL MOVING FRAME
C
     XA = X1 - DX
     YA = X2 - DY
     ZA = X3 - DZ
```

```
      D1     = CTETA * XA
      D2     = STETA * ZA
      XLOCAL  = D1 + D2
      D3     = STETA * XA
      D4     = CTETA * ZA
      ZLOCAL  = D4 - D3
      YLOCAL  = X2 DY VY TT * + -
C
C COMPUTING THE GOLDAK SOURCE
C
      XX = XLOCAL * XLOCAL
      YY = YLOCAL * YLOCAL
      ZZ = ZLOCAL * ZLOCAL
     AA = YY YY *
     BB = ZZ ZZ *
     AA = AA BB +
     AA = SQRT (AA)
     DIST = YY - 144

C F Computation
C
    F = 0
    IF( YLOCAL .GE. 0.0 ) F = 1
    IF( YLOCAL .GE. DIST ) F = 1
C
     RETURN
     END

 5/ FORTRAN
     FUNCTION F(X)
C
C F= 1 ACTIVATION OF ELEMENT
C F= -1 DEACTIVATION OF ELEMENT
C F=0 NO EFFECT
C
     F=-1
     RETURN
     END

; Y0UNGS MODULUS E (N/mm^2) FOR ALUMINUM
;
 10 / 1 (0 , 73000) (20 , 73000) (100 , 70000) (200 , 63000) --
    (300 , 55000) (400 , 37000) (500 , 15000) (600 , 100) --
    (700 , 10)

; YIELD STRENGTH (N/mm^2) FOR ALUMINUM 2519
 20 / -21 -22
 21 / 1 (0 , 400) (20 , 400) (25 , 378) (50 , 356) (75 , 334) --
     (100 , 312) (125 , 289) (150 , 267) (175 , 245) --
```

```
     (200 , 223) (225 , 201) (250 , 179) (275 , 157) --
     (300 , 135) (325 , 112) (350 , 75) (375 , 40) (400 , 35) --
     (425 , 30) (450 , 25) (475 , 20) (500 , 15) (525 , 10) --
     (550 , 5) (575 , 3) (600 , 2) (700 , 1)

 22 / 1 (0 , 152) (20 , 152) (25 , 144) (50 , 135) (75 , 127) --
     (100 , 118) (125 , 110) (150 , 102) (175 , 93) --
     (200 , 85) (225 , 76) (250 , 68) (275 , 60) --
     (300 , 51) (325 , 43) (350 , 28) (375 , 15) (400 , 13) --
     (425 , 11) (450 , 9) (475 , 8) (500 , 6) (525 , 4) --
     (550 , 2) (575 , 2) (600 , 2) (700 , 1)

; YIELD STRENGTH (N/mm^2) FOR ALUMINUM 2319
 23 / -24 -25
 24 / 1 (0 , 250) (20 , 250) (25 , 239) (50 , 229) (75 , 218) --
     (100 , 208) (125 , 197) (150 , 186) (175 , 176) --
     (200 , 165) (225 , 155) (250 , 144) (275 , 134) --
     (300 , 123) (325 , 112) (350 , 75) (375 , 40) (400 , 35) --
     (425 , 30) (450 , 25) (475 , 20) (500 , 15) (525 , 10) --
     (550 , 5) (575 , 3) (600 , 2) (700 , 1)

 25 / 1 (0 , 95) (20 , 95) (25 , 91) (50 , 87) (75 , 83) --
     (100 , 79) (125 , 75) (150 , 71) (175 , 67) --
     (200 , 63) (225 , 59) (250 , 55) (275 , 51) --
     (300 , 47) (325 , 43) (350 , 28) (375 , 15) (400 , 13) --
     (425 , 11) (450 , 9) (475 , 8) (500 , 6) (525 , 4) --
     (550 , 2) (575 , 2) (600 , 2) (700 , 1)

; THERMAL STRAINS FOR ALUMINUM
 30 / -31 -31
 31 / 1 (20 , 0) (100 , 0.00224) (200 , 0.00474) --
       (300 , 0.00741) (400 , 0.00988) (500 , 0.01235) --
       (600 , 0.01482) (700 , 0.01729)

 32 / 1 (20 , -0.00448) (100 , -0.00224) (200 , 0.00026) --
       (300 , 0.00293) (400 , 0.00540) (500 , 0.00787) --
       (600 , 0.01034) (700 , 0.01281)

; ISOTROPIC STRAIN HARDENING FOR ALUMINUM 2519
 40 / -41 -51
 41 / 7 (20 , 45) (316 , 46) (371 , 47) (550 , 48)
 45 / 1 (0 , 386.1) (.1 , 468.8)
 46 / 1 (0 , 117.2) (.1 , 137.8)
 47 / 1 (0 , 41.37) (.1 , 62.05)
 48 / 1 (0 , 5) (.1 , 7.5)
 51 / 7 (20 , 55) (316 , 56) (371 , 57) (550 , 58)
 55 / 1 (0 , 152) (.1 , 185)
 56 / 1 (0 , 46) (.1 , 54)
 57 / 1 (0 , 16) (.1 , 24)
```

```
 58 / 1 (0 , 1.9) (.1 , 2.9)

; ISOTROPIC STRAIN HARDENING FOR ALUMINUM 2319
 60 / -61 -71
 61 / 7 (20 , 65) (316 , 66) (371 , 67) (550 , 68)
 65 / 1 (0 , 241) (.1 , 255)
 66 / 1 (0 , 117.2) (.1 , 137.8)
 67 / 1 (0 , 41.37) (.1 , 62.05)
 68 / 1 (0 , 5) (.1 , 7.5)
 71 / 7 (20 , 75) (316 , 76) (371 , 77) (550 , 78)
 75 / 1 (0 , 95) (.1 , 115)
 76 / 1 (0 , 46) (.1 , 54)
 77 / 1 (0 , 16) (.1 , 24)
 78 / 1 (0 , 1.9) (.1 , 2.9)

RETURN
SAVE DATA 21

SEARCH DATA 21

; THERMAL LOAD

ASSIGN 19 TRAN12.TIT BINARY
TEMPERATURE TRANSIENT METALLURGY CARD
DEASSIGN 19

TRANSIENT NON-LINEAR STATIC
BEHAVIOUR METALLURGY 2 PLASTIC
METHOD DIRECT SGI ORDER 1
ALGORITHM BFGS ITERATION 80
PRECISION ABSOLUTE DISPLACEMENT 1 FORCE 10
INITIAL CONDITION
  ELEMENTS GROUP $BEAD1$  / IS -1
TIME INITIAL 0
   50 STEP 0.5 / STORE 0
   60 STEP 1.0   / STORE 0
  100 STEP 10.0  / STORE 0
 1000 STEP 100.0 / STORE 0
 5000 STEP 500.0 / STORE 10
RETURN

SAVE DATA TRAN 24
DEASSIGN 19
```

1.4 MECH2.DAT

```
SEARCH DATA 10
;
DEFINITION
```

```
;
 T-WELD STEP BY STEP
;
OPTION THERMOMECHANICAL THREE DIMENSION
;
RESTART GEOMETRY
;
MATERIAL
;
 ELEMENTS GROUP $PLATES$ / E=-10 YIELD=-20 LX=LY=LZ=-30--
  MODEL=3 NU=0.34 PHAS=2 SLOPE=-40
;
 ELEMENTS GROUP $BEAD1$ / E=-10 YIELD=-23 LX=LY=LZ=-30--
  MODEL=3 NU=0.34 PHAS=2 SLOPE=-60
;
 ELEMENTS GROUP $BEAD2$ / STATE=-4 E=-10 YIELD=-23 LX=LY=LZ=-30--
  MODEL=3 NU=0.34 PHAS=2 SLOPE=-60

CONSTRAINTS
 NODES   95      INTER /   UZ
 NODES   6623    INTER /   UZ
 NODES   17361   INTER /   UZ
 NODES   7      INTER /   UZ
 NODES   23794   INTER /  UX UY
;
LOAD
;
1 WELDING / NOTHING
;
TABLE
  4 /  FORTRAN
       FUNCTION F(X)
       DIMENSION X(5)
C ACTIVATION
C
C  VARIABLES
C
        X1=X(1)
        X2=X(2)
        X3=X(3)
        TT=X(4)
C
C VELOCITY VY=-6.
        VY  = -6.
C
      M1 = -1
      PI = acos ( M1 )
C CONSTANTS OF THE SOURCE
C
```

```
      A      = 30 ;DEPTH OF THE MOLTEN ZONE ALONG X AXIS
      ALIMIT  = 30
      A2LIMIT = -ALIMIT
      B      = 30 ;WIDTH OF THE MOLTEN ZONE ALONG Y AXIS
      BLIMIT  = 30
      B2LIMIT = -BLIMIT
      C1      = 24 ;LENGTH OF THE MOLTEN ZONE ALONG Z AXIS
      C2      = 80
      C1LIMIT  = 24
      C2LIMIT  = 80
      C1LIMIT = -C1LIMIT
      C2LIMIT = -C2LIMIT
C
C INITIAL POSITION OF THE SOURCE IN LOCAL FRAME
C
       DX = -4.12
       DY = 30300.
       DZ = 14.45
C
C ANGLE OF ROTATION OF FRAME ABOUT Y AXIS
C
      TETA = 135. 180. / pi *
C CALCULATION OF SINE AND COSINE OF TETA
C
     CTETA = COS(TETA)
     STETA = SIN(TETA)
C
C CALCULATION OF THE COORDINATES OF THE GAUSS POINT IN THE MOVING FRAME
C CALCUALTION OF THE POSITION OF THE SOURCE
C
C CALCULATION OF COORDINATES IN THE LOCAL MOVING FRAME
C
     XA = X1 - DX
     YA = X2 - DY
     ZA = X3 - DZ
     D1     = CTETA * XA
     D2     = STETA * ZA
     XLOCAL  = D1 + D2
     D3     = STETA * XA
     D4     = CTETA * ZA
     ZLOCAL  = D4 - D3
     YLOCAL  = X2 DY VY TT * + -
C
C COMPUTING THE GOLDAK SOURCE
C
     XX = XLOCAL * XLOCAL
     YY = YLOCAL * YLOCAL
     ZZ = ZLOCAL * ZLOCAL
    AA = YY YY *
```

```
      BB = ZZ ZZ *
      AA = AA BB +
      AA = SQRT (AA)
      DIST = YY - 144.
C
C F Computation
C
     F = 0
     IF( YLOCAL .GE. 0.0 ) F = 1
     IF( YLOCAL .GE. DIST ) F = 1
C
      RETURN
      END

 5/ FORTRAN
      FUNCTION F(X)
C
C F= 1 ACTIVATION OF ELEMENT
C F= -1 DEACTIVATION OF ELEMENT
C F=0 NO EFFECT
C
      F=-1
      RETURN
      END

; Y0UNGS MODULUS E (N/mm^2) FOR ALUMINUM
;
 10 / 1 (0 , 73000) (20 , 73000) (100 , 70000) (200 , 63000) --
     (300 , 55000) (400 , 37000) (500 , 15000) (600 , 100) --
     (700 , 10)

; YIELD STRENGTH (N/mm^2) FOR ALUMINUM 2519
 20 / -21 -22
 21 / 1 (0 , 400) (20 , 400) (25 , 378) (50 , 356) (75 , 334) --
      (100 , 312) (125 , 289) (150 , 267) (175 , 245) --
      (200 , 223) (225 , 201) (250 , 179) (275 , 157) --
      (300 , 135) (325 , 112) (350 , 75) (375 , 40) (400 , 35) --
      (425 , 30) (450 , 25) (475 , 20) (500 , 15) (525 , 10) --
      (550 , 5) (575 , 3) (600 , 2) (700 , 1)

 22 / 1 (0 , 152) (20 , 152) (25 , 144) (50 , 135) (75 , 127) --
      (100 , 118) (125 , 110) (150 , 102) (175 , 93) --
      (200 , 85) (225 , 76) (250 , 68) (275 , 60) --
      (300 , 51) (325 , 43) (350 , 28) (375 , 15) (400 , 13) --
      (425 , 11) (450 , 9) (475 , 8) (500 , 6) (525 , 4) --
      (550 , 2) (575 , 2) (600 , 2) (700 , 1)

; YIELD STRENGTH (N/mm^2) FOR ALUMINUM 2319
 23 / -24 -25
```

```
 24 / 1 (0 , 250) (20 , 250) (25 , 239) (50 , 229) (75 , 218) --
     (100 , 208) (125 , 197) (150 , 186) (175 , 176) --
     (200 , 165) (225 , 155) (250 , 144) (275 , 134) --
     (300 , 123) (325 , 112) (350 , 75) (375 , 40) (400 , 35) --
     (425 , 30) (450 , 25) (475 , 20) (500 , 15) (525 , 10) --
     (550 , 5) (575 , 3) (600 , 2) (700 , 1)

 25 / 1 (0 , 95) (20 , 95) (25 , 91) (50 , 87) (75 , 83) --
     (100 , 79) (125 , 75) (150 , 71) (175 , 67) --
     (200 , 63) (225 , 59) (250 , 55) (275 , 51) --
     (300 , 47) (325 , 43) (350 , 28) (375 , 15) (400 , 13) --
     (425 , 11) (450 , 9) (475 , 8) (500 , 6) (525 , 4) --
     (550 , 2) (575 , 2) (600 , 2) (700 , 1)

; THERMAL STRAINS FOR ALUMINUM
 30 / -31 -31
 31 / 1 (20 , 0) (100 , 0.00224) (200 , 0.00474) --
       (300 , 0.00741) (400 , 0.00988) (500 , 0.01235) --
       (600 , 0.01482) (700 , 0.01729)

 32 / 1 (20 , -0.00448) (100 , -0.00224) (200 , 0.00026) --
       (300 , 0.00293) (400 , 0.00540) (500 , 0.00787) --
       (600 , 0.01034) (700 , 0.01281)

; ISOTROPIC STRAIN HARDENING FOR ALUMINUM 2519
 40 / -41 -51
 41 / 7 (20 , 45) (316 , 46) (371 , 47) (550 , 48)
 45 / 1 (0 , 386.1) (.1 , 468.8)
 46 / 1 (0 , 117.2) (.1 , 137.8)
 47 / 1 (0 , 41.37) (.1 , 62.05)
 48 / 1 (0 , 5) (.1 , 7.5)
 51 / 7 (20 , 55) (316 , 56) (371 , 57) (550 , 58)
 55 / 1 (0 , 152) (.1 , 185)
 56 / 1 (0 , 46) (.1 , 54)
 57 / 1 (0 , 16) (.1 , 24)
 58 / 1 (0 , 1.9) (.1 , 2.9)

; ISOTROPIC STRAIN HARDENING FOR ALUMINUM 2319
 60 / -61 -71
 61 / 7 (20 , 65) (316 , 66) (371 , 67) (550 , 68)
 65 / 1 (0 , 241) (.1 , 255)
 66 / 1 (0 , 117.2) (.1 , 137.8)
 67 / 1 (0 , 41.37) (.1 , 62.05)
 68 / 1 (0 , 5) (.1 , 7.5)
 71 / 7 (20 , 75) (316 , 76) (371 , 77) (550 , 78)
 75 / 1 (0 , 95) (.1 , 115)
 76 / 1 (0 , 46) (.1 , 54)
 77 / 1 (0 , 16) (.1 , 24)
 78 / 1 (0 , 1.9) (.1 , 2.9)
```

```
RETURN
SAVE DATA 25

SEARCH DATA 25

; THERMAL LOAD

ASSIGN 19 TRAN12.TIT BINARY
TEMPERATURE TRANSIENT METALLURGY CARD
DEASSIGN 19

ASSIGN 19 TRAN24.TIT BINARY

TRANSIENT NON-LINEAR STATIC
BEHAVIOUR METALLURGY 2 PLASTIC
METHOD DIRECT SGI ORDER 1
ALGORITHM BFGS ITERATION 80
PRECISION ABSOLUTE DISPLACEMENT 1 FORCE 10
INITIAL CONDITION RESTART CARD LAST
TIME INITIAL 5000
  5050 STEP 0.5  / STORE 0
  5060 STEP 1.0   / STORE 0
  5100 STEP 10.0  / STORE 0
  6000 STEP 100.0 / STORE 0
 10000 STEP 500.0 / STORE 10
RETURN

SAVE DATA 24
DEASSIGN 19
```

1.5 METALLURGY.DAT

```
MATERIAL 1 PHASE 2
REACTION
 1 2 DISSOLUTION TABLE 10 N TABLE 11
TABLE
 10 / 3610 15644 3000 545
 11 / 0 0
MATERIAL 2 PHASE 2
REACTION
 1 2 DISSOLUTION TABLE 12 N TABLE 13
TABLE
 12 / 3610 15644 3000 545
 13 / 0 0
END
```

Vita

Justin David Francis was born on October 7, 1973 to David and Karen Francis in Hackensack, NJ. After attending high school in Washingtonville, NY, Justin attended Virginia Tech for four years and received a B.S. in Mechanical Engineering. Through working in industry for an additional four years, his interest in structural design and analysis grew. After obtaining greater and greater professional responsibilities in the field of structural analysis, it was decided to return to Virgina Tech to obtain a master's degree in Aerospace Engineering, with a concentration in Structures and Structural Dynamics.